REPORT DOCUMENTATION PAGE	Form Approved OMB No. 0704-0188

1. AGENCY USE ONLY (Leave blank)	2. REPORT DATE 1/96	3. REPORT TYPE AND DATES COVERED Final Technical Report for 11/1/91-3/31/95

4. TITLE AND SUBTITLE

Microstructure and Reliability of Ceramics

5. FUNDING NUMBERS

AFOSR

F4962092-J0034

2306/BS

6. AUTHOR(S)

Michael J. Readey

7. PERFORMING ORGANIZATION NAME(S) AND ADDRESS(ES)

Carnegie-Mellon University
5000 Forbes Avenue
Pittsburgh, PA 15213-3890

8. PERFORMING ORGANIZATION

AFOSR-TR-96

0091

9. SPONSORING/MONITORING AGENCY NAME(S) AND ADDRESS(ES)

NA

AFOSR/NE
Building 410, Bolling AFB DC
20332-6448

AGENCY REPORT NUMBER

F49620-92-J-0034

19960320 093

11. SUPPLEMENTARY NOTES

12a. DISTRIBUTION/AVAILABILITY STATEMENT

APPROVED FOR PUBLIC RELEASE; DISTRIBUTION IS UNLIMITED.

12b. DISTRIBUTION CODE

13. ABSTRACT (Maximum 200 words)

The aim of this program was to investigate the role of microstructure on the reliability of ceramics, in particular those ceramics having pronounced R-curve behavior and thus the property of flaw tolerance, where the failure stress is minimally affected by processing defects or by damage accumulated in service. Hence, flaw-tolerant ceramics should show decreased strength variability and thus exhibit higher structural reliability. The program examined the effect of increasing R-curve behavior on the strength variability of ceramics toughened by phase transformation or grain bridging. The principal result of this work is that high reliability will only result in materials having both a strongly rising R-curve *and* a narrow intrinsic flaw population. The strong R-curve allows for stable crack extension under in-service conditions, and the narrow flaw population ensures that strength variability will be minimized in as-processed materials. These criteria are readily satisfied in zirconia ceramics by careful control of processing contaminants and heat-treatment schedules. In monolithic ceramics such as alumina, achieving a rapidly rising R-curve is more complex, involving tailoring the grain shape and grain boundary toughness through the use of additives.

14. SUBJECT TERMS	15. NUMBER OF PAGES 192
Microstructure, Ceramics, Reliability, R-Curve, T-Curve	16. PRICE CODE

17. SECURITY CLASSIFICATION OF REPORT	18. SECURITY CLASSIFICATION OF THIS PAGE	19. SECURITY CLASSIFICATION OF ABSTRACT	20. LIMITATION OF ABSTRACT
UNCLASSIFIED	UNCLASSIFIED	UNCLASSIFIED	

COMPLETED PROJECT SUMMARY

TITLE: Microstructure and Reliability of Ceramics
PRINCIPAL INVESTIGATOR: Michael J. Readey
INCLUSIVE DATES: 11/1/91 - 3/31/95
CONTRACT NUMBER: AFOSR No. F49620-92-J0034
RESEARCH PERSONNEL: Desiderio Kovar (Ph.D. received 5/95)
Celeste L. McCallen (M.S. received 5/93)
Patrick D. McNamara (M.S. received 5/93)

PUBLICATIONS:
1. "Correlations between flaw tolerance and reliability in zirconia," M.J. Readey, C.L. McCallen, P.D. McNamara, and B.R. Lawn, J. Mat. Sci., 28 6768-52 (1993).
2. "Microstructure, R-Curve Behavior, and Reliability of Structural Ceramics," M.J. Readey, International Symposium on Development and Applications of New Ceramics and Metal Alloys. Edited by Drew and Mostaghaci, Canadian Institute of Materials. p. 387-398 (1993).
3. "Role of Grain Size in Strength Variability of Alumina," D. Kovar and M.J. Readey, J. Am. Ceram. Soc., 77 [7] 1928-38 (1994).
4. "Effect of Glass Additions on the Indentation-Strength Behavior of Alumina," H.L. O'Donnell, M.J. Readey, and D. Kovar, J. Am. Ceram. Soc., 78 [4] 849-56 (1995).
5. "Microstructure, Flaw Tolerance, and Reliability of Ce-TZP and Y-TZP Ceramics," M.J. Readey and C.L. McCallen, J. Am. Ceram. Soc., 78 [10] 2769-76 (1995).
6. "Grain Size Distributions and Strength Variability of High-Purity Alumina," D. Kovar and M.J. Readey, J. Am. Ceram. Soc., in press (1996).
7. "Effect of Grain Shape on Strength Variability of Alumina Ceramics," M.J. Readey and D. Kovar, Fracture Mechanics of Ceramics, Volumes 11-12. Edited by R.C. Bradt, D.P.H. Hasselman, D. Munz, M. Sakai, and V.Y. Shevchenko. In press (1996).
8. "Effect of Heat-Treatment on Grain Size, Phase Assemblage, and Mechanical Properties of 3 mole % Y-TZP," L. Ruiz and M.J. Readey, J. Am. Ceram. Soc., in press (1996).
9. "Crack Stability and Strength Variability in Alumina Ceramics with T-Curve Behavior," D. Kovar, S.J. Bennison, and M.J. Readey, J. Am. Ceram. Soc., submitted (1996).

ABSTRACT OF OBJECTIVES AND ACCOMPLISHEMENTS:
The aim of this program was to investigate the role of microstructure on the reliability of ceramics, in particular those ceramics having pronounced R-curve behavior and thus flaw tolerance, where the failure stress is minimally affected by processing defects or by damage accumulated in service. Hence, flaw-tolerant ceramics should show decreased strength variability and thus exhibit higher structural reliability. The goal of this program was to investigate the effect of increasing R-curve behavior on the strength variability of ceramics toughened by phase transformation or grain bridging. Specifically, we examined the influence of microstructure on the reliability of ceramics, with the ultimate goal of providing the foundation for the design and fabrication of ceramic microstructures with greatly improved mechanical properties. Our results may be summarized as follows:

(i) The degree of flaw tolerance in zirconia ceramics is directly related to the degree of R-curve behavior. Also, the variability in strength decreases dramatically as the R-curve becomes stronger.

(ii) In alumina ceramics, increasing the grain size in high-purity alumina enhances both R-curve behavior and flaw tolerance, but strength variability is unaffected. This behavior was modeled by showing that the locally varying residual stresses contribute to the crack tip stress intensity, resulting in a variability in fracture toughness. This variability in toughness offsets any improvement in reliability due to enhanced flaw tolerance.

(iii) The shape of the R-curve in high-purity alumina ceramics is very sensitive to the grain morphology. In elongated grains, the R-curve rises sufficiently to promote some stable crack extension prior to failure, leading to a decrease in strength variability and improved reliability.

(iv) High reliability will only result in materials having both a strongly rising R-curve *and* a narrow intrinsic flaw population. The strong R-curve allows for stable crack extension under in-service conditions, and the narrow flaw population ensures that strength variability will be minimized in as-processed materials. These criteria are readily satisfied in zirconia ceramics by careful control of processing contaminants and heat-treatment schedules. In monolithic ceramics such as alumina, achieving a rapidly rising R-curve is more complex, involving tailoring the grain shape and grain boundary toughness through the use of additives.

MICROSTRUCTURE AND RELIABILITY OF CERAMICS

4

Publications in Progress

MICROSTRUCTURE AND RELIABILITY OF CERAMICS

I. INTRODUCTION

A. Objectives

The aim of this program was to investigate the role of microstructure on the reliability of ceramics, in particular those ceramics having pronounced R-curve behavior. R-curve (or T-curve) behavior refers to the phenomenon exhibited by many tough, structural ceramics, whereby the materials fracture toughness is a strong increasing function of crack size. In ceramics such as zirconia, the increase in toughness arises due the volumetric expansion (~ 5%) that occurs when small grains or precipitates in the material undergo a martensitic phase transformation from tetragonal to monoclinic symmetry. When this transformation takes place in the stress field of a propagating crack, the expansion induces compressive stresses that counteract the far field applied stresses, thereby reducing the local crack tip stress intensity and increasing the fracture toughness. In non-transforming ceramics such as alumina, the increase in toughening is due to grain bridging, where interlocking grains behind the crack tip "bridge" the two crack surfaces, relieving some of the stress at the crack tip. As the crack continues to propagate, more bridges are activated, progressively increasing the macroscopic fracture toughness.

An important consequence of R-curve behavior in ceramics is flaw tolerance, where the strength is insensitive to the initial flaw size. In fact, strength no longer follows conventional Griffith theory for these materials, but is controlled entirely by the shape and magnitude of the R-curve. This property has far-reaching implications with respect to the design of structural ceramics, namely that the failure stress will be minimally affected by processing defects or by damage accumulated in service. Hence, flaw-tolerant ceramics should show decreased strength

variability and thus exhibit higher structural reliability than ceramics characterized by a single-valued fracture toughness.

The goal of this program was to investigate the effect of increasing R-curve behavior on the strength variability of ceramics toughened by phase transformation or grain bridging. Specifically, we examined the influence of microstructure on the reliability of ceramics, with the ultimate goal of providing the foundation for the design and fabrication of ceramic microstructures with greatly improved mechanical properties. In FY92 and 93, we concentrated on the processing and characterization of zirconia and ultra-high purity alumina ceramics having controlled microstructures, assessing strength variability as a function of microstructural features such as grain size and degree of phase transformation. In FY94 and 95, we focused more on non-transforming alumina ceramics, exploring details such as the role of grain size distribution, grain shape, and the influence of grain boundary phases on flaw tolerance, R-curve behavior, and strength variability. Our results may be summarized as follows:

(i) We showed that controlling the heat-treatment temperature in Mg-PSZ and Ce-TZP led to control of R-curve behavior. We also showed that the degree of flaw tolerance was directly related to the degree of R-curve behavior; the stronger the R-curve the more flaw tolerant the material. Finally, we showed that in zirconia materials, the variability in strength decreases dramatically as the R-curve becomes stronger, e.g. the Weibull modulus increased by a factor of three in Mg-PSZ having a strong R-curve compared one with a lower, single-value fracture toughness.

(ii) We confirmed our hypothesis that ceramics having little R-curve behavior, such as Y-TZP, typically have high variability strength that is also insensitive to changes in microstructure.

(iii) We demonstrated that the strength and fracture toughness of Y-TZP ceramics could be further enhanced by controlled heat-treatments at elevated temperatures. For example, first sintering Y-TZP at low temperature followed by heat-treatment at higher temperatures leads to a ceramic with remarkable strength (~ 1 GPa) and high toughness (~ 10 MPa.m$^{1/2}$), a combination of properties rarely achieved in Y-TZP.

(iv) In alumina ceramics, we showed that the influence of microstructure on strength variability is much more complicated than in zirconia. For example, increasing the grain size in high-purity alumina enhances both R-curve behavior and flaw tolerance, but strength variability is unaffected. We modeled this behavior by showing that the locally varying residual stresses due to crystallographic thermal expansion anisotropy contribute to the crack tip stress intensity, resulting in a variability in fracture toughness. This variability in toughness offsets any improvement in reliability due to enhanced flaw tolerance.

(v) We demonstrated that the shape of the R-curve in high-purity alumina ceramics is very sensitive to the grain morphology. While increasing the average grain size enhances R-curve behavior, elongated grains tend to make the R-curve rise faster than equiaxed grains. The result of this subtle difference is important. In equiaxed alumina, the slowly rising R-curve implies cracks do not undergo stable extension, meaning failure is determined by the initial flaw size much like a Griffith material; there is no benefit from an increasing R-curve whatsoever.

However in elongated grains, the R-curve rises sufficiently to promote some stable crack extension prior to failure. Thus alumina having elongated grains shows a decrease in strength variability and improved reliability.

(vi) We also showed that flaw history plays an important role in whether reliability will be affected. For example, only in Mg-PSZ and Ce-TZP, and coarse-grained, alumina having elongated grain morphologies is the R-curve sufficiently steep to allow stable extension of preexisting flaws - leading to flaw tolerance and enhanced reliability. In addition, flaws having associated residual tensile stresses (i.e., indentations or hard particle impacts) will propagate stably with the application of an externally applied stress, and thus show flaw tolerance and enhanced reliability. However in alumina having equiaxed grain morphologies, natural processing flaws with no residual stresses show no stable crack propagation, and thus are not afforded the beneficial effects of the rising R-curve.

(vii) Perhaps the most significant result of this program is that high reliability will only result in materials having both a strongly rising R-curve *and* a narrow intrinsic flaw population. The strong R-curve allows for stable crack extension under in-service conditions, and the narrow flaw population ensures that strength variability will be minimized in as-processed materials. These criteria are readily satisfied in zirconia ceramics by careful control of processing contaminants and heat-treatment schedules. In monolithic ceramics such as alumina, achieving a rapidly rising R-curve is more complex, involving tailoring the grain shape and grain boundary toughness through the use of additives, an area of on-going research for the principal investigator.

B. Achievements

Eight papers have been published during FY93-96; a ninth paper is currently in review. Three additional papers are near completion and will be submitted for review in the first quarter of 1996. The work in these papers is summarized in the following abstracts, and the papers themselves are appended.

Paper 1. "Correlations between flaw tolerance and reliability in zirconia"

Interrelations between flaw tolerance and reliability in Y-TZP, Ce-TZP and Mg-PSZ ceramics are investigated. Indentation-strength tests indicate an enhanced flaw tolerance with increasing R-curve behavior from tetragonal-monoclinic martensite transformation. The Weibull modulus of unindented specimens increases with enhanced tolerance. However, even the most tolerant zirconia show persistent scatter in strength, implying that variability in material microstructure may be as important a factor in reliability evaluation in these materials as variability in flaw size.

Paper 2. "Microstructure, R-Curve Behavior, and Reliability of Structural Ceramics"

Today's structural ceramics often show an increasing fracture toughness with crack extension, or R-curve behavior. Theoretically, such R-curve behavior should improve the material's mechanical reliability by reducing the variability in strength. However, some toughening mechanisms can contribute to an increase in strength variability, depending on the scale of the microstructure relative to the flaw size. This factor is currently lacking in many models of reliability. This paper reviews the relationships between R-curve behavior and

reliability, and then discusses the influence of microstructure on strength variability. Criteria are then proposed to direct the design and engineering of ceramic microstructures for high reliability.

Paper 3. "Role of Grain Size in Strength Variability of Alumina"

Relationships between grain size and strength variability in alumina were investigated. Results are presented for an ultra-high-purity alumina with a narrow grain size distribution and an equiaxed grain morphology at three grain sizes ranging from 5 to 27 um. Vickers indentations are used to introduce controlled flaws into the specimens. It is found that increasing the grain size leads to enhanced flaw tolerance owing to a rising R-curve. However, contrary to recent theoretical predictions, no reduction in strength variability is found with increasing grain size. It is proposed that increasing variability in local fracture toughness with grain size offsets any improvement in reliability. This suggests that an upper bound to the reliability of grain-bridging materials may exist.

Paper 4. "Effect of Glass Additions on the Indentation-Strength Behavior of Alumina"

The effect of small calcium aluminosilicate (CAS) glass additions on the microstructure and flaw tolerance of alumina ceramics is investigated, and the results compared to a high-purity alumina. The high-purity alumina specimens were dense with microstructure consisting of a uniform grain size distribution and equiaxed grain morphology. Additions of only 1 wt% glass phase resulted in a bimodal grain size distribution containing large, elongated grains within a fine-grain matrix. Indentation-strength tests indicated enhanced flaw tolerance with the bimodal microstructure, even though both materials hand nominally the same average grain size. The

strength on unindented specimens was also observed to decrease with glass additions. Observations of crack paths show a greater propensity for bridging in the glass-containing alumina due to the presence of coarse, elongated grains and perhaps a lower grain boundary toughness. however, crack extension occurs transgranularly when the size of the coarsest grains becomes too large. This suggests that an optimum in flaw tolerance will be achieved with an elongated grain morphology and intermediate grain size.

Paper 5. "Microstructure, Flaw Tolerance, and Reliability of Ce-TZP and Y-TZP Ceramics"

Ce-TZP and Y-TZP ceramics were heat-treated for various times and temperatures in order to vary the microstructure. Flaw tolerance was investigated using the indentation-strength test. Reliability was quantified using conventional two-parameter Weibill statistics. Some Ce-TZP specimens were indented at slightly elevated temperatures where no transformation was observed. Results indicated that the Ce-TZP specimens were extremely flaw tolerant, and showed a relatively high Weibull modulus that scaled with both R-curve behavior and flaw tolerance. Y-TZP, on the other hand, with very little if any R-curve behavior or flaw tolerance, had a low Weibull modulus. The results also show that flaw history, i.e., whether or not a transformation zone exists along the wake of the crack, has a significant influence on strength. Strength was much less dependent on initial crack size when the crack had an associated transformation zone, whereas strength was highly dependent on cracks typical of natural processing defects. It is argued that the improvement in reliability, flaw tolerance, and dependence on flaw history are all ramifications of pronounced R-curve behavior.

Paper 6. "Grain Size Distributions and Strength Variability of High-Purity Alumina"

Two batches of high-purity alumina ceramics having an equiaxed grain morphology were manufactured with a mean grain size of approximately 10 um. A low-temperature heat treatment performed prior to sintering on one batch of specimens resulted in a narrow grain size distribution. The other batch of specimens was fired in a conventional manner and exhibited a broader grain size distribution. Mechanical tests performed on these specimens indicated little difference in the flaw tolerance or T-curve behavior of the aluminas, despite the presence of coarser grains in the conventionally fired alumina. Observations of cracks in these high-purity aluminas revealed that large grains ruptured transgranularly and therefore did not act as effective bridging sites. Strength tests on polished specimens indicated that the alumina with the broad grain size distribution exhibited greater strength variability than the alumina with the narrow grain size distribution. A simple analysis shows that because of the shallow T-curve behavior observed in both aluminas, stable crack extensions should not occur from natural flaws. The strength of these high-purity alumina is therefore controlled by the initial flaw size and the initial toughness. The increase strength variability in the alumina with the broad grain size distribution is rationalized in terms of a wider distribution of critical flaws.

Paper 7. "Effect of Grain Shape on Strength Variability of Alumina Ceramics"

In this study, the strength variability of several aluminas having similar average grain sizes but equiaxed or elongated grain morphologies are compared and correlated to their flaw tolerance and T-curve behavior. It was found that coarse-grained microstructures having elongated grain morphologies exhibited significantly more flaw tolerance and T-curve behavior

than their fine-grain, equiaxed counterparts. Moreover, only the coarse-grained, elongated alumina showed a T-curve sufficient to cause stable crack extension prior to failure. In addition, the Weibull modulus for this flaw-tolerant alumina was more than twice that of fine-grained, elongated aluminas. Tests with indented specimens conclusively demonstrated that improvements in reliability in these materials are not due solely to changes in the critical flaw size distribution, but rather to a combination of flaw size distribution and T-curve behavior.

Paper 8. "Effect of Heat-Treatment on Grain Size, Phase Assemblage, and Mechanical Properties of a 3 mole % Y-TZP"

The effect of heat-treatment on the grain size, phase assemblage, and mechanical properties of a 3 mole percent Y-TZP ceramic was investigated. Specimens were initially sintered for two hours at 1450°C to near theoretical density; some specimens were then heat treated at 1550°C, 1650°C, 1750°C or 1850°C to coarsen the microstructure. The average grain size increased with heat treatment from < 0.5 μm to ~ 10 μm. Phase analyses revealed predominantly tetragonal and cubic phases below 1750°C, with a significant decrease in tetragonal content and increase in monoclinic content for temperatures > 1750°C. The maximum fraction of tetragonal phase that transformed during fracture corresponded with the largest tetragonal grain size of ~ 5-6 μm. Strength was on the order of 1 GPa, and was surprisingly insensitive to heat-treatment temperature and grain size, contrary to previous studies. The fracture toughness increased from 4 MPa.m$^{1/2}$ to 10 MPa.m$^{1/2}$ with increasing grain size, owing to an increasing transformation zone size. Grain sizes larger than 5-6 μm spontaneously transformed to monoclinic phase during cooling. Such critical grain sizes are much larger than found in past investigations, and may be due to the greater fraction of cubic phase present which

decreases the strain energy arising from crystallographic thermal expansion anisotropy of the

tetragonal phase.

Paper 9. "Crack Stability and Strength Variability in Alumina Ceramics with T-Curve Behavior"

Four batches of alumina were manufactured, characterized, and tested to determine the

influence of microstructure on strength variability. Two batches of materials were produced

from high-purity starting powders and had an equiaxed grain morphology, one with a mean grain

size of 5 um and the other with a mean grain size of approximately 10 um. Two batches of

material with similar mean grain sizes were also manufactured from a lower purity starting

powder which resulted in materials with an elongated grain shape and broad grain size

distribution. Mechanical tests indicated that only the coarse-grained, lower purity alumina

exhibited strong flaw tolerance and T-curve behavior. In-situ crack growth studies confirmed that

this was the only material for which significant stable crack extension occurred from flaws free

of contact-induced residual stresses. Strength tests on polished specimens indicated hat the

highest mean strength was achieved in fine-grained materials with little or no flaw tolerance.

However, the lowest strength variability was measured in the coarse grained, lower purity

alumina which exhibited strong T-curve behavior. The improved mechanical reliability that was

observed in this material are rationalized in terms of T-curve behavior and its resultant influence

on crack stability.

APPENDIX 1

Correlations between flaw tolerance and reliability in zirconia

M. J. READEY, C. L. McCALLEN, P. D. McNAMARA
Department of Materials Science and Engineering, Carnegie Mellon University, Pittsburgh, PA 15213, USA

B. R. LAWN
Materials Science and Engineering Laboratory, National Institute of Standards and Technology, Gaithersburg, MD 20899, USA

Interrelations between flaw tolerance and reliability in Y-TZP, Ce-TZP and Mg-PSZ ceramics are investigated. Indentation–strength tests indicate an enhanced flaw tolerance with increasing R-curve behaviour from tetragonal → martensite transformation. The Weibull modulus of unindented specimens increases with the enhanced tolerance. However, even the most tolerant zirconias show persistent scatter in strength, implying that variability in material microstructure may be as important a factor in reliability evaluation in these materials as variability in flaw size.

1. Introduction

It is now well established that many engineering ceramics demonstrate pronounced crack-resistance (R-curve) behaviour, where fracture toughness increases with crack extension. One class of ceramics that shows particularly strong R-curves is zirconia, from transformation toughening [1–3]. A consequence of R-curve behaviour is "flaw tolerance", meaning that the strength becomes less sensitive to initial flaw size relative to conventional ceramics which obey the Griffith failure criterion [4–6]. Recently, it has been suggested that flaw-tolerant ceramics may also exhibit a reduced variability in strength, with a consequent improved reliability [7–9]. While flaw tolerance has been extensively studied in alumina ceramics [4, 6, 10], the same is not true of zirconia ceramics. Moreover, definitive evidence for improved reliability due to flaw tolerance is not generally available.

The purpose of this preliminary study was to establish a correlation between flaw tolerance and reliability in Y-TZP, Ce-TZP and Mg-PSZ ceramics subjected to various heat treatments. Previous studies of similar materials have reported pronounced R-curve behaviour in Mg-PSZ and Ce-TZP ceramics [5,11,12], but little or none in Y-TZP ceramics [13]. First, we determined the flaw tolerance characteristics of our materials using indentation flaws [4, 6, 10]. Then we evaluated the strength variability of unindented specimens using conventional Weibull statistics. Conclusions were drawn concerning the competitive roles of flaw size and microstructural variability on the Weibull modulus.

2. Experimental procedure

2.1. Material processing

Y-TZP (3 mol %), Ce-TZP (12 mol%) and Mg-PSZ

(9 mol %) were chosen for study because of their well-documented toughness properties [11–17] and microstructural characteristics [17]. The toughening arises from transformation of constrained tetragonal (t) phase to monoclinic (m) phase. In TZP the t-phase pre-exists as complete grains, in PSZ as precipitates within a cubic matrix. Our general aim was to produce zirconias with different microstructures, and hence different flaw tolerances. More specifically, the aim was to vary the R-curves of our selected materials without altering the fundamental nature of the flaw populations, so that we might observe the influence of flaw tolerance on reliability in a well-controlled material system.

Specimens approximately 25 mm diameter by 4 mm thick were prepared by pressing powders to 70 MPa in a hardened steel die. The green compacts were then cold-isostatically pressed to 250 MPa, and heat treated for various times and temperatures. All materials were embedded in powder of the same composition to minimize volatilization, and sintered at specified temperatures and times in air using heating and cooling rates of $5\,^{\circ}C\,min^{-1}$. The Mg-PSZ materials were subjected to additional post-sintering ageing heat treatments [14], after cooling directly from the sintering temperature at $10\,^{\circ}C\,min^{-1}$. Heat-treatment details are included in Table I.

2.2. Microstructure analysis

Densities of the sintered ceramics were determined using Archimedes' method. Grain sizes were determined from scanning electron micrographs of polished and thermally etched surfaces using an image analysis system. Precipitate sizes in Mg-PSZ were measured on fracture surfaces after chemically etching in concentrated HF acid to remove the cubic matrix.

TABLE I Sintering/heat-treatment schedules for zirconia ceramics. (Mg-PSZ ageing carried out after quenching specimens from the sintering temperature)

Zirconia	Sintering temp. (°C)	Sintering time (min)	Ageing temp. (°C)	Ageing time (min)
Y-TZP [a]	1450	120	–	–
	1575	120	–	–
Ce-TZP [b]	1450	120	–	–
	1450	3000	–	–
Mg-PSZ [c]	1700	120	1400	0
	1700	120	1400	40
	1700	120	1400	60

[a] SY-Ultra, Z-Tech Corporation, Bow, NH, USA.
[b] TZ-12CE, Tosoh Ceramics, Tosoh Corporation, Tokyo.
[c] TZ-9MG, Tosoh Ceramics, Tosoh Corporation, Tokyo.

X-ray diffraction (XRD) phase analysis was conducted on both as-polished surfaces and subsequent fracture surfaces. Integrated intensities of m and t $\{1\,1\,1\}$ peaks were measured using a non-linear curve-fitting program. The m-phase fractions were evaluated using the method of Porter and Heuer [18]. The t-phase fractions that transformed during fracture were then determined as differences in m-phase fraction in the polished and fracture surfaces.

2.3. Flaw tolerance and reliability
The flaw tolerance of the zirconia ceramics was assessed using the indentation–strength test [4, 6, 10]. The discs were ground to a thickness of 2 mm and the prospective test surfaces diamond-polished to a finish of 1 μm. A Vickers microhardness indentation was placed at the centre of each test surface, at loads between 3 and 300 N. A small drop of oil was then placed on the indentation site to minimize environmentally assisted slow crack growth. The specimens were then rapidly loaded ($\approx$ 250 MPa s^{-1}) to failure in biaxial flexure using a flat-on-3-ball technique, with the indented surfaces on the tensile side. Strengths were determined from the equations of linear elasticity for thin plates. (We acknowledge these materials can show a marked non-linearity in their stress–strain responses, resulting in a shift of the neutral axis during loading. Thus our calculations will overestimate the actual strength [5].) The specimens were subsequently inspected to determine which failures originated from the indentation. Those which did not were excluded from the data set.

Strength variability for unindented specimens was quantified using conventional Weibull statistics. A minimum sample of 50 specimens of each batch of material was prepared by grinding and polishing, as discussed earlier. The specimens were broken in biaxial flexure without indentation, with the polished surfaces on the tensile side. The ensuing strength data were then analysed using a two-parameter Weibull function [19, 20].

3. Results
3.1. Density and grain size
All the materials had a density of > 98% theoretical in their as-sintered state. The microstructures of the Y-

TABLE II Physical properties of zirconia ceramics

Zirconia	Ageing treatment (°C min^{-1})	Density (Mg m^{-3})	Grain size (μm)	Precipitate size (nm)
Y-TZP	1450/120	6.03	0.31	–
	1575/120	6.03	0.86	–
Ce-TZP	1450/120	6.17	0.56	–
	1450/3000	6.18	2.1	–
Mg-PSZ	1400/0	5.68	40	160
	1400/40	5.66	40	280
	1400/60	5.59	40	380

TZP and Ce-TZP ceramics were relatively uniform and equiaxed. The mean grain size of these two materials increased with heat treatment (final size $\approx$ 2.2 μm). For the Mg-PSZ the microstructures were less regular, and coarser (grain size $\approx$ 40 μm). The latter grain size was independent of post-sintering ageing time. Details are included in Table II.

3.2. Phase microstructure
XRD of as-polished surfaces revealed no m-phase in the as-sintered Y-TZP and Ce-TZP ceramics, suggesting that the grain sizes are well below those necessary for spontaneous transformation to the m-phase during cooling [21]. On the other hand, as seen in Fig. 1, significant transformation occurred during fracture, especially at the coarser grain sizes. The degree of transformation was substantially higher in Ce-TZP than in Y-TZP, consistent with a much higher steady-state toughness [17].

XRD of as-polished surfaces of Mg-PSZ again revealed no m-phase prior to ageing. However, some m-phase was observed after post-sintering ageing, indicating that a fraction of the precipitates must have coarsened beyond the critical size. SEM inspection of acid-etched surfaces indeed revealed ever-coarsening lenticular precipitate structures in these materials [18], over a particle length range 160–380 nm (Table II). The amount of transformation of the residual t-phase precipitates during subsequent fracture varied with ageing time, with a peak at $\approx$ 40 min, as seen in Fig. 1; accordingly, we refer to the three Mg-PSZ materials represented in Fig. 1 as under-aged, peak-aged, and over-aged.

3.3. Indentation flaws
Examinations of the indentation sites on polished zirconia surfaces revealed considerable variability. In the Y-TZP materials the indentations showed the well-known radial crack pattern. However, only at the higher loads were the patterns "well developed", i.e. symmetrical with arms extending a distance of more than one impression half-diagonal from each corner. At the lower loads the patterns were more asymmetrical, with one or more ill-formed radial cracks less than one-tenth of an impression half-diagonal. Observations in Nomarski illumination showed evidence for significant contact-induced transformation zones surrounding the hardness impressions. These zones exert
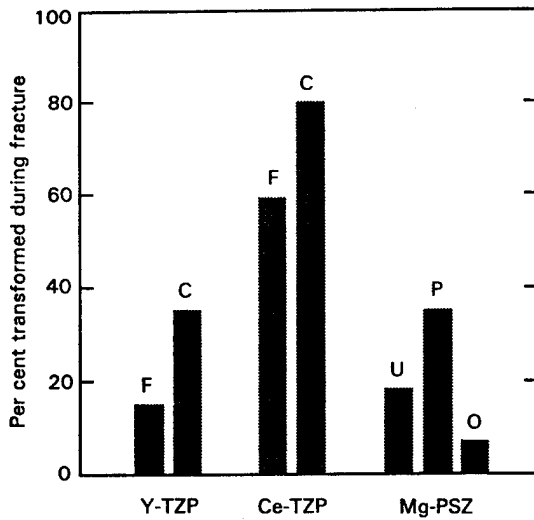
Figure 1 Percentage of t-phase transformed to m-phase during fracture of zirconia ceramics, as determined by comparative measurements on polished and fracture surfaces. For Y-TZP and Ce-TZP the fraction of transforming t-phase grains increases with change from finer (F) to coarser (C) grain scale. For Mg-PSZ the fraction increases with ageing from its initial value in the as-sintered state (under-aged, U) to a maximum (peak-aged, P) and then decreases (over-aged, O).

considerable compressive hoop stresses in the extra-hardness region, thereby "trapping" the incipient radial cracks in a subthreshold propagation state [22].

In the Ce-TZP and Mg-PSZ materials, the indentation fracture patterns were always ill formed, with little or no sign of radial extension beyond the hardness impression, except occasionally in the over-aged Mg-PSZ at the highest loads. These materials showed pronounced transformation zones outside the impression.

3.4. Flaw tolerance and Weibull modulus
3.4.1. Y-TZP

Indentation-strength data for the as-indented Y-TZP ceramics are plotted in Fig. 2. The two materials show a parallel dependence on indentation load, close to the classical $-1/3$ slope (dashed line, logarithmic co-ordinates) characteristic of materials with single-valued toughnesses [4, 6]. Slight deviations toward a lower slope are observed at low loads; ultimately, the strength cuts off abruptly, corresponding to failures from competing processing flaws (boxes at left). The data for the coarser grained material lie just below their finer grained counterparts, indicating a slightly reduced toughness. We note that the indentation data show considerable scatter, reflecting some kind of intrinsic variability in the indentation flaw K-field in these materials.

Weibull plots for unindented Y-TZP are shown in Fig. 3. The strength distributions for the two grain sizes are comparable, with relatively low Weibull moduli $m = 7.4$ (coarse) and $m = 9.0$ (fine).

3.4.2. Ce-TZP

Comparative indentation–strength data are plotted for Ce-TZP ceramics in Fig. 4. As with the Y-TZP, the
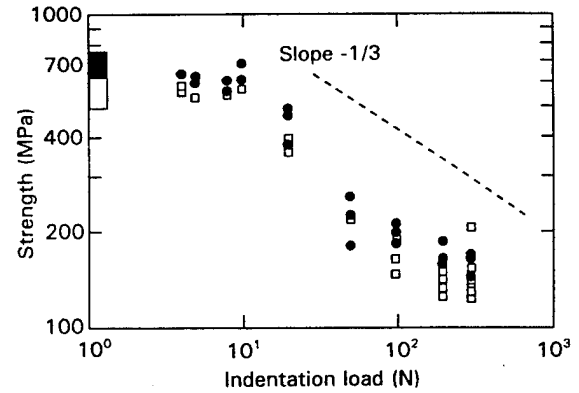

Figure 2 Strength as a function of indentation load for Y-TZP ceramics. Materials show strong sensitivity to load, and only slight dependence on grain size (cf. classical strength versus load$^{-1/3}$ dependence, - - -). (●) Fine grain, (□) coarse grain.
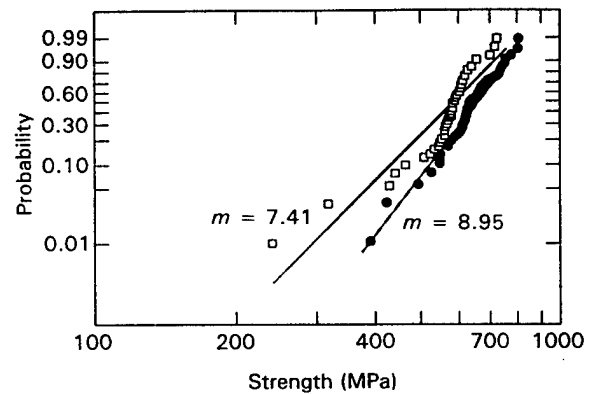

Figure 3 Weibull plots for Y-TZP ceramics. Note comparable Weibull moduli. (●) Fine grain, (□) coarse grain.
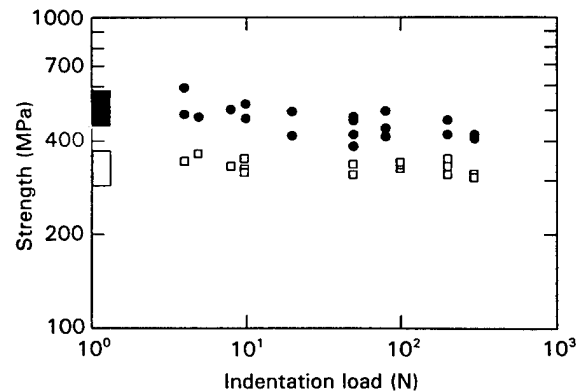

Figure 4 Strength as a function of indentation load for Ce-TZP ceramics. Materials show strong flaw tolerance (cf. Fig. 2). Coarser material shows lower strength but greater flaw tolerance. (●) Fine grain, (□) coarse grain.

finer grain-sized material is stronger. Now, however, the strengths are nearly invariant with indentation load, diminishing by $< 5\%$ over the load range for the coarser material and $< 15\%$ for the finer. The strength data no longer cut off abruptly at the levels for failure from natural flaws (boxes at left), but approach these levels asymptotically. These zirconias are therefore, relatively flaw tolerant, indicative of a ma-
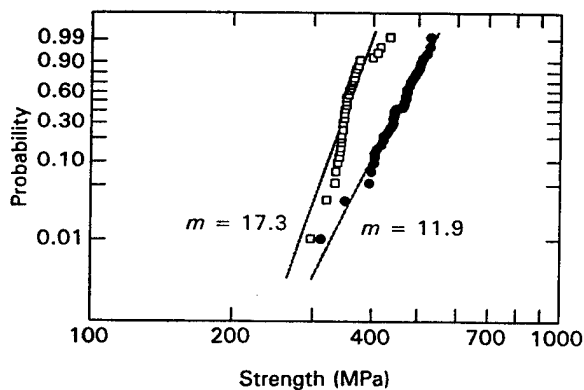
Figure 5 Weibull plots for Ce-TZP ceramics. Coarser material shows higher Weibull modulus. (●) Fine grain, (□) coarse grain.

Figure 6 Strength as a function of indentation load for Mg-PSZ ceramics. Materials show enhanced strength and flaw tolerance, in order (●) peak-aged, (□) under-aged and (▲) over-aged.

terial with a pronounced R-curve. Note that, notwithstanding this flaw tolerance, the strength data still show substantial scatter.

Weibull diagrams for Ce-TZP specimens without indentations are shown in Fig. 5. The Weibull modulus of both Ce-TZP materials is significantly higher than for the Y-TZP, $m = 17.3$ for coarse-grain and $m = 11.9$ for fine-grain material, suggesting a correlation with degree of flaw tolerance.

3.4.3. Mg-PSZ

Indentation–strength data for the Mg-PSZ ceramics are plotted in Fig. 6. The peak-aged material exhibits the highest strengths, followed by the under-aged and the over-aged materials. This is consistent with previous studies [11,14]. The degree of flaw tolerance shows the same trend, i.e. highest for the peak-aged and lowest for the over-aged material.

The Weibull data for the three materials are plotted in Fig. 7. Again, the Weibull modulus correlates with degree of flaw tolerance: $m = 20.0$ for peak-aged, $m = 10.3$ for under-aged, and $m = 6.3$ for over-aged material.

4. Discussion

We have demonstrated flaw tolerance, i.e. failure stress independent of initial flaw size, in zirconia ceramics using the indentation–strength test. This flaw tolerance is especially pronounced in Ce-TZP and Mg-PSZ materials, less so in Y-TZP. In the Ce-TZP and Mg-PSZ, the tolerance increases systematically with increasing degree of t–m transformation during fracture – the same mechanism responsible for the relatively strong R-curves in these two zirconias [9, 11, 14, 17, 21]. This increase in transformation activity reflects an increase in Weibull modulus for unindented, polished specimens that fail from processing flaws. There is, therefore, an implied correlation between flaw tolerance, hence R-curve, and reliability.

In addressing this potential correlation, we need to consider the nature of the flaws in our zirconia ceramics. We recall from Section 3.3 that indentation cracks tend not to be well developed in these materials, especially in Ce-YZP and Mg-PSZ; they remain
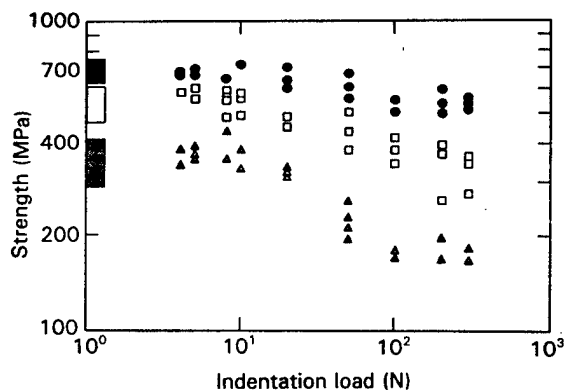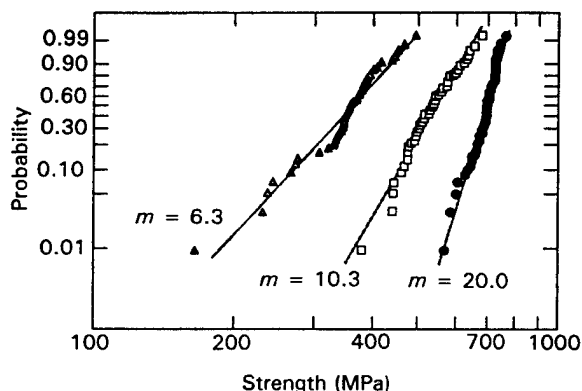

Figure 7 Weibull plots for Mg-PSZ ceramics. Highest Weibull modulus in order (●) peak-aged, (□) under-aged and (△) over-aged.

constricted at the impression corners within an outer encasing compressive transformation zone [22]. In contrast to other flaw-tolerant ceramics like coarse-grained aluminas where radial cracks are generally well developed [10, 23, 24], the critical conditions for failure are governed more by the mechanics of crack initiation than of crack propagation [23, 24]. The mechanics of initiation within residual contact fields is complex, even in materials with single-valued toughness [24]; the superposition of a transformation surround zone adds to this complexity [22]. Nevertheless, working analytical treatments of this problem are not beyond the bounds of indentation fracture mechanics [22].

The strong similarities in indentation flaw tolerance in such apparently disparate ceramics as our toughened zirconias (notably Figs 4 and 6) and coarsened aluminas [25] are of special interest in light of the above differences in radial crack configuration. Notwithstanding the fact that the radial cracks are comparatively ill-developed in the zirconias, the strength in both material types remains strongly independent of indentation impression size (typically over a range 25–250 μm in diagonal) relative to a classical flaw-size$^{-1/2}$ (load$^{-1/3}$) response. Moreover, the strengths for low-load indentations in these materials, in contrast to materials without strong toughening (such as

the Y-TZP in Fig. 2), are asymptotic to the strengths for unindented specimens. In this sense indentations may indeed be considered truly representative of natural flaws. These characteristics suggest that all flaws, regardless of history, are R-curve stabilized [4, 8, 26, 27], so reducing the sensitivity of strength to initial flaw size. Such flaw insensitivity is not seen in materials with single-valued toughness like glass [24]; there, the scatter in strength in the subthreshold region is typically more than an order of magnitude higher than in the postthreshold radial crack region. In glass there is no R-curve mechanism to negate the inherent susceptibility of initiation conditions to small geometrical fluctuations in the size and location of flaw nuclei within the immediate (strongly inhomogeneous) indentation stress fields [24].

The impressive insensitivity of strength to flaw size implicit in Figs 4 and 6 lead us to seek an alternative explanation for the observed strength scatter in our zirconia ceramics, namely in the microstructural variation. Preliminary quantitative analyses of polished surfaces in the SEM reveal a considerable point-to-point variability in grain size in our TZP zirconias. Similar determinations of precipitate size and spacing in the PSZ have yet to be made, but cursory SEM examinations do indicate some tendency for variability in precipitate size. In this context, we may recall from Section 3.4 the strong influence of precipitate size on the strength of Mg-PSZ. The implication is that fluctuations in precipitate size may profoundly influence the shape of the local short-crack R-curve, with consequent variation in specimen-to-specimen strengths. Again, it is the distribution in the underlying microstructural characteristics, rather than in the flaw size, that principally determines the variability in these materials. There are profound implications here concerning reliability in material design, with a shift in emphasis from traditional flaw elimination to microstructural characterization and processing control [23].

This shift in emphasis raises stochastic issues. Does the Weibull distribution remain a valid measure of reliability in such cases [7–9, 27]? In the present study we have retained the Weibull diagram simply as a vehicle for data display. Insights into such complex stochastic problems may await the use of computer algorithms to simulate flaw evolution in representative microstructures [28].

References

1. R. M. McMEEKING and A. G. EVANS, J. Am. Ceram. Soc. 65 (1982) 242.
2. A. G. EVANS and R. M. CANNON, Acta Metall. 34 (1986) 761.
3. M. J. READEY, R. W. STEINBRECH and A. H. HEUER, Materials Research Society Symposium Proceedings Vol. 78, edited by P. F. Becher, M. V. Swain and S. Somiya (MRS Press, Pittsburgh, PA, 1987) p. 107.
4. R. F. COOK, B. R. LAWN and C. J. FAIRBANKS, J. Am. Ceram. Soc. 68 (1985) 604.
5. D. B. MARSHALL, ibid. 69 (1986) 173.
6. S. J. BENNISON and B. R. LAWN, J. Mater. Sci. 24 (1989) 3169.
7. K. KENDALL, N. McN. ALFORD, S. R. TAN and J. D. BIRCHALL, J. Mater. Res. 1 (1986) 120.
8. R. F. COOK and D. R. CLARKE, Acta Metall. 36 (1988) 555.
9. D. K. SHETTY and J. S. WANG, J. Am. Ceram. Soc. 72 (1989) 1158.
10. L. M. BRAUN, S. J. BENNISON and B. R. LAWN, ibid. 75 (1992) 3049.
11. M. J. READEY, PhD thesis, Case Western Reserve University (1987).
12. D. K. SHETTY, J. Am. Ceram. Soc. 76 (1993) 961.
13. R. M. ANDERSON and L. M. BRAUN, ibid. 73 (1990) 3059.
14. R. H. HANNINK and M. V. SWAIN, J. Aust, Ceram. Soc. 18 (1982) 53.
15. V. GROSS and M. V. SWAIN, ibid. 12 (1986) 1.
16. K. TSUKUMA and M. SHIMADA, Am. Ceram. Soc. Bull. 65 (1986) 1386.
17. D. J. GREEN, R. H. J. HANNINK and M. V. SWAIN, "Transformation Toughening of Ceramics" (CRC Press, Boca Raton, FL, 1989) p. 90.
18. D. L. PORTER and A. H. HEUER, J. Am. Ceram. Soc. 62 (1979) 298.
19. G. QUINN, ibid. 73 (1990) 2374.
20. J. D. SULLIVAN and P. H. LAUZON, J. Mater. Sci. Lett. 5 (1986) 1245.
21. M. V. SWAIN and L. R. F. ROSE, J. Am. Ceram. Soc. 69 (1986) 511.
22. L. M. BRAUN and R. F. COOK, private communication (1993).
23. B. R. LAWN, "Fracture of Brittle Solids", 2nd Edn (Cambridge University Press, Cambridge, 1993) Chs 9, 10.
24. S. LATHABAI, J. RÖDEL, B. R. LAWN and T. P. DABBS, J. Mater. Sci. 26 (1991) 2157.
25. P. CHANTIKUL, S. J. BENNISON and B. R. LAWN, J. Am. Ceram. Soc. 73 (1990) 2419.
26. Y.-W. MAI and B. R. LAWN, Ann. Rev. Mater. Sci. 16 (1986) 415.
27. K. KENDALL, N. McN. ALFORD and J. D. BIRCHALL, Materals Research Society Symposium Proceedings, Vol. 78, edited by P. F. Becher, M. V. Swain and S. Somiya (MRS Press, Pittsburgh, PA, 1987) p. 189.
28. W. CURTIN, private communication (1992).

22

APPENDIX 2

MICROSTRUCTURE, R-CURVE BEHAVIOR, AND RELIABILITY
OF
STRUCTURAL CERAMICS

M.J. Readey
Department of Materials Science and Engineering
Carnegie Mellon University
Pittsburgh, Pennsylvania 15213
United States

ABSTRACT

Today's structural ceramics often show an increasing fracture toughness with crack extension, or R-curve behavior. Theoretically, such R-curve behavior should improve the material's mechanical reliability by reducing the variability in strength. However, some toughening mechanisms can contribute to an increase in strength variability, depending on the scale of the microstructure relative to the flaw size. This factor is currently lacking in many models of reliability. This paper reviews the relationships between R-curve behavior and reliability, and then discusses the influence of microstructure on strength variability. Criteria are then proposed to direct the design and engineering of ceramic microstructures for high reliability.

INTRODUCTION

The mechanical properties of structural ceramics have become quite impressive over the past decade. For example, magnesia partially-stabilized zirconia (Mg-PSZ) ceramics have fracture toughness values of over 15 MPam$^{1/2}$; silicon nitride ceramics have strengths of nearly 1 GPa. As a consequence of these desirable properties, these materials are now considered for demanding structural applications such as wear components in paper mills, and pistons, valves and rotors in automotive engine applications, to name but a few.

However, designers are not always interested in the average mechanical properties of a component, but the variability in properties. For example, a silicon nitride turbocharger rotor with an average strength of 1 GPa is extraordinary. But if the standard deviation about the mean is 200 MPa, and if the engine designer uses a 3σ criterion for design, then the strength of nearly all (99.7%) of the components will be between 400 and 1600 MPa. If the designer wishes to ensure high reliability in the application, then it is the 400 MPa value which is of interest, and not necessarily the average value. Thus if we are take advantage of the useful properties of advanced structural ceramics, then we must achieve high reliability by reducing the variability in strength.

RELIABILITY IN STRUCTURAL CERAMICS

In many engineering ceramics, reliability is defined as the probability of failure at a prescribed service stress: a low probability of failure implies a high reliability. Structural ceramic components are often regarded as mechanically unreliable because of a large variability in strength. This variability is most often expressed (inversely) as the Weibull modulus, i.e., a high Weibull modulus implies a small variability in strength. Thus for high reliability one attempts to seek materials with a high Weibull modulus.

The strength of many ceramic materials is controlled mainly by a critical flaw size, as described by the Griffith relation:

$$\sigma = \frac{K_{IC}}{\Psi c^{1/2}}$$

where σ is the strength, K_{IC} is the fracture toughness, c is the critical flaw size, and Ψ is a constant relating to the geometry of the crack. In such ceramics, the variability in strength is thus generally attributed to a broad distribution of flaws.

This flaw sensitivity for ceramics has posed considerable problems in structural design. How does one ensure that a given component does not contain a large flaw, or develop them in service? The problem is exacerbated by the fact that it is not the average flaw size, but that failure is caused by a single critical flaw. Non-destructive evaluation (NDE) and proof-testing could in principle allow the engineer to screen out components with unacceptably large flaws. However, in ceramics the small flaw sizes (typically on the order of a few tens of microns) lie well below the detection limits of present-day NDE technology. In the case of proof-testing, sub-critical crack growth is commonly observed in ceramics, suggesting that in spite of successfully passing the proof-test, the component may still fail in service. Furthermore, eliminating potentially defective components greatly increases the cost of those components that do survive.

To circumvent the limitations of NDE and proof-testing, some ceramic processors have argued that reliability can only be improved by narrowing the flaw size distribution via improved processing methods, e.g., colloidal processing under clean-room conditions, thereby eliminating large-scale processing defects. While this approach has experimentally been shown to result in considerably higher average strengths, it has not yet properly demonstrated that it leads to improved reliability. Moreover, there can be no guarantee that the component will develop strength degrading post-processing flaws in service, e.g. due to hard particle impacts. In such materials the single errant surface defect may degrade the strength by over an order of magnitude. This approach has the further disadvantage of being demanding of processing facilities, and is economically impractical for large-scale production.

Ideally, the most effective approach to improved reliability is to engineer ceramics that are less flaw-sensitive in the first place. Under these circumstances, conventional ceramic processing would be possible. Furthermore, one need not worry about processing or in-service defects, since strength is less dependent on defect size. We refer to such ceramics as being "flaw-tolerant". The only remaining question is can we successfully manufacture flaw-tolerant ceramics?

R-CURVE BEHAVIOR AND FLAW TOLERANCE

It is now generally recognized that the fracture toughness of many structural ceramics cannot be characterized by a single-valued fracture toughness, as implied by the Griffith relation. These ceramics demonstrate crack resistance (R-curve) behavior, whereby the fracture toughness increases with increasing crack size, as illustrated in Figure 1. It is also recognized that the origins of R-curve behavior in ceramics
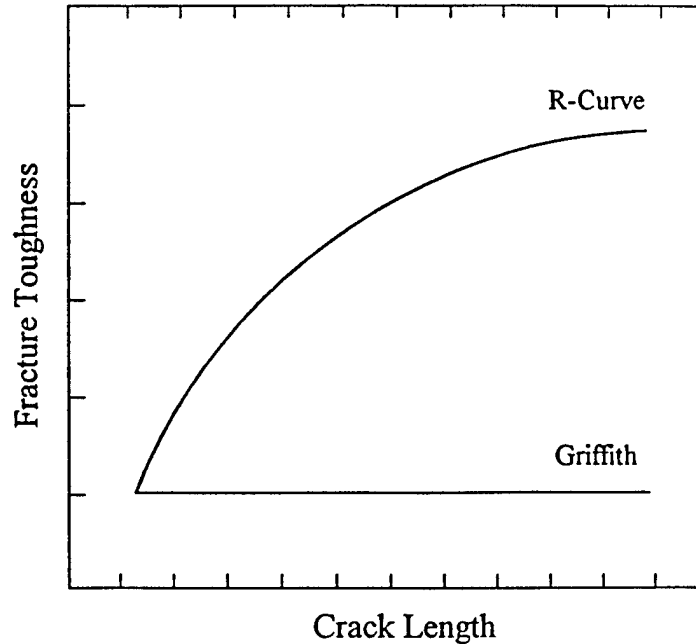
Figure 1. Schematic illustration showing a material having a single-valued fracture toughness (K_{Ic}), and one where the fracture toughness increases with increasing crack size (R-curve behavior).

are material related, and are associated with cumulative interactions between a propagating crack and a restraining microstructure. One of the first materials to demonstrate R-curve behavior is Mg-PSZ. In Mg-PSZ ceramics, the mechanism of toughening is the volume expansion (~5%) which occurs when small precipitates in the material undergo a martensitic transformation from the tetragonal to monoclinic symmetry. When the transformation nucleates in the stress field of a propagating crack, the volume expansion induces compressive traction forces behind the crack tip, thereby reducing the local crack tip stress intensity, and increasing the fracture toughness (1-6).

More recently, R-curve behavior has been observed in non-transforming ceramics such as alumina and silicon nitride. In alumina, the increase in toughness is due to grain bridging, where interlocking grains "bridge" the two crack surfaces behind the propagating crack, relieving some of the stress at the crack tip. As the crack continues to advance, more bridging grains are activated, progressively increasing the macroscopic fracture toughness (7-10).

In silicon nitride the increase in toughening with crack extension is less clear, but appears to closely related to the morphology of the silicon nitride grains: the more elongated the grain structure the more pronounced the R-curve behavior. Presumably, these elongated grains act to increase the toughness in many ways: crack deflection, as grain bridges, and as whisker-reinforcements.

The implication of R-curve behavior in these materials is profound. Specifically, failure is no longer governed by the Griffith criterion, but by the shape and magnitude of the R-curve. This is demonstrated in Figure 2, which plots the applied stress intensity as a function of the square root of crack length. From linear elastic fracture mechanics, we know the applied stress intensity (assuming Mode I loading) is given by:

$$K_I = \Psi \sigma_{app} c^{1/2}$$

Thus K_I is linear with respect to the square root of crack length, with the slope of the line proportional to the applied stress. Now on the second axis of Figure 2, we plot the material fracture toughness (R-curve) versus the square root of crack length. Crack propagation is then governed by the balance between the applied stress intensity and fracture toughness. This can be described as follows (the reader is referred to an excellent discussion by Broek on this topic (11)): upon loading to some applied stress, K_I for some initial crack length c_o is below the material's fracture toughness, and no crack propagation ensues. Increasing σ_{app} further increases K_I, to a point where it equals or exceeds the fracture toughness. In this case, $K_I > K_R$,* and crack extension ensues. However, as the crack extends, K_R increases to a point where it equals K_I. At this point the system is in mechanical equilibrium, and the crack arrests. Increasing σ_{app} causes crack extension to continue up to a critical length, c^*, where the K_I line becomes tangent to K_R. Again, the system is in mechanical equilibrium, but any infinitesimal increase in stress will result in K_I always greater than K_R, and the crack propagates in an unstable fashion to failure. Note that the new fracture criteria is such that:

$$K_I = K_R$$

but also that:

$$\frac{dK_I}{dc} = \frac{dK_R}{dc}$$

This condition is more commonly known as the tangency condition for failure. Note the implications of this new failure criteria: (1) strength is determined by the shape of the R-curve, and (2) considerable stable crack growth occurs prior to failure. Also note that it is the final crack length (c^*) that determines failure, and not the initial crack length (c_o). Thus strength becomes independent (or at least less dependent) on the initial flaw size! Moreover, taking this argument to its logical limit, any flaw size less than c^* should lead to the same strength - the material becomes flaw tolerant. The implication of this to reliability is apparent; high reliability will be achieved by ensuring that all flaws are smaller than c^*. This should be relatively straightforward, since materials having strong R-curve behavior are observed to have several hundred microns (and in some cases millimeters) of crack extension.

FLAW TOLERANCE IN CERAMICS

The relationship between flaw tolerance and R-curve behavior was first demonstrated with alumina ceramics by Lawn and coworkers using Vickers indentations to control the initial flaw size (9,12). As schematically shown in Figure 3, the strength of materials having a single valued toughness (K_{IC}) depend strongly on the indentation load (increasing the indentation load increases the indentation crack size). However, materials showing strong R-curve behavior deviated significantly from this behavior. Specifically, the strength was independent of indentation load over a wide range. Lawn later showed that this "plateau" strength correlated to the increasing portion of the fracture toughness curve up to an indentation crack size which correlated to c^*. For indentation cracks larger than c^*, the strength decreased and tended to the Griffith relation. Further studies by McCallen and Readey on Y-TZP and Ce-TZP ceramics (13), and by McNamara and Readey on Mg-PSZ (14) have confirmed that this is a general result: strong R-curve behavior leads to flaw tolerance.

---

* Note: In terms of stress intensities, it is customary to distinguish between a single-valued fracture toughness, K_{IC}, from a fracture toughness which increases with crack extension. This latter toughness exhibits R-curve behavior, and is therefore denoted K_R.
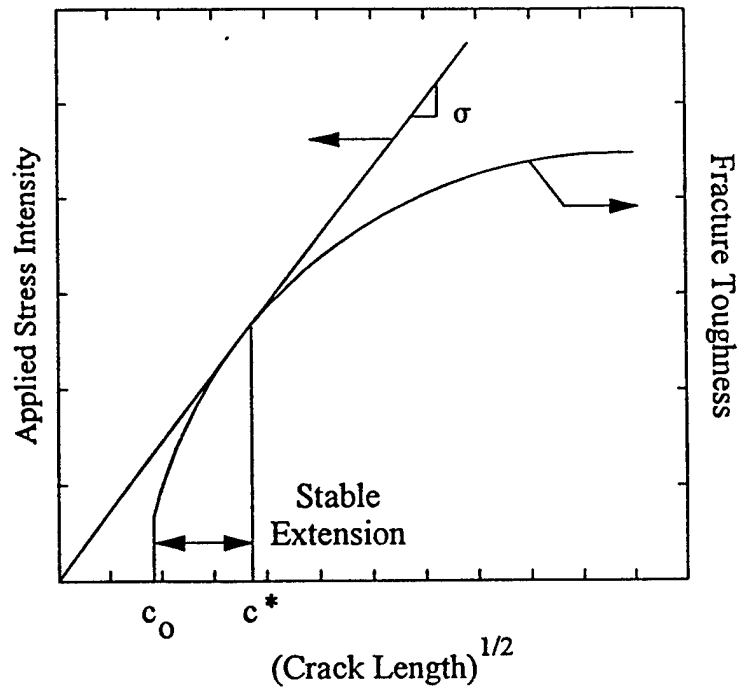
Figure 2. Schematic illustration showing how R-curve behavior leads to stable extension prior to failure. Note that strength depends only on c^*, and not on c_o.
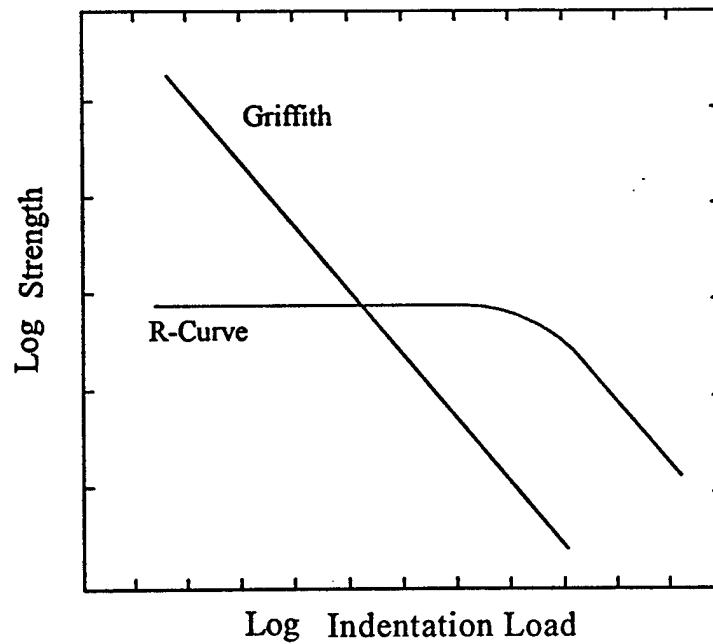

Figure 3. Schematic illustration of how strength depends on indentation load for materials which have a single-valued fracture toughness (Griffith) and those having R-curve behavior.

R-CURVE BEHAVIOR AND RELIABILITY

The natural conclusion we draw from the property of flaw tolerance is that the reliability of a ceramic will be greatly improved due to this insensitivity to flaw size. Furthermore, the improvement in reliability scales with the degree of R-curve behavior. Experimentally this has been verified in Mg-PSZ by McNamara and Readey (Figure 4) (14).

We might assert that ceramics exhibiting R-curve behavior, because of their insensitivity to flaw size, should manifest zero variability in strength (i.e., the plateau region in the strength-indentation load plot of Figure 3). This would suggest an infinite Weibull modulus. Experimentally, however, we observe that strength variability does persist in R-curve ceramics, although it is generally lower than "conventional" ceramics. Surprisingly, there is little if any improvement in reliability of alumina ceramics in spite of strongly increasing R-curve behavior (Figure 5) (15). This suggests that the feasibility of improving reliability by incorporating strong R-curve behavior depends on the toughening mechanism.

THE ROLE OF TOUGHENING MECHANISM ON RELIABILITY

In order to understand why R-curve behavior leads to an improvement in reliability for Mg-PSZ ceramics but not for alumina ceramics, we must investigate the role of microstructure and the influence of toughening mechanism on reliability. We begin by considering the mechanism of grain bridging. As mentioned earlier, grain bridging increases the fracture toughness of alumina ceramics by having interlocking grains bridge the two crack surfaces, effectively shielding the crack tip from the applied stress. As detailed by Bennison and Lawn (10), the bridging grains in alumina are further clamped in place by compressive residual stresses in the microstructure. The residual stresses arise because of anisotropy in thermal contraction of neighboring alumina grains during cooling from the processing temperature, given by:

$$\sigma_R = E\Delta\alpha\Delta T$$

where σ_R is the residual stress, E is Young's modulus, $\Delta\alpha$ is the difference in crystallographic thermal expansion coefficients, and ΔT is the temperature difference from room temperature to the temperature where stress relaxation can occur. The bridging mechanism is schematically shown in Figure 6. Intuitively, one would expect that as the grains increase in size, so does the length of the bridging ligament. Thus coarse grained aluminas would tend to show greater R-curve behavior than fine grained aluminas. This has been experimentally verified by many investigators. (15,16)

However, mechanical equilibrium requires that the compressive stresses be balanced by tensile stresses. Hence some grain facets will be in compression while others are in tension - with the total stresses summing to zero. Now consider a crack about to extend along an alumina grain boundary. Also assume that the size of the crack is on the same order of magnitude as the grain size, as schematically shown in Figure 7a. Under these circumstances, the sign and the magnitude of the residual stresses along the grain facet will strongly influence the local crack tip stress intensity. For example, if the facet is in compression, then as the crack begins to extend from an applied load, the compressive stress stabilize the crack from further growth, resulting in a macroscopic increase in the fracture toughness (Figure 7b).

Just the opposite effect occurs if the boundary is in tension. In this case, the tensile stress destabilizes the crack, "pulling" the crack forward. Here, the measured fracture toughness decreases as the crack extends across the boundary (Figure 7b). Thus the net result of the random nature of the residual
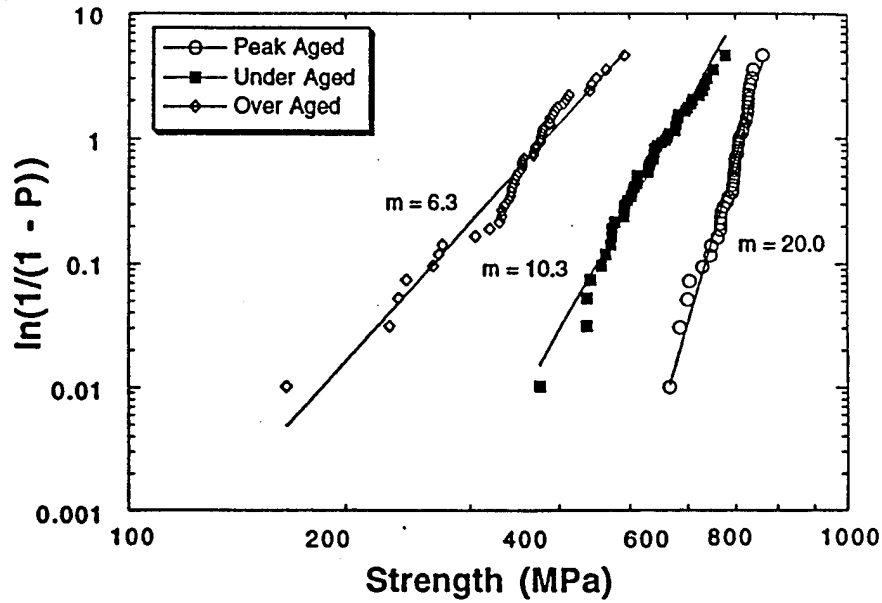
Figure 4. Weibull plot for various Mg-PSZ ceramics. "Underaged" corresponds to moderate R-curve behavior, "Peakaged" to maximum R-curve behavior, and "Overaged" to no R-curve behavior. Note that the variability in strength decreases with increasing degree of R-curve behavior, e.g., the Weibull modulus increases by over a factor of 3.
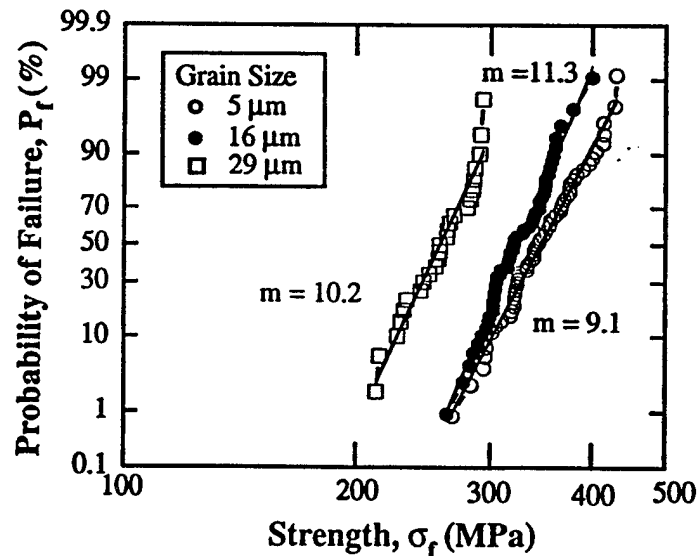

Figure 5. Probability of failure plot for alumina ceramics having different grain sizes. In alumina, R-curve behavior increases with increasing grain size. However, no improvement in reliability was measured.
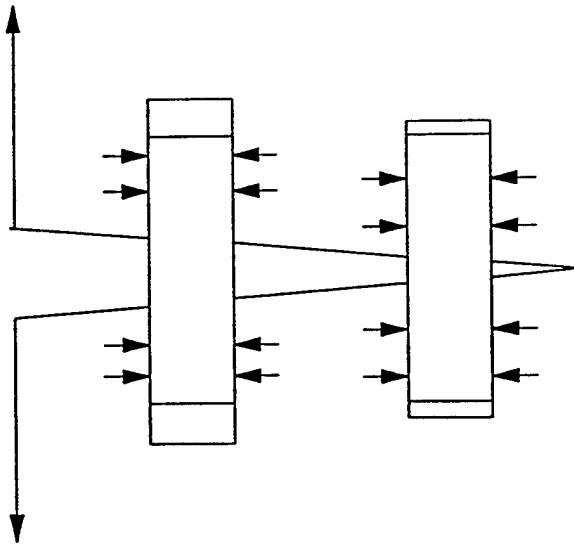
Figure 6. Schematic showing the mechanism of grain bridging.

stresses is that there will be considerable variation in the initial region of the R-curve. If we then allow the crack to continue propagating, as shown in Figure 8a, then clearly we will obtain a different R-curve each time we make a measurement, owing to the random distribution of residual stresses. This means that during the early stages of crack extension, when the crack size is still on the same scale of the grain size, the R-curves we measure will have considerable variability, and will need to be plotted as a "band", as shown in Figure 8b. (Note that as the crack becomes large relative to the microstructure, the influence of the alternating residual stresses becomes less important.)

Now consider the situation where the crack size is much larger than the microstructural feature responsible for the enhanced toughness. This is schematically shown in Figure 9a. (We illustrate the idea with smaller grains, but we imply generality; the "grains" in Figure 9a may be the tetragonal particles in zirconia ceramics, where the size is on the order of one micron.) In this case, any distribution of residual stresses will influence the crack tip stress intensity only over a small scale. Hence the variability in the R-curve will be significantly decreased, as shown in Figure 9b.

We now examine the influence on the variability in toughness on the variability in strength. Consider the schematic shown in Figure 11a for the material having little variability in R-curve behavior. If we test two specimens having exactly the same flaw size (c*), then it is likely that the specimens will have different strengths, depending on where the tangent point intersect each material's toughness curve (schematically shown as the top and bottom of the "band" in toughness, respectively). Nonetheless, the difference in the slopes of the lines is small, indicating a small difference in strength.

Contrast this to the situation where there is considerable variability in toughness. Again, if two specimens are tested with the same final flaw size, these may have dramatically different strengths, by virtue of the variability in the R-curve (Figure 10b). Thus, even though both materials have the same initial and final fracture toughness values, as well as similar shapes to the R-curves, the material with the larger variability in toughness has the larger variability in strength.

Figure 7. Schematic illustration showing a crack growing into a grain boundary facet (a), where the crack size is comparable to the grain size. (b) The fracture toughness either increases or decreases as the crack extends along the grain boundary, depending on the sign of the residual stresses.

Figure 8. Schematic illustration showing a crack extending into the material (a) The distribution of the residual stresses implies a different fracture toughness curve for different specimens, resulting in a "band" delineating the minimum and maximum fracture toughness values (b).

(a)   (b)
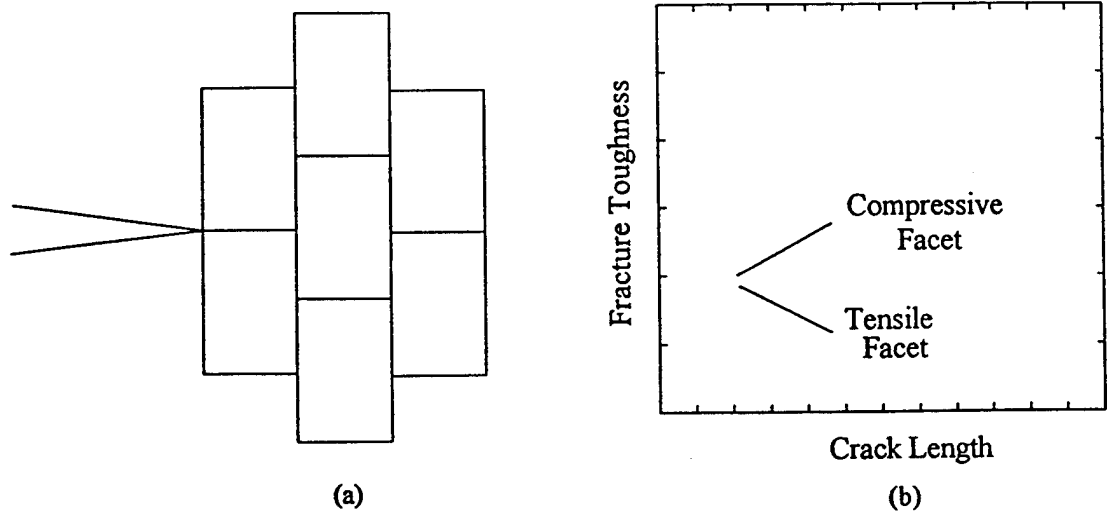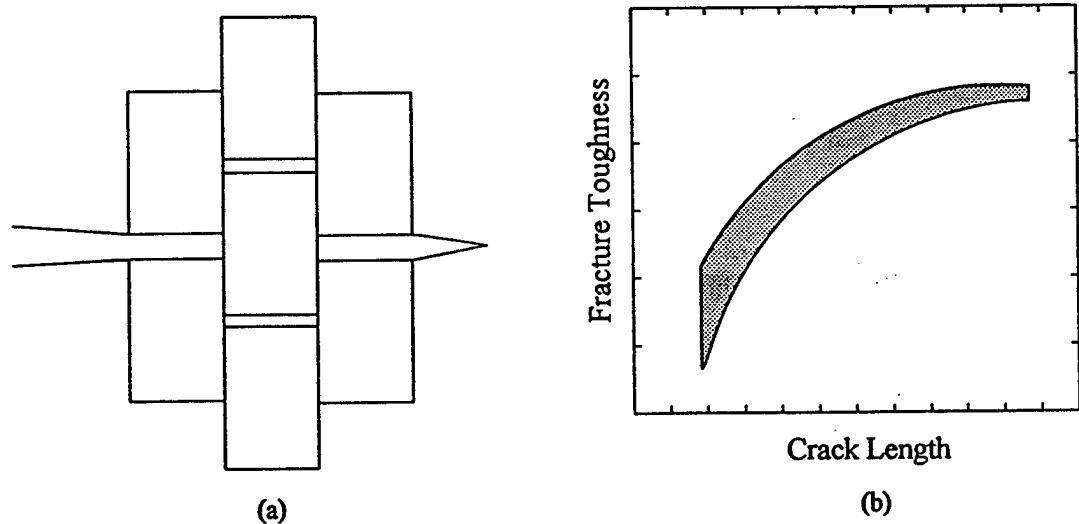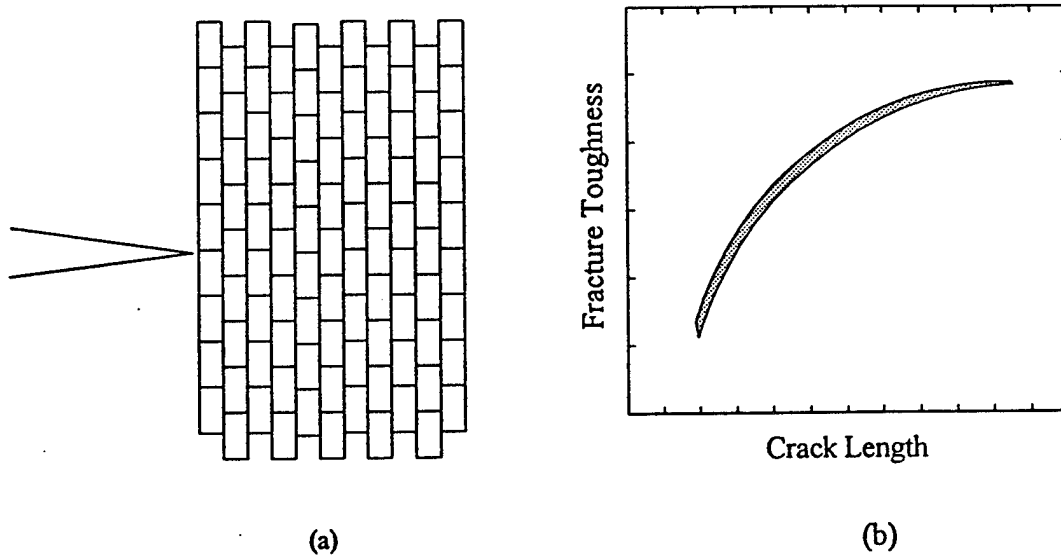
Figure 9. Schematic illustration showing a crack growing into a grain boundary facet (a), where the crack size is considerably larger than the microstructural feature leading to R-curve behavior. (b) The fracture toughness is only moderately influenced by the residual stresses as it extends along the grain boundary.

(a)   (b)
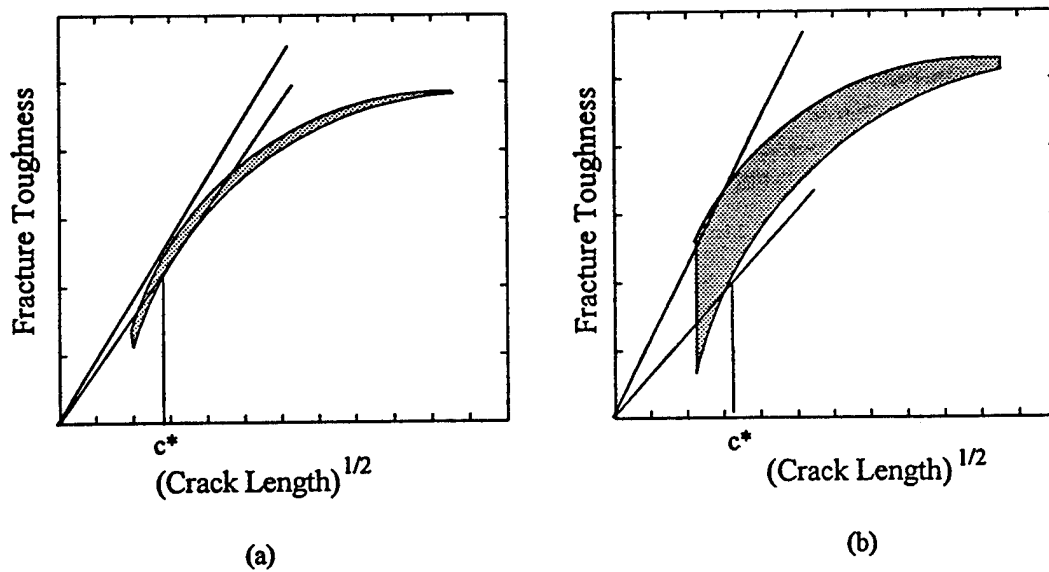
Figure 10. Schematic illustration showing the influence of variability in R-curve on strength. In material (a), little variability contributes only slightly to the variability in strength, whereas the material in (b) has considerable variability in toughness, with a consequent increase in the variability in strength. Note that both materials have the same initial and final toughness values, similar shapes to the R-curve, and the identical c* values.

We now can rationalize the experimental data discussed earlier. In the case of transformation-toughened zirconia ceramics, the scale of the microstructural features responsible for toughening is on the order of 1 micron or less. Thus we would expect little variability in the measured R-curves for these materials. Hence the increasing flaw tolerance afforded by a rising fracture toughness curves dramatically increases reliability.

On the other hand, the microstructural feature for toughening in alumina ceramics is the grain size. Thus as the grain size increases (to a few tens of microns) then we would expect the variability in toughness to increase as well. This variability adversely affects reliability, and in alumina leads to no improvement in reliability, in spite of strong R-curve behavior.

CONCLUSIONS

Given this rather qualitative view of R-curve behavior and reliability, we can now make some general predictions regarding high reliability in ceramic materials. In general, ceramics must have sharply rising R-curves giving substantial stable crack growth prior to failure. This imparts considerable flaw tolerance to the material. Finally, the scale of the microstructural feature responsible for the R-curve behavior must be small relative to "practical" flaw sizes, defined as flaw sizes in the range of 50-100μm. This will lead to small variability in fracture toughness from one specimen to the next, and result in a material with very high reliability.

ACKNOWLEDGMENTS

REFERENCES

1. M.J. Readey, A.H. Heuer, and R.W. Steinbrech, "Crack Propagation in Mg-PSZ", pp. 107-120 in Mat. Res. Symp. Proc. Vol 78. Ed. by S. Somiya, M.V. Swain, and P.F. Becher ((Materials Research Society, Pittsburgh) 1987.

2. M.J. Readey, A.H. Heuer, and R.W. Steinbrech, "Annealing of Test Specimens of High-Toughness Magnesia Partially-Stabilized Zirconia", J. Am. Ceram. Soc. 71 [1] C-2-C-6 (1988).

3. A.G. Evans, and A.H. Heuer, "Review-Transformation Toughening in Ceramics: Martensitic Transformations in Crack-Tip Stress Fields", J. Am. Ceram. Soc. 63 [5-6] 241-48 (1980).

4. R.M. McMeeking, and A.G. Evans, "Mechanics of Transformation Toughening in Brittle Materials", J. Am. Ceram. Soc. 65 [5] 242-46 (1982).

5. A.G. Evans, and R.M. Cannon, "Toughening of Brittle Solids by Martensitic Transformations", Acta metall. 34 761-800 (1986).

6. M.J. Readey, K_R-Curve Behavior in MgO Partially-Stabilized ZrO$_2$, Ph.D. Thesis, Case Western Reserve University, 1987.

7. Y.W. Mai, and B.R. Lawn, "Crack-Interface Bridging as a Fracture Resistance Mechanism in Ceramics: II, Theoretical Fracture Mechanics Model", J. Am. Ceram. Soc., 70 [4] 289-94 (1987).

8. R. Knehans, and R.W. Steinbrech, "Effect of Grain Size on the Crack Resistance Curves of Al$_2$O$_3$ Bend Specimens", pp. 613-19 in Science of Ceramics, Volume 12. Ed. by P. Vincenzini (Ceramurgica, Italy) 1984.

9. C.J. Fairbanks, B.R. Lawn, R.F. Cook, and Y.W. Mai, "Microstructure and the Strength of Ceramics", pp. 23-37 in Fracture Mechanics of Ceramics, Vol. 8. Ed. by R.C. Bradt, A.G. Evans, D.P.H. Hasselman, and F.F. Lange (Plenum Publishing Corporation) 1986.

10. S.J. Bennison, and B.R. Lawn, "Role of Interfacial Grain-Bridging Sliding Friction in the Crack-Resistance and Strength Properties of Nontransforming Ceramics", Acta metall., 37 [10] 2659-2671 (1989).

11. D. Broek, Elementary Engineering Fracture Mechanics, 3rd ed. (Martinus Nijhoff, Boston) 1982, pp. 193-195.

12. R.F. Cook, B.R. Lawn, and C. J. Fairbanks, "Microstructure-Strength Properties in Ceramics: I, Effect of Crack Size on Toughness", J. Am. Ceram. Soc. 68 [11] 604-15 (1985).

13. C.S. McCallen, and M.J. Readey, "Microstructure, R-Curve Behavior, Flaw Tolerance, and Reliability of Y-TZP and Ce-TZP Ceramics", to be published in the Journal of the American Ceramic Society.

14. P.D. McNamara and M.J. Readey, "R-Curve Behavior, Flaw Tolerance and Reliability of Mg-PSZ Ceramcs", to be published in the Journal of the American Ceramic Society.

15. D. Kovar and M.J. Readey, ""The Role of Microstructure on the Variability in Toughness and Strength", to be published in the Journal of the American Ceramic Society.

16. P.Chantikul, S.J. Bennison, and B.R. Lawn, "Role of Grain Size in the Strength and R-Curve Properties of Alumina", J. Am. Ceram. Soc., 73 [8] 2419-27 (1990).

APPENDIX 3

Role of Grain Size in Strength Variability of Alumina

Desiderio Kovar* and Michael J. Readey*,†

Department of Materials Science and Engineering, Carnegie Mellon University, Pittsburgh, Pennsylvania 15213

Relationships between grain size and strength variability in alumina were investigated. Results are presented for an ultra-high-purity alumina with a narrow grain size distribution and an equiaxed grain morphology at three grain sizes ranging from 5 to 27 μm. Vickers indentations are used to introduce controlled flaws into the specimens. It is found that increasing the grain size leads to enhanced flaw tolerance owing to a rising R-curve. However, contrary to recent theoretical predictions, no reduction in strength variability is found with increasing grain size. It is proposed that increasing variability in local fracture toughness with grain size offsets any improvement in reliability. This suggests that an upper bound to the reliability of grain-bridging materials may exist.

I. Introduction

A NUMBER of ceramic systems, including coarse-grained alumina, transformation-toughened zirconia, silicon nitride, and many whisker-reinforced ceramic composites, exhibit rising crack-growth resistance with crack extension or R-curve behavior.[1-4] An important and now well-established result of R-curve behavior is flaw tolerance; ceramics that have a strong R-curve show a decreased dependence of strength on initial flaw size.[5] This has profound implications from an engineering standpoint, namely that flaw-tolerant ceramics should show decreased strength variability and therefore exhibit higher reliability.

Enhanced reliability due to R-curve behavior was first suggested by Kendall *et al.* (based on the work of Hartsock and McLean). Kendall observed low strength variability in Mg-PSZ ceramics having a strong R-curve.[6,7] Conversely, considerable variability in strength was observed in Mg-PSZs having very little if any R-curve behavior. As both PSZs had similar flaw populations, Kendall attributed the improved reliability directly to the increasing fracture toughness. Since then, a number of investigators have associated R-curve behavior with high reliability. For example, Li and Yamanis found that silicon nitride having pronounced R-curve behavior also exhibited a high Weibull modulus.[4] Ramachandran *et al.* found that a Weibull modulus as high as 39 can be attained in a Ce-TZP/Al₂O₃ composite with a very strong R-curve. In contrast, they found a much lower Weibull modulus in 2Y-TZP ceramics having very little R-curve.[8] Based on these and other experimental observations, it is now widely believed that toughened ceramics with a rising fracture toughness are inherently more reliable than "conventional" ceramics having a constant fracture toughness.

In many cases, the correlation between reliability and R-curve behavior has been inferred from materials having

vastly different microstructures and thus potentially different flaw populations (e.g., single-phase alumina versus alumina reinforced with SiC whiskers). Consequently, it is quite possible that the observed improvement in reliability was more a result of a change in the critical flaw size, rather than an increasing crack resistance. Moreover, improvements in reliability have been observed in many ceramic materials that have a single-valued fracture toughness. For example, Rogeaux and Boch demonstrated that a Weibull modulus of 16 can be attained in fine-grained alumina by careful processing.[9] Similarly, Hamano *et al.* found that it was possible to produce silicon carbide with a fine grain size that had a Weibull modulus of 16.2.[10] Readey *et al.* reported a Weibull modulus of 24 for a commercially available, fine-grained alumina that was conventionally processed from spray-dried powders.[11]

Attempts to distinguish between the effect of R-curve behavior versus that of a changing flaw size distribution on reliability were first made by Ramachandran *et al.* by processing Ce-TZP/Al₂O₃ specimens containing monosized, spherical pores in order to maintain a constant flaw population.[8] They showed that the strength was essentially independent of pore size in these materials. However, in their study, only the surface trace of the strength-limiting pores was measured, giving no indication of the actual depth and hence the severity of the flaw. Moreover, it is not clear that such spherical pores act as Griffith-like flaws. The strength of a material containing a spherical pore is usually governed by the size of the incipient cracks emanating from the pore and the ratio of the size of the pore to that of the cracks. In fact, no size dependence on the strength is predicted based on the stress concentration near a spherical flaw in the absence of cracks, even for a material with a constant fracture toughness. Thus, it remains unclear whether R-curve behavior by itself leads to a reduction in strength variability.

Models accounting for the improved reliability of materials with R-curve behavior have primarily relied upon empirical curve fits to the R-curve in order to obtain a closed form solution for the strength. For example, Kendall *et al.* described the R-curve in Mg-PSZ ceramics using a power-law function:

$$K_R = Ac^n \tag{1}$$

where K_R is the fracture resistance, c is crack length, and A and n are fitting parameters.[12] They incorporated Eq. (1) into the standard Griffith relation, giving

$$\sigma_{fr} = \frac{A}{\sqrt{\pi}c^{0.5-n}} \tag{2}$$

where σ_{fr} is the fracture stress. The result of Kendall's analysis is that large values of n (indicating a steep R-curve) lead to a decreased dependence of strength on flaw size. Thus, for a given distribution of flaw sizes, the variability in strength in materials with a rising R-curve should be reduced compared to materials with a constant fracture toughness. Cook and Clarke extended Kendall's analysis by including the possibility that cracks may be under the influence of local residual stresses from impact damage.[13] They found similar results in that they predicted a weaker dependence of strength on flaw size with increasing n, even in the presence of residual stresses. However, they also concluded that simple power-law R-curves do not

completely describe the strength behavior of toughened ceramics. Other empirical functions have also been used to describe *R*-curves in order to establish a link between reliability and *R*-curve behavior.[3] Regardless of the form of the equations, all of these models give the same basic result; increasing the magnitude of the *R*-curve should lead to an increase in the reliability of the material. While these empirical models have been useful in motivating investigations linking *R*-curve behavior and reliability, no systematic experimental study has yet emerged.

The goal of this study is to examine the effect of increasing *R*-curve behavior on the strength variability of materials toughened by grain bridging. In this paper, we describe the conditions necessary to obtain materials having highly controlled microstructures and flaw populations. We then evaluate the strength variability of these materials using well-known engineering parameters. Finally, we propose a simple qualitative model to correlate the results with specific microstructural features. We are currently developing a more detailed fracture mechanics model to account for our results.

II.   Experimental Procedure

Alumina was chosen as a model material for study because the microstructure can be controlled by heat treatment, and because *R*-curve behavior due to grain bridging has been observed in coarse-grained aluminas.[14,15] The fracture mechanics of grain bridging has also been extensively modeled by Lawn *et al*.[16-19] Based on these models, the principal factors controlling the *R*-curve include the grain size, grain shape, coefficient of friction between the grains, and the magnitude of the residual stresses due to thermal expansion anisotropy (TEA).[18] In this study, we aim to vary the degree of *R*-curve behavior in alumina by increasing only the grain size, while simultaneously maintaining all other microstructural features constant. To achieve this goal it was necessary to produce our own materials under carefully controlled processing conditions.

(1)   Processing

An ultra-high-purity alumina powder (AKP-50, Sumitomo Chemical America, New York, NY) with a purity >99.99%[‡] was uniaxially pressed (as-received) at 28 MPa into disk-shaped specimens approximately 25 mm in diameter and 3 mm thick. A high-purity graphite die was used to minimize the introduction of metal ion impurities into the samples.[§] The specimens were then individually isostatically pressed to 280 MPa to further increase the green density and to remove density gradients due to uniaxial pressing. The final green density was approximately 57% of the theoretical density (ρ_{th} = 3.98 g/cm³). The specimens were then packed in loose powder of identical composition to the compacts, placed in high-purity alumina crucibles, and fired in air at 1600°C for 5 h using a MoSi₂ resistance furnace with a heating rate of 5°C/min and a cooling rate of 10°C/min. To increase the grain size, some specimens were given additional heat treatments at 1720°C for up to 48 h.

(2)   Characterization

Bulk density measurements were made on fired specimens using the Archimedes method with distilled water as the medium. To facilitate microstructural characterization, specimens were ground, polished to a 1-μm finish using a diamond slurry, and then thermally etched for 15 to 30 min approximately 50°C below the maximum sintering temperature. Optical and scanning electron photomicrographs were used to obtain grain size and grain aspect ratio measurements using a computer-assisted image analysis system (Image 1.45, National Institutes of Health, Bethesda, MD) by measuring the area, major axis, and minor axis of at least 500 grains. The grain size

was computed from the area assuming that each grain was spherical and the mean grain size was multiplied by 1.5 to correct for stereological effects. The aspect ratio was calculated from the ratio of the major axis to the minor axis, obtained from two-dimensional measurements.

(3)   Mechanical Testing

(A)   Strength: Strength measurements were made on disk-shaped specimens approximately 20 mm in diameter that were ground to a nominal 2.5-mm thickness, polished on the prospective tensile surface, and then fractured in biaxial tension according to ASTM standard F394-78 (flat on 3-ball technique).[20] Biaxial flexure disks were used in this study to eliminate possible edge effects. The tests were performed using an MTS servohydraulic testing machine (MTS 810, MTS Systems Corp., Minneapolis, MN) at a stressing rate of approximately 50 MPa/s. The thickness, the diameter, and the maximum load were measured for each specimen, from which the strength was calculated using standard thin-plate theory.

(B)   Flaw Tolerance: Vickers indentations were used to introduce controlled flaws into the polished surface of the specimens. Indentation loads were varied between 2 and 200 N and a drop of diffusion pump oil was placed on the indentation immediately following indentation to minimize the effects of moisture. In addition, some specimens were left unindented to determine the natural strength of the material. All indented specimens were examined using an optical or scanning electron microscope (SEM) following fracture to confirm that the failure originated from the indentation. Specimens where the crack intersected the indentation impression were assumed to have failed from the indentation. Only the data from those specimens that failed from the indentation were used in the analysis.

(C)   Strength versus Crack Size: In order to examine the effect of initial flaw size on strength, some specimens were annealed for 4 h at 1100°C to remove the residual stress field caused by the indentation. (The annealing time and temperature were determined from subsequent studies of strength and will be discussed further in Section III(2).) The maximum crack length after annealing was measured using optical microscopy. The shape of the indentation cracks was determined by viewing specimen fracture surfaces in a SEM and under oblique lighting conditions in an optical macroscope at low magnifications. A variation in the fracture surface morphology was clearly visible between the initial radial indentation crack and the fast fracture region. Surface crack lengths measured before fracture were found to correspond to the surface crack traces observed on the fracture surface.

(D)   Reliability: Because large changes in grain size most likely affect the intrinsic flaw population of the material, it was necessary to incorporate controlled flaws into the specimens to evaluate the influence of only the grain size on strength variability. This was accomplished by indenting the polished surface of specimens at each grain size using a constant indentation load. A minimum of 30 samples were fractured for each grain size and indentation load. Loads of 5 and 100 N were used in this study and were considered representative of small and large flaws, respectively. The strengths were then ranked and the probability of failure was calculated. A Gaussian distribution was assumed rather than the more traditional Weibull distribution because the variability in the strength-limiting flaw size tended to be normally distributed. (In fact, the strength data fit a Gaussian distribution exceptionally well, whereas a poor fit was obtained assuming either a two- or three-parameter Weibull distribution.) The probability of failure was estimated from

$$P_f = \frac{i - 0.5}{N} \tag{3}$$

where P_f is the probability of failure, *i* is the *i*th data point in the ranking, and *N* is the total number of strength values. By plotting the estimate of the probability of failure (in probability coordinates) vs the strength, the data are linearized and the magnitude of the slope is the standard deviation. The coefficient

---

of variation, defined as the ratio of the standard deviation to the mean strength, was used as a quantitative measure of the reliability and can be considered analogous to the more conventional Weibull modulus.

III. Results

(1) Characterization

SEM photomicrographs of polished and thermally etched samples are shown in Figs. 1(a–c). The densities of all of the materials were very high and ranged from 98.6% of the theoretical density for the fine-grained material to a maximum of 99.2% in the coarsest-grained material. The grain size distribution appears narrow and the grain shape appears equiaxed. (Note that the micrographs are at different magnifications to emphasize the self-similarity in microstructures.)

The grain size distributions are shown in Figs. 2(a–c). The mean grain size ($\bar{d}$) for the three materials was 5, 16, and 27 μm, respectively. In order to investigate how the distribution changed as the grain size was increased, the grain size was normalized by the mean grain size. It can be seen that little difference exists in the three distributions, indicating that the grain size distribution remained self-similar as the grain size was increased. Furthermore, the mean aspect ratio and the aspect ratio distribution remained constant as the grain size increased (Figs. 3(a–c)). The mean aspect ratio for all materials was

approximately 1.5, indicating that the grain shape was more or less equiaxed in all three materials.

(2) Mechanical Tests

Strength as a function of indentation load is shown in Figs. 4(a–c) for each of the three grain sizes. Each data point represents a minimum of five specimens and the error bars represent one standard deviation about the mean. The hatched region on the left portion of each graph represents the natural strength of the unindented material. The solid line represents the theoretical behavior of a material with a constant fracture toughness and has been shown by Lawn to have a slope of $-1/3$.[21] From the strength data it is apparent that the mean natural strength decreases as the grain size is increased, consistent with results in previous studies.[18] However, the dependence of strength on the indentation load and therefore the initial crack size is also reduced as the grain size is increased. This phenomenon is also consistent with the work of other investigators and is known in the literature as flaw tolerance.[5,21] Flaw tolerance has been attributed to the increasing degree of R-curve behavior as the grain size is increased.[21]

The probability of failure vs strength is plotted in Figs. 5 and 6. It is seen that at low indentation loads ($P = 5$ N), where the cracks are small, the fine-grained alumina had the highest mean strength and that as the grain size was increased the mean strength was reduced, consistent with the indentation strength data. More importantly, the strength variability as determined
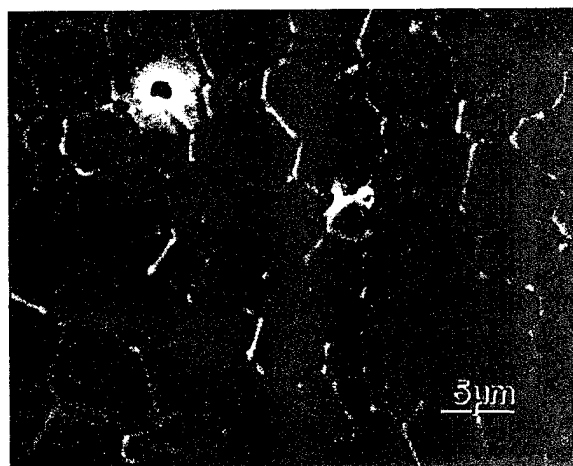
(a)
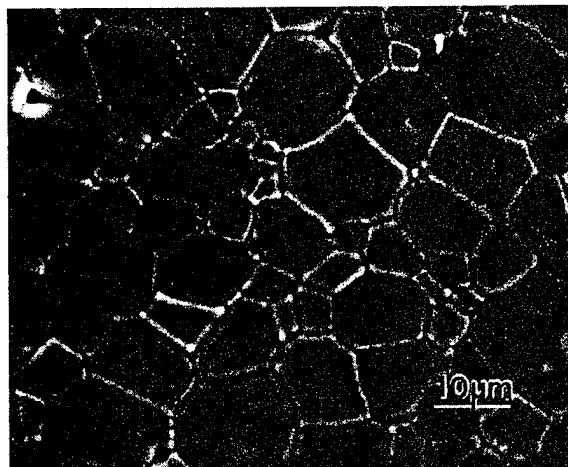
(b)
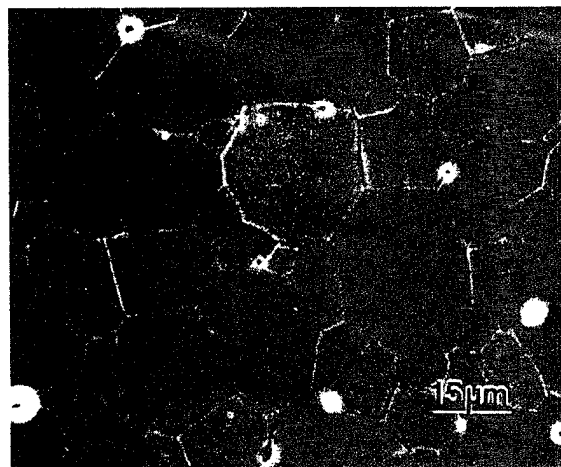
(c)

Fig. 1. SEM micrographs of polished and thermally etched specimens for alumina ceramics with an average grain size of (a) 5, (b) 16, and (c) 27 μm taken at different magnifications. Note the self-similarity between the materials and the high density and equiaxed morphology of the microstructures.

Fig. 2. Grain size distributions for each of the three aluminas shown in Fig. 1. The shape of the grain size distributions remain self-similar as the grain size is increased.
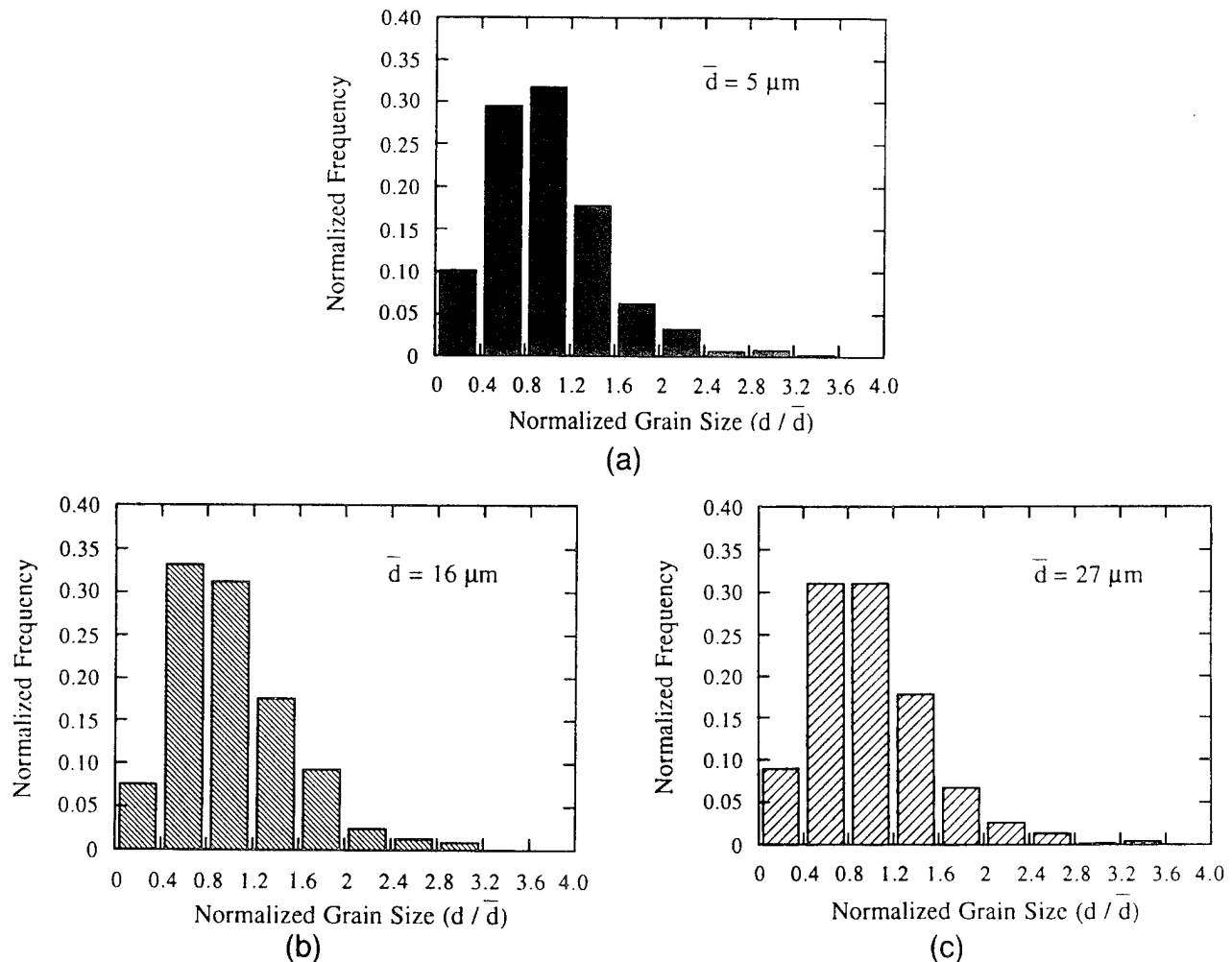
by the coefficient of variation (C_v) was similar in all three materials. The minor differences fall well within the 90% confidence limits and are not statistically different. *Thus at small indentation loads, coarse-grained alumina did not show an improvement in reliability compared to fine-grained alumina.*

At the higher indentation load ($P = 100$ N), where the indentation cracks were larger, the mean strength increased with increasing grain size, consistent with the flaw tolerance data. In general, all materials exhibited less variability in strength at this indentation load compared to the lower indentation load. However, in this case, the fine-grained material had slightly lower strength variability compared to the coarse-grained alumina although these values may not be statistically different. The mean strengths, standard deviations, and coefficients of variation for all three materials at both indentation loads are summarized in Table I.

Although controlled indentation flaws were used to evaluate the strength characteristics of our materials, indentation cracks were not necessarily equivalent in the aluminas with different grain sizes, even at the same indentation load. Optical photomicrographs of indentation cracks at indentation loads of 5 and 100 N are shown in Figs. 7(a–c) and 8(a–c), respectively, for the three aluminas. At a load of 5 N, indentation cracks in all three materials were very irregular. Radial cracking was not limited to the corners of the indentation impressions and crack lengths were highly variable. Nonetheless, the variability in the crack lengths, as measured by the coefficient of variation, was approximately equal for all three materials at low indentation loads. However, at an indentation load of 100 N, the indentation cracks in the fine-grained alumina were always well developed and indentation crack lengths showed little variability. In contrast, cracking was far more irregular and there was evidence of chip-out in the coarser aluminas. A small amount of lateral cracking was observed at all indentation loads but increased dramatically above 100 N in all three materials. A summary of the mean crack lengths, standard deviations, and coefficients of variation is presented in Table II.

In order to simulate natural flaws (i.e., processing flaws), some of the samples were indented and then annealed to remove the residual stress from the indentations using a technique similar to that used by Anderson and Braun.[22] This approach has the advantage that the stress intensity solutions for such a crack geometry are readily available, permitting a direct calculation of the fracture toughness as a function of crack size and crack geometry. A small amount of crack healing was observed during the annealing process but no discernible differences in crack

Table I.   Strength Statistics for Indented Specimens*

$\bar{d}$ (μm)	P (N)	σ (MPa)	C_v (%)
5	5	347 ± 38	10.9
16	5	324 ± 28	8.8
27	5	258 ± 28	9.3
5	100	143 ± 8	5.8
16	100	163 ± 13	8.1
27	100	166 ± 11	7.1

*At an indentation load of 5 N, the fine-grained material had the highest mean strength and the mean strength decreased with increasing grain size. The variability in strength at this indentation load was similar in all three aluminas. At an indentation load of 100 N the fine-grained material had the lowest mean strength and the strength increased with grain size. The variability in strength at this indentation load was slightly lower in the fine-grained alumina compared to the coarser-grained aluminas.
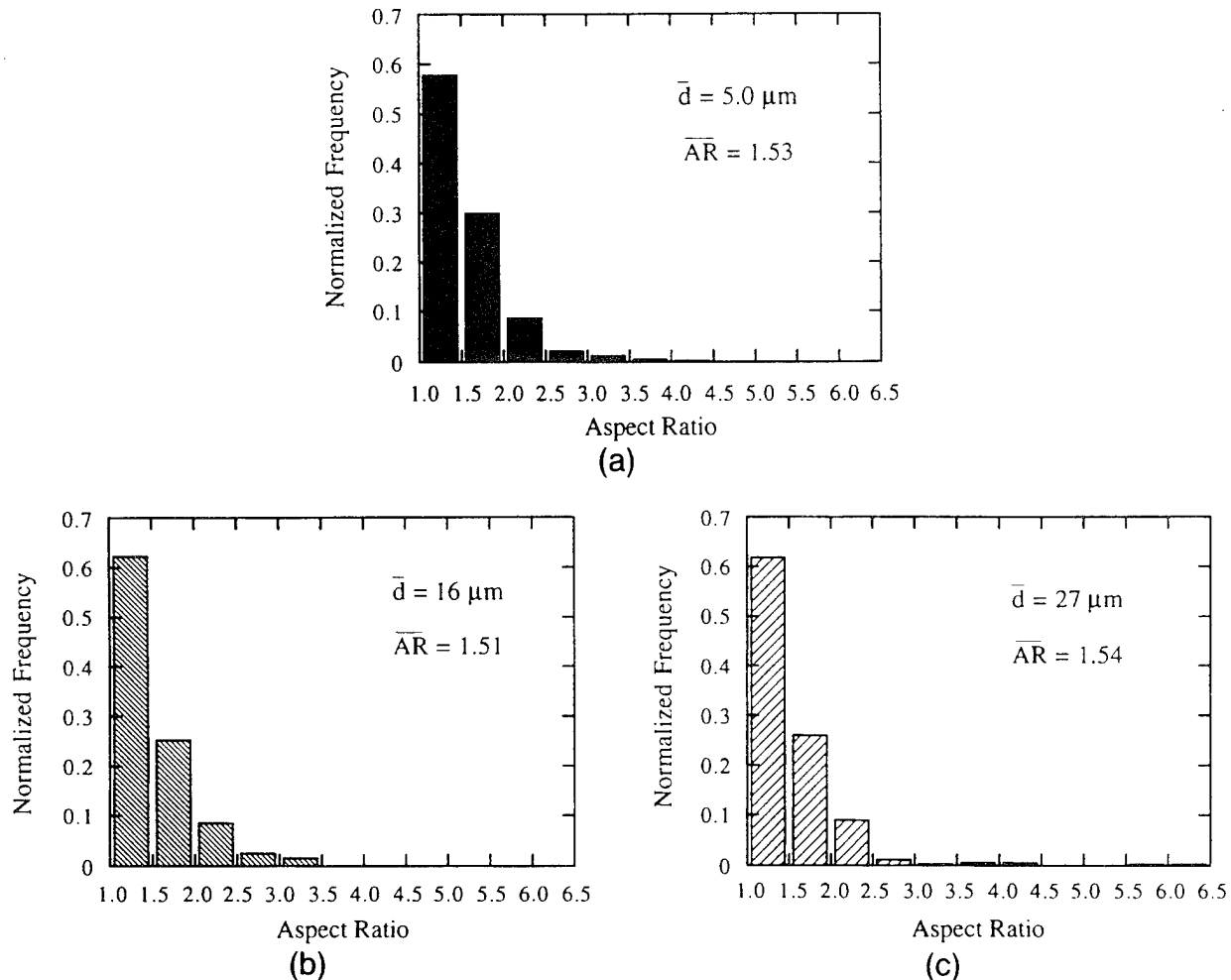
43

Fig. 3. Aspect ratio distributions for the aluminas with a grain size of (a) 5, (b) 16, and (c) 27 μm. The grain shape is nearly equiaxed and does not change as the grain size is increased.

Table II.   Indentation Crack Length*

$\bar{d}$ (μm)	P (N)	c (μm)	C_v (%)
5	5	22.4 ± 4.8	21.2
16	5	24.3 ± 4.5	18.5
27	5	28.9 ± 7.1	24.6
5	100	221 ± 11	5
16	100	191 ± 20	10
27	100	195 ± 24	13

*The mean crack size increases with increasing grain size at small indentation loads (5 N). More importantly the variability in the crack sizes, as measured by the coefficient of variation (C_v), is large and approximately equal in all three materials. At large indentation loads (100 N) the mean crack size is largest in the fine-grained material. The variability in the crack size at large indentation loads is smallest in the fine-grain material where the indentations are well formed.

Table III.   Indentation Crack Length after Annealing Treatment*

$\bar{d}$ (μm)	P (N)	c (μm)	C_v (%)
5	100	163 ± 15	9
27	100	188 ± 47	25

*A summary of indentation crack length data are shown for specimens that were indented at a load of 100 N and then annealed to remove the residual stress from the indentation. The variability in the crack size is much larger in the coarse-grained material.

healing behavior were observed as a function of grain size. A summary of these results is shown in Table III.

Fracture strength as a function of indentation crack size for *annealed* specimens is plotted (logarithmic coordinates) in Figs. 9(a,b) for fine- and coarse-grained materials, respectively.[†] The strength of the fine-grained material showed a

power-law dependence on the crack size with a slope of -0.47 and a small amount of scatter about this line. For an ideally brittle material with a constant fracture toughness, Griffith's law predicts a slope of -0.50. Evidence that the residual stress was removed can be seen by comparing the strength values at a given indentation load: the strength values following annealing were 40–45% higher than before annealing for the same indentation load. This compares favorably to the theoretical prediction of a 52% increase in strength following annealing.[21] Although some crack healing did occur during annealing, the amount of healing was generally quite small and could not account for the increase in strength.

The coarse-grained material showed little if any reduction in strength as a function of crack size, consistent with the notion of flaw tolerance. However, the scatter in the strength values about the mean was considerably larger in the coarse-grained material compared to the fine-grained material, indicating that no

[†]The range of indentation loads used in this test was lower than for that of the unannealed specimens. This is because failure from natural flaws began to predominate at indentation loads below 30 N. Moreover, lateral cracking became severe if indentation loads exceeded 100 N.
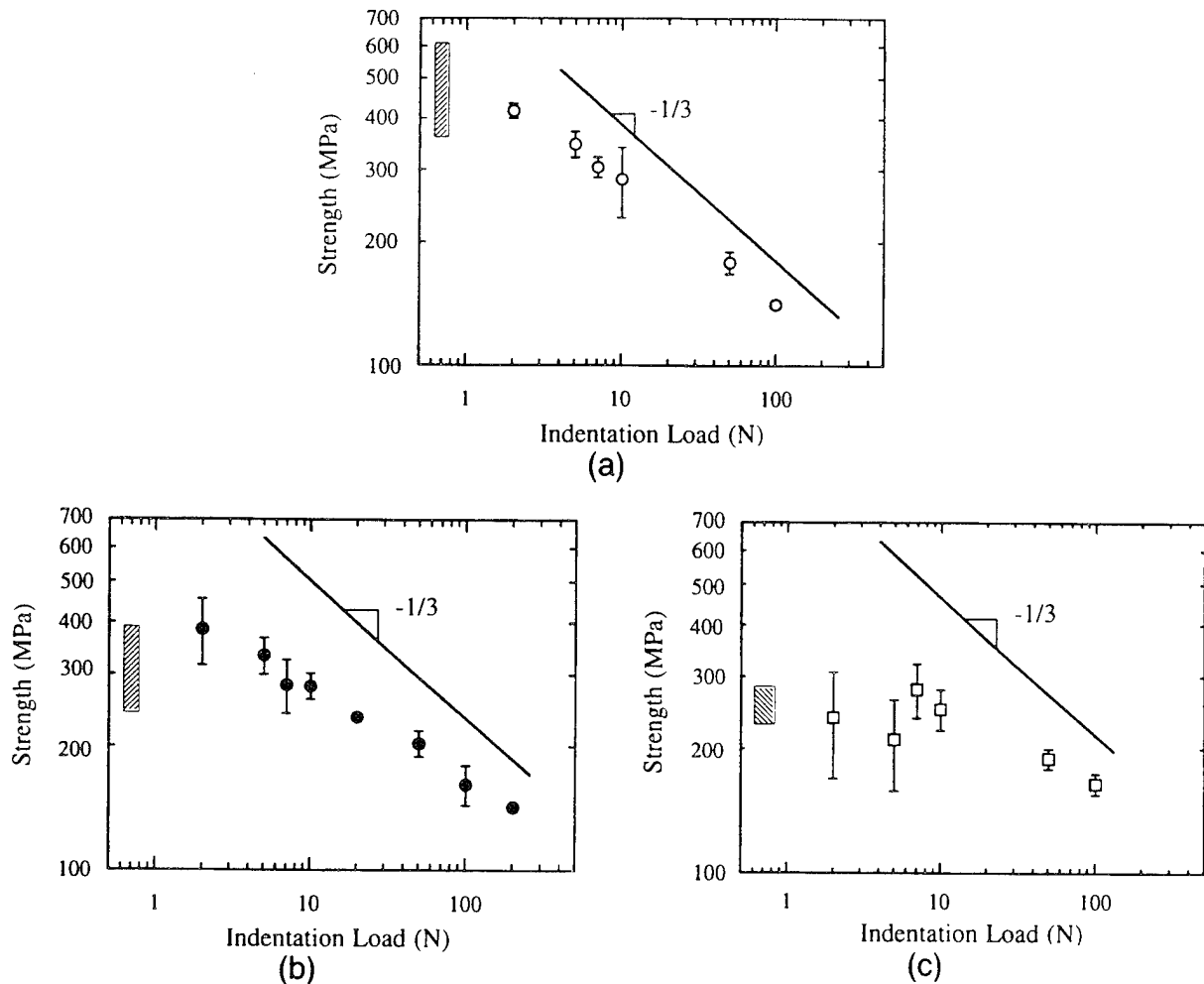
Fig. 4. Plots of strength vs indentation load for alumina with a grain size of (a) 5, (b) 16, and (c) 27 μm. The hatched region on the left portion of each graph represents the natural strength of the unindented material. The solid line represents the expected behavior for a material with a constant fracture toughness. It is seen that the natural strength of the fine-grained is highest and that the strength decreases with increasing grain size. However, flaw tolerance, as measured by the deviation from a $-1/3$ slope, increases with grain size.

improvement in reliability was found as the grain size was increased in annealed specimens.

IV. Discussion

The results of the strength tests on indented specimens indicate that increasing the grain size in alumina, although greatly enhancing the flaw tolerance, does not lead to a reduction in strength variability and hence an improvement in reliability. At small indentation loads, where the distribution in initial crack sizes produced by the indentations was approximately equal in all of the materials, no discernible difference in strength variability was measured. At large indentation loads where the initial crack size distribution in the fine-grained material was much narrower than in the coarse-grained material, the fine-grained material exhibited similar, if not lower, strength variability compared to the coarse-grained material. In addition, the strength variability in all three aluminas decreased significantly when the variability in the indentation crack size decreased (i.e., at large indentation loads). Therefore, the initial crack size distribution does appear to play at least some role in controlling the strength variability of alumina contrary to previous discussions of flaw tolerance. However, the differences in the variability in the indentation crack sizes themselves are clearly an indication that other microstructural factors also affect the strength variability.

To understand why no improvement in reliability was observed in coarse-grained alumina, the factors that control the strength variability must first be examined. We begin by considering the stress intensity at the tip of an indentation crack from the perspective of a global observer as the sum of two terms: (i) the stress intensity field, K_{app}, resulting from the far-field applied stress and (ii) the tensile residual field, K_{res}, resulting from the indentation.[21] Thus

$$K_{tot} = K_{app} + K_{res} \qquad (4)$$

where K_{app} and K_{res} are given by[21]

$$K_{app} = \sigma_{app} Y \sqrt{\pi c} \qquad (5)$$

$$K_{res} = \frac{\chi P}{c^{3/2}} \qquad (6)$$

where σ_{app} is the applied stress, Y is a crack geometry factor, c is the crack length, χ is the residual stress parameter associated with the indentation, and P is the indentation load. At fracture, $K_{tot} = T$ and $\sigma_{app} = \sigma_{fr}$ where T and σ_{fr} are the fracture toughness and strength of the material, respectively. (The fracture toughness is defined as the sum of the intrinsic fracture toughness, T_0, and any contribution from crack-tip shielding, T_μ.) Thus

$$\sigma_{app} = \frac{T}{Y\sqrt{\pi c}} - \frac{\chi P}{Y\sqrt{\pi c^2}} \qquad (7)$$

(Note that the strength of an indented material will always be less than an unindented material having the same crack size, but without the associated residual stress.) Experimentally, strength
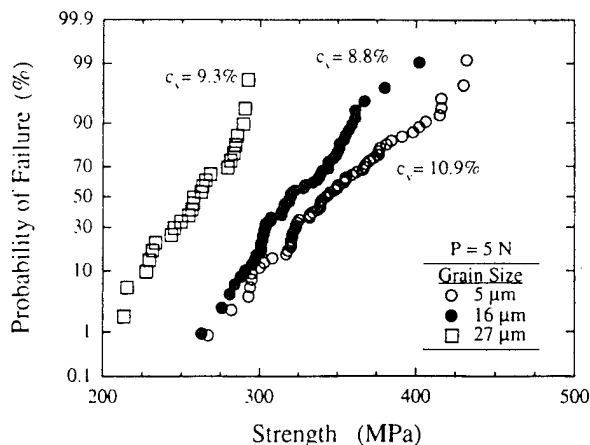
Fig. 5. Plot of probability of failure vs strength for samples that were polished and then indented with a Vickers indentor at a load of 5 N to introduce a controlled flaw. The fine-grained material has the highest mean strength and the coarsest material has the lowest mean strength. The variability in strength, as measured by the coefficient of variation (C_v), is similar in all materials.
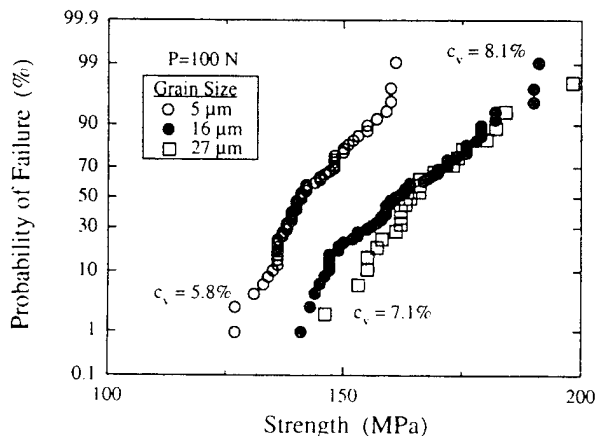

Fig. 6. Plot of probability of failure vs strength for samples that were polished and then indented with a Vickers indentor at an indentation load of 100 N. At this indentation load the fine-grained material has the lowest mean strength and the coarsest material has the highest mean strength. The variability in strength is slightly lower in the fine-grained material.

and crack length can be measured on individual specimens and the indentation load, P, is known. The crack geometry factor can be computed once the crack geometry is known. We cannot, however, measure or compute the fracture resistance *and* the residual stress parameter unambiguously, and thus we cannot identify with certainty the critical parameter that controls strength variability.

However, by removing the residual stress through annealing, the residual stress term in Eq. (7) is eliminated and the fracture stress is simply given by

$$\sigma_{fr} = \frac{T}{Y\sqrt{\pi c}} \qquad (8)$$

If we assume that the fracture toughness and the surface correction factor are constant, then the variability in strength is attributed solely to the variation in indentation flaw sizes. However, a simple statistical calculation shows that this only accounts for a fraction of the total variability in strength, indicating that the remaining variability in strength must be attributed to

(i) variability in Y, (ii) variability in T, or (iii) both (i) and (ii).[††] The surface correction factor can be computed directly from the depth and length of a crack.[24] For the materials used in this study, deviation from the half-penny value of $Y = 0.713$ was found to be minimal and variability in the geometrical parameter due to variability in the crack length to crack depth ratio was generally less than 5%. It was therefore assumed that the surface correction factor was a constant equal to the half-penny value in all specimens. *This suggests that the variability in fracture toughness is the primary source of strength variability in these alumina ceramics.* We now address this issue in more detail.

The fracture toughness of annealed specimens was calculated from the indentation crack size and the measured strength. The results are shown in Figs. 10(a,b) for the fine-grained material and the coarse-grained material, respectively.[‡‡] The fine-grained material had a mean fracture toughness of 3.8 MPa·m$^{1/2}$ with a standard deviation of 0.5 MPa·m$^{1/2}$ $(C_v = 13\%)$. The variability in fracture toughness appeared to remain fairly constant as a function of crack length, at least over the scale of crack sizes that were analyzed. The coarse-grained material had a lower mean toughness of 3.1 MPa·m$^{1/2}$ and a much larger standard deviation of 0.9 MPa·m$^{1/2}$ $(C_v = 29\%)$, more than twice the variability of the fine-grained material. While it is undoubtedly true that some of the variability in the fracture toughness was due to systematic experimental error in the measurement of crack length, load, and specimen dimensions, this error has been determined to be relatively small, and more importantly, is independent of grain size. The difference in variability in fracture toughness as a function of grain size is therefore attributed to a real material effect which will be discussed further below and in greater detail in a future paper.

(1) Effect of Variability of Fracture Resistance on Strength

The traditional explanation for the variability in strength in ceramics is that ceramics contain a distribution of strength-limiting flaws. From the Griffith criterion (Eq. (8)), it is apparent that a distribution in critical flaw sizes will cause a distribution in strength for a material with a constant fracture resistance. However, it is also possible that variability in strength may arise from variability in the fracture toughness. Consider a material that has a flat or non-rising R-curve but exhibits toughness variability due to microstructural influences, schematically shown in Fig. 11. (We will suggest the physical basis for the toughness variability in the following section.) Now consider that we superimpose the applied stress intensity as a function of the square root of crack length. Using the tangency construction as the failure criterion,[24] it can be seen that the strength will vary between σ_1 and σ_2, *even for materials having identical crack sizes.* In reality, materials do not contain a single flaw size but instead contain a distribution of flaws. The combined effect of variability in fracture toughness and a distribution in the critical flaw sizes is a further increase in the variability in strength, as illustrated in Fig. 12. Thus, there are two possible causes of variability in strength in a material with a constant fracture toughness, variability in fracture toughness itself as well as variability in initial crack size.[§§]

We now consider a material that has an increasing fracture toughness or R-curve, schematically illustrated in Fig. 13. It is apparent that even in a material with R-curve behavior, variability in the fracture toughness can result in variability in strength. However, as the R-curve becomes more pronounced, the variability in strength is reduced.[12,13]

[††]Errors in measurement of maximum applied load and the specimen dimensions account for only a few percent of the total variability in strength.

[‡‡]To calculate fracture toughness from annealed specimens, it was assumed that no stable crack extension occurred during fracture. While this is contrary to current theories about R-curve behavior, experimental evidence based on the short-crack R-curve behavior of alumina supports this assumption (see Appendix).[19] Further details and ramifications of this result will be discussed in a future paper.

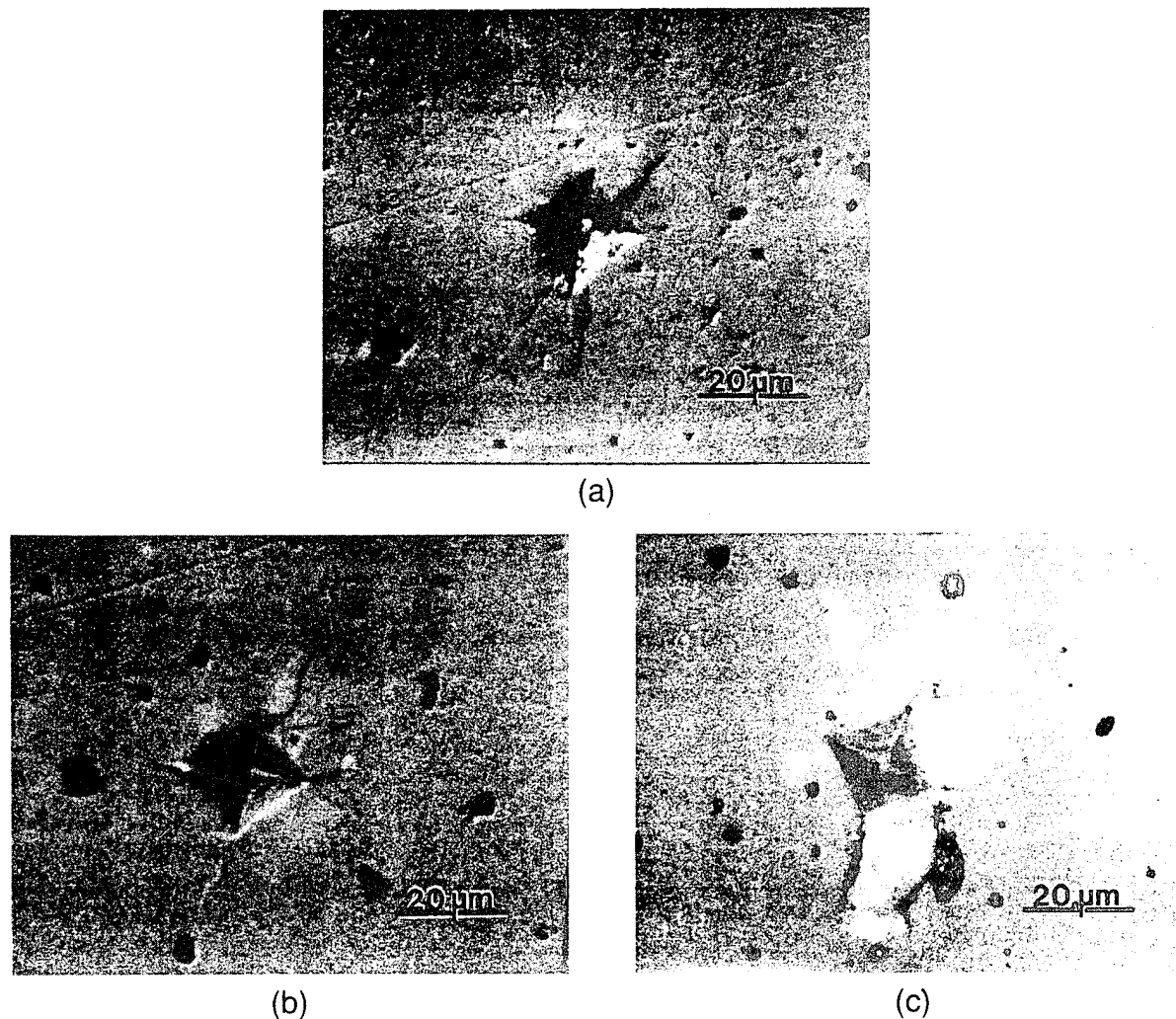[§§]Assuming a constant flaw geometry.

(a)

(b)

(c)

Fig. 7. Optical photomicrographs of samples with a grain size of (a) 5, (b) 16, and (c) 27 μm that were polished and then indented at loads of 5 N. All of the materials exhibit an irregular crack pattern and highly variable crack lengths.

(2) Microstructural Origins of Variability in Fracture Toughness

We now consider the microstructural origins of variability in fracture toughness in alumina ceramics. In this paper we suggest a physical basis for the existence of such variability. We begin by noting that in a grain-bridging material such as alumina, the fracture toughness is composed of three terms, the intrinsic fracture toughness, T_0, a term reflecting the residual stress distribution from thermal expansion anisotropy, T_{tea}, and the stabilizing field due to bridging, T_{br}:[17]

$$T = T_0 + T_{tea} + T_{br} \qquad (9)$$

The intrinsic toughness is often equated to the grain boundary toughness, as these materials fail primarily in an intergranular fashion, and is therefore considered a constant. T_{tea} results from the crack growing into a residual stress field resulting from crystallographic thermal expansion anisotropy. In the bridging model proposed by Bennison and Lawn, this term was only important during crack growth along the first grain facet. In reality, a propagating crack is subjected to a continually varying residual stress field owing to the random orientation of grains and, consequently, T_{tea} varies markedly during crack extension.

The distribution of residual stresses also contributes to variability in the bridging component of the toughness. For example, in the Bennison and Lawn model, the clamping stresses from the thermal expansion anisotropy are considered constant. In fact, the distribution of residual stresses will inevitably result

in a corresponding distribution of clamping stresses from one grain bridge to the next, giving rise to considerable variability in T_{br} during crack extension.[25]

Now consider the role of microstructure, namely the grain size, in the variability in fracture toughness. In fine-grained aluminas, T_{br} is small and can be neglected, implying a nearly R-curve, but with some degree of variability due to T_{tea} (Fig. 12). Increasing the grain size increases the bridging contribution to toughness, T_{br}, giving rise to pronounced R-curve behavior. However, the variability in T_{br} as well as T_{tea} also scales with microstructure. Thus, increasing the grain size results in R-curve behavior and flaw tolerance, but also introduces greater variability in fracture toughness, as schematically illustrated in Fig. 13.

Returning now to the experimental results, it was found that at small indentation loads, Vickers indentations produced cracks with similar morphologies (viz., irregular) and with approximately equal size distributions. However, there was no discernible difference in strength variability in any of the aluminas that were tested. Furthermore, the variability in the fracture toughness increased as the grain size was increased. Thus two competing effects appear to control reliability; increasing the grain size leads to a more pronounced R-curve and thus decreases the strength variability. However, at the same time, increasing the grain size also leads to greater variability in the fracture toughness, which increases the strength variability. These two effects essentially cancel each other, resulting in
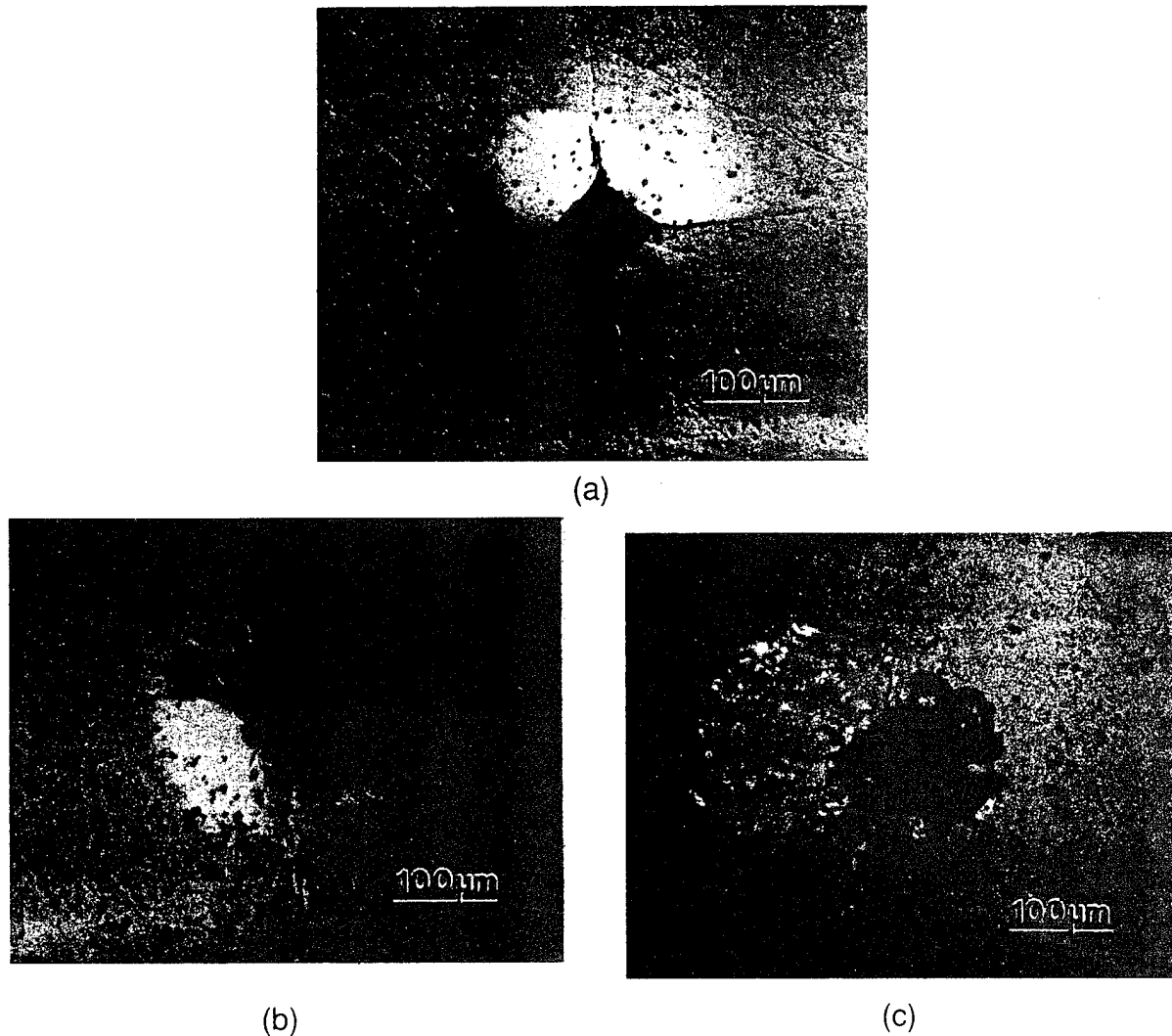
(a)

(b)

(c)

Fig. 8. Optical photomicrographs of samples with a grain size of (a) 5, (b) 16, and (c) 27 μm which were polished and then indented at loads of 100 N. Indentation cracks in the fine-grained material are well-developed and uniform. The coarser-grained materials, however, exhibit an irregular crack pattern and less uniform crack lengths.

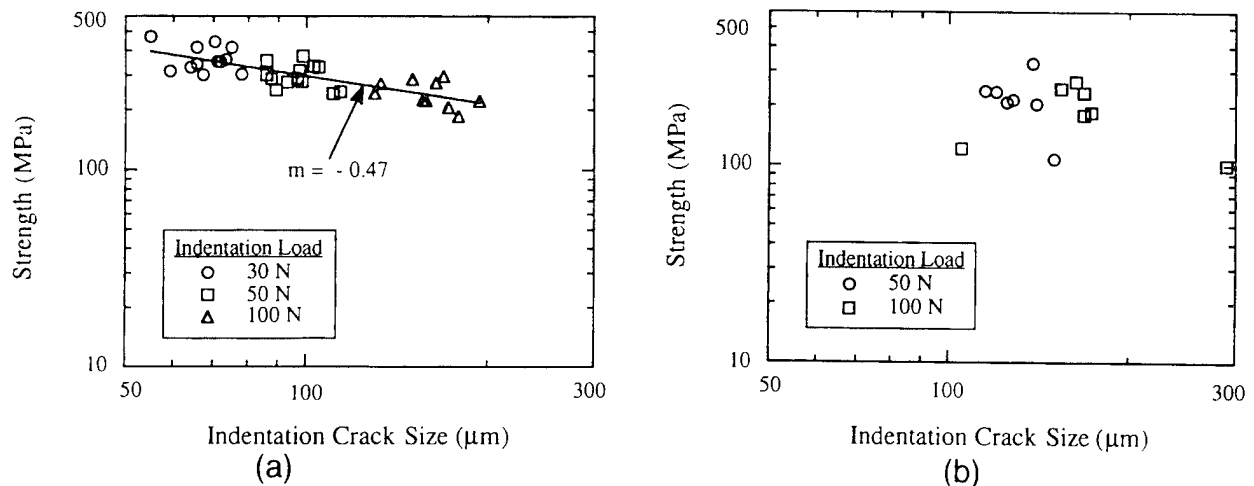
(a)

(b)

Fig. 9. Fracture strength as a function of indentation crack size at a grain size of (a) 5 and (b) 27 μm in specimens that were polished, indented, and then annealed to remove the residual stress from the indentation. The fine-grained alumina showed good agreement with Griffith's law and little scatter. In contrast, the scatter in strength in the coarse-grained was much larger.
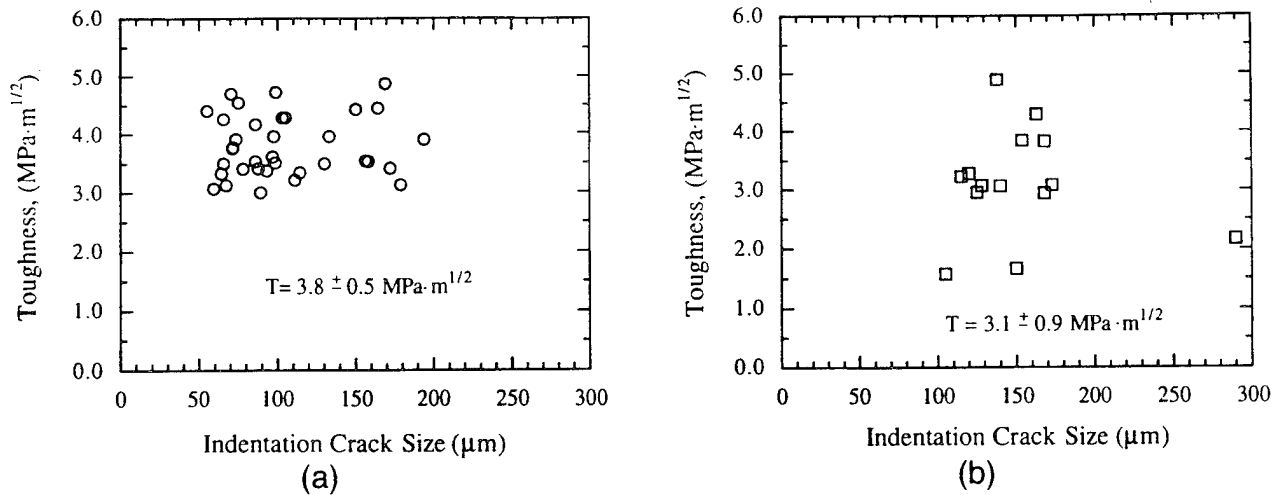
Fig. 10. Plots of short-crack fracture resistance vs indentation crack length for alumina with grain sizes of (a) 5 and (b) 27 μm determined from the strength of indented and annealed specimens. The fracture toughness of the fine-grained alumina is slightly higher and much less variable than that of the coarse-grained alumina.
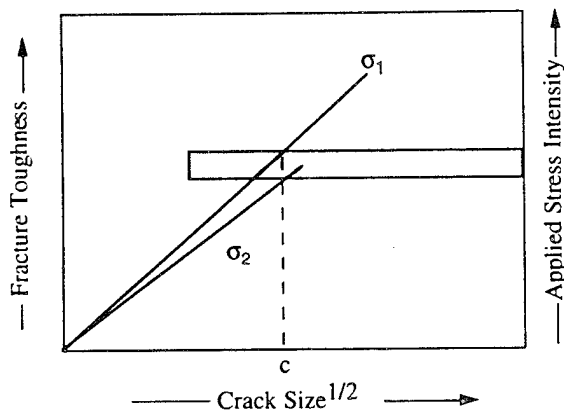

Fig. 11. Schematic illustration of fracture toughness vs the square root of crack length for a material with a flat R-curve but with variability in the fracture toughness. Variability in the fracture toughness leads to variability in strength, even at a constant critical flaw size.
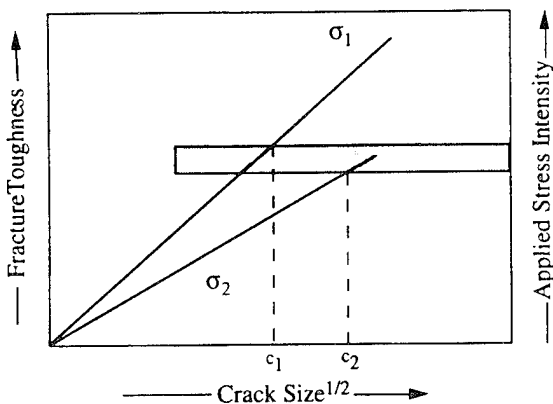

Fig. 12. Schematic illustration for a material with a flat R-curve and a distribution in critical flaw sizes. Both the variability in fracture toughness as well as the variability in the critical flaw size contribute to the variability in strength.
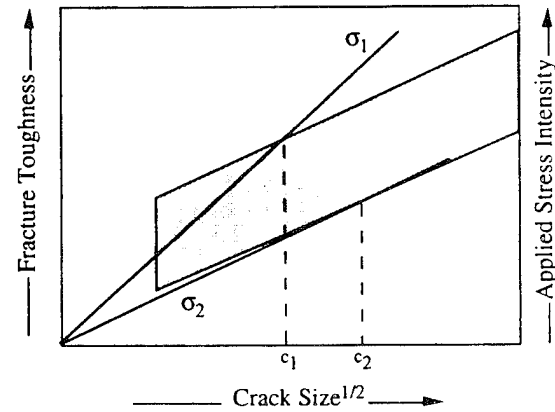
Fig. 13. Schematic plot of fracture toughness as a function of crack length for a material with a rising R-curve and variability in the R-curve. Although this material exhibits a pronounced R-curve and flaw tolerance, it does not show improved reliability compared to the fine-grained material due to variability in fracture toughness. Note that we must invoke greater variability in fracture toughness in the coarse-grained material to result in the same variability in strength as in the fine-grained material.

cracks appear irregular at small indentation loads but are well developed in the fine-grained material at large indentation loads (cracks are fairly irregular in the coarse alumina, even at high indentation loads). In the case of the fine-grained aluminas, the size of the indentation crack becomes large in comparison to the grain size at high indentation loads. In contrast, in the coarse-grained materials, even at high indentation loads, the size of the cracks is never more than 10 times the grain size. The variability in the crack size as well as the strength is lowest in the fine-grained alumina at large indentation loads. Either decreasing the indentation load or increasing the grain size leads to decreased reliability. Thus, in equiaxed, single-phase materials such as the alumina ceramics examined in this study, we surmise that the crack must be large in comparison to the grain size in order for the variability in the fracture toughness and hence the variability in strength to be small.

V.   Conclusions

It is possible to produce conventional ceramics with low strength variability by carefully processing the materials to control the initial flaw size distribution. The strength of these

little if any net result on the strength variability at small indentation loads.

The scale of the microstructure with respect to the initial flaw size also appears to affect the reliability of alumina. This can be seen in the micrographs of indentations in Figs. 7 and 8, where
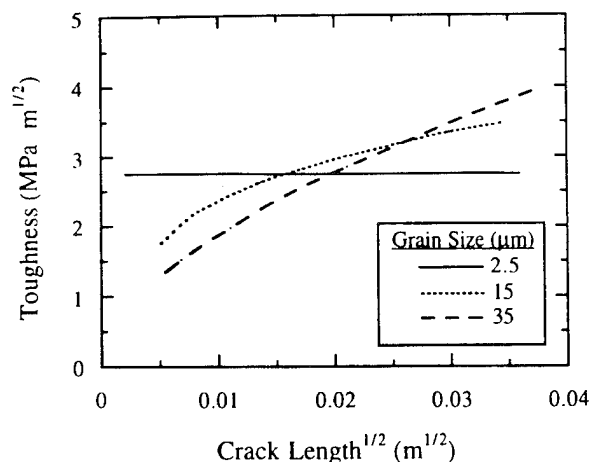
Fig. 14. Data after Braun *et al.* are plotted as toughness and a function of the square root of crack length for aluminas with a mean grain size of 2.5, 15, and 35 μm.[19] Using the graphical tangency construction, it is seen that no stable crack extension from natural flaws is predicted from these *R*-curves.

materials, however, is highly sensitive to damage introduced while in service. Hence a material that is highly reliable in the laboratory may not be reliable in engineering applications. One possible alternative to the flaw elimination approach is to design and process ceramic microstructures that exhibit *R*-curve behavior, thereby imparting the property of flaw tolerance.

The efficacy of this approach in achieving high reliability was investigated in this study using alumina as a model material. Alumina ceramics having different mean grain sizes but self-similar grain size distributions and grain shapes were examined for flaw tolerance and strength variability. While the flaw tolerance increased dramatically as a function of grain size, no improvement in reliability was found for equivalent flaw populations. In addition, the initial size distribution was found to play an important role in determining the strength variability contrary to current arguments of flaw tolerance. It was suggested that variability in fracture toughness strongly influences the variability in strength in alumina ceramics and that the variability in fracture toughness increases with grain size. Although flaw-tolerance becomes more pronounced with increasing grain size, the concomitant increase in the variability in fracture toughness offsets any improvement in reliability. This suggests that significant improvements in reliability owing to *R*-curve behavior will result when the microstructural features responsible for the increasing fracture toughness are small relative to the critical flaw sizes.

APPENDIX

Braun *et al.* have calculated the short-crack *R*-curves for aluminas with similar grain sizes to those used in this study.[19] Because the flaw tolerance plots (strength vs indentation load) for their materials are almost identical to those used in this study, we will assume that the *R*-curves are also similar. In Fig. 14, the data of Braun are replotted as fracture toughness vs the square root of crack length. It is seen that as the grain size is increased, the *R*-curves become more pronounced. However, upon applying the tangency construction, we predict that *none* of these materials would exhibit stable crack extension prior to fracture in the absence of a residual stress field. Thus, we believe that it is unlikely that stable crack extension takes place

in any of these materials when the failure origin is a natural processing defect or when the residual stress associated with an indentation is annealed away.

References

[1]D. B. Marshall, "Strength Characteristics of Transformation-Toughened Zirconia," *J. Am. Ceram. Soc.*, **69** [3] 173–80 (1986).

[2]C. W. Li and J. Yamanis, "Super Tough Silicon Nitride with *R*-curve Behavior," *Ceram. Eng. Sci. Proc.*, **10** [7–8] 632–45 (1989).

[3]N. Ramachandran and D. K. Shetty, "Rising Crack Growth Resistance Behavior of Toughened Alumina and Silicon Nitride," *J. Am. Ceram. Soc.*, **74** [10] 2634–41 (1991).

[4]P. F. Becher, "Microstructural Design of Toughened Ceramics," *J. Am. Ceram. Soc.*, **74** [2] 255–66 (1991).

[5]Y. W. Mai and B. R. Lawn, "Crack Stability and Toughness in Brittle Materials," *Annu. Rev. Mater. Sci.*, **16**, 415–39 (1986).

[6]K. Kendall, N. McN. Alford, and J. D. Birchall, "Weibull Modulus of Toughened Ceramics"; pp. 189–97 in *Materials Research Society Symposia Proceedings*, Vol. 78. Edited by P. F. Becher, M. V. Swain, and S. Somiya. Materials Research Society, Pittsburgh, PA, 1986.

[7]D. L. Hartsock and A. F. McLean, "What the Designer with Ceramics Needs," *Am. Ceram. Soc. Bull.*, **63** [2] 266–70 (1984).

[8]N. Ramachandran, L. Y. Chao, and D. K. Shetty, "*R*-curve Behavior and Flaw Insensitivity of Ce-TZP/Al₂O₃ Composite," *J. Am. Ceram. Soc.*, **76** [4] 961–69 (1993).

[9]B. Rogeeaux and P. Boch, "Influence of an Ultrasonic Assistance to Powder Compaction on the Weibull Modulus of Sintered Alumina," *J. Mater. Sci. Lett.*, **4**, 403–404 (1985).

[10]Y. Hamano, M. Yamaguchi, and S. Nagoano, "Sintered Silicon Carbide"; pp. 251–60 in *Ceramics for High Performance Applications III. Reliability.* Edited by E. M. Lenoe, R. Nathan Katz, and J. J. Burke. Plenum Press, New York, 1983.

[11]M. J. Readey, T. K. Brog, and J. Sibold, "Effect of Processing Method on the Weibull Modulus in Alumina Ceramics"; presented at the 92nd Annual Meeting of the American Ceramic Society, Dallas, TX, April 25, 1990 (Engineering Ceramics Division, Paper No. 70-C-90).

[12]K. Kendall, N. McN. Alford, S. R. Tan, and J. D. Birchall, "Influence of Toughness on the Weibull Modulus of Ceramic Bending Strength," *J. Mater. Res.*, **1** [1] 120–23 (1986).

[13]R. F. Cook and D. R. Clarke, "Fracture Stability, *R*-Curves and Strength Variability," *Acta Metall.*, **36** [3] 555–62 (1989).

[14]H. Hübner and W. Jillek, "Sub-Critical Crack Extension and Crack Resistance in Polycrystalline Alumina," *J. Mater. Sci.*, **12**, 117–25 (1977).

[15]R. Steinbrech, R. Knehans, and W. Schaarwächter, "Increase of Crack Resistance During Slow Crack Growth in Al₂O₃ Bend Specimens," *J. Mater. Sci.*, **18**, 265–70 (1983).

[16]R. F. Cook, B. R. Lawn, and C. J. Fairbanks, "Microstructure–Strength Properties in Ceramics: I, Effect of Crack Size on Toughness," *J. Am. Ceram. Soc.*, **68** [11] 604–15 (1985).

[17]S. J. Bennison and B. R. Lawn, "Role of Interfacial Grain-Bridging Sliding Friction in the Crack Resistance and Strength Properties of Nontransforming Ceramics," *Acta Metall.*, **37** [10] 2659–71 (1989).

[18]P. Chantikul, S. J. Bennison, and B. R. Lawn, "Role of Grain Size in the Strength and *R*-curve Properties of Alumina," *J. Am. Ceram. Soc.*, **73** [8] 2419–27 (1990).

[19]L. M. Braun, S. J. Bennison, and B. R. Lawn, "Objective Evaluation of Short-Crack Toughness Curves Using Indentation Flaws: Case Study on Alumina-Based Ceramics," *J. Am. Ceram. Soc.*, **75** [11] 3049–577 (1992).

[20]ASTM F394-78, "Biaxial Flexure Strength (Modulus of Rupture) of Ceramic Substrates"; pp. 422–26 in *ASTM Annual Book of Standards*, Vol. 15.02, Section 15. American Society for Testing and Materials, Philadelphia, PA, 1994.

[21]B. R. Lawn, *Fracture of Brittle Solids*, 2nd ed. Cambridge University Press, Cambridge, U.K., 1993.

[22]R. M. Anderson and L. M. Braun, "Technique for the *R*-curve Determination of Y-TZP Using Indentation Produced Flaws," *J. Am. Ceram. Soc.*, **73** [10] 3059–62 (1990).

[23]G. C. Sih, *Handbook of Stress Intensities*. Lehigh University Press, Bethlehem, PA, 1983.

[24]D. Broek, *Elementary Engineering Fracture Mechanics*, 4th ed.; pp. 202–208. Martinus Nijhoff Publishers, Dordrecht, Netherlands, 1986.

[25]B. R. Lawn, N. P. Padture, L. M. Braun, and S. J. Bennison, "Model for Toughness Curves in Two-Phase Ceramics: I, Basic Fracture Mechanics," *J. Am. Ceram. Soc.*, **76** (9) 2235–40 (1993).   □

50

APPENDIX 4

Effect of Glass Additions on the Indentation–Strength Behavior of Alumina

Heather L. O'Donnell,[†] Michael J. Readey,[*,‡,§] and Desiderio Kovar[*]

Department of Materials Science and Engineering, Carnegie Mellon University, Pittsburgh, Pennsylvania   212212

The effect of small calcium aluminosilicate (CAS) glass additions on the microstructure and flaw tolerance of alumina ceramics is investigated, and the results compared to a high-purity alumina. The high-purity alumina specimens were dense with microstructures consisting of a uniform grain size distribution and equiaxed grain morphology. Additions of only 1 wt% glass phase resulted in a bimodal grain size distribution containing large, elongated grains within a fine-grain matrix. Indentation–strength tests indicated enhanced flaw tolerance with the bimodal microstructure, even though both materials had nominally the same average grain size. The strength of unindented specimens was also observed to decrease with glass additions. Observations of crack paths show a greater propensity for bridging in the glass-containing alumina due to the presence of coarse, elongated grains and perhaps a lower grain boundary toughness. However, crack extension occurs transgranularly when the size of the coarsest grains becomes too large. This suggests that an optimum in flaw tolerance will be achieved with an elongated grain morphology and intermediate grain size.

I. Introduction

A LUMINA is perhaps the most widely used advanced ceramic today. Unfortunately, as with most ceramics, alumina is brittle and therefore prone to catastrophic failure. Several studies have indicated that the fracture toughness of alumina can be greatly enhanced by modifying the microstructure, in particular by increasing the grain size.[1,2] In nontransforming ceramics such as alumina, the dominant toughening mechanism is known as "grain bridging," where interlocking grains along the crack wake partially shield the crack tip from the applied stress. These materials also demonstrate pronounced crack resistance behavior, or R-curve behavior; the fracture toughness increases with crack extension due to the growing number of bridging grains. An important consequence of R-curve behavior in ceramics is flaw tolerance, meaning strength is insensitive to the initial flaw size. Indeed, it has been suggested that strength in these ceramics no longer follows conventional Griffith theory, but is controlled entirely by the shape and magnitude of the R-curve.[3] This property has far-reaching implications with

respect to the design of structural components, namely that the failure stress will be minimally affected by damage accumulated in service. Moreover, it suggests that the stringent processing conditions required for flaw elimination[4] may be somewhat relaxed.

The micromechanics of grain bridging have been extensively modeled by Bennison and Lawn[5] and account for those microstructural features responsible for R-curve behavior and flaw tolerance in nontransforming ceramics. Specifically, both the crack resistance and flaw tolerance become more pronounced with increasing grain size, as this increases the pullout distance prior to complete grain separation. Some of the first experimental evidence of flaw tolerance in alumina was provided by Cook and co-workers.[6] They measured the flaw tolerance of several commercially available materials and observed that the degree of flaw tolerance scaled with average grain size. Subsequent experimental efforts by Lawn and co-workers have been directed at fabricating more controlled microstructures in order to isolate the effect of grain size.[7–9] These results showed unequivocally that flaw tolerance increased with increasing grain size. More recently, Braun et al. demonstrated that this enhanced flaw tolerance was linked to stronger R-curve behavior in the coarser materials.[10] These results were also consistent with direct R-curve measurements conducted by Steinbrech and co-workers[11–13] and Vekinis et al.[14] in alumina ceramics having different average grain sizes.

While some studies have examined grain bridging in ceramics having a broad grain size distribution, notably the recent work by Hay and White,[15] many of the previous studies of flaw tolerance and fracture toughness in alumina ceramics have focused on microstructures consisting of uniform grain size distributions with equiaxed grain morphologies. Hence investigations isolating the effect of grain size distribution have heretofore not been explicitly attempted in alumina. Furthermore, the importance of grain shape has generally not been addressed experimentally, although it is now recognized that this is an important microstructural parameter in enhancing toughness, as demonstrated by whisker-reinforced composites and self-reinforced silicon nitride and silicon carbide.[16–18]

The objective of this study is to compare the flaw tolerance of two alumina-based ceramics, a high-purity alumina containing a uniform grain size distribution and an alumina containing a small amount of glass phase, which exhibits a bimodal microstructure consisting of coarse grains within a fine grain matrix. In particular we aim to compare the flaw tolerance of aluminas that are both nominally fine-grained, with similar *average* grain sizes. Moreover, because the microstructures of aluminas containing a glassy intergranular phase often consist of elongated grains, our study provides some insight into the role of grain shape on the flaw tolerance of alumina ceramics.

II. Experimental Procedure

(1) Material Processing

Previous research by the authors[19] has shown that alumina having a uniform grain size distribution and equiaxed grain

morphology can be fabricated from high-purity alumina powders. Kaysser *et al.* and Padture have both demonstrated that alumina having a bimodal microstructure can be formed by adding small amounts (~1%) of a calcium aluminosilicate (CAS) glass to high-purity alumina powders.[20,21] Furthermore, the large grains in the bimodal microstructure had elongated morphologies. Based on these studies, we synthesized two different alumina microstructures, one containing a uniform grain size distribution and an equiaxed grain morphology, and a second containing a bimodal grain size distribution consisting of large elongated grains. For convenience, we refer to these as "uniform" and "bimodal," respectively (although we recognize that microstructural changes other than grain size distribution can also occur with glass additions). Preparation and evaluation of the high-purity, uniform alumina is described in detail elsewhere.[19] For the bimodal microstructure, a calcium aluminosilicate (CAS) glass frit (SP1384, Specialty Glass, Oldsmar, FL) was first pulverized in ethanol using a mortar and pestle. The glass powder was then dry ball-milled with a high-purity alumina powder (AKP-50, Sumitomo Chemical America, New York) for 12 h using high-purity alumina media (99.5%).

Disk-shaped specimens were formed by uniaxially pressing the powders at 28 MPa (4 ksi) in a graphite die, followed by isostatic pressing at 280 MPa (40 ksi), resulting in specimens approximately 27 mm in diameter and 3 mm thick. The powder compacts were then sintered for specified times and temperatures to produce dense microstructures having nominally the same average grain size. The heating and cooling rates were maintained at 5°C/min. All heat-treatment details are included in Table I.

(2) Microstructural Characterization

The sintered densities of the aluminas were determined by Archimedes' method using water as the medium. The microstructures were examined by first grinding and polishing sintered samples to a 1 μm diamond finish using standard ceramographic techniques. A few of the polished samples were thermally etched at 1500°C for 30 min in order to reveal the grain boundaries. The microstructures of these samples were then analyzed using optical and scanning electron microscopy. The grain size distributions for the materials were determined by digitally scanning several representative SEM micrographs of thermally etched surfaces into a personal computer. A commercial software package (Image 1.45, National Institute of Health, Bethesda, MD) was then used to measure the grain area, and maximum and minimum diameters of at least 500 grains per microstructure. The equivalent spherical grain diameters were computed from the measured areas, assuming the grains were spherical. The average grain size was multiplied by 1.5 to account for stereological effects resulting from the two-dimensional measurements. The grain aspect ratio was determined from the ratio of the major to minor diameter of an ellipse fit to the grain shape.

(3) Flaw Tolerance and R-Curve Behavior

Flaw tolerance was investigated using the indentation–strength test.[5,6] Thirty biaxial flexure specimens approximately 22 mm in diameter were ground to a uniform thickness of 2 mm, and the prospective tensile surface polished to a 1 μm diamond finish. A Vickers diamond microhardness indentation was then placed at the center of each specimen, using loads between 2 and 100 N. A drop of silicone oil was placed on the indent to minimize further crack growth due to environmental effects. The specimens were then rapidly loaded to failure

(~250 MPa·s⁻¹) in biaxial flexure (flat-on-3 ball configuration, ASTM F 394-78), with the indented surface as the tensile surface. The load was monitored with an on-line data acquisition system; the maximum load at failure was used to determine the strength. Strength was calculated from equations of linear elasticity for thin plates.[22] All specimens were subsequently checked to ensure that failure occurred from the indent. Those that did not fail from the indent were excluded from the analysis. At least three specimens were used at each indentation load. In addition, several *un*indented specimens were fractured to determine the "natural" strength of the aluminas.

Toughness curves were determined from the indentation-strength data using the technique proposed by Braun *et al.*[10] As our high-purity alumina is similar to that used in the Braun study, we have used their calibrated values for ψ and χ, terms reflecting the shape of the indentation crack, specimen geometry, and the residual stress associated with the elastic/plastic response of the alumina under the contact indentor, respectively. We have assumed that these values are also valid for the glass-containing alumina.[††]

III. Results

(1) Microstructural Analysis

SEM micrographs of polished and thermally etched surfaces of the pure and glass-containing aluminas are shown in Figs. 1(a) and (b), respectively (note the different magnifications). For the pure alumina, the microstructure consists of small, equiaxed grains approximately 5 μm in diameter. The grain size distribution also appears relatively uniform. The microstructure of the glass-containing alumina is dramatically different, as shown in Fig. 1(b). The microstructure in these samples is bimodal, consisting of large (up to 50 μm in length), elongated grains within a fine-grain matrix. The measured densities of the two aluminas are comparable: 3.91 g/cm³ for the pure alumina and 3.88 g/cm³ for the glass-containing alumina. Physical property data are summarized in Table II. A few isolated pores are located at grain boundaries in the pure alumina. The glass-containing alumina tended to have somewhat larger pores, possibly associated with inadequate mixing of the alumina powder and glass frit. Some intragranular porosity is also visible in the larger, elongated grains.

The grain size distributions for the two materials are shown in Figs. 2(a) and (b). The distribution for the pure alumina appears lognormal, with a slight tail extending to larger grain sizes (Fig. 2(a)). The average grain size measured 5.0 ± 2.8 μm. No grains larger than 18 μm were observed. The distribution for the glass-containing alumina is similar, except that a greater number of grains are clustered around a smaller grain size of about 1.5 μm. The distribution also appears lognormal, with a tail extending to larger grain sizes. The average grain size measured 3.4 ± 3.5 μm; a few grains were as large as 30 μm. The similarity in the distributions for the pure and

---

[††] In addition, we have implicitly assumed that Ψ and χ are invariant with indentation load and crack length. Smith and Scattergood[23] and more recently Dransmann *et al.*[24] have demonstrated that Ψ and χ in fact change slightly as a function of load and crack length, leading to shallower *R*-curves. These changes were not accounted for in the present study, due to the difficulty in measuring indentation crack depths on fracture surfaces. We therefore recognize that the calculated *R*-curves most likely overestimate the toughness and degree of *R*-curve behavior exhibited by the pure and glass-containing aluminas.

Table I. Sintering Schedules for Alumina Ceramics

Alumina	Starting powder	Sintering temperature (°C)	Sintering time (h)
Uniform	High-purity alumina*	1600	5
Bimodal	High-purity alumina* + 1 wt% CAS glass frit†	1590	5

*AKP-50, Sumitomo Chemical America, New York. †SP1384, Specialty Glass, Oldsmar, FL.
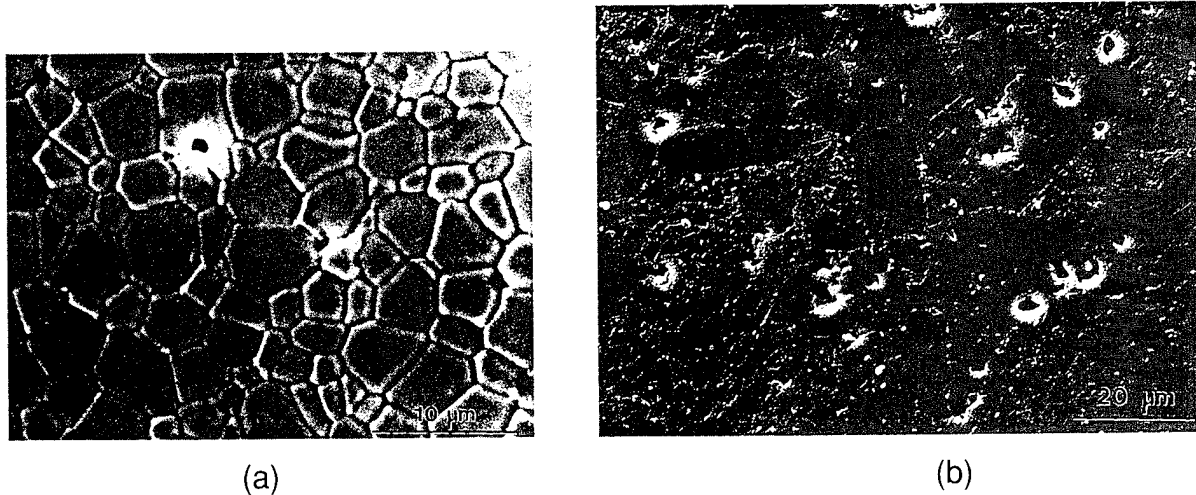
Fig. 1. Scanning electron micrographs of polished and thermally etched surfaces: (a) pure alumina showing uniform grain size distribution and equiaxed grain morphology; (b) glass-containing alumina with bimodal grain size distribution consisting of coarse, elongated grains within a fine-grain matrix. Note the difference in magnifications.

Table II. Physical Properties of Alumina Ceramics

Alumina	Sintered density (g/cm³)	Grain size, d (μm)	Maximum grain size, d_{max} (μm)	Aspect ratio, AR_{ave}
Uniform	3.91 ± 0.02	5.0 ± 2.8	12	1.53
Bimodal	3.88 ± 0.02	3.4 ± 3.5	20	1.96

glass-containing aluminas is somewhat surprising, given the obvious differences in microstructure. In fact, the glass-containing alumina has a slightly smaller average grain size compared to the pure alumina.

In order to better illustrate the uniform and bimodal nature of the two microstructures, the grain size distributions are replotted in Figs. 3(a) and (b) in coordinates of area fraction versus grain size. This method plots the cumulative area of all grains falling within a specified size interval relative to the total area of all grains measured. This takes into account the fact that the large grains tend to be few in number, but represent a significant fraction of total area measured. As shown in Figs. 3(a) and (b), the uniform and bimodal nature of the grain size distributions can be clearly seen in this representation; the pure alumina

shows a relatively uniform distribution, whereas the glass-containing alumina shows the large grains present in the microstructure (nearly 30% by area).

The aspect ratio distributions for the two aluminas are shown in Figs. 4(a) and (b). The distributions are also lognormal, with a long tail extending towards higher aspect ratios. The average aspect ratio for the pure alumina is 1.53, indicating that the grain morphology is relatively equiaxed. The aspect ratio of the glass-containing alumina increases to 1.96, confirming that on average the grains have developed a more elongated morphology, consistent with observations from Fig. 1.

(2) Indentation–Strength and Toughness

The indentation–strength data are shown in Figs. 5(a) and (b) for the uniform (pure) and bimodal (glass-containing) alumina,
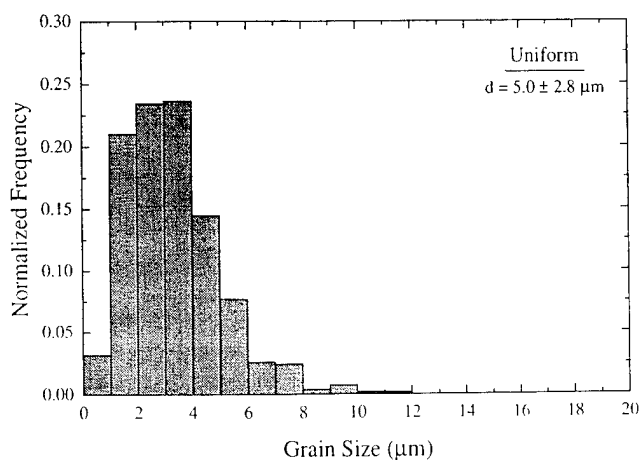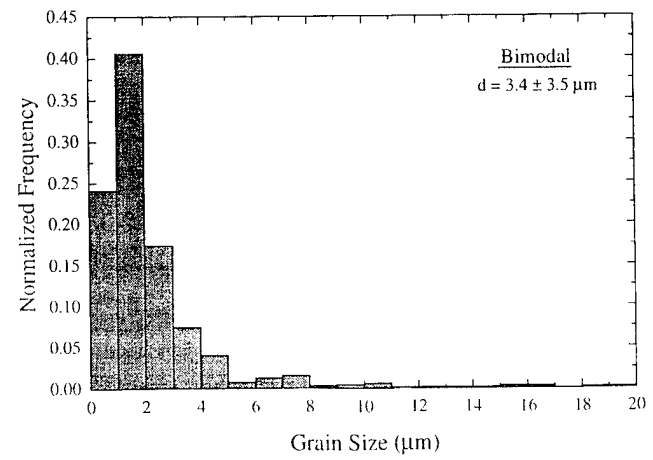
Fig. 2. Grain size distributions for (a) pure alumina, and (b) glass-containing alumina.

Fig. 3. Grain size distributions replotted in terms of area fraction. (a) Pure alumina showing relatively uniform distribution, and (b) glass-containing alumina showing presence of coarse grains.
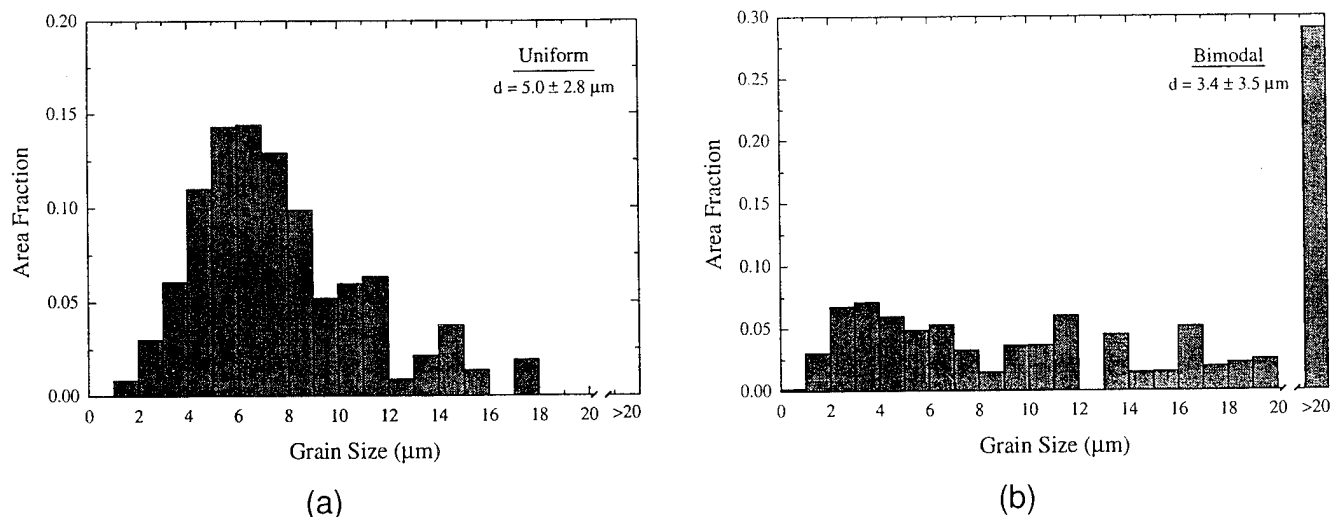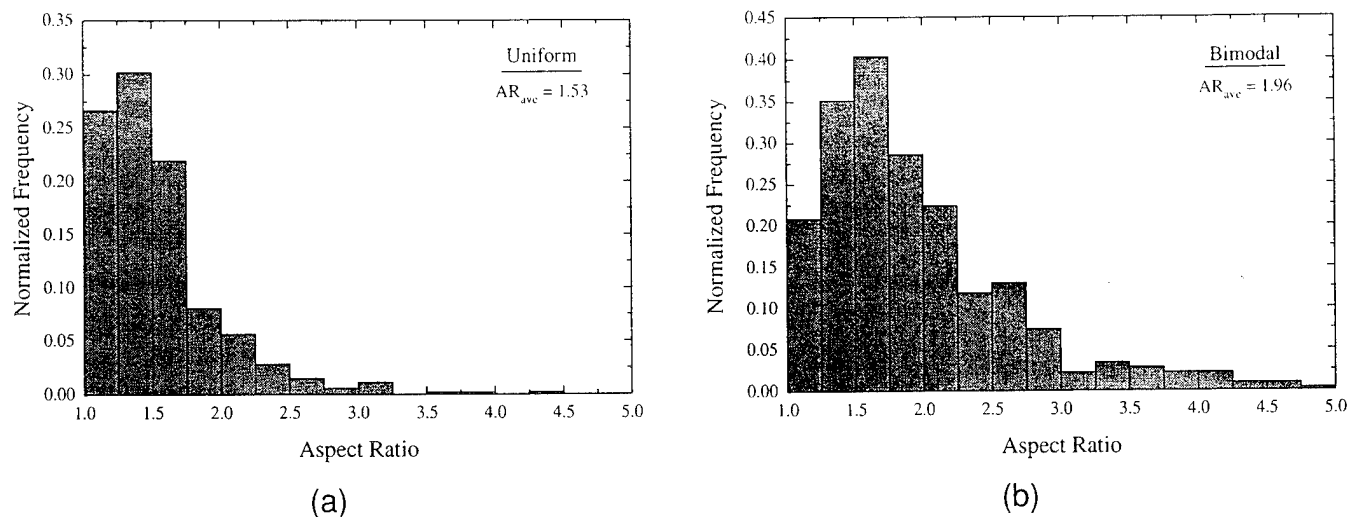

Fig. 4. Aspect ratio distributions for (a) pure alumina showing nearly equiaxed grain morphology, and (b) glass-containing alumina showing a more elongated grain morphology.

respectively. The strength of the uniform alumina decreases sharply with increasing indentation load, following a linear relationship with a slope close to $-1/3$, indicating a single-value fracture toughness and little or no flaw tolerance.[25] The strength of the bimodal alumina departs from this linear behavior (Fig. 5(b)), decreasing only modestly over the entire range of indentation load, indicating enhanced flaw tolerance. For comparison, we have also plotted the data from the study by Chantikul et al.[8] for an equiaxed, high-purity alumina having an average grain size of 21 μm. Note that in spite of an average grain size of ~4 μm, the bimodal alumina in this study has the flaw tolerance of a much coarser alumina.

The *un*indented strength of the uniform alumina is almost twice that of the bimodal alumina. However, at high indentation loads, the strength of the uniform alumina was *lower* than the bimodal alumina. This is consistent with other investigators,[8] who also observed a cross-over in the indentation–strength responses when comparing alumina ceramics with a single-valued fracture toughness and pronounced *R*-curve behavior.

Toughness curves obtained from the indentation–strength data are shown in Fig. 6 for the uniform and bimodal aluminas. For the uniform microstructure, the initial toughness is ~2.5 MPa·m$^{1/2}$ and increases quickly to a plateau toughness near 3 MPa·m$^{1/2}$ in approximately 200 μm of crack extension. In contrast, the bimodal alumina has an initial toughness of ~2.2

MPa·m$^{1/2}$ and increases more slowly to about 3.7 MPa·m$^{1/2}$ over nearly a millimeter of crack extension. Moreover, the plateau toughness is not yet attained in the bimodal alumina, indicating even higher toughness values may be achieved with extended crack growth. Considering that the two materials have the same average grain size, the presence of coarser, elongated grains and the glassy grain boundary phase contribute significantly to the rising *R*-curve and higher plateau toughness.

(3) Fracture Mode

The fracture surfaces of the uniform and bimodal aluminas are shown in Figs. 7(a) and (b), respectively. The uniform alumina with the equiaxed microstructure failed in a predominantly intergranular fashion, whereas the bimodal alumina failed in both an intergranular and transgranular mode. Some of the larger, elongated grains in the bimodal alumina failed by transgranular fracture (denoted "T" in the figure), whereas the surrounding fine-grained matrix failed intergranularly (denoted "I" in the figure).

Typical crack paths in the bimodal aluminas are shown in Figs. 8(a) and (b). Mixed-mode fracture can be readily observed (Fig. 8(a)); the crack propagated in an intergranular fashion through the fine-grain matrix, but also around some of the larger, elongated grains. Several grain bridges can also be observed (the arrowed features in the figure). Figure 8(b) shows
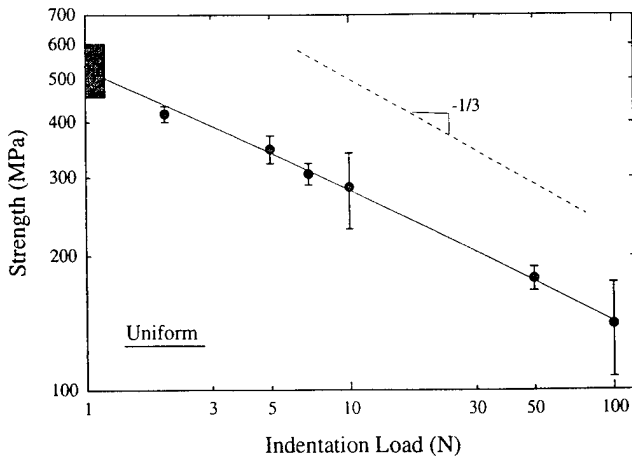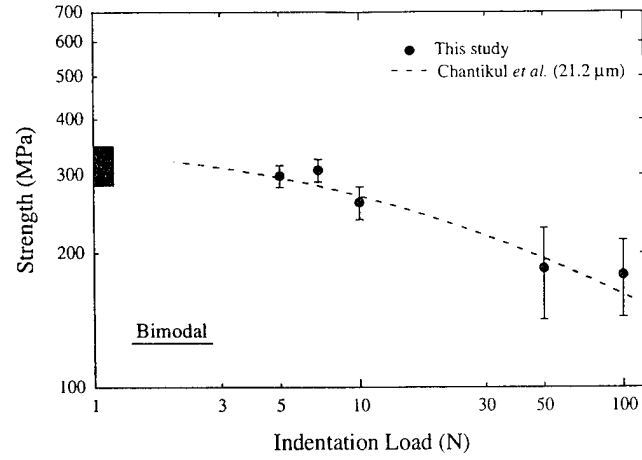
(a)   (b)

Fig. 5. Indentation-strength data for (a) uniform and (b) bimodal alumina. The uniform alumina shows near linear behavior, whereas the bimodal alumina deviates markedly from linearity, indicative of stronger R-curve behavior. The natural strength of the uniform alumina is also greater than the glass-containing alumina (the hatched boxes).

Fig. 6. R-curves derived from the indentation-strength data. The toughness of the uniform alumina rises quickly to the plateau value of approximately 3 MPa·m$^{1/2}$. The fracture toug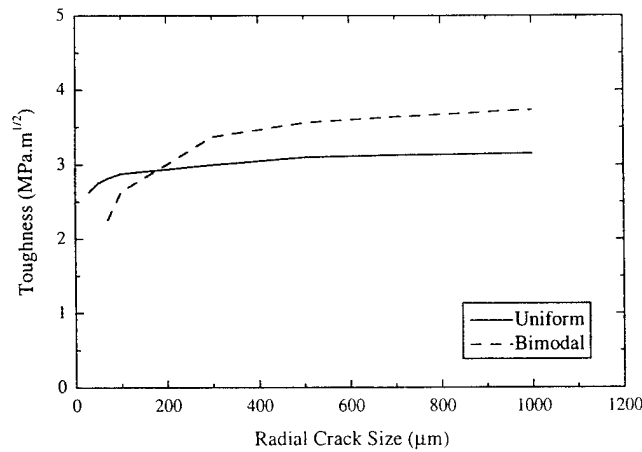hness of the bimodal alumina begins at a slightly lower value, and increases more slowly to a higher toughness of 3.7 MPa·m$^{1/2}$.

both intergranular and transgranular fracture. Transgranular fracture predominates whenever the grain size is too large, or whenever the crack trajectory is more or less normal to a major grain facet (in particular the long edge of the grain). Many cases were observed where large alumina grains fractured in a transgranular fashion by small cleavage steps ("T" in Fig. 8(b)). Elastic bridges were also commonly observed, particularly when cracks would propagate across a grain, arrest, and then reinitiate at some remote grain boundary ("B" in Fig. 8(b)).

IV. Discussion

(1) Microstructure

The presence of a small amount of glass phase had a significant influence on grain size distribution and grain shape. The pure alumina had an equiaxed microstructure, whereas the alumina containing only 1 wt% of a glass phase resulted in a considerable fraction of large, elongated grains, even for comparable processing times. The effect of CAS glass additions on microstructure development in alumina was studied in detail by Kaysser and co-workers.[20] These investigators observed microstructures consisting of predominantly coarse grains apparently resulting from discontinuous grain growth. In comparison, the

(a)   (b)

**Fig. 7.** SEM micrographs of fracture surfaces: (a) uniform alumina, and (b) bimodal alumina. The fine-grained, equiaxed alumina failed in a predominantly intergranular fashion, whereas the bimodal structures showed mixed mode fracture, with transgranular fracture occurring in some of the larger grains. "T" denotes regions of transgranular fracture; "I" denotes regions of intergranular fracture.
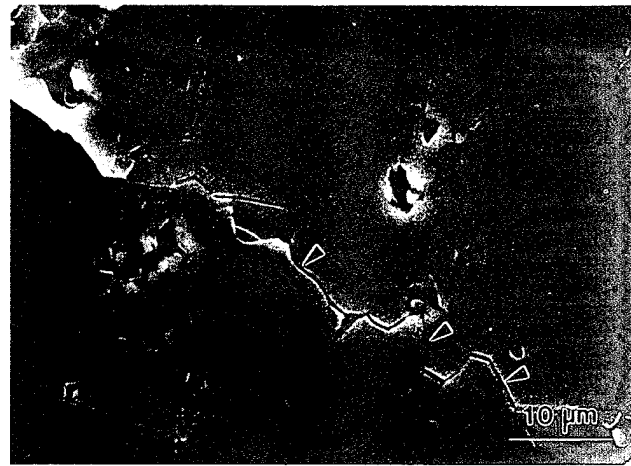
(a)
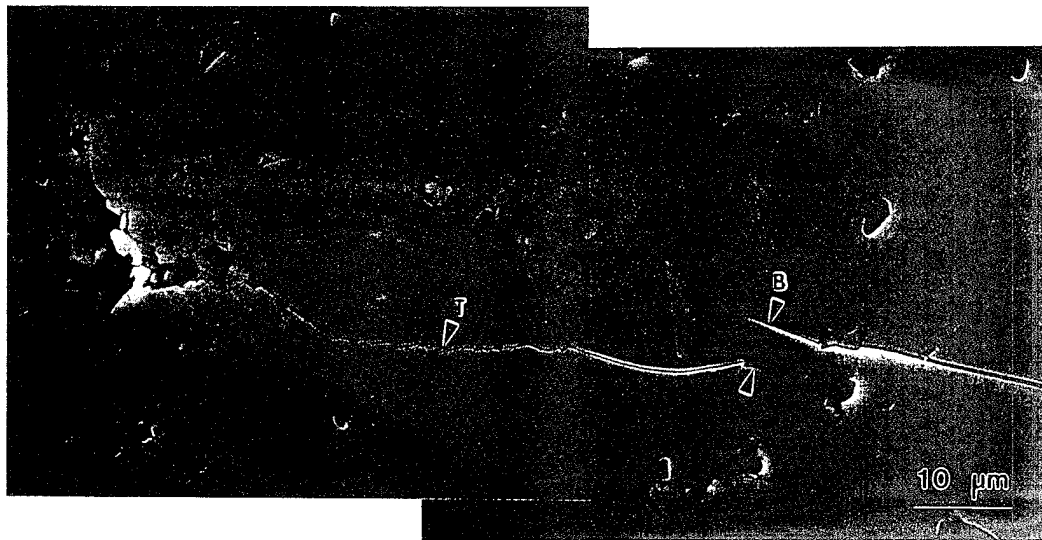
(b)

Fig. 8. SEM micrographs of typical crack paths in bimodal alumina. (a) Coarse grains tend to promote bridge formation (the arrowed features). (b) Grains that are too large tend to fail in a transgranular fashion, often by cleavage ("T"). Elastic bridges are also commonly observed ("B"). Secondary cracks are occasionally observed in bridging grains (the arrowed feature).

microstructure in the glass-containing alumina produced in this study was much more bimodal. The smaller fraction of large grains suggests that our materials are at the early stages of discontinuous grain growth and that prolonged heating at elevated temperatures would most likely continue growth of the coarse grains at the expense of the finer grains in the matrix until eventually the entire microstructure consists of larger grains, as observed by Kaysser.

The existence of coarse, faceted grains is also a common feature during grain growth in the presence of a liquid phase. Faceting is known to result from either a solution–reprecipitation process or simple enhanced diffusion through the liquid phase. In either case, a low-energy equilibrium grain structure is formed; i.e., the long edges of the faceted grains are usually perpendicular to ⟨0001⟩ directions corresponding to low-energy (0001) boundaries.[26] Discontinuous grain growth in the presence of a liquid phase is not well understood, but is believed to be due primarily to a combination of two effects. One, the liquid is unable to wet all boundaries due to interfacial energy arguments,[27] thus allowing some grains to grow faster than others due to enhanced diffusion through the liquid phase. Second, larger than average grains, when combined with the fast diffusion path provided by the wetting liquid phase, act as potent nucleation sites for rapid growth of an abnormal grain.[28] (Note, however, that in alumina growth of abnormal grains is

anisotropic; growth of the low-energy (001) boundaries is much slower than the other higher energy boundaries.[20])

(2) Flaw Tolerance and R-Curve Behavior

The strength–indentation response of the equiaxed alumina is consistent with previous studies conducted by Lawn and coworkers. Fine-grained alumina shows the near ideal $-1/3$ slope on a strength–indentation load plot, indicating a single-value fracture toughness. This is also consistent with other investigators who have determined that the fracture toughness for fine-grain alumina is nearly constant with increasing crack extension. However, despite the similarity in *average* grain size, the strength in the bimodal microstructure is less sensitive to the increasing size of the indentation flaws, suggesting a stronger crack resistance curve, consistent with the calculated R-curves. These results are also in agreement with the recent work of Padture.[21] Moreover, it is clear from observations of surface crack traces that this enhanced flaw tolerance is due largely to grain bridging of the coarse, elongated grains in the microstructure. The fine grains in the matrix (which are actually smaller than the uniform microstructure) play little to no role in the bridging process; we observed many more active bridging sites with the bimodal microstructure.

It is important to note that any fracture process that involves intergranular fracture must also involve the grain boundary

fracture toughness. In comparing the flaw tolerance of our uniform and bimodal alumina, we have ignored the role of grain boundary fracture toughness, and hence the propensity for cracks to propagate along grain boundaries. For example, assuming that the CAS glass wets some fraction of grain boundaries, then the fracture toughness of such an interphase boundary should not be equal to that of a grain boundary devoid of a siliceous phase. Nonetheless, both aluminas propagate in a primarily intergranular fashion (with the exception of some extremely coarse grains that fracture in a transgranular mode), suggesting that the grain boundary toughnesses are less than the intrinsic toughness of alumina (sapphire). While it has been suggested that the grain boundary toughness in debased aluminas plays a secondary role to the bridging grain size,[29] we recognize that the grain boundary toughness for the glass-containing alumina is probably lower than that for the pure alumina, thereby promoting intergranular fracture and thus potentially enhancing the toughness by increasing the number of active bridging sites. Ideally, we would like to isolate the effect of grain size distribution in high-purity alumina, thereby allowing us to compare directly materials with equivalent grain boundary toughnesses. Currently we are studying the fracture properties of such microstructures processed by controlling processing conditions. Our results will be reported in a future paper.[30]

It is interesting to compare the data for our glass-containing, bimodal alumina with a small average grain size (~4 μm) to the data of Chantikul *et al.* for pure alumina having an equiaxed grain morphology and an average grain size of ~21 μm. The similarity in indentation–strength responses suggests that the microstructure need not consist entirely of coarse grains in order to impart a significant degree of flaw tolerance. Ostensibly, the presence of a small fraction of coarse grains in the glass-containing alumina is sufficient. The implication here is that the number of bridging sites in more uniform microstructures is much less than previously believed; some investigators have suggested that every other grain must effectively be a bridge in order to attain fracture toughness values measured experimentally. Perhaps more importantly, the similarity in our data also indicates that average grain size is *not* a useful parameter in characterizing the microstructure, and that the grain size distribution is much more pertinent to flaw tolerance. This presumes, of course, a predominantly intergranular mode of fracture that takes advantage of the coarser bridging grains; grain boundaries that are too strong simply facilitate transgranular fracture and do not contribute markedly to a rising toughness.

While it is impossible to separate the effects of grain size, grain shape, and grain boundary toughness on flaw tolerance from the results of this study, observations of crack extension in the glass-containing alumina do provide some insight into the importance of grain shape. For instance, elongated grains appear to be more effective bridging sites than equiaxed grains due to the longer pullout distance during crack extension. This is also implicit in the bridging model proposed by Bennison and Lawn, which accounts for grain shape by extending the load–displacement function (*P–u*) to larger crack opening displacements. These observations are also consistent with several other studies of crack propagation in toughened ceramics. For example, it is now recognized that it is the elongated nature of silicon carbide whiskers that results in high fracture toughness of whisker-reinforced composites.[16] In addition, strong *R*-curve behavior and high plateau fracture toughnesses are observed in silicon nitride ceramics having elongated grain morphology.[17] More recently, Padture demonstrated a greatly improved fracture toughness in silicon carbide ceramics having elongated grain structures.[18] Hence it is now clear that tough ceramics can be achieved by tailoring the grain shape. In fact, we believe that flaw tolerance and *R*-curve behavior are much more sensitive to grain shape than to grain size. We are currently conducting a more systematic study of grain shape effects in alumina ceramics to confirm this hypothesis.

Our results also indicate that grains that are too large often fail by transgranular fracture, and that the probability of transgranular fracture is related to the grain orientation relative to the crack front. For instance, the largest grains in the glass-containing aluminas had a long dimension of ~50 μm and a short dimension of ~25 μm. When the crack intersects the large grain normal to the long dimension, the crack tends to continue, propagating through the grain unimpeded. However, when the crack intersects the grain normal to the minor diameter, the crack is almost always deflected. Because toughening appears to be maximized with intergranular fracture, this observation suggests that the ideal grain dimension for high toughness should be ~25 μm long with an aspect ratio greater than 2,[‡‡] although these values will depend on the grain boundary toughness.

One discrepancy that was manifest from observations of fracture surfaces and surface crack traces is the apparent absence of grain bridging pullout on fracture surfaces, compared to the degree of bridging observed on surface traces. Indeed, one might conclude from fractography that no bridging occurs in the glass-containing alumina. We reconcile this discrepancy by noting that during our analysis of surface crack traces, occasionally small, secondary cracks were observed to propagate through bridging grains. Evidently, as the crack opening displacement increases, localized stresses on the bridges themselves become high enough to initiate an intragranular crack, ultimately leading to bridge failure and thus the appearance of complete transgranular fracture on fracture surfaces. In other words, grains that serve effectively as bridges may subsequently fail prematurely before attaining their maximum pullout distance. This further suggests that fractographic analyses that attempt to identify bridging events or quantify critical flaw sizes in such ceramics are dubious at best, as argued for some time now by Lawn *et al.*[31]

Finally we note that enhanced flaw tolerance in the glass-containing alumina comes at the expense of strength, a feature now commonly observed in many flaw-tolerant ceramics. The bimodal aluminas in this study had a low strength, in spite of a small average grain size. This suggests that strength in these materials is related to the presence of coarse grains in the microstructure. While there is still some controversy among those in the fracture community over the mechanism, evidently the large grains promote crack extension along grain facets due to the large residual stresses associated with the anisotropic thermal expansion of alumina. Thus while large, elongated grains are necessary to promote strong bridging, they also limit the strength in alumina.

V. Conclusions

The addition of a small amount of glass phase dramatically affects the microstructure of nominally high-purity alumina ceramics. Large, elongated grains develop in glass-containing alumina that increase the crack resistance behavior due to grain bridging over extended pullout distances. However, grains that grow beyond some optimum size fail by transgranular fracture and do not contribute to bridging. These large grains also have a deleterious effect on strength. This suggests criteria for designing microstructures to be both strong yet flaw tolerant in monolithic ceramics toughened by grain bridging: (i) elongated grains are necessary for strong bridging; (ii) the fraction of coarse, abnormal grains should be minimized; and (iii) grain boundaries should be sufficiently weak so as to effect intergranular fracture, but not so weak so as to allow crack extension at unreasonably low loads.

---

‡‡Not surprisingly, Si_3N_4, SiC_w–Al_2O_3, and *in situ* reinforced SiC ceramics that exhibit the highest fracture toughnesses also have grain dimensions on this order.

References

[1]H. Hübner and W. Jillek, "Sub-Critical Crack Extension and Crack Resistance in Polycrystalline Alumina," *J. Mater. Sci.*, **12**, 117–25 (1977).

[2]R. Steinbrech, R. Knehans, and W. Schaarwächter, "Increase in Crack Resistance during Slow Crack Growth in Al_2O_3 Bend Specimens," *J. Mater. Sci.*, **18**, 265–270 (1983).

[3]D. Broek, pp. 202-205 in *Elementary Engineering Fracture Mechanics*, 4th ed. Kluwer Academic Publishers, Dordrecht, Netherlands, 1986.

[4]F. Lange, "Powder Processing Science and Technology for Increased Reliability," *J. Am. Ceram. Soc.*, **72** [1] 3–15 (1989).

[5]S. J. Bennison and B. R. Lawn, "Role of Interfacial Grain-Bridging Sliding Friction in the Crack-Resistance and Strength Properties of Nontransforming Ceramics," *Acta Metall.* **37** [10] 2659–71 (1989).

[6]R. F. Cook, B. R. Lawn, and C. J. Fairbanks, "Microstructure-Strength Properties in Ceramics," *J. Am. Ceram. Soc.*, **68** [11] 604–15 (1985).

[7]B. R. Lawn, S. W. Freiman, T. L. Baker, D. D. Cobb, and A. C. Gonzalez, "Study of Microstructural Effects in the Strength of Alumina Using Controlled Flaws," *J. Am. Ceram. Soc.*, **67** [4] C-67–C-69 (1984).

[8]P. Chantikul, S. J. Bennison, and B. R. Lawn, "Role of Grain Size in the Strength and *R*-Curve Properties of Alumina," *J. Am. Ceram. Soc.*, **73** [8] 2419–27 (1990).

[9]S. J. Bennison and B. R. Lawn, "Flaw Tolerance in Ceramics with Rising Crack Resistance Characteristics," *J. Mater. Sci.*, **24** [9] 3169–75 (1989).

[10]L. M. Braun, S. J. Bennison, and B. R. Lawn, "Objective Evaluation of Short-Crack Toughness Curves using Indentation Flaws: Case Study on Alumina-Based Ceramics," *J. Am. Ceram. Soc.*, **75** [11] 3049–57 (1992).

[11]R. Knehans and R. W. Steinbrech, "Effect of Grain Size on Crack Resistance Curves of Al_2O_3 Bend Specimens," *Sci. Ceram.*, **12**, 613–19 (1983).

[12]A. Reichl, "Ermittlung und Bedeutung von Rißwiderstandskurven für oxidische Keramiken mit und ohne Umwandlungsverstärkung"; Ph.D. Thesis. Universität Dormund, Germany, 1990.

[13]R. W. Steinbrech, A. Reichl, and W. Schaarwächter, "*R*-Curve Behavior of Long Cracks in Alumina," *J. Am. Ceram. Soc.*, **73** [7] 2009–2015 (1990).

[14]G. Vekinis, M. F. Ashby, and P. W. R. Beaumont, "*R*-Curve Behavior of Al_2O_3 Ceramics," *Acta Metall. Mater.*, **38** [6] 1151–62 (1990).

[15]J. C. Hay and K. W. White, "Grain-Bridging Mechanisms in Monolithic Alumina and Spinel," *J. Am. Ceram. Soc.*, **76** [7] 1849–54 (1993).

[16]P. F. Becher, "Microstructural Design of Toughened Ceramics," *J. Am. Ceram. Soc.*, **74** [2] 255–69 (1991).

[17]C. W. Li and J. Yamanis, "Super Tough Silicon Nitride with *R*-Curve Behavior," *Ceram. Eng. Sci. Proc.*, **10** [7–8] 632–645 (1989).

[18]N. P. Padture, "In Situ-Toughened Silicon Carbide," *J. Am. Ceram. Soc.*, **77** [2] 519–23 (1994).

[19]D. Kovar and M. J. Readey, "Role of Grain Size in the Strength Variability of Alumina," *J. Am. Ceram. Soc.*, **77** [7] 1928–38 (1994).

[20]W. A. Kaysser, M. Sprissler, C. A. Handwerker, and J. E. Blendell, "Effect of Liquid Phase on the Morphology of Grain Growth in Alumina," *J. Am. Ceram. Soc.*, **70** [5] 339–43 (1987).

[21]N. P. Padture and H. M. Chan, "Improved Flaw Tolerance in Alumina Containing 1 vol% Anorthite via Crystallization of the Intergranular Glass," *J. Am. Ceram. Soc.*, **75** [7] 1870–75 (1992).

[22]"Standard Test Method for Biaxial Flexure Strength (Modulus of Rupture) of Ceramic Substrates," ASTM, F-394-78; pp. 422-426 in *ASTM Annual Book of Standards*. Vol. 15.02, Section 15. American Society for Testing and Materials, Philadelphia, PA, 1994.

[23]S. M. Smith and R. O. Scattergood, "Crack-Shape Effects for Indentation Fracture Toughness Measurements," *J. Am. Ceram. Soc.*, **75** [2] 305–15 (1992).

[24]G. W. Dransmann, R. W. Steinbrech, A. Pajares, R. Guiberteau, A. Dominguez-Rodriguez, and A. H. Heuer, "Indentation Studies on Y_2O_3-Stabilized ZrO_2: II, Toughness Determination from Stable Growth of Indentation-Induced Cracks," *J. Am. Ceram. Soc.*, **77** [5] 1194–201 (1994).

[25]B. R. Lawn; p. 265 in *Fracture in Brittle Solids*, 2nd ed. Cambridge University Press, Cambridge, U.K. 1993.

[26]C. A. Powell-Dogan and A. H. Heuer, "Microstructure of 96% Alumina Ceramics: I, Characterization of the As-Sintered Materials," *J. Am. Ceram. Soc.*, **73** [12] 3670–76 (1990).

[27]D. Y. Kim, S. Wiederhorn, B. J. Hockey, C. A. Handwerker, and J. E. Blendell, "Stability and Surface Energies of Wetted Grain Boundaries in Aluminum Oxide," *J. Am. Ceram. Soc.*, **77** [2] 444–53 (1994).

[28]D. Kolar, "Discontinuous Grain Growth in Multiphase Ceramics"; pp. 529–45 in Ceramic Transactions, Vol. 7. *Sintering of Advanced Ceramics*. Edited by C. A. Handwerker, J. E. Blendell, and W. A. Kaysser. American Ceramic Society, Westerville, OH, 1990.

[29]N. Padture, H. M. Chan, B. R. Lawn, and M. J. Readey, "The Role of Crystallization of an Intergranular Glassy Phase in Determining Grain Boundary Residual Stresses in Debased Aluminas," *Mater. Res. Soc. Symp. Proc.*, **170**, 245–50 (1990).

[30]D. Kovar and M. J. Readey, "The Role of Grain Size Distribution on Strength Variability of High-Purity Alumina Ceramics," *J. Am. Ceram. Soc.*, in review.

[31]B. R. Lawn, L. M. Braun, S. J. Bennison, and R. F. Cook, "Reply to 'Comment on "Role of Grain Size in the Strength and *R*-Curve Properties of Alumina'," *J. Am. Ceram. Soc.*, **76** [7] 1900–901 (1993).   □

APPENDIX 5

journal

Microstructure, Flaw Tolerance, and Reliability of Ce-TZP and Y-TZP Ceramics

Michael J. Readey*

Glass and Electronic Ceramics, MS 0333, Organization 1845, Sandia National Laboratories, Albuquerque, New Mexico 87185-0333

Celeste L. McCallen*,†

Department of Materials Science and Engineering, Carnegie Mellon University, Pittsburgh, Pennsylvania 15213

Ce-TZP and Y-TZP ceramics were heat-treated for various times and temperatures in order to vary the microstructure. Flaw tolerance was investigated using the indentation–strength test. Reliability was quantified using conventional two-parameter Weibull statistics. Some Ce-TZP specimens were indented at slightly elevated temperatures where no transformation was observed. Results indicated that the Ce-TZP specimens were extremely flaw tolerant, and showed a relatively high Weibull modulus that scaled with both *R*-curve behavior and flaw tolerance. Y-TZP, on the other hand, with very little if any *R*-curve behavior or flaw tolerance, had a low Weibull modulus. The results also show that flaw history, i.e., whether or not a transformation zone exists along the wake of the crack, has a significant influence on strength. Strength was much less dependent on initial crack size when the crack had an associated transformation zone, whereas strength was highly dependent on cracks typical of natural processing defects. It is argued that the improvement in reliability, flaw tolerance, and dependence on flaw history are all ramifications of pronounced *R*-curve behavior.

I. Introduction

THE considerable variability in strength of ceramic components often limits their use in demanding structural applications. This variability has traditionally been attributed to the presence of a broad size distribution of strength-limiting flaws. These flaws are often present in the material after processing in the form of remnant porosity, inclusions, firing cracks, etc., or result from damage acquired during service. Recent studies have suggested that ceramics exhibiting a rising fracture resistance with crack extension (*R*-curve behavior) will have a smaller variability in strength, and thus be more reliable as components.[1-6] Kendall *et al.*[1] were the first to postulate such a correlation, noting that Mg-PSZ ceramics having strong *R*-curve behavior also exhibited a high Weibull modulus. They subsequently derived a simple empirical model to account for the improvement in reliability. Cook and Clark[3] and later Tandon *et al.*[6] extended this model to include residual stresses, and

showed, at least theoretically, that *R*-curve behavior decreases variability in strength, and that the decrease is linked directly to the shape of the fracture resistance curve. More recently, Shetty and Wang[5] studied the effect of flaw size on strength and reliability in ceramics having various degrees of *R*-curve behavior. Their results indicated that ceramics having strong *R*-curve behavior showed stable crack extension prior to failure, and that the fracture strength was insensitive to the initial flaw size. These materials also had higher Weibull moduli.

In spite of the strong (empirical) evidence suggesting the link between flaw tolerance and enhanced reliability, no study has yet emerged that has investigated the role of initial flaw size on the variability in strength in ceramic materials. The purpose of this paper is to examine the relationships among microstructure, flaw tolerance, and reliability in two zirconia ceramics, namely Ce-TZP and Y-TZP. Studies have shown that Ce-TZP has strong *R*-curve behavior, whereas Y-TZP has a nearly single-valued fracture toughness more typical of "conventional" ceramics.[7-12] In this study, the fracture toughness (or *R*-curve behavior) was controlled by varying the grain size via heat treatment. Flaw tolerance and reliability were then investigated using well-known fracture mechanics tests. It is worth pointing out that because the propensity of the tetragonal phase to undergo the stress-induced phase transformation is very sensitive to small changes in microstructure, controlling the heat-treatment schedule can dramatically vary the transformation characteristics of the TZP while leaving the intrinsic flaw population largely unaffected. This permits examination of toughness and strength variability under conditions of a nearly constant flaw population.

II. Experimental Procedure

(1) Material Processing

Y-TZP (3 mol%) (SY5.2, Z-TECH, Inc., Bow, NH) and Ce-TZP (12 mol%) (12CE, TOSOH U.S.A., Bound Brook, NJ) were selected for this study because of their well-documented toughness properties[10,11,13-15] and microstructural characteristics. Disk-shaped specimens approximately 25 mm in diameter by 4 mm thick were prepared by uniaxially pressing as-received powders to 70 MPa (10 ksi) in a hardened steel die using a dilute solution of stearic acid as a lubricant. The green compacts were then isostatically pressed to 280 MPa (40 ksi) to increase the green density. The specimens were placed in high-purity alumina crucibles, and sintered in air using a $MoSi_2$ resistance furnace for various times and temperatures. All materials were embedded in powder of the same composition to minimize volatilization and impurity pickup. Heating and cooling rates of $5°C \cdot min^{-1}$ were used for all heat treatments. The specific heat treatments are detailed in Table I.

(2) Microstructural Analysis

Densities of the sintered specimens were measured using the Archimedes method using distilled water as the medium. Accuracy in measurement was estimated at ± 0.02 g·cm^{-3}. Several specimens from each heat treatment were polished to a 1 μm diamond finish and thermally etched at 1400°C for 15 min in order to reveal the microstructure. Grain size distributions were determined by measuring the area of at least 200 grains using image analysis software (Image Version 1.45, National Institute of Health, Bethesda, MD), then converting the area into grain diameters assuming the grains were spherical. No additional corrections were made to account for the stereological effects resulting from 2D images.

Phase analysis was conducted using X-ray diffraction on polished and fractured surfaces. The integrated intensities of the *t*- and *m*-ZrO$_2$ {111} peaks were measured using a nonlinear Voigt function (Peakfit, Jandel Scientific, Corte Madera, CA), and the fraction of *m*-phase calculated using the method developed by Heuer and Porter.[16] The fraction of *t*-ZrO$_2$ that transformed to the more stable *m*-ZrO$_2$ during fracture was then determined as the difference in *t*-ZrO$_2$ phase fraction between the polished and fractured surfaces.

(3) Flaw Tolerance and Reliability

The flaw tolerance of the TZP ceramics was assessed using the indentation-strength test.[17-19] Biaxial flexure disks approximately 22 mm in diameter were initially ground on both sides to a nominal thickness of 2 mm. The prospective tensile surfaces of the disks were then polished to a 1 μm diamond finish. Vickers indentations were placed in the center of the tensile surface of each disk using loads ranging from 4 to 300 N. A drop of silicone oil was applied to minimize any environmentally assisted subcritical crack growth. Specimens were then loaded to failure using the flat-on-three-ball geometry at a loading rate of ~250 MPa·s^{-1}. The fracture strength was then calculated from the load at failure using linear elastic solutions[‡] derived for thin plates.[20] After fracture, all indented specimens were inspected to ensure that failure had occurred from the indent; any specimen that did not fail from the indent was excluded from the analysis.

The variability in strength for *un*indented specimens was determined in a similar fashion and quantified using conventional two-parameter Weibull statistics.[21] Approximately 50 specimens from each heat treatment were ground and polished as discussed earlier. The specimens were then broken in biaxial flexure, using the polished surface as the tensile side. The Weibull modulus was computed from

$$P_f = 1 - \exp\left(\frac{\sigma}{\sigma_0}\right)^m \qquad (1)$$

where P_f is the probability of failure, σ is the failure stress, σ_0 is a normalizing stress, and m is the Weibull modulus. The probability of failure was calculated from[22]

$$P_f = \frac{i - 0.5}{n} \qquad (2)$$

where i is the ith bar in the strength ranking, and n is the total number of specimens tested. The Weibull modulus was then determined by linear regression from the usual plots of ln ln $[1/(1 - P_f)]$ versus ln σ.

III. Results and Discussion

(1) Microstructural Analysis

The Archimedes method showed that all fired specimens densified to greater than 98% of the theoretical density. This was also supported by the lack of any significant porosity on SEM micrographs of fine and coarse-grain microstructures in Y-TZP (Figs. 1(a,b)) and Ce-TZP (Figs. 2(a,b)). The average grain size for the fine-grained Y-TZP was approximately 0.4 μm, and increased to ~0.8 μm with additional heat treatment. The grain size distributions also tended to scale with average grain size, indicating reasonably self-similar microstructures. The average grain sizes of the Ce-TZP ceramics were larger, 0.6 μm, and increased with extended heat treatments to ~2.1 μm. The grain size distribution was broader in the case of the Ce-TZP, but also tended to scale in a self-similar manner with heat treatment. The densities and grain size data are summarized in Table I.

(2) Phase Analysis

X-ray diffraction analysis indicated that polished surfaces of both Ce-TZP and Y-TZP did not contain *m*-ZrO$_2$ in any of the heat treatments, indicating that the grain size was always smaller than the critical grain size at which the *t*-ZrO$_2$ phase spontaneously transforms to *m*-symmetry upon cooling to room temperature. Figure 3 shows the percent of the *t*-phase transformed scales with grain size, suggesting that the coarse-grain specimens have a higher toughness compared with their fine-grain counterparts. The Ce-TZP specimens also showed a greater fraction of grains transformed during fracture, indicative of a higher toughness relative to the Y-TZP.[23]

(3) Flaw Tolerance and Weibull Modulus

(A) Y-TZP: Figure 4 shows the indentation–strength data for as-indented Y-TZP specimens. The fine-grain Y-TZP has a slightly greater strength than the coarse-grain Y-TZP. However, both fine- and coarse-grain materials show very similar strength characteristics. At low loads the strength is independent of indentation load, and approaches the natural strength of the material (the shaded boxes at the left of the figure). However, at larger indentation loads the strength decreases markedly with increasing indentation load, typical of a material having a single-valued fracture toughness. At high indentation loads ($P > 200$ N), the strength data again appear to become less dependent on indentation load. This is most likely due to the presence of lateral indentation cracks that begin to dominate the fracture process, and is not related to flaw tolerance.

Figure 5 shows the Weibull plot for the *un*indented fine-grain and coarse-grain Y-TZP specimens. The strength distributions were nearly identical, with relatively low Weibull moduli of

Table I.   Sintering Schedules and Physical Properties of Zirconia Ceramics

Material	Sintering temperature (°C)	Sintering time (h)	Sintered density (g/cm³)	Grain size (μm)
Y-TZP[†]	1450	2	6.03 ± 0.02	0.39 ± 0.10
	1575	2	6.03 ± 0.02	0.81 ± 0.02
Ce-TZP[‡]	1450	2	6.17 ± 0.02	0.56 ± 0.27
	1450	52	6.18 ± 0.02	2.1 ± 1.0

[†]SY5.2 Ultra, Z-Tech, Bow, NH. [‡]TZ-12CE, Tosoh Ceramics, Tokyo, Japan.
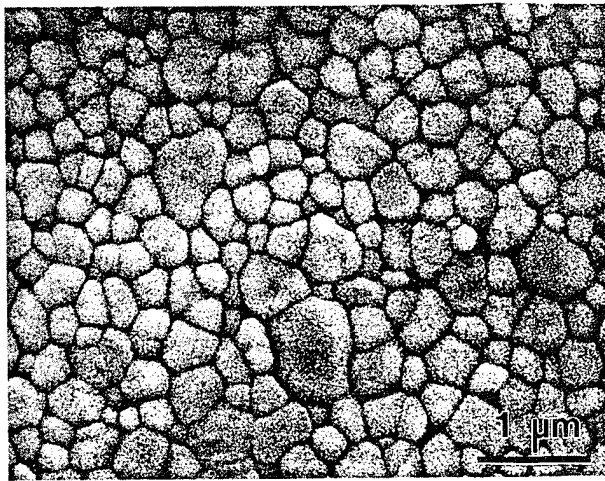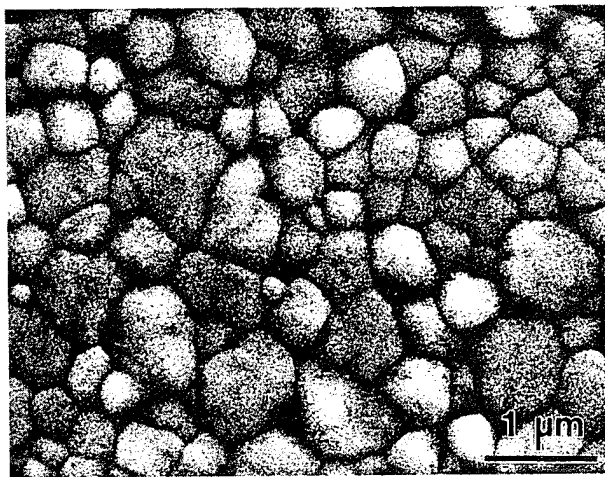
Fig. 1. SEM micrographs of thermally etched surfaces of Y-TZP sintered for 2 h at (a) 1450° and (b) 1575°C.
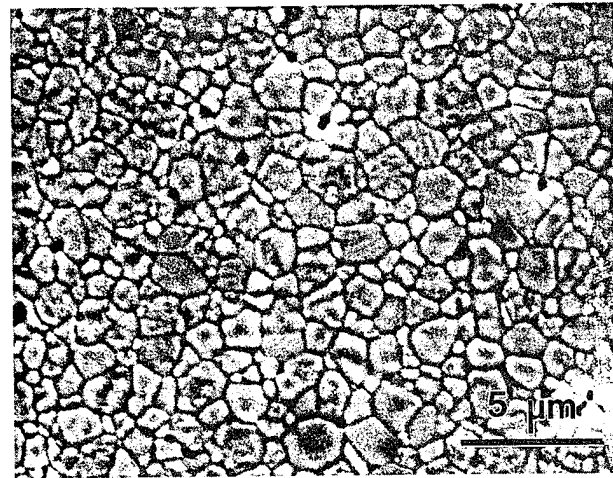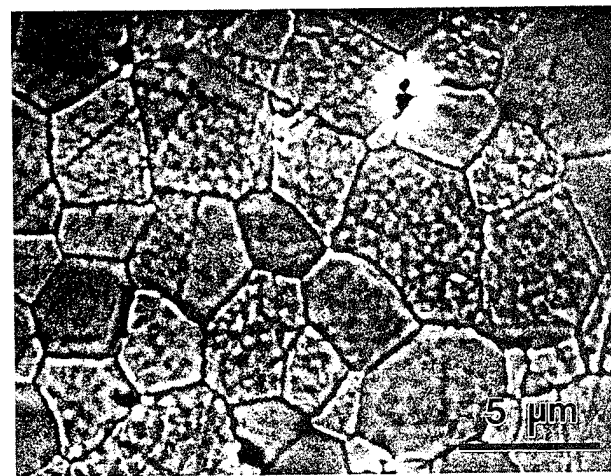
Fig. 2. SEM micrographs of thermally etched surfaces of Ce-TZP sintered at 1450°C for (a) 2 and (b) 52 h.

$m = 8.2$ and $m = 8.3$ for the fine- and coarse-grain ceramics, respectively.[§]

(B) Ce-TZP: The strength–indentation data for the Ce-TZP specimens are shown in Fig. 6. As with the Y-TZP, the strength of the fine-grain material is greater than for the coarse-grain Ce-TZP. However, in this case, the strength of the fine-grain Ce-TZP decreases only modestly (<15%) over the load range. Moreover, the strength of the coarse-grain Ce-TZP was nearly independent of indentation load. This insensitivity of strength to indentation size is consistent with the strong R-curve behavior observed by Yu and Shetty.[§] The strength of the indented Ce-TZP specimens also approaches the natural strength of the materials (the shaded boxes at the left of the figure), suggesting a similarity between "natural" and indentation flaws.

Weibull distributions for *un*indented Ce-TZP specimens are shown in Fig. 7. The Weibull moduli for both Ce-TZP materials are considerably higher than for Y-TZP. The coarse-grain Ce-TZP has a Weibull modulus of $m = 17.3$ compared to $m = 11.9$ for the fine-grain material, indicating a strong correlation with flaw tolerance and R-curve behavior. Furthermore, note that the strength data for the coarse-grain Ce-TZP are much less linear than for the fine-grain material. While this has traditionally been viewed as due to a different flaw population, we believe it
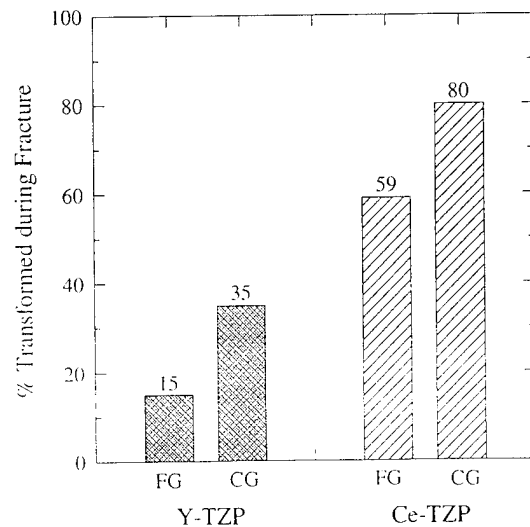

Fig. 3. Percentage of tetragonal grains that transformed to monoclinic symmetry during fracture. The fraction transformed increases with grain size in both TZPs, but is much greater in Ce-TZP.

[§]Note: These represent mroe accurate values than those reported in an earlier work.[21]
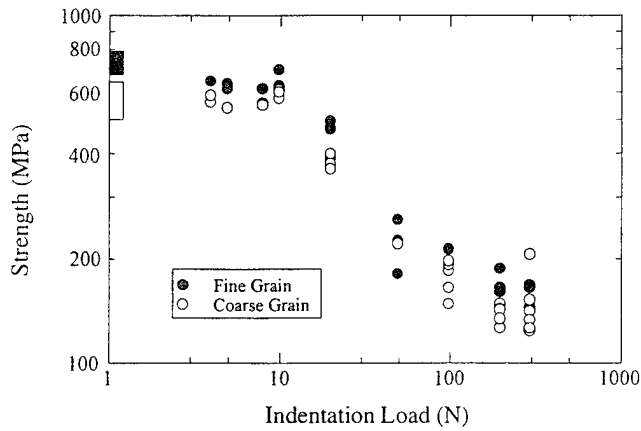
Fig. 4. Strength as a function of indentation load for fine- and coarse-grain Y-TZP ceramics. Both materials show a strength plateau at low loads, then strength decreases rapidly with further increases in indentation load. The fine-grain ceramics have a slightly higher strength. The boxes at the left of the diagram correspond to the natural (unindented) strengths of the ceramics.
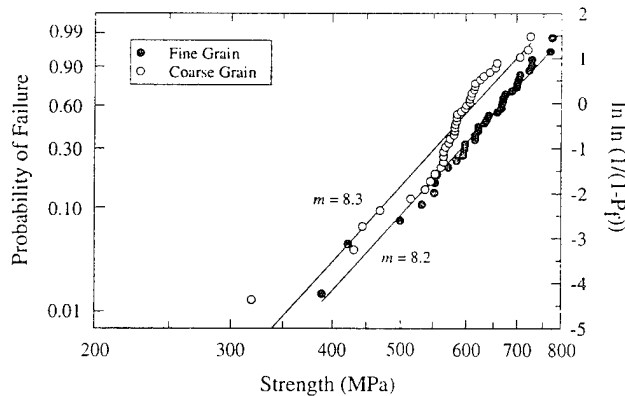

Fig. 5. Weibull plots for unindented fine- and coarse-grain Y-TZP ceramics. The Weibull moduli are low, indicating a broad distribution of strengths. The values are nearly identical, consistent with the indentation–strength data. The fine-grain material also shows a slightly greater strength.
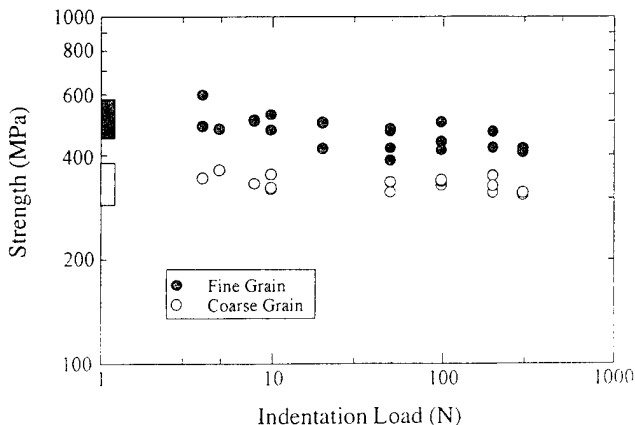

Fig. 6. Strength as a function of indentation load for Ce-TZP ceramics. Both materials show strong flaw tolerance; i.e., strength is nearly independent of indentation load over the entire range tested. The fine-grain ceramics also have a higher strength. The boxes at the left of the diagram correspond to the natural (unindented) strengths of the ceramics.

is a direct consequence of strong R-curve behavior. For example, it has been suggested by Kovar and Readey[25] as well as by Rödel[26] that Weibull plots for materials having strong R-curve behavior should have a characteristic "S"-shape, as demonstrated here. Specifically, flaws that are either very small or very large relative to the scale of the R-curve will undergo little stable extension prior to failure, and thus will behave more like Griffith flaws. Flaws on the same dimensional scale as the R-curve experience the full effect of the rising toughness behavior, extending in a stable fashion prior to failure. Theoretically, strength is least sensitive to flaws in this latter size range, resulting in a higher Weibull modulus relative to the modulus determined by the extremes in flaw size. Hence a Weibull plot describing the strength distribution arising from the entire range of flaw sizes should have a characteristic S-shape. Further details on flaw size and Weibull modulus are discussed in the forthcoming paper by Kovar and Readey.[25]

Based on the indentation–strength results given above, Ce-TZP ceramics are shown to be significantly more flaw tolerant than their Y-TZP counterparts. Moreover, the flaw tolerance scales with the amount of t–m transformation during fracture. This transformation imparts considerable R-curve behavior owing to transformation toughening, as experimentally demonstrated by Ramachandran and Shetty.[4] Prior analyses by Bennison and Lawn,[19] as well as Cook et al.,[27] have suggested that such flaw tolerance is a direct consequence of R-curve behavior, a correlation now widely accepted by the ceramics community. Such a correlation is strengthened by the fact that Y-TZP, which has very little R-curve behavior, exhibits flaw tolerance only at very low indentation loads. In general, the indentation–strength characteristics are more typical of a ceramic having a single-valued fracture toughness. Our results also suggest that the correlation betwen R-curve behavior and flaw tolerance in TZP ceramics can be extended to include reliability; high reliability, at least when defined in terms of strength variability, is obtained with very flaw-tolerant ceramics. Hence, pronounced R-curve behavior results in enhanced flaw tolerance and dramatically improved reliability.

However, the flaw tolerance indicated by our indentation–strength tests data assumes that the indentation cracks generated at different loads are self-similar, varying only in size. Close observation of indentation cracks shows that this is not the case: well-developed cracks emanating from the four corners of the indentation impression were observed only in Y-TZP at indentation loads greater than ~10 N (Fig. 8(a)). At lower loads, one or more radial cracks were constrained at the impression corners. At very low loads, no cracks were observed at all. Furthermore, no radial cracking was observed in Ce-TZP at any of the loads used in this study (Fig. 8(b)). Cook and Braun[28,29] have observed similar results in Y-TZP ceramics, and argued that the
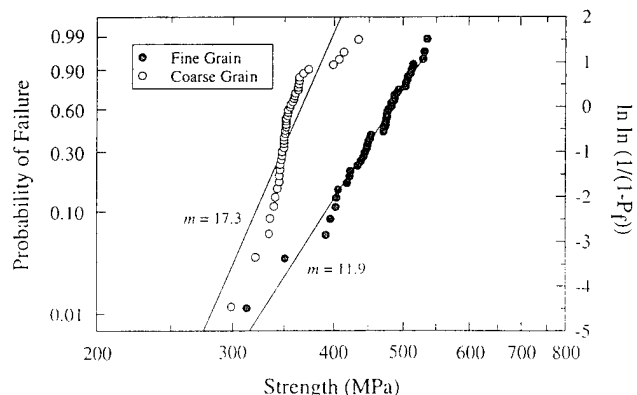

Fig. 7. Weibull plots for Ce-TZP ceramics. The Weibull modulus increases significantly with grain size. The fine-grain material also shows greater strength, but the coarse-grain ceramic shows less variability in strength. The coarse-grain data are also nonlinear, most likely a result of the strong R-curve behavior (see text).

presence of the transformation zone surrounding the indentation impression has a strong influence on the formation and geometry of the radial cracks. For example, below a critical indentation load, the residual tensile field from the indentation is balanced by the compressive field produced by the transformation, thereby "trapping" radial cracks within the transformation zone. At even lower loads, the transformation-induced compressive stresses overwhelm the indentation tensile stresses responsible for crack initiation.[30] Thus, in our Ce-TZP ceramics, where extensive *t–m* transformation results in a significant compressive zone surrounding the indent impression, the indentation loads are always subthreshold; i.e., no radial cracks are ever observed even at very high indentation loads.

Based on our data and observations of indentation crack morphology, we now conclude that flaw tolerance in Ce-TZP (and in Y-TZP at low loads) is associated more with a change in crack morphology to subthreshold indentations than to insensitivity to crack size. Strictly speaking, one should not refer to such behavior as flaw tolerance, as this implies a near constant strength over a wide range of flaw sizes. Rather, we consider these Ce-TZPs remarkably damage tolerant, as the coarse-grained Ce-TZP shows most dramatically; the strength is nearly

independent of impression size, even when the size of the impression diagonal varied by over an order of magnitude over the loading range used, as shown in Fig. 9.

Given the relative independence of strength on the size of the indentation impression in Ce-TZP ceramics, we further investigated the role of the surrounding transformation zone on strength. In this series of tests, coarse-grain Ce-TZP specimens were indented at room temperature at various loads, and then annealed at 500°C for 1 h to remove the residual compressive stresses by retransforming the monoclinic grains back to tetragonal symmetry. Raman microprobe analysis was used to ascertain the degree of reverse *m–t* transformation; all evidence indicated that the 500°C annealing treatment caused complete retransformation. These annealed specimens were then broken as usual, and the strengths compared to those specimens that were not annealed. The results, shown in Fig. 10, indicate that there is no difference in strength between annealed and unannealed indentation flaws. Furthermore, we found no evidence for the transformation zone to reform during loading; observations using Nomarski interference contrast showed no surface uplift around the indent impression even after preloading to 80% of the failure load. This strongly suggests that strength is governed more by the stress required to *initiate* a crack from the indentation impression, and that this stress is independent of both the impression size and surrounding stress state.

The ability to cause the reverse *m–t* transformation at relatively low temperatures suggested that well-developed indentations could be formed by indenting specimens at temperatures
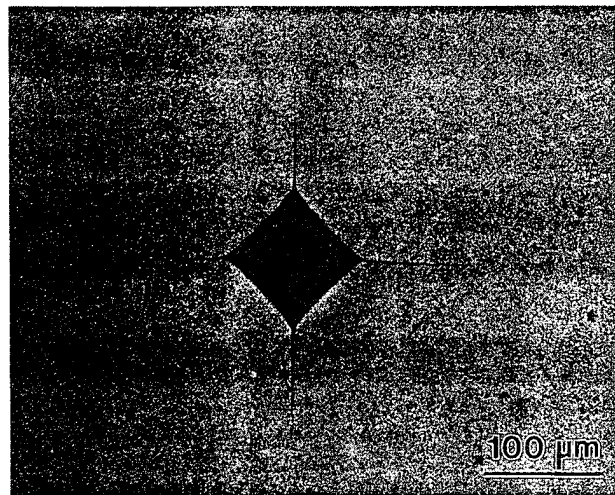
(a)
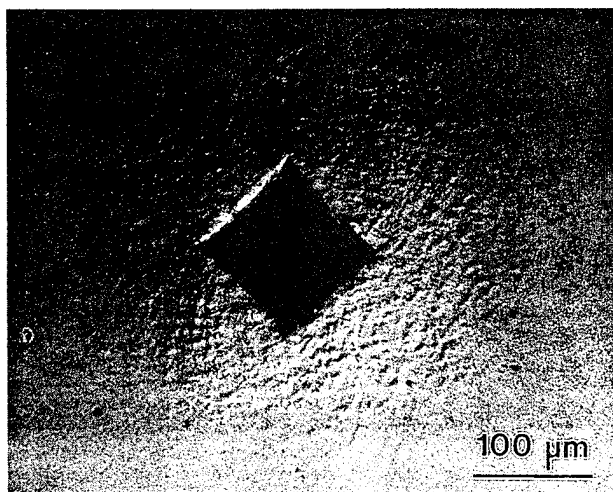
(b)

Fig. 8. Optical micrographs of 100 N indentations in (a) coarse-grain Y-TZP, and (b) coarse-grain Ce-TZP. Nomarski interference contrast was used to observe surface uplift caused by the attendant *t–m* transformation during indentation. Fully developed radial cracks form in Y-TZP, whereas no cracks were observed in Ce-TZP.
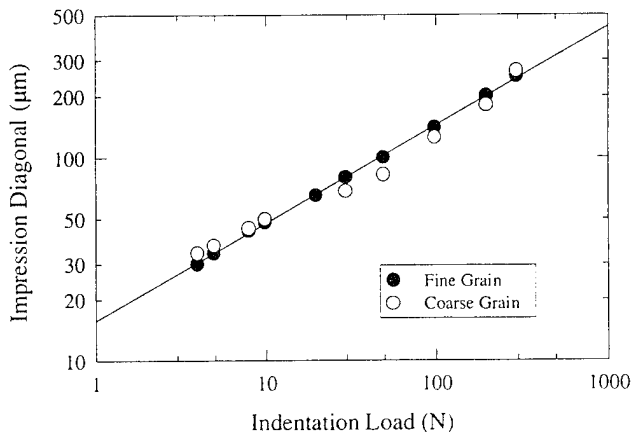
Fig. 9. Indent impression diagonal as a function of indentation load for the two Ce-TZP ceramics. The impression size increases by nearly an order of magnitude over the load range, and was independent of grain size. No radial cracking was observed at any load.
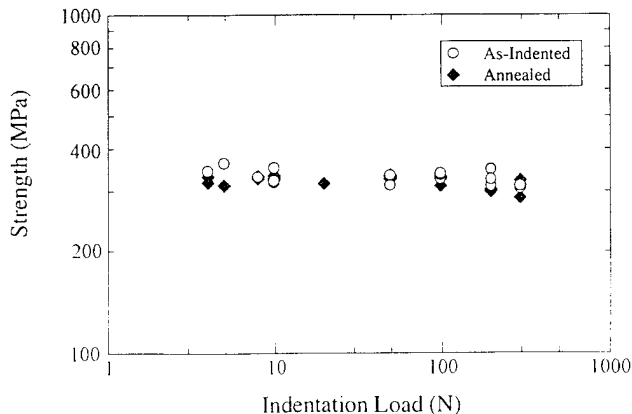
Fig. 10. Strength as a function of indentation load for coarse-grain Ce-TZP ceramics that were tested either as-indented or indented and then annealed at 500°C for 1 h to remove the surrounding transformation zone. Strength was independent of local stress state.

where the transformation is no longer thermodynamically favorable, as demonstrated by Tikare and Heuer.[31] In this study, we determined that well-developed indentation cracks could be formed at temperatures as low as 350°C, at least for indentation loads greater than approximately 30 N. Moreover, Raman microprobe analysis confirmed that no transformation zone was present around the cracks. Based on these results, we then "hot-indented" several coarse-grain Ce-TZP specimens over a range of indentation loads. The flaw tolerance of these hot-indented specimens was then assessed as in previous tests. The results of the indentation–strength test of the hot-indented, coarse-grained Ce-TZP specimens are shown in Fig. 11. At loads less than 30 N, no cracks were observed and the strength was relatively independent of impression size, as discussed previously. However, at larger loads, well-developed cracks were visible, and the strength decreased with increasing indentation load, although less so than predicted from theory.[32] This is not surprising because these materials are known to have rapidly rising R-curves and thus should be flaw tolerant. Finally, we note that because these indentation cracks were not influenced by the presence of a transformation zone, they are more representative of natural flaws, i.e., flaws such as pores or agglomerates that are processing-related and do not have an associated residual stress.

The ability to form well-developed indentation cracks by indenting at elevated temperatures also allowed us to investigate the role of flaw history on strength. In another series of experiments, hot-indented, coarse-grain Ce-TZP specimens were slowly loaded (in biaxial flexure) to further extend the indentation cracks. Since this was performed at room temperature, any crack extension was associated with a corresponding t–m transformation. This is shown in Fig. 12, which clearly shows the transformation zone surrounding the portion of the crack that was propagated at room temperature (about 50 μm, shown by the arrowed features). It should be noted that such a crack is typical of in-service cracks (e.g., scratches and hard particle impacts) that *do* have some associated residual stress component. In these specimens, presumably the fracture toughness is increasing during crack propagation owing to transformation toughening (note the surface uplift in the figure). Thus, for cracks of identical sizes, we could examine the importance of flaw history on strength, viz., whether or not a natural flaw is as severe as an in-service crack of the same size. To investigate this relationship, several specimens were hot-indented at 50 to 300 N, and the resulting indentation crack sizes measured optically. Biaxial flexure strengths were then measured as before. A second batch of specimens was also hot-indented at either 50 or 100 N. However, these materials were subsequently

loaded slowly in order to propagate the crack. Once significant crack extension was observed, the sample was removed from the fixture and the total crack size measured optically. The specimens were then fast-fractured in biaxial flexure. Figure 13 shows the strength of the coarse-grain Ce-TZP as a function of crack size for both as-indented cracks (c_0) and extended cracks ($c_0 + \Delta c$). As shown in the figure, the strengths of specimens containing extended cracks were consistently greater than those specimens containing only as-indented cracks, even when the overall crack sizes were the same. This indicates that flaw history is an important component to strength in materials that have pronounced R-curve behavior.

Such insensitivity of strength to extended indentation cracks (i.e., in-service cracks) can be explained using the conventional tangent construction described by Broek,[33] shown in Fig. 14(a). For instance, consider the case of a hot-indented crack of size c_0 that has no surrounding transformation zone. Application of a sufficient stress will result in stable extension of the crack to a size $c_0 + \Delta c$, with the accompanying formation of a transformation zone (provided the temperature is below the M_s temperature for the t–m phase transformation). This in turn increases the fracture toughness according to the R-curve. Further increases in applied stress lead to continued stable extension
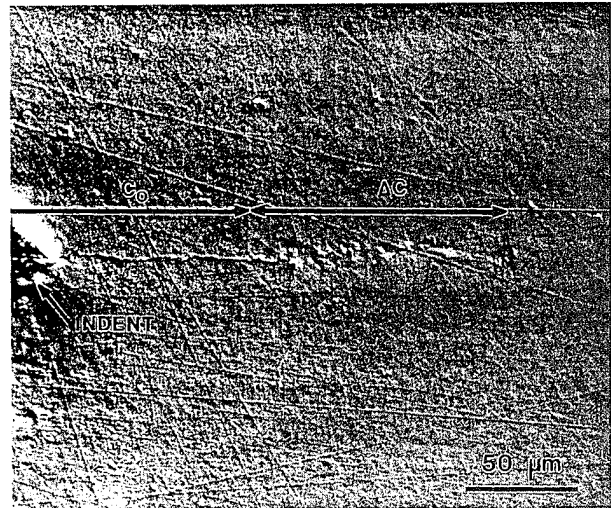
Fig. 12. Optical micrograph of a coarse-grain Ce-TZP specimen that was first indented at 350°C to produce well-developed radial cracks. These cracks were then extended at room temperature under conditions of slow loading. Nomarski interference contrast shows surface uplift due to t–m transformation during room-temperature crack propagation.
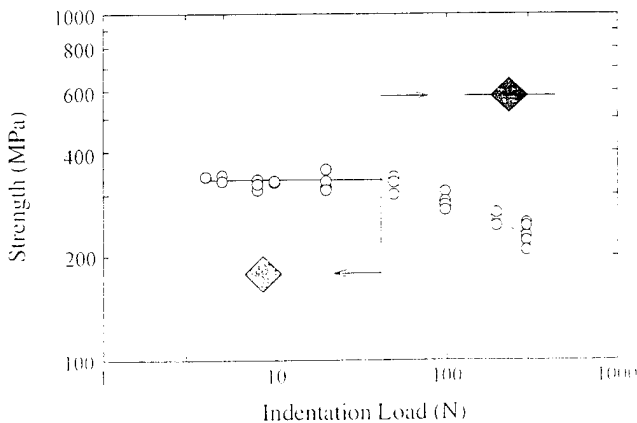
Fig. 11. Room-temperature strength as a function of indentation load for coarse-grain Ce-TZP indented at 350°C. Below approximately 30 N, no cracks were observed and strength was invariant with indentation load. At loads greater than 30 N, well-developed radial cracks formed, and strength decreased with increasing load (and indent crack size).
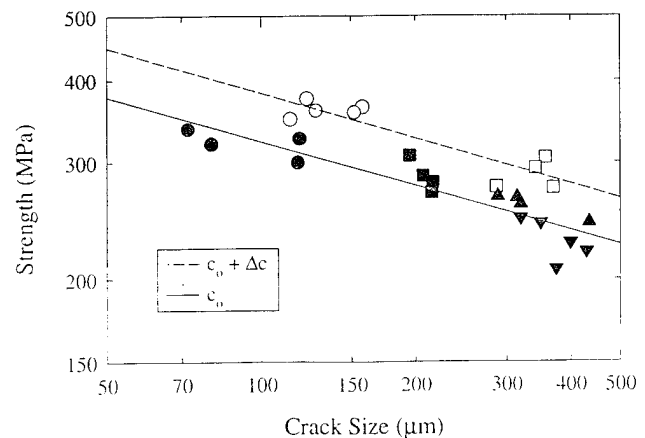
Fig. 13. Strength as a function of initial crack size for cracks that were formed by indenting at 350°C (c_0), and extended at room temperature ($c_0 + \Delta c$): (○,●) 50, (□,◼) 100, (▲) 200, (▼) 300 N.

until the crack attains a critical size, c^*, upon which any additional stress results in crack instability. Strength, σ, is therefore defined as the stress at the critical crack length, c^*. The important point to be made is that because *stable* crack growth precedes failure, any crack size between c_0 and c^* will result in the same strength, σ. Thus strength is independent of flaw size; the material exhibits flaw tolerance.

However, now consider the situation for hot-indented (natural) cracks of *different* initial flaw sizes, as shown in Fig. 14(b). Because there is no associated transformation zone, all cracks act like "initial" flaws, c_0, with a fracture toughness given by the initial point on the R-curve. Larger initial flaws imply that the R-curve is merely *shifted* to the right, i.e., R-curves originating at c_0^1 and c_0^2 in Fig. 14(b). Strength is now strongly linked to the *initial* flaw size, as indicated by the tangent construction, although the dependence is less than what would be predicted by the conventional Griffith analysis due to stable crack extension prior to failure.

The implications of Fig. 14 are clear, namely that flaw history plays an important role in the strength characteristics of ceramics demonstrating pronounced R-curve behavior, notably

Ce-TZP ceramics. Since the rising R-curve mitigates the effect of in-service flaws, the strength of a component should not degrade significantly if subsequent crack extension occurs under in-service conditions, provided that the flaw does not grow beyond some critical value determined by the slope and peak toughness described by the R-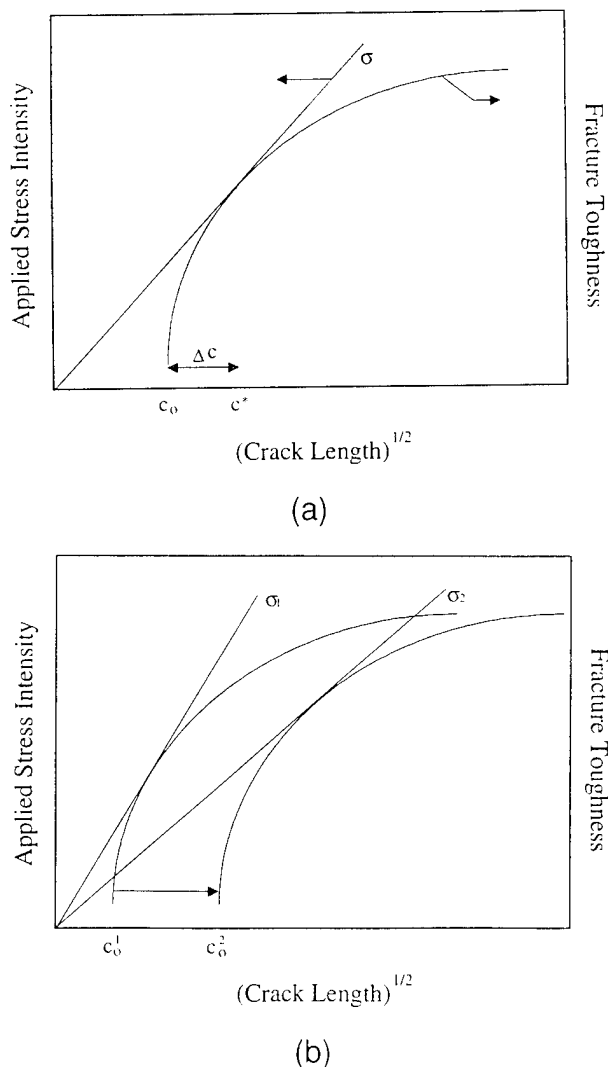curve. This has real advantages in structural applications, for instance a component that has been proof-tested to a certain design stress should maintain mechanical integrity in spite of subsequent crack growth (environmentally assisted or otherwise). This suggests that ceramics having strong R-curve behavior should have a higher reliability than flaw-sensitive ceramics characterized by a single-valued toughness, as borne out by our own Weibull tests on Y-TZP and Ce-TZP.

On the other hand, the strength of a component does appear to be *dependent* on the size of natural flaws in spite of pronounced R-curve behavior, although the dependence is less than that predicted by the Griffith failure criterion. This is contrary to current arguments suggesting that initial flaw size is not important in the strength of flaw-tolerant ceramics. This is a rather subtle yet important point, since a natural implication of the flaw tolerance concept is that removing processing defects (i.e., by clean-room processing) is unnecessary in producing reliable components. Our data suggest that processing defects *are* important, and that decreasing the scale of the initial flaw size will result in both an increase in strength and a decrease in strength variability. However, there is a practical limit to increasing the strength by decreasing the flaw size. For instance, once the flaw size is below the scale of the microstructural feature contributing to enhanced toughness (i.e., the zone size in transformation toughened ceramics), then no further improvement in strength will be observed. Below this size limit, these defects no longer tend to be failure origins. Rather, cracks nucleate elsewhere in the system and eventually cause failure.[34]

(a)

(b)

Fig. 14. Schematic illustration of the influence of flaw history on strength of ceramics having strong R-curve behavior: (a) Initial flaws (c_0) grow by an amount (Δc) to final critical flaw size c^*. Thus all flaws less than c^* will result in a constant strength, σ. (b) Initial flaws of different sizes, c_0^1 and c_0^2, begin at the same initial value of toughness; crack extension increases the fracture toughness, but along displaced R-curves. The strength, σ_1 and σ_2, in this case is strongly dependent on the initial flaw size, but less so than would be predicted from the Griffith failure criterion.

IV. Conclusions

We have shown that Ce-TZP ceramics having pronounced R-curve behavior are more flaw tolerant and have a greater Weibull modulus than Y-TZP ceramics having single-valued fracture toughness. We have also shown that the strength insensitivity to indentations in Ce-TZP is more due to subthreshold indentation loads failing to produce well-developed radial cracking patterns. Strength was also independent of the presence of a compressive region surrounding the indentation impression, suggesting that the strength insensitivity was related to the stress required to nucleate cracks from evidently innocuous indentation impressions.

Well-developed cracks were produced in Ce-TZP by indenting at elevated temperatures, and strength then showed a modest dependence on indentation-flaw size, although much less than predicted by the Griffith criterion. Furthermore, and perhaps more importantly, our results indicate that flaw history is a critical component to strength; strength is sensitive to the size of natural flaws and relatively insensitive to the size of in-service induced cracks. These results were explained using the tangent construction, arguing that the R-curve is not fixed but shifts with initial flaw size.

Perhaps the most significant result of our work is that high reliability will only be achieved in materials having both a strong R-curve *and* narrow flaw population. The strong R-curve allows for stable crack extension without causing failure, ideal for crack extension under in-service conditions, and the narrow flaw population ensures that the R-curve begins at more or less the same location. Thus we conclude that future directions in structural ceramics research should include both process refinement to reduce the size and range of sizes of processing defects, and microstructural design to engineer strong R-curve behavior into ceramic components.

References

[1]K. Kendall, N. McN. Alford, S. R. Tan, and J. D. Birchall, "Influence of Toughness on Weibull Modulus of Ceramic Bending Strength," *J. Mater. Res.*, **1** [1] 120–23 (1986).

[2]D. L. Hartstock and A. F. McLean, "What the Designer with Ceramics Needs," *Am. Ceram. Soc. Bull.*, **63** [2] 266–70 (1984).

[3]R. F. Cook and D. R. Clarke, "Fracture Stability, *R*-Curves and Strength Variability," *Acta Metall.*, **36** [3] 555–62 (1988).

[4]N. Ramachandran, L. Chao, and D. K. Shetty, "*R*-Curve Behavior and Flaw Insensitivity of Ce-TZP/Al₂O₃ Composites," *J. Am. Ceram. Soc.*, **75** [4] 961–69 (1993).

[5]D. K. Shetty and J. Wang, "Crack Stability and Strength Distribution of Ceramics and Exhibit Rising Crack-Growth-Resistance (*R*-Curve) Behavior," *J. Am. Ceram. Soc.*, **72** [7] 1158–62 (1989).

[6]R. Tandon, D. J. Green, and R. F. Cook, "Strength Variability in Brittle Materials with Stabilizing and Destabilizing Resistance Fields," *Acta Metall. Mater.*, **41** [2] 399–408 (1993).

[7]R. M. Anderson and L. M. Braun, "Technique for the *R*-Curve Determination of Y-TZP Using Indentation-Produced Flaws," *J. Am. Ceram. Soc.*, **73** [10] 3059–62 (1990).

[8]C.-S. Yu and D. K. Shetty, "Transformation Yielding, Plasticity, and Crack-Growth-Resistance (*R*-Curves) Behavior of Ce-TZP," *J. Mater. Sci.*, **25** [4] 2025–35 (1990).

[9]C.-S. Yu and D. Shetty, "Transformation Zone Shape, Size and *R*-Curve Behavior of Ce-TZP," *J. Am. Ceram. Soc.*, **72** [8] 921–28 (1989).

[10]D. B. Marshall, "Strength Characteristics of Transformation-Toughened Zirconia," *J. Am. Ceram. Soc.*, **69** [3] 173–80 (1986).

[11]K. Tsukuma and M. Shimada, "Strength, Fracture Toughness, and Vickers Hardness of Ce-TZP," *J. Mater. Sci.*, **20** [4] 1178–84 (1985).

[12]R. W. Steinbrech; unpublished work, 1990.

[13]M. V. Swain, "Grain-Size Dependence of Toughness and Transformability of 2 mol% Y-TZP," *J. Mater. Sci. Lett.*, **5**, 1159–62 (1986).

[14]P. F. Becher and M. V. Swain, "Grain-Size-Dependent Transformation Behavior in Polycrystalline Tetragonal Zirconia," *J. Am. Ceram. Soc.*, **75** [3] 493–502 (1992).

[15]D. J. Green, R. H. J. Hannink, and M. V. Swain; pp. 90–103 in *Transformation Toughening of Ceramics*. CRC Press, Boca Raton, FL, 1989.

[16]D. L. Porter and A. H. Heuer, "Microstructural Development in Mg-Partially Stabilized Zirconia," *J. Am. Ceram. Soc.*, **62** [5–6] 298–305 (1979).

[17]S. J. Bennison, N. P. Padture, J. L. Runyun, and B. R. Lawn, "Flaw Insensitive Ceramics," *Philos. Mag. Lett.*, **64** [4] 191–95 (1991).

[18]P. Chantikul, S. J. Bennison, and B. R. Lawn, "Role of Grain Size in the Strength and R-Curve Properties of Alumina," *J. Am. Ceram. Soc.*, **73** [8] 2419–27 (1990).

[19]S. J. Bennison and B. R. Lawn, "Flaw Tolerance in Ceramics with Rising Crack Resistance Characteristics," *J. Mater. Res.*, **24** [9] 3169–75 (1989).

[20]ASTM Standard F394-78, "Biaxial Flexure Strength (Modulus of Rupture) of Ceramic Substrates"; pp. 422–26 in *ASTM Annual Book of Standards*, Vol. 15.02, Section 15. American Society for Testing and Materials, Philadelphia, PA, 1978.

[21]R. H. Doremus, "Fracture Statistics: A Comparison of the Normal, Weibull, and Type 1 Extreme Value Distributions," *J. Appl. Phys.*, **54** [1] 193–98 (1983).

[22]J. D. Sullivan and P. H. Lauzon, "Experimental Probability Estimators for Weibull Plots," *J. Mater. Sci. Lett.*, **5** [12] 1245–47 (1986).

[23]R. M. McMeeking and A. G. Evans, "Mechanics of Transformation-Toughening in Brittle Materials," *J. Am. Ceram. Soc.*, **65** [5] 242–46 (1985).

[24]M. J. Readey, C. L. McCallen, P. D. McNamara, and B. R. Lawn, "Correlations between Flaw Tolerance and Reliability in Zirconia," *J. Mater. Sci.*, **28** [12] 6748–52 (1993).

[25]D. Kovar and M. J. Readey; unpublished work.

[26]J. Rödel; personal communication, 1994.

[27]R. F. Cook, C. J. Fairbanks, B. R. Lawn, and Y.-W. Mai, "Crack Resistance by Interfacial Bridging: Its Role in Determining Strength Characteristics," *J. Mater. Res.*, **2** [3] 345–56 (1987).

[28]R. F. Cook, L. J. Braun, and W. R. Cannon, "Trapped Cracks at Indentation: I, Experiments on Y-TZP," *J. Mater. Sci.*, **29** [8] 2133–42 (1994).

[29]R. F. Cook and L. M. Braun, "Trapped Cracks at Indentation: II, Fracture Mechanics Model," *J. Mater. Sci.*, **29** [8] 2192–204 (1994).

[30]S. Lathabai, J. Rödel, B. R. Lawn, and T. P. Dabbs, "Fracture Mechanics Model for Subthreshold Indentation Flaws: I, Equilibrium Fracture," *J. Mater. Sci.*, **26** [8] 2157–68 (1991).

[31]V. Tikare and A. H. Heuer, "Temperature-Dependent Indentation Behavior of Transformation-Toughened Zirconia-Based Ceramics," *J. Am. Ceram. Soc.*, **74** [3] 593–97 (1991).

[32]B. R. Lawn, *Fracture of Brittle Solids*, 2nd ed., Chs. 9 and 10. Cambridge University Press, Cambridge, U. K., 1993.

[33]D. B. Broek, *Elementary Engineering Fracture Mechanics*, 4th ed.; pp. 130–34. Kluwer Academic Publishers, Dordrecht, Netherlands, 1986.

[34]D. Kovar and M. J. Readey, "Role of Grain Size in the Strength Variability of Alumina," *J. Am. Ceram. Soc.*, **77** [7] 1928–38 (1994).

APPENDIX 6

72

Grain Size Distributions and Strength Variability of High-Purity Alumina

Desiderio Kovar[*,†]

Department of Materials Science and Engineering, Carnegie Mellon University, Pittsburgh, Pennsylvania 15213

Michael J. Readey[*]

Glass and Electronic Ceramics, Sandia National Laboratories, Albuquerque, New Mexico 87185-0333

Two batches of high-purity, alumina ceramics having an equiaxed grain morphology were manufactured with a mean grain size of approximately 10 μm. A low-temperature heat treatment performed prior to sintering on one batch of specimens resulted in a narrow grain size distribution. The other batch of specimens was fired in a conventional manner and exhibited a broader grain size distribution. Mechanical tests performed on these specimens indicated little difference in the flaw tolerance of *T*-curve behavior of the aluminas, despite the presence of coarser grains in the conventionally fired alumina. Observations of cracks in these high-purity aluminas revealed that large grains ruptured transgranularly and therefore did not act as effective bridging sites. Strength tests on polished specimens indicated that the alumina with the broad grain size distribution exhibited greater strength variability than the alumina with a narrow grain size distribution. A simple analysis shows that, because of the shallow *T*-curve behavior observed in both aluminas, stable crack extension should not occur from natural flaws. The strength of these high-purity aluminas is therefore controlled by the *initial* flaw size and the *initial* toughness. The increased strength variability in the alumina with the broad grain size distribution is rationalized in terms of a wider distribution of critical flaws.

I. Introduction

IT IS now well established that many alumina ceramics exhibit rising toughness or *T*-curve behavior, and that the magnitude of the *T*-curve behavior is a function of grain size.[1-4] It has also been shown that the flaw sensitivity for materials that display *T*-curve behavior is reduced compared to materials with a single-valued toughness.[5,6] Such flaw tolerance implies significant improvements in mechanical reliability in coarse-grained aluminas. However, recent experimental evidence indicates that reliability is *not* improved in alumina by merely increasing the mean grain size. Instead, it was found that local variability in the fracture toughness also increases with grain size and offsets improvements in reliability due to increasing flaw tolerance.[7]

Since dramatic improvements in reliability have been measured in other grain-bridging ceramics that demonstrate pronounced *T*-curve behavior (i.e., Si_3N_4), it is possible that other

microstructural variables such as the width of the grain size distribution or the grain shape may play a greater role in increasing reliability than merely the average grain size. For example, Hirosaki *et al.* found that a coarse-grained, elongated silicon nitride with a broad grain size distribution had a Weibull modulus of 53;[8] others have reported Weibull moduli of between 14 and 39 for similar materials.[9,10] In light of these results, it is not clear whether the high reliability observed in these silicon nitride ceramics is due to the coarse grain size, elongated grain shape (resulting in a strong *T*-curve), or a narrow distribution of critical flaws.

Recently, we demonstrated increased flaw tolerance in alumina ceramics containing 1% glass and attributed this increase to a broad grain size distribution; the coarse grains act as effective bridging sites.[11] In this study, we investigate the role of grain size distribution on the flaw tolerance and strength variability of ultra-high-purity alumina. Specifically, we intend to determine if the presence of a small number of coarse grains introduced by broadening the grain size distribution (while keeping the mean grain size constant) improves the flaw tolerance and, if so, whether the improved flaw tolerance translates into reduced strength variability.

II. Experimental Procedure

In order to control the width of the grain size distribution while simultaneously keeping all other microstructural variables constant, it was necessary to manufacture specimens in our own laboratory using a high-purity starting powder. Many of the details regarding the processing and mechanical testing have been discussed previously[7] and thus only a short summary will be given here.

(1) Processing

An ultra-high-purity alumina powder[‡] (Sumitomo AKP-50, Sumitomo Chemical Company, New York, NY) was uniaxially pressed in a graphite die at 28 MPa into disk-shaped compacts approximately 25 mm in diameter and 2.75 mm thick, and subsequently isostatically pressed at 280 MPa. The specimens were packed in powder of identical composition and placed in a high-purity alumina crucible to be fired.

The specimens were divided into two batches and were fired in air using a $MoSi_2$ furnace and the firing profiles shown in Fig. 1. One batch was continuously heated at a rate of 10°C/min to 1700°C and then held at temperature for 25 h in order to sinter the powder compacts and simultaneously coarsen the microstructure (the dashed line in Fig. 1). The other batch of specimens was given a precoarsening treatment prior to sintering to make the microstructure more uniform.[12,13] This was accomplished by step-heating during the ramp cycle; beginning at 1000°C, the temperature was held for 4 h and then increased

in increments of 200°C up to the sintering temperature (the solid line in Fig. 1). Both batches of specimens were sintered at 1700°C for 25 h.

(2)   Microstructure Characterization

Densities were determined using Archimedes' method with water as the immersion medium. In order to analyze the microstructure, specimens were ground and polished to a 1 μm mirrorlike finish using diamond pads and diamond slurries and subsequently thermally etched at 1600°C for 15 min to reveal the grain boundaries. Representative SEM photomicrographs of the microstructure were then digitized using a scanner. A semiautomated image analysis was performed on the digitized images in order to determine the area, major axis, and minor axis of each grain (Image 1.52, NIH, Bethesda, MD). Over 600 grains were measured from three different specimens for each batch of alumina in order to sample a representative number of grains. The equivalent circular diameter was determined from the area, assuming that each grain was spherical, using the formula[14]

$$d = 2 \sqrt{\frac{A}{\pi}} \tag{1}$$

where d is the grain diameter and A is the area. The three-dimensional mean grain size, $\bar{d}$, was calculated by multiplying the mean equivalent circular diameter by 1.5.

Two different methods were used to represent the grain size distributions. The first is the conventional plot of frequency versus grain size, in which the number of grains falling within a specific size interval (normalized by the total number of grains counted) is plotted versus the grain size. This method gives equal weight to all grains, independent of size, and therefore is not sensitive to small changes at the extremes of the distribution. Presumably, coarse grains have a greater influence on macroscopic mechanical properties such as fracture toughness and strength compared to fine grains. Therefore, a method of plotting the data was desired that gives a more representative weighting to the large grains. This was accomplished by plotting the *area fraction* versus the grain size. The area fraction was calculated by first transforming the grain size data into areas, classifying the areas into uniform intervals, followed by normalizing the sum of the cumulative area in each interval by the total area of all grains that were measured.
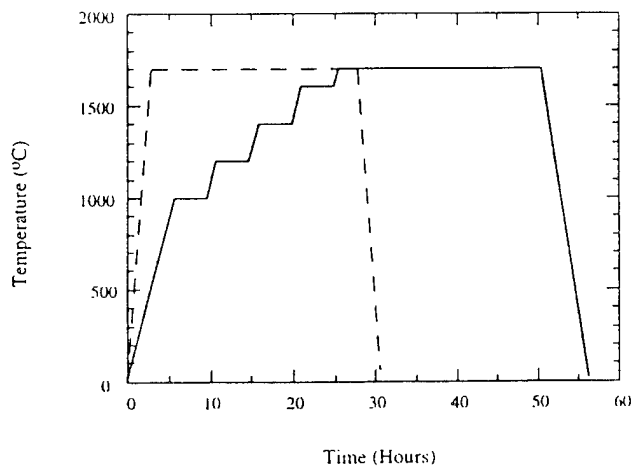

Fig. 1. The dashed line is the heating profile for specimens that were continuously heated at 10°C/min to 1700°C and then held at that temperature for 25 h. The solid line is the heating profile for specimens that were heated slowly (3°C/min) to 1000°C and then soaked at that temperature for 4 h before being heated an additional 200°C. This was repeated every 200°C until the temperature reached 1700°C, after which the temperature was held for 25 h. The cooling rate for both batches of specimens was 10°C/min.

The aspect ratio was determined directly from the ratio of the major axis to the minor axis. The major and minor axes were determined by obtaining a best fit to an ellipse for each grain. Because the aspect ratio was used only as a relative comparison between the two materials, no attempt was made at correcting the aspect ratio to account for the fact that the data were obtained from a two-dimensional plane of polish.

(3)   Mechanical Tests

Mechanical tests were performed to determine the influence of microstructure on the strength and fracture properties. Strength as a function of indentation load was used as a measure of flaw tolerance for each material and was also used to calculate short-crack T-curve behavior. In addition, strengths of unindented specimens were determined and the variability in strengths correlated to mechanical reliability.

(A)   Flaw Tolerance Tests: Disk-shaped specimens were ground to a nominal 2.5 mm thickness and polished on one side to a mirrorlike finish to remove preexisting surface damage. The polished surfaces were then indented at loads ranging from 5 to 200 N using a Vickers diamond indenter. A drop of silicone oil was applied to the indentation to minimize environmentally assisted subcritical crack growth prior to strength testing. Specimens were fractured using a servo-hydraulic testing machine at a high stressing rate of approximately 20000 MPa/s (to minimize the effects of static fatigue) according to ASTM F394-78.[15] The load at fracture was measured with a load cell and, in conjunction with the specimen dimensions, used to calculate the strength based on thin plate theory.

After fracture, all of the indented specimens were analyzed using optical microscopy in bright-field and Nomarski contrast modes to determine the origin of fracture. Only data from specimens in which the critical crack intersected the indentation impression were used in this study. Fracture surfaces of some of the specimens were examined in the SEM to determine the shape of the indentation crack.

(B)   T-Curves: T-curves were calculated from the flaw tolerance data using the technique developed by Braun et al.[16] Using this technique, it is possible to deconvolute the short-crack T-curves of materials with no assumptions about the shape of the T-curve or the toughening mechanism.

The underlying equations that govern crack extension for a flaw in the presence of residual stress due to an indentation are given by

$$T(c) \leq \sigma_A \psi \sqrt{c} + \frac{\chi P}{c^{3/2}} \tag{2a}$$

and

$$T(c) = T_0 + T_\mu(c) \tag{2b}$$

where $T(c)$ is the crack-length-dependent toughness, σ_A is the applied stress during loading, ψ is the crack shape parameter, c is the crack length, χ is the material-dependent residual stress parameter, P is the indentation load, T_0 is the intrinsic grain-boundary toughness, and $T_\mu(c)$ is the crack-tip shielding term due to grain bridging.[17] While the indentation load is known and the strength is calculated from the load, χ and ψ must be determined independently in order to calculate the T-curve.

Initially, we intended to calculate ψ and χ directly from SEM observations of fracture surfaces. However, for the aluminas investigated in this study, dimensions of the initial indentation crack were difficult to determine. For this reason, ψ, and χ were determined for a control alumina having similar purity, but a fine grain size of 5 μm. Indentation cracks ($P = 100$ N) in these specimens were readily apparent on fracture surfaces and allowed accurate determination of the crack shape. ψ was calculated from measurements of crack length, c, and crack depth, a, and the equation[18]

$$\psi = \frac{1.12 \sqrt{\pi a/c}}{\int_0^{\pi/2} \left[1 - \left(\frac{c^2 - a^2}{c^2} \right) \sin^2(\theta) \right]^{1/2} d\theta} \tag{3}$$

χ was obtained from

$$\chi = \xi \sqrt{\frac{E}{H}} \qquad (4)$$

where ξ is a material-independent parameter $= 0.016$,[19] E is Young's modulus, and H is the hardness. Young's modulus was determined acoustically using the pulsed-overlap technique;[20] hardness was determined from the measurement of the indentation impression diagonals and Lawn's expression for hardness.[17] Once these parameters were determined for the fine-grain control alumina, we assumed that they were also valid for the coarser aluminas examined in this study.

(C) Strength: Disk-shaped specimens were used to measure the natural, *unindented* strength of each material in order to eliminate edge effects that are often present in other loading configurations. All specimens were polished to a 1 μm finish and then fractured in air in the same manner as described in Section II(3)(A). A minimum of 24 specimens were then used for each batch of alumina. Selected specimens were then examined in a SEM in an attempt to determine the origin of failure. The strength values were ranked and the probability of failure, P_t, calculated using the following estimator:

$$P_t = \frac{i - 0.5}{n} \qquad (5)$$

where i is the ith sample to be ranked and n is the total number of samples tested. The data were then plotted using a traditional Weibull scale (plotting $\log \{\ln(1/(1 - P_t))\}$ versus $\log$ strength).

III. Results

(1) Characterization

The densities of the step-heated and continuously heated aluminas were, respectively, 99.0% and 99.1% of theoretical. SEM photomicrographs of polished and etched surfaces of representative specimens from the two batches of materials are shown in Figs. 2(a) and (b). The microstructures appear similar; a few small pores (1–5 μm) are located at triple points and along grain boundaries. Occasional intragranular porosity is also observed. The step-heated specimens, however, appear to have a more uniform grain size distribution than the continuously heated specimens. For example, grains as large as 55 μm are visible in the continuously fired specimens, while the step-heated specimens appear to have a maximum grain size of approximately 35 μm. The grain shape in both materials appears equiaxed.

From the quantitative image analyses, the mean grain size of both materials was determined to be approximately 10 μm. The grain size distributions based on number fraction are shown in Figs. 3(a) and (b). The grain size distribution in the step-heated material is narrow with a standard deviation of 4.9 μm. In contrast, the continuously heated alumina with the broader distribution has a standard deviation of 5.6 μm. More importantly, a small number of coarse grains (>25 μm) are present in the continuously heated specimens, indicated by the tail in the distribution. When these data are replotted based on area fractions (Figs. 4(a) and (b)), the presence of the larger grains becomes more apparent. In fact, in the continuously heated alumina, about 11% of the area on a two-dimensional plane of polish, is made up of grains with a mean grain size of 38 μm or larger. In contrast, less than 1% of the area on a polished surface is made up of grains larger than 38 μm in the step-heated material.

The aspect ratios for the step-heated and continuously heated aluminas were 1.53 ± 0.52 and 1.62 ± 0.66, respectively, indicating that the grain shapes were statistically equivalent and approximately equiaxed.

(2) Mechanical Properties

(A) Flaw Tolerance: Strength as a function of indentation load is plotted (log–log scale) for each batch of alumina in Fig. 5. Each data point represents the mean strength from a minimum of four specimens, and the error bars indicate one standard deviation about the mean. The solid line is the predicted behavior for a Griffith-like material with a single-valued toughness (slope $= -1/3$).[17] From Fig. 5, it is clear that the materials behave similarly. No plateau in the strength is observed at small indentation loads, indicating only a modest degree of flaw tolerance. More importantly, from the similarity in data, it is apparent that the presence of a small number of large grains in an otherwise uniform microstructure *does not* significantly affect the flaw tolerance in these high-purity alumina ceramics.

(B) T-Curves: SEM observations of indentation cracks ($P = 100$ N) in the fine-grained control alumina revealed that the shape of the cracks was semielliptical with a crack length of 208 ± 7 μm and a crack depth of 193 ± 19 μm. Inserting these values into Eq. (3) gives $\psi = 1.26 \pm 0.07$. The hardness of the control material was 18.2 ± 0.4 GPa and Young's modulus was 391 GPa which, using Eq. (4), yields $\chi = 0.074 \pm 0.004$ (compared with previous estimates of $\chi = 0.071$–0.076 for similar aluminas.[16,19] Assuming self-similarity in the crack morphologies with the fine-grain control alumina, short-crack

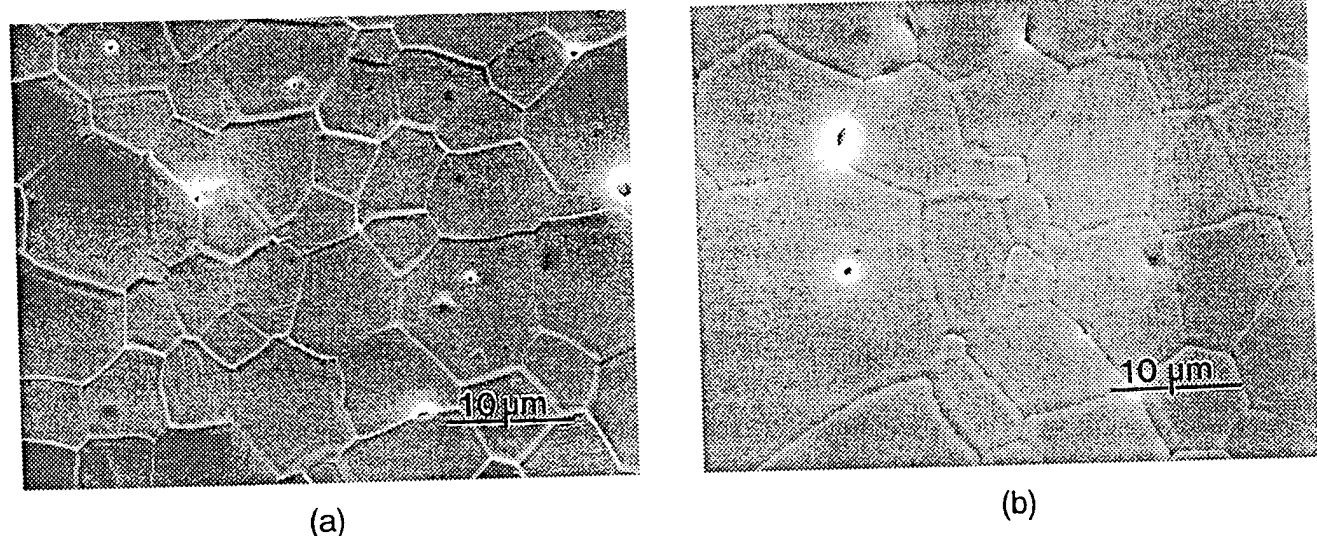
(a)   (b)

Fig. 2. Scanning electron micrographs of polished and thermally etched specimens for specimens that were (a) step-heated and (b) continuously heated. The density of both batches of material is approximately 99% of theoretical with occasional small pores present at triple junctions, along grain boundaries, and in the bulk. The grain shape appears equiaxed in both aluminas.
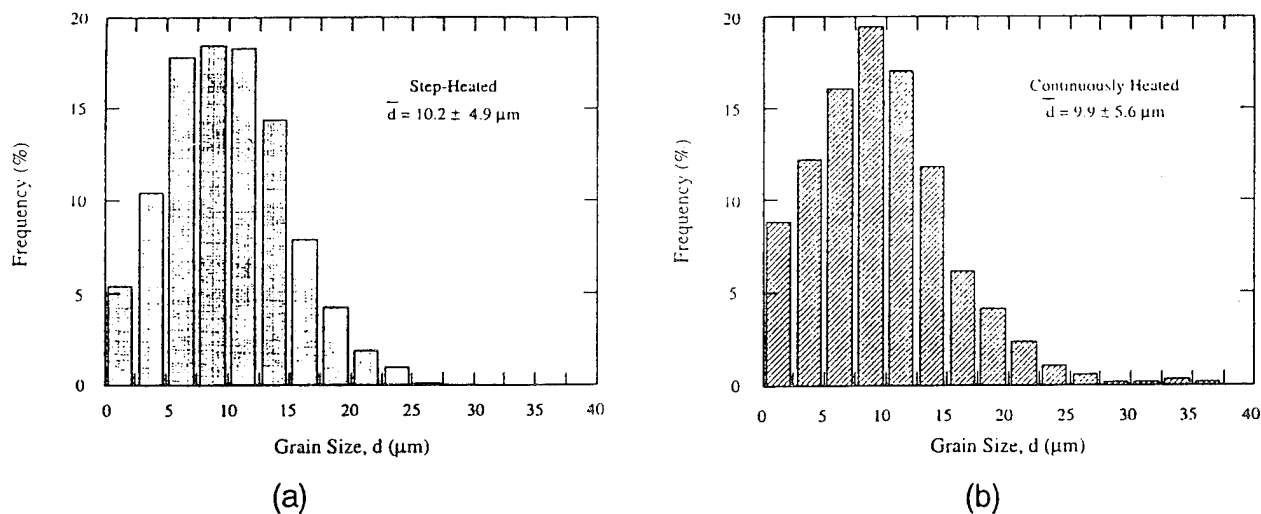
Fig. 3. Grain size distributions for (a) step-heated and (b) continuously heated specimens. Normalized frequency is shown as a function of grain size. The mean grain size in both materials is approximately 10 μm. Grain size distributions are similar, although a slight tail exists in the continuously heated alumina at grain sizes larger than about 25 μm.

T-curves were then determined from the flaw tolerance data for the continuously heated and step-heated aluminas. The results are shown in Figs. 6(a) and (b). The materials exhibit nearly identical behavior with an initial toughness of approximtely 3.5 MPa·m$^{1/2}$ rising to a toughness of approximately 5.5 MPa·m$^{1/2}$ over a crack extension of 800 μm.

(C) Strength: Weibull plots for polished specimens for each material are shown in Fig. 7. The materials exhibit qualitatively similar behavior; the data are clearly nonlinear indicating that the strength characteristics are not adequately described by a two-parameter Weibull distribution. In the high-strength region, both sets of data have a steep slope indicative of a relatively high Weibull modulus. However, an abrupt change of slope occurs in both plots at approximately 300 MPa, below which the data show much greater variability in strength.

Nevertheless, the mean strengths for both aluminas are similar; the step-heated material has a strength of 396 MPa while the continuously heated material has a strength of 373 MPa. Although statistically there is no difference between the mean strengths, *there is a difference in the strength variability.* The step-heated material with the narrow grain size distribution has a standard deviation of 90 MPa compared to a standard deviation of 132 MPa for the continuously heated material with the broader grain size distribution. The difference in strength

variability can be attribued almost entirely to a few low-strength specimens in the continuously heated alumina. For example, one specimen had a strength of only 75 MPa.

Selected specimens from each batch of material were examined using an optical microscope and an SEM in order to determine the origin of failure. Viewing the fracture surfaces in the SEM, no pores larger than approximately 25 μm were detected. Similarly, no large agglomerates were found near the specimen surface where the failure is most likely to have originated (recalling that these are bend specimens). The critical flaw was therefore thought to be associated with large grains or clusters of large grains. In both aluminas (but with greater frequency in the continuously heated alumina), a few clusters of abnormally large grains were detected at or near the fracture surface of the specimens as shown in Fig. 8 (the arrowed feature). It should be noted that because so few of these clusters of abnormal grains were present in only a limited number of specimens, these grains were not detected in the analyses of the grain size distributions.

IV. Discussion

(1) Flaw Tolerance

Although these materials did show a small degree of flaw tolerance as evidenced by the slight deviation from ideal behav-
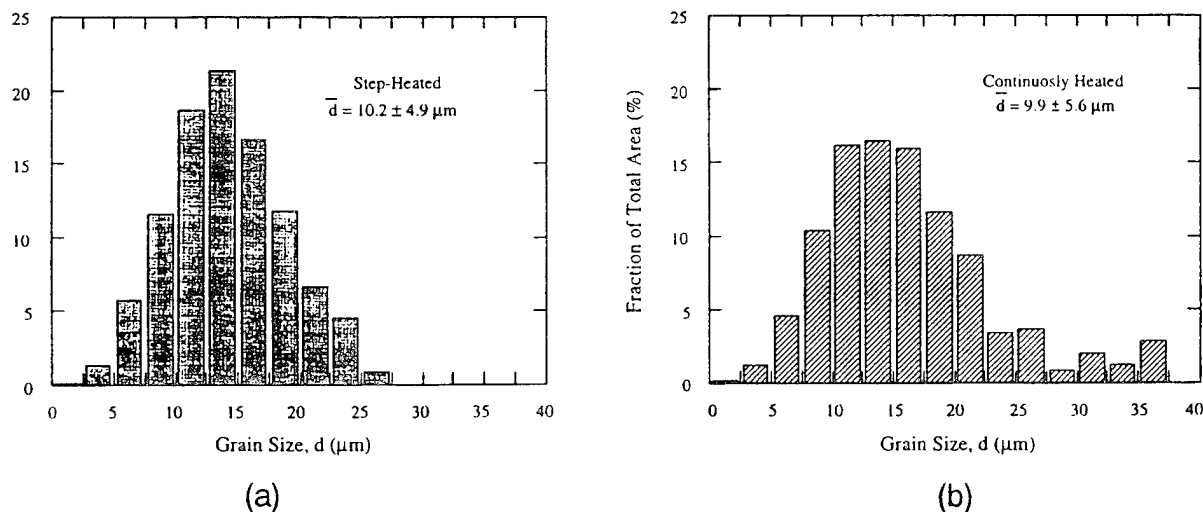

Fig. 4. The data from Figs. 3(a) and (b) are replotted as fraction of the total area versus grain size on the abscissa, revealing that a significantly greater fraction of the area is occupied by large grains in the continuously heated alumina vis á vis the step-heated alumina.
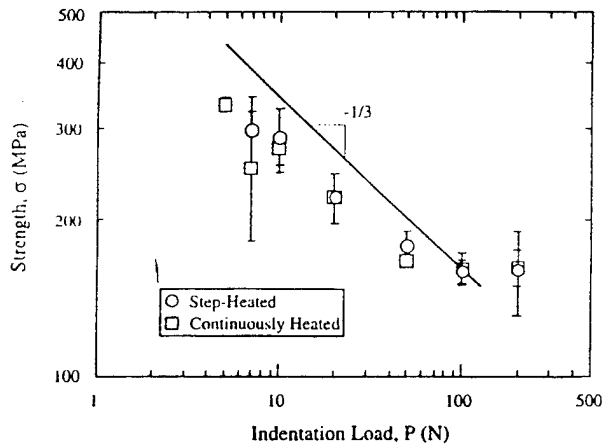
Fig. 5. Strength as a function of indentation load for step-heated and continously heated aluminas. Each data point represents a minimum of four specimens, and the error bars represent one standard deviation. The materials exhibit similar behavior with only modest deviation from Griffith-like behavior ($-1/3$ slope), indicating that the presence of larger grains in the continuously heated alumina does not appreciably affect the flaw tolerance. The plateau in strength at large indentation loads is likely due to lateral cracking.[29]

ior shown in Fig. 5, neither material exhibited a plateau in the strength at low indentation loads, indicating that the presence of large grains in the alumina with a broad distribution did not appreciably improve flaw tolerance relative to the alumina with a narrow distribution in grain sizes.[*] Observations of crack extension on polished surfaces as well as fractographic analyses on fractured surfaces indicated that larger grains fractured transgranularly with little or no pullout and thus did not contribute to toughening by grain bridging; most of the grain bridging was provided by smaller grains, which fractured intergranularly (Fig. 9). Because large grains do not appreciably contribute to bridging in these aluminas, further broadening of the grain size distribution would not be expected to improve flaw tolerance.

---

[*]We distinguish here between the large grains (~40 μm) observed in *all* of the rapidly-fired specimens and the relatively few abnormal grains (>100 μm) present in both rapidly fired and step-fired specimens.

It should be emphasized that this phenomenon is not universal to all nontransforming ceramics, since the crack path is ultimately influenced by a number of factors including grain boundary toughness, bulk toughness, grain size and grain shape. For example, Cook *et al.* has shown that aluminas with similar mean grain sizes can show substantial flaw tolerance.[21] However, with respect to microstructural design, our results suggest that there may be a limit to the efficacy of increasing the grain size to promote grain bridging in high-purity ceramics with "strong" grain boundaries, such as in the aluminas used in this study. More potent grain bridging in coarse-grained alumina requires weakening the grain boundaries, achieved by the introduction of elements that segregate to the grain boundaries, or by incorporating weak second phases along the grain boundaries.[11,21,22]

(2) T-Curve Behavior and Crack Stability

The modest *T*-curve behavior displayed by both batches of aluminas also influences the measured strength distribution. Consider, for example, that in ceramics having *T*-curve behavior, catastrophic failure occurs when the total crack driving force exceeds the fracture toughness:

$$K_{app} > T(c) \tag{6a}$$

and

$$\frac{dK_{app}}{dc} > \frac{dT(c)}{dc} \tag{6b}$$

where K_{app} is the applied stress intensity, $T(c)$ is the apparent toughness of the material, and c is the critical flaw size. For a natural, processing flaw, the applied stress intensity is given by

$$K_{app} = \sigma_{app} \psi \sqrt{c} \tag{7}$$

Superimposing $T(c)$ over plots of K_{app} versus the square root of crack length permits a graphical description of the failure criteria by means of the now well-known "tangency construction."[23]

Assuming that the short-crack *T*-curves calculated for the aluminas used in this study are correct,[†] then we see that a

---

[†]There is some debate in the literature about whether χ and ψ can be treated as material constants. Since these were not determined directly for the coarse-grained aluminas, we cannot address these assumptions. However, Bleise *et al.*[24] and Krause[25] have shown that corrections to ψ result in *T*-curves that rise even more slowly than those calculated here.
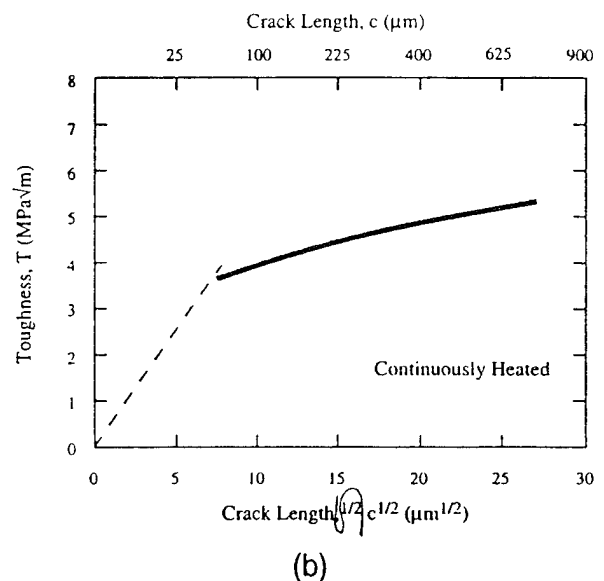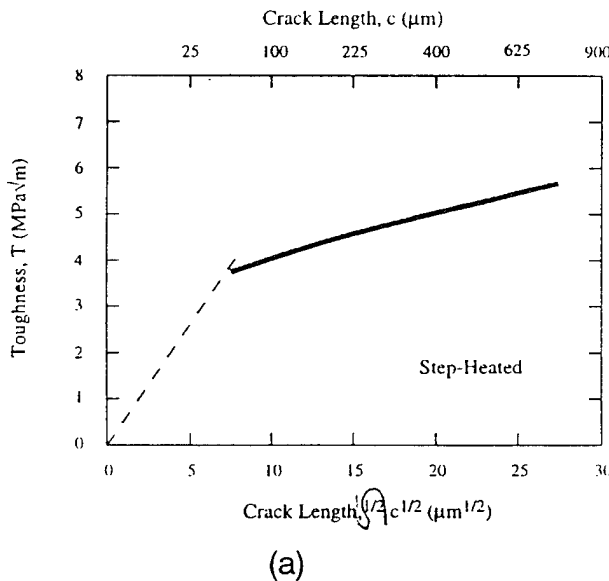

(a)

(b)

Fig. 6. Apparent fracture toughness versus the square root of crack length for (a) the step-heated and (b) continuously heated aluminas determined from the data in Fig. 5. The fracture toughness rises slightly from an initial value of 3.5 to approximately 5.5 MPa·m$^{1/2}$ over 800 μm of crack extension.
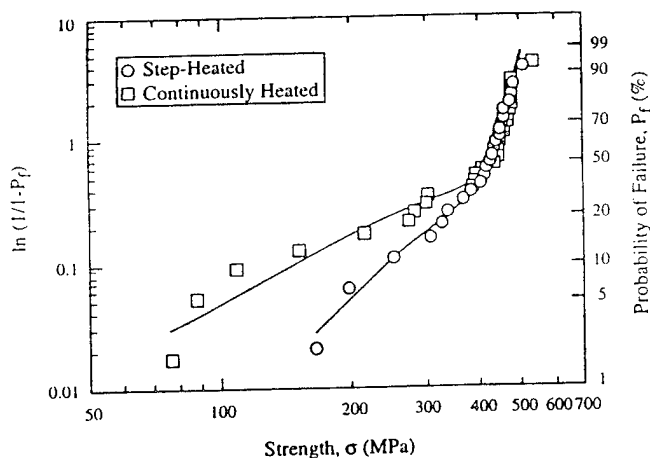
Fig. 7. Weibull plot for step-heated and continuously heated aluminas. The alumina with a narrow distribution in grain sizes shows reliability superior to the material with a broad distribution in grain sizes. A distinct tail is visible in the continuously heated alumina with a broad grain size distribution indicative of partially concurrent flaw populations.

Fig. 9. Optical micrograph of a crack in a polished and thermally etched specimen with a broad grain size distribution is shown. Most of the crack deflection and bridging occurs at small to medium size grains (indicated by "B") while large grains fracture transgranularly (indicated by "T") *without* grain pullout.

graphical tangency construction (Figs. 6(a) and (b)) predicts that *no stable extension should occur from natural flaws, and thus the strength is dependent only on the initial flaw size and the initial fracture toughness.* Indeed, in many ceramics that exhibit thermal expansion anisotropy, including alumina, initial crack extension along tensile grain facets reduces the apparent toughness and may actually lead to strength degradation if the T-curve does not rise rapidly enough to ensure stable crack extension prior to failure.[26]

In the case of ceramics having modestly rising T-curves such as those in this study, differences may exist between the strength measured from certain natural flaws and from postprocessing flaws such as particle impact damage. Postprocessing flaws are associated with strong residual stresses that significantly influence the relationships governing crack extension. In contrast, for natural processing flaws, residual stresses may be greatly reduced or even nonexistent.[tt] This can best be illustrated by considering failure from a postprocessing flaw such as

an indentation. For indentation damage, the apparent toughness is modified by the addition of a stabilizing term resulting from the indentation-induced residual stress:[tt17]

$$T(c) = T_0 + T_\mu - \frac{\chi P}{c^{3/2}} \tag{8}$$

Comparing Eq. (8) to the crack extension criteria in Eqs. 6a and 6b, we see that the effect of the indentation residual stress is to greatly reduce the apparent toughness of the material at small crack sizes.

The distinction between failure from processing and postprocessing flaws is illustrated in Fig. 10, where catastrophic failure is compared in the *same material* for (1) a flaw free of residual

---

[tt]Residual stresses may also develop upon cooling from processing temperature in the vicinity of certain types of natural flaws (e.g., inclusion particles or at pores that lie along grain boundaries in thermally anisotropic materials such as alumina) which will also affect the strength.
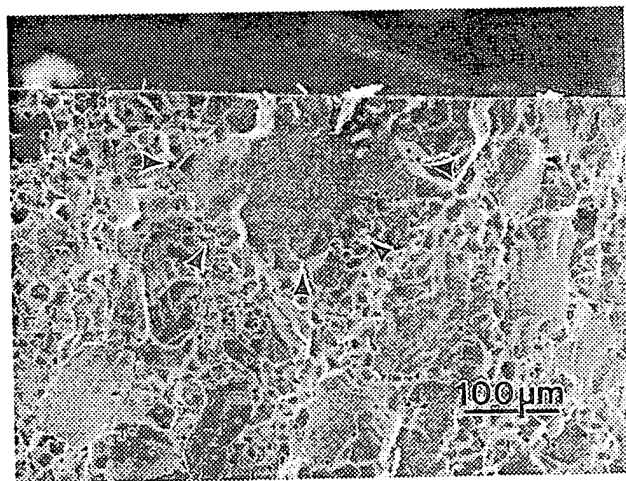

[tt]Rather than incorporating the indentation-induced residual stress field into the applied stress field acting on the flaw, as is usually done,[18] we have incorporated the residual field into the apparent toughness of the material. This has the advantage of allowing us to use Eqs. (6a) and (6b) and the familiar linear graphical tangency construction to determine the failure criterion directly.

Fig. 8. SEM micrograph of the fracture surface in the vicinity of the failure origin for the alumina with a broad grain size distribution that failed at a stress of 284 MPa. No large agglomerates or pores are present, and it appears that a large grain (marked by arrows) was the cause of failure.
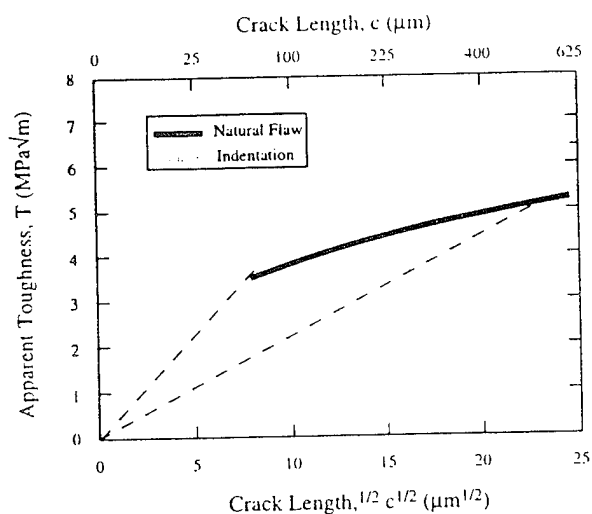
Fig. 10. T-curves for the alumina with a broad grain size distribution. The shaded line represents the T-curves for indentation flaws at an indentation load of 100 N. The dark line represents the T-curve in the same material for a flaw free of tensile residual stresses (such as for a natural flaw). Graphical tangency analyses show that no stable crack extension would be predicted from natural flaws; however, postprocessing defects should grow stably prior to failure.

stresses, and (2) an indentation crack at a load of 100 N. In materials that exhibit *T*-curve behavior, we see that the combination of the stabilizing field from crack-tip shielding (e.g., T_μ) and the indentation residual stress lead to stable crack extension from the postprocessing defect. However, no stable crack extension is predicted from the natural flaw, despite the rising toughness. Thus, while the strength of the natural flaw is *directly dependent on the initial flaw size and the initial toughness*, for postprocessing flaws with an attendant tensile residual stress, the strength of a specimen is not directly related to the initial flaw size or initial fracture toughness. Instead, the *strength is dependent on both the shape and magnitude of the T-curve*, as well as the magnitude of the impact or indentation. The strength for materials with modest *T*-curves that contain both natural and postprocessing flaws (the case for many materials in service applications) is therefore very much dependent on the history of the critical flaw. This issue will be addressed in greater detail in a future paper.[27]

(3) Strength Variability

The strength distributions from the two batches of polished specimens (Fig. 7) did not fit a two- or three-parameter Weibull distribution, making a quantitative comparison of the reliability of the two materials difficult. For instance, the shape of the curves suggests that multiple flaw populations were operative in these materials. As stated in Section III(2)(C), fractographic evidence supports the notion that large grains are related to failure in both batches of materials. In addition, a small fraction of abnormally large grains were observed in both aluminas, but with a greater frequency in the continuously heated alumina. This suggests that two independent flaw distributions were responsible for failure in these aluminas: one associated with the normal distribution of grains and a second from the distribution of abnormal grains.[§§] If, as appears to be the case in these materials, all specimens contain flaws of one type and *some* specimens contain flaws of a second type, the flaw populations are said to be partially concurrent.[28] Under these conditions, the total probability of failure, P_T from partially concurrent flaw populations is given by

$$P_T = 1 - \left\{ (1 - P_B) \exp\left[-\left(\frac{\sigma_M}{\sigma_{uA}}\right)^{m_A} \right] \right\}$$
$$- \left\{ (P_B) \exp\left[-\left(\frac{\sigma_M}{\sigma_{uA}}\right)^{m_A} - \left(\frac{\sigma_M}{\sigma_{uB}}\right)^{m_B} \right] \right\} \qquad (9)$$

where P_B is the probability of failure associated with flaw distribution B, σ_M is the maximum stress in the specimen, σ_{uA} is the scale parameter for flaw distribution A, σ_{uB} is the scale parameter for flaw distribution B, m_A and m_B are the respective Weibull moduli for flaw distributions A and B. The data from Fig. 7 were fitted using a nonlinear least-squares algorithm using P_B, σ_{uA}, σ_{uB}, m_A, and m_B as fitting parameters; the results are shown in Table I. For this analysis, it was assumed that all specimens contained flaws of type A (associated with normal grains), and that some specimens contained flaws of type B (associated with abnormally large grains). The fitted lines are plotted as solid lines in Fig. 7; there is excellent agreement between the data and the partially concurrent flaw population model.

The utility of Eq. (9) is that it allows us, in theory, to separate the two contributions to strength variability: (1) the presence of abnormally large grains, and (2) the role of broadening the distribution of normal grains. Using this technique, the probability of failure from abnormally large grains (type B) was estimated to be 42% in the continuously heated material and only 25% in the step-heated material. These results are consistent with the observations that there was a much greater probability of finding abnormally large grains in the continuously

Table I. Best-Fit Values of the Parameters Resulting from Fitting Eq. (9) to the Strength Data*

	Step-Heated	Continuously Heated
m_A	14	21
m_B	4	2
σ_{uA} (MPa)	454	467
σ_{uB} (MPa)	301	300
P_B (%)	25	42

*Note that the continuously fired material exhibits a greater probability of containing an abnormal grain.

heated material. When we consider failures from flaws of type A (normal grains) only, we find similar strength variability in the continuously heated specimens and the step-heated specimens, given the number of specimens that were tested and the number of fitting parameters necessary for the model. No statistical difference was found in Weibull modulus (14 versus 21) or scale parameter (454 versus 467 MPa) between the two materials.

V. Conclusions

Two batches of highly pure alumina ceramics were manufactured with an equiaxed grain morphology and a mean grain size of 10 μm. One batch was step-heated and contained a narrow distribution of grain sizes while the other batch was continuously heated and contained a broader distribution of grain sizes. Both materials showed similarly modest degrees of flaw tolerance, indicating that broadening the distribution in grain sizes did not enhance *T*-curve behavior. Observations of crack paths suggested that there may exist an upper limit to the size of grains that can act as bridges in these aluminas; grains larger than this upper limit fracture transgranularly with no apparent pullout.

Analysis of the short-crack *T*-curves revealed that although both batches of aluminas exhibited a rising toughness, neither material should exhibit stable crack extension prior to failure from many types of natural flaws. This implies that in the case of *processing defects* such as pores and agglomerates, the strength is determined by *initial flaw size* and *initial fracture toughness*. Therefore, when failure initiates from these processing defects, these ceramics see none of the beneficial effects of *T*-curve behavior such as flaw tolerance and associated improvements in reliability.

However, in the case of postprocessing damage involving residual stress fields, the combination of a rising fracture toughness (even the minor amount observed here) and the stabilizing influence of the residual stress associated with the flaw will result in considerable stable crack extension. It is therefore possible for a material that shows no stable crack extension from natural flaws to exhibit flaw tolerance from postprocessing damage and hence show improved reliability in the presence of postprocessing damage.

Lastly, it was found that both of the materials tested contain two distributions of natural flaws. Based on the shape of the strength distributions and fractography, it was determined that the two flaw distributions are partially concurrent. No significant improvement in reliability was detected as the grain size distribution was broadened, even if the influence of abnormal grains is eliminated altogether. The effect of the heat treatment is to, in fact, increase the fraction of abnormal grains, which has a much greater influence on the strength distribution in high-purity, equiaxed alumina ceramics.

These results have important implications toward the design and production of advanced ceramics. For many ceramics with modest *T*-curve behavior, stable crack extension may not precede catastrophic failure from natural flaws, even in coarse microstructures. In this case, the elimination of large-scale defects (agglomerates, pores, abnormal grains, etc.) through careful processing can improve the reliability that is measured in the laboratory. However, the strength will still be sensitive to

---

[§§]We refrain from stating that the grains themselves were the failure origins. Postmortem analysis indicated only the presence of the abnormal grains near the high-stress regions in the bend specimens.

damage that may evolve in service, and thus the reliability of a component may be compromised in aggressive environments. To produce truly reliable ceramics, the strength of a material must be insensitive to both processing and postprocessing flaws. This can be accomplished only if the *T*-curve is sufficiently steep to cause stable crack extension from *all* types of flaws.

References

[1]H. Hübner and W. Jillek, "Sub-Critical Crack Extension and Crack Resistance in Polycrystalline Alumina," *J. Mater. Sci.*, **12**, 117–25 (1977).

[2]R. W. Steinbrech and O. Schmenkel, "Crack Resistance Curves of Surface Cracks in Alumina," *J. Am. Ceram. Soc.*, **71** [5] C-271–C-273 (1988).

[3]P. Chantikul, S. J. Bennison, and B. R. Lawn, "Role of Grain Size in the Strength and *R*-Curve Properties of Alumina," *J. Am. Ceram. Soc.*, **73** [8] 2419–72 (1990).

[4]G. Vekinis, M. F. Ashby, and P. W. R. Beaumont, "*R*-Curve Behaviour of Al_2O_3 Ceramics," *Acta Metall. Mater.*, **38** [6] 1151–62 (1990).

[5]S. J. Bennison and B. R. Lawn, "Flaw Tolerance in Ceramics with Rising Crack Resistance Characteristics," *J. Mater. Sci.*, **24**, 3169–75 (1989).

[6]N. Ramachandran, L. Y. Chao, and D. K. Shetty, "*R*-Curve Behavior and Flaw Insensitivity of Ce-TZP/Al_2O_3 Composite," *J. Am. Ceram. Soc.*, **76** [4] 961–69 (1993).

[7]D. Kovar and M. J. Ready, "The Role of Grain Size in Strength Variability of Alumina," *J. Am. Ceram. Soc.*, **77** [7] 1928–38 (1994).

[8]N. Hirosaki, Y. Akimune, and M. Mitomo, "Effect of Grain Growth of β-Silicon Nitride on Strength, Weibull Modulus, and Fracture Toughness," *J. Am. Ceram. Soc.*, **76** [7] 1892–94 (1993).

[9]C. W. Li and J. Yamanis, "Super Tough Silicon Nitride with *R*-Curve Behavior," *Ceram. Eng. Sci. Proc.*, **10** [7–8] 622–45 (1986).

[10]P. Dusza and P. Sajgalík, "Mechanical Properties of Si_3N_4 + β-Si_3N_4 Whisker Reinforced Alumina," *J. Eur. Ceram. Soc.*, **9** [1] 9–17 (1992).

[11]H. O'Donnel, M. J. Ready, and D. Kovar, "Effect of Glass Additions on the Indentation Strength Behavior of Alumina," *J. Am. Ceram. Soc.*, **78** [4] 849–56 (1995).

[12]M.-Y. Chu, M. N. Rahaman, and L. C. De Jonghe, "Effect of Heating Rate on Sintering and Coarsening," *J. Am. Ceram. Soc.*, **74** [6] 1217–25 (1991).

[13]M.-Y. Chu, L. C. De Jonghe, M. K. F. Lin, and F. J. T. Lin, "Precoarsening to Improve Microstructure and Sintering of Powder Compacts," *J. Am. Ceram. Soc.*, **74** [11] 2902–11 (1991).

[14]J. C. Russ, Computer Assisted Microscopy—The Measurement and Analysis of Images. Plenum Press, New York, 1990.

[15]F 394-78, Standard Test Method for Biaxial Flexure Strength (Modulus of Rupture) of Ceramic Substrates, Vol. 15.02, *Glass; Ceramics Whitewares*. Edited by P. C. Fazio *et al.* American Society for Testing and Materials, Philadelphia, PA, 1978.

[16]L. M. Braun, S. J. Bennison, and B. R. Lawn, "Objective Evaluation of Short Crack Toughness Curves Using Indentation Flaws: Case Study on Alumina-Based Ceramics," *J. Am. Ceram. Soc.*, **75** [11] 3049–57 (1992).

[17]B. R. Lawn, *Fracture of Brittle Solids*, 2nd ed. Cambridge University Press, Cambridge, UK, 1993.

[18]P. C. Paris and G. C. M. Sih, "Stress Analysis of Cracks"; pp. 30–82 in *Fracture Toughness Testing and Its Applications*. American Society for Testing and Materials, Philadelphia, PA, 1965.

[19]G. R. Anstis, P. Chantikul, B. R. Lawn, and D. B. Marshall, "A Critical Evaluation of the Indentation Techniques for Measuring Fracture Toughness: I. Direct Crack Measurements," *J. Am. Ceram. Soc.*, **64** [9] 533–38 (1981).

[20]G. V. Blessing, "The Pulsed Ultrasonic Velocity Method for Determining Material Dynamic Elastic Moduli"; pp. 47–57 in *Dynamic Elastic Modulus Measurements in Materials*, ASTM STP 1045. Edited by A. Wolfenden. American Society for Testing and Materials, Philadelphia, PA, 1990.

[21]R. F. Cook, B. R. Lawn, and C. J. Fairbanks, "Microstructure–Strength Properties in Ceramics: I. Effect of Crack Size on Toughness," *J. Am. Ceram. Soc.*, **68** [11] 604–15 (1985).

[22]R. F. Cook, "Segregation Effects in the Fracture of Brittle Materials: Ca-Al_2O_3," *Acta Metall. Mater.*, **38** [6] 1083–110 (1990).

[23]D. Broek, *Elementary Engineering Fracture Mechanics*, 4th ed. Kluwer Academic Publishers, Dordecht, The Netherlands, 1991.

[24]D. Bleise and R. W. Steinbrech, "Flat *R*-Curve from Stable Propagation of Indentation Cracks in Coarse-Grained Alumina," *J. Am. Ceram. Soc.*, **77** [2] 315–22 (1994).

[25]R. F. Krause, "Flat and Rising *R*-curves for Elliptical Surface Cracks from Indentation and Superposed Flexure," *J. Am. Ceram. Soc.*, **77** [1] 172–78 (1994).

[26]S. J. Bennison and B. R. Lawn, "Role of Interfacial Grain-Bridging Sliding Friction in the Crack-Resistance and Strength Properties of Nontransforming Ceramics," *Acta Metall.*, **37** [10] 2659–71 (1989).

[27]D. Kovar and M. J. Ready, "Strength Variability in Ceramics with Increasing Fracture Toughness," unpublished work.

[28]C. A. Johnson, "Fracture Statistics of Multiple Flaw Distributions"; pp. 365–86 in Fracture Mechanics of Ceramics, Vol. 5, *Surface Flaws, Statistics, and Microcracking*. Edited by R. C. Bradt, A. G. Evans, D. P. H. Hasselman, and F. F. Lange. Plenum Press, New York, 1983.

[29]R. F. Cook and D. H. Roach, "The Effect of Lateral Crack Growth on the Strength of Contact Flaws in Brittle Materials," *J. Mater. Res.*, **1** [4] 589–600 (1986).   □

APPENDIX 7

THE EFFECT OF GRAIN SHAPE ON STRENGTH VARIABILITY OF ALUMINA CERAMICS

Michael J. Readey
Glass and Electronic Ceramics
Sandia National Laboratories
Albuquerque, NM 87185-0333

Desiderio Kovar
Department of Materials Science and Engineering
Carnegie Mellon University
Pittsburgh, PA 15213

INTRODUCTION

During the past several years, various theories have emerged suggesting that ceramics having flaw tolerance due to an increasing fracture toughness (R or T-curve behavior) will also have an improved reliability, usually defined in terms of variability in strength.[1-3] This is an attractive approach to achieving reliable structural components, primarily because failure becomes less dependent on the size of either processing or in-service generated defects. Thus, defect-free components via expensive cleanroom processing are not required, and long-term reliability is ensured due to enhanced damage tolerance.

The link between high reliability and a rising fracture toughness is motivated by the encouraging results of transformation-toughened ceramics, namely Mg-PSZ and Ce-TZP.[2,4] In these ceramics, high Weibull moduli are typically observed in ceramics having a high fracture toughness, and low Weibull moduli are associated with zirconias having a low fracture toughness. Indeed, a systematic investigation on Mg-PSZ by Readey and McNamara demonstrated that the Weibull modulus correlates directly with enhanced T-curve behavior and flaw tolerance.[5]

However, results in monolithic, non-transforming ceramics toughened mainly by grain bridging have been less promising. For example, Kovar and Readey have shown that there is *no* improvement in reliability in spite of enhanced flaw tolerance in high-purity alumina ceramics having controlled grain sizes and equiaxed grain morphologies.[6] This same conclusion was also obtained by Rodel and co-workers on a similar material.[7]

Many systematic studies involving grain-bridging in alumina ceramics have focused on grain size as the critical microstructural feature responsible for the enhanced fracture

toughness. However, recent experimental evidence on high-purity aluminas doped with a small amount of a calcium aluminosilicate glass has suggested that grain *shape* may in fact be more important with respect to grain bridging.[8] This is not surprising; witness that elongated microstructures in silicon nitride ceramics exhibit much higher fracture toughnesses than typically achieved in silicon nitride having an equiaxed grain morphology.[9,10]

In this study, the strength variability of several aluminas having similar average grain sizes but equiaxed or elongated grain morphologies are compared and correlated to their flaw tolerance and T-curve behavior. Specifically, we address the issue of whether coarse grain microstructures having elongated grain morphologies result in greater flaw tolerance and reduced variability in strength.

EXPERIMENTAL PROCEDURE

Processing

Equiaxed microstructures were fabricated from ultra-high purity alumina powder (99.997% purity, AKP-50, Sumitomo Chemical Company). Microstructures containing elongated grains were prepared from commercial-purity alumina powder (99.7%, A-16SG, ALCOA), the predominant impurities being MgO, Na_2O, SiO_2 as well as trace quantities of CaO and FeO. Both powders were free of large agglomerates and relatively uniform in shape and size with mean particle sizes of 0.3 and 0.5 μm for the AKP-50 and A-16SG, respectively.

Powder compacts approximately 25 mm in diameter by 3 mm thick were prepared by first uniaxially pressing as-received powders in a high-purity graphite die (AF-Grade, POCO Graphite Inc.) at compaction pressures between 20 and 28 MPa. These disks were then isopressed at 280 MPa to minimize gradients in green density. The green compacts were then placed in high-purity alumina crucibles, packed in powder of the same composition, and sintered in air to 1600°C for a period of 5 hours. Some specimens were then given an additional heat-treatment at 1700°C for 25 hours in order to coarsen the microstructure. Heating and cooling rates were typically 5°C/min and 10°C/min, respectively.

Microstructure Characterization

Density measurements were conducted on all sintered aluminas using Archimedes' method with distilled water as the immersion medium. Densities were further corrected for the water temperature, and typically had an accuracy of ±0.02 g/cm³. Quantitative information concerning the microstructure was obtained by first grinding and polishing one surface of the disks, followed by a thermal-etch treatment at 1500°C for 15 minutes to reveal the grain boundaries. Optical or scanning electron micrographs were then taken of representative areas, and the grain boundaries highlighted manually. These highlighted images were then digitized using a 300 dpi scanner, and the images converted to black and white binary images. The area of individual grains were then measured using a commercial image analysis program (Image 1.41, National Institute of Health). The two dimensional grain size (diameter) was calculated from the areas assuming spherical grains. The aspect ratio of each grain was calculated by fitting an ellipse to each grain and calculating the ratio of the major to minor axes. At least 500 grains were measured for each heat-treatment condition in order to obtain reliable statistics.

Mechanical Properties

Strength measurements were made on disk-shaped specimens using a biaxial flexure test according to ASTM standards (flat-on-3 balls).[11] Prior to testing, as-fired specimens were ground flat and polished on one side to a mirror-like finish using one micron diamond paste. The tensile surface was the polished surface in all cases. The specimens were centered on the three support balls, and loaded to failure at a rapid loading rate of 20 GPa/sec in order to minimize environmentally assisted slow crack growth. Strength was then calculated from the maximum load using thin plate theory.[11]

The indentation strength in bending (ISB) test was used to assess the flaw tolerance of the aluminas, as well to calculate the fracture toughness curves (T-curves).[12,13] Disk-shaped specimens that were polished on one side were indented with a Vickers indentor using loads 2 and 200 N. Immediately following the indentation, a drop of silicone oil was placed on the indent to exclude moisture from the indentation cracks. Specimens were then fractured as usual. After fracture, all specimens were examined using an optical or scanning electron microscope (SEM) to ensure failure originated from the indentation. Those specimens that did not fail from indentations were excluded from the analysis.

T-curves were calculated from the ISB data based on the technique of Braun *et al.*[14] Details on calibrating the indentation coefficients ψ and χ are given elsewhere.[6] The shape of the crack was determined by observing the fracture surface of indented specimens and noting the crack length and depth. Crack shape parameters for elliptical cracks were then calculated from the crack length measurements.[15]

The variability in strength was evaluated as a function of microstructure by measuring both the indented and unindented strengths of approximately 30 specimens from each material. The strength data were then ranked and each datum assigned a probability of failure according to:

$$P_f = \frac{i-0.5}{N} \qquad (1)$$

where i is ranking, and N is the total number of specimens tested. For the unindented specimens, two parameter Weibull statistics were used to determine the variability in strength, using the maximum likelihood estimator technique to calculate the Weibull modulus.[16] For the indented specimens, the flaw sizes were normally distributed, and a Gaussian distribution was used to describe the strength distribution. In this case, the strength variability was defined by the coefficient of variation by taking the ratio of the mean strength to the sample standard deviation. (In this way, the coefficient of variation is analogous to the Weibull modulus; it is a direct measure of the breadth of the strength distribution.)

RESULTS

Microstructure

Densities for all four aluminas were greater than 98 % of theoretical. Details are shown in Table 1. SEM photomicrographs of the microstructures from representative sintered specimens that were polished and thermally etched are shown in Figure 1. From the micrographs, it is evident that aluminas fired at 1600°C had a significantly finer microstructure than those heat-treated at 1700°C. In the case of the high-purity alumina, the grains are equiaxed, with a relatively narrow grain size distribution that remains

self-similar during coarsening. The commercial-purity alumina has a broader grain size distribution, with pockets of small grains surrounding larger grains. In addition, many grains are tabular or elongated in shape with one or more flat, faceted edges. Previously, it has been demonstrated in similar aluminas that flat grain boundaries and tabular grain shapes are due to the presence of a traces impurities forming a liquid phase at the grain boundaries during sintering, leading to solution-reprecipitation phenomenon that lowers the overall grain boundary energy.[17] Average grain sizes and aspect ratios are shown in Table 1. For the sake of clarification, these aluminas will be referred to as "f" (fine) or "c" (coarse) grained microstructures consisting of "eq" (equiaxed) or "el" (elongated) grain morphologies.

Indentation-Strength

Strength as a function of indentation load for the high-purity and commercial-purity aluminas are shown in Figure 2. The solid lines represent the theoretical behavior expected for materials that have a constant fracture toughness[12]; the natural strength of polished (unindented) specimens is indicated by a hatched box on the left hand side of each plot. Comparing the natural strength of the four aluminas, it is apparent that strength decreases with increasing grain size for both the commercial-purity and high-purity aluminas. Furthermore, the strength at similar mean grain sizes is lower for the commercial-purity aluminas than for the high-purity aluminas. These results are consistent with the results of previous investigations using similar aluminas.[13]

The indentation-strength response of the f-eq alumina exhibits classical brittle behavior with a slope very close to the theoretical value of -1/3, while the f-el alumina and the c-eq alumina both exhibit a slight deviation from -1/3 behavior. In contrast, the c-el alumina shows the greatest deviation from Griffith-like behavior with almost no dependence of strength on indentation load at small loads, albeit at the expense of a lower unindented strength. At large indentation loads, a plateau in the indentation-strength response is apparent in both coarse aluminas. This behavior is generally attributed to extensive lateral cracking and is not associated with flaw tolerance.[18]

Strength Variability

Weibull plots for polished (unindented) specimens are shown for the four aluminas in Figure 3. The f-eq alumina has the highest mean strength followed by the c-eq alumina, the f-el alumina, and the c-el alumina. The Weibull moduli and characteristic strengths as determined using the MLE method along with the confidence limits obtained from the parametric bootstrap technique are shown in Table 2. The Weibull moduli vary from 7.8 and 5.3 for the fine-grained and coarse-grained high-purity aluminas, respectively, to 9.2 and 14.8 for the fine-grained and coarse-grained commercial-purity aluminas. From the confidence limits, a statistical difference in Weibull modulus exists between the c-el aluminas and all of the other aluminas and also between the c-eq and the f-el alumina. Thus, only the c-el alumina, which exhibits strong flaw tolerance, shows a statistically significant higher Weibull modulus.

Strength Variability from Controlled Flaws

Strictly speaking, it is not possible to determine if the differences in strength variability observed in Figure 3 are due to flaw tolerance or whether they are instead due to a narrowing of the critical flaw distribution (*i.e.*, because of different powder sources).

Thus, strength tests were also conducted on specimens containing controlled indentation flaws at an indentation load of 100 N; the results are plotted using a probability scale in Figure 4. This indentation load was chosen because it was sufficiently large to ensure that failure always occurred from the indentation cracks and yet the extent of lateral cracking was minimized.

As expected from the indentation-strength responses of the aluminas, the f-eq alumina exhibits the lowest mean strength for indented specimens. The c-eq and f-el materials have comparable strengths which are slightly higher, while c-el alumina has the highest mean strength. The coefficient of variation, C_v, determined for each data set is not statistically different among any of the materials; it ranged from 5.7 to 6.7%. Thus, although the mean strength increases with flaw tolerance, the strength variability measured from controlled, indentation defects does not appear to be sensitive to the microstructure. These results imply that the enhanced flaw tolerance in coarse-grained aluminas does not directly lead to a reduction in the strength variability of alumina.

Crack lengths were measured in an attempt to quantify the critical flaw size distribution; a summary of the radial crack sizes is shown in Table 3 for each alumina. The f-eq had the largest flaw size and exhibited the least variability, with a coefficient of variation of 5.0%. Cracks sizes in the other materials were typically smaller, but showed an increase in variability; the coefficient of variation ranged from 8.3% to 11.7%. Thus, although controlled indentation flaws (at a constant indentation load) were used to initiate failure in all of the specimens, the critical flaw size distributions were *not* equivalent in these materials. Moreover, while the strength variability does not appear to be sensitive to the microstructure, the indentation crack lengths are clearly linked to the scale of the microstructure; variability in crack size increases with grain size and grain aspect ratio. Most significant, however, is the fact that although the variability in the indentation flaw sizes increases with grain size and aspect ratio, the strength variability is not affected by changes in the critical flaw size distribution for indented specimens.

T-Curve Behavior

The indentation-strength technique provides a relatively simple way to determine the fracture toughness at very small crack sizes comparable to the scale of the microstructure. T-curves determined from the indentation-strength method and lines corresponding to the maximum strength (i.e., tangent construction) are shown for the four aluminas in Figure 5. The T-curve for the f-eq alumina is almost flat indicating that the fracture toughness of this material is nearly constant. The f-el and c-eq aluminas have similar T-curves that rise from 3.5 MPa.m$^{1/2}$ at a crack length of 50 μm to 4.5-5 MPa.m$^{1/2}$ after 700 μm of crack extension. The c-el alumina exhibits the most pronounced T-curve rising rapidly from a toughness of 2.8 MPa.m$^{1/2}$ at 70 μm to more than 5 MPa.m$^{1/2}$ at a crack length of 700 μm.

There are a number of important features that are apparent from these T-curves; most notably, increases in T-curve behavior in alumina do not come without penalty. Consistent with previous observations in alumina and other grain-bridging ceramics, the increase in toughness at long crack lengths comes at the expense of the short-crack toughness.[19] This is particularly apparent in c-el material where the long-crack toughness is highest and the initial toughness is lowest of all of the aluminas. Another important point is that even the most pronounced T-curves rise relatively gradually in these materials. In fact, the tangency construction predicts stable crack extension from natural flaws occurs only for the c-el alumina (Fig. 5). This suggests that, with the exception of the c-el alumina, strength is dependent on the *initial* flaw size. Hence little benefit is derived from the T-curve in terms of reducing variability in strength.

DISCUSSION

Flaw Tolerance

The experimental results indicate that both grain size and grain shape play a role in determining the fracture behavior of alumina. Increasing the mean grain size only modestly increases the flaw tolerance and T-curve behavior of high-purity alumina having equiaxed grain morphologies. In contrast, the coarse-grained commercial-purity aluminas having elongated grain morphologies exhibited much stronger flaw tolerance. Such improved flaw tolerance results from a combination factors. For one, the elongated grain morphology results in a high fraction of large grains which can act as effective bridges. Second, the crack paths in the commercial-purity aluminas tended to be much more tortuous. Evidently the minor impurities present in the commercial-purity alumina powders promote intergranular fracture necessary for strong grain bridging. Thus, it appears it is the combination of weaker boundaries and large, elongated grains that are responsible for the improvement in flaw tolerance in the aluminas used in this study. For example, it was shown that neither large grains (c-eq alumina) nor an elongated grain morphology (f-el) by themselves lead to improvements in flaw tolerance. Strong flaw tolerance in the c-el alumina results due to the presence large, elongated grains and equally important, weak grain boundaries which are needed to generate a tortuous crack path necessary to get strong mechanical interlocking of the bridges.

Strength Variability

Weibull plots for polished specimens from Figure 3 indicate that, in general, strength variability decreases with increasing flaw tolerance, provided the T-curve responsible for the flaw tolerance is considerable. Similar results were found by Ting et al. for a series of alumina ceramics where the highest Weibull modulus was obtained for a material with a broad grain size distribution and an elongated grain shape while the poorest reliability was obtained for an equiaxed alumina with a narrow grain size distribution.[20] In addition, Hoffman and Petzow both found similar results for silicon nitride.[10] Ting et al. argued that the improvement in reliability in materials with increased heterogeneity in the microstructure was due a narrowing in the critical flaw size distribution. They suggested that in materials that have a narrow grain size distribution, the presence of a few large grains in only some of the specimens results in a large scatter in strength because the strength is controlled by these large grains. In contrast, materials with heterogeneous microstructures contain a more uniform dispersion of large grains and therefore, these materials exhibit less variability in strength. On the other hand, Hoffman and Petzow argued that it is T-curve behavior rather than a narrowing in the initial flaw size that is responsible for the improvement in reliability in silicon nitride ceramics.[10] Evaluating whether it is T-curve behavior or changes in the critical flaw size distribution that leads to improvements in reliability involves quantifying the critical flaw size distribution, which is experimentally difficult, particularly in coarse-grained ceramics.

Introducing controlled critical flaws through the use of indentations allows one to isolate the influence of flaw size on strength variability. In our tests, strength tests on specimens indented at an indentation load of 100 N revealed that there was essentially *no* difference in the variability in strength in aluminas with vastly different microstructures. However, measurements of the distribution in critical crack sizes, showed that distribution in the size of the cracks varied greatly depending on the material. Cracks in the coarse-grained elongated alumina had more than twice the variability compared to the fine-grained, equiaxed alumina, yet no difference in strength variability was detected. This

suggests that narrowing of the critical crack sizes distribution by itself cannot account for the improvement reliability measured in coarse-grained ceramics such as the c-el alumina in this study. This suggests that a combination of a narrow flaw population *and* strong T-curve is necessary for improved reliability in ceramics toughened by grain bridging.

CONCLUSIONS

Fine-grained and coarse-grained aluminas containing either equiaxed or elongated grain structures were fabricated from commercial-purity and high-purity alumina powders. Compared to the high-purity aluminas, the commercial-purity aluminas having a coarse grain size and elongated grain structures exhibited significantly more pronounced flaw tolerance and T-curve behavior. Thus, microstructural features other than just mean grain size were found to be important in determining the fracture properties of alumina. T-curve behavior determined from indentation strength tests suggested that only the coarse-grained, elongated-grain alumina had a T-curve sufficient to cause stable crack extension prior to failure, a requirement for any observable improvement in reliability. In the high-purity aluminas as well as the fine-grained commercial-purity aluminas, however, it is likely that little or no stable extension occurs prior failure. Thus strength in these materials is dependent solely on the critical flaw size.

Strength tests on polished specimens showed the commercial-purity aluminas had a lower mean strength than the high-purity aluminas and the coarse-grained aluminas exhibited a lower mean strength compared to the fine-grained aluminas. An analysis of the mean strength versus grain size revealed that the differences in the critical flaw size alone could not account for the differences in mean strength. Instead, a combination of changes in flaw size as well as T-curve behavior were shown to be responsible for the differences in strength and flaw tolerance. T-curve behavior was also found to have a profound influence on the strength variability of alumina. For example, the Weibull modulus for the coarse-grained, commercial-purity alumina was almost twice that of the fine-grained, high-purity material. Tests with indented specimens conclusively demonstrated that improvements in reliability in these materials are not due solely to changes in the critical flaw size distribution but rather a combination of flaw size distribution and T-curve behavior.

Acknowledgements

REFERENCES

1. K. Kendall, N. McN. Alford, S.R. Tan, and J.D. Birchall, The Influence of Toughness on Weibull Modulus of Ceramic Bending Strength, *J. Mater. Res.*, 1:120 (1986).
2. D.K. Shetty and J.S. Wang, Crack Stability and Strength Distribution of Ceramics that Exhibit a Rising Crack Growth Resistance (R-Curve) Behavior, *J. Am. Ceram. Soc.*, 72:1158 (1989).

3. R.F. Cook and D.R. Clarke, Fracture Stability, R-curves, and Strength Variability, *Acta metall.*, 36:555 (1992).

4. M.J. Readey, P.D. McNamara, C.L. McCallen, and B.R. Lawn, Correlations Between Flaw Tolerance and Reliability in Zirconia Ceramics, *J. Mat. Sci.*, 28:6748 (1993).

5. M.J. Readey and P.D. McNamara, R-Curve Behavior, Flaw Tolerance, and Strength Variability in Mg-PSZ, submitted to the *J. Am. Ceram. Soc.*, (1995).

6. D. Kovar and M.J. Readey, The Effect of Grain Size on Strength Variability of Alumina, *J. Am. Ceram. Soc.*, 77:1928 (1994).

7. J. Seidel, N. Claussen and J. Rodel, Reliability of Alumina Ceramics: Effect of Grain Size, *J. Europ. Ceram. Soc.*, 15:395 (1995).

8. H.L. O'Donnell, M.J. Readey and D. Kovar, Effect of Glass Additions on the Indentation Strength Behavior of Alumina, *J. Am. Ceram. Soc.*, 78:849 (1995).

9. P. Becher, Advances in the Design of Toughened Ceramics, *J. Ceram. Soc. Jap. Int. Ed.*, 99:962 (1991).

10. M.J. Hoffman and G. Petzow, Microstructural Design of Si_3N_4 Based Ceramics, *in* "Silicon Nitride Ceramics: Scientific and Technological Advances," Vol 287, Materials Research Society Proceedings, I.W. Chen, ed. MRS Publishers, Boston (1989).

11. ASTM F 394-78, Standard Test Method for Biaxial Flexure Strength (Modulus of Rupture), in Annual Book if ASTM Standards, Vol. 15.02, P.C. Fazio, ed. American Society for Testing and Materials,Philadelphia (1978).

12. B.R. Lawn, Fracture of Brittle Solids, 2nd edition. Cambridge University Press, Cambridge (1993).

13. P. Chantikul, S.J. Bennison and B.R. Lawn, "Role of Grain Size in the Strength and R-Curve Properties of Alumina, *J. Am. Ceram. Soc.*, 73:2419 (1990).

14. L.M. Braun, S.J. Bennison and B.R. Lawn, Objective Evaluation of Short Crack Toughness Curves Using Indentation Flaws: Case Study on Alumina-Based Ceramics, *J. Am. Ceram. Soc.*, 64:533 (1981).

15. P.C. Paris and G.C.M. Sih, Stress Analysis of Cracks, in Fracture Toughness Testing and its Applications. American Society for Testing and Materials, Philadelphia (1965).

16. C.A. Johnson and W.T. Tucker, Weibull Estimators for Pooled Fracture Data, *in* "Life Prediction Methodologies and Data for Ceramic Materials", C.R. Brinkman and S.F. Duffy, eds. American Society for Testing and Materials, Philadelphia (1994).

17. W.A. Kaysser, M. Sprissler, C.A. Handweker, and J.E. Blendell, Effect of a Liquid Phase on the Morphology of Grain Growth in Alumina, *J. Am. Ceram. Soc.*, 70:339 (1987).

18. R.F. Cook, E.G. Liniger, R.W. Steinbrech, and F. Deueler, Sigmoidal Indentation-Strength Characteristics of Polycrystalline Alumina, *J. Am. Ceram. Soc.*, 77:303 (1994).

19. N.P. Padture, J.L. Runyan, S.J. Bennison, L.M. Braun, and B.R. Lawn, Model for Toughness Curves in Two-Phase Ceramics, *J. Am. Ceram. Soc.*, 76:2241 (1993).

20. J.M. Ting, R.Y. Lin and Y.H. Ko, Effect of Powder Characteristics on Microstructure and Strength Characteristics of Sintered Alumina, *Am. Ceram. Soc. Bull.*, 70:1167 (1991).

Table 1. Physical properties of alumina ceramics.

Alumina	Heat-Treatment	Density (g/cm^3)	Grain Size (µm)	Aspect Ratio
High-Purity*	1600°C/5h	3.91	5.0 ± 2.6	1.5
High-Purity*	1600°C/5h + 1700°C/25h	3.93	10.2 ± 4.9	1.5
Commercial-Purity**	1600°C/5h	3.93	4.0 ± 3.9	2.1
Commercial-Purity**	1600°C/5h + 1700°C/25h	3.91	12.8 ± 11.4	2

* AKP-50, 99.997% purity, Sumitomo Chemical Company.
**A16-SG, 99.7% purity, ALCOA

Table 2. Characteristic strengths, Weibull moduli including 90% confidence limits (m_5 and m_{95}) for the four aluminas. Note that only the c-el shows any statistically significant reduction in strength variability.

Alumina	σ_o (MPa)	m	m_5	m_{95}
f-eq	507	7.8	6.1	10.5
c-eq	369	5.3	4.2	7.1
f-el	346	9.2	7.4	11.9
c-el	243	14.8	12.1	19.8

Table 3. A comparison of the indentation crack lengths generated from a 100 N Vickers indentation. Note that the f-eq alumina exhibits significantly less variability in crack length relative to the other aluminas.

Alumina	Crack Length (μm)	Coefficient of Variation (%)
f-eq	221 ± 11	5
c-eq	182 ± 21	11.7
f-el	181 ± 15	8.3
c-el	192 ± 22	11.6
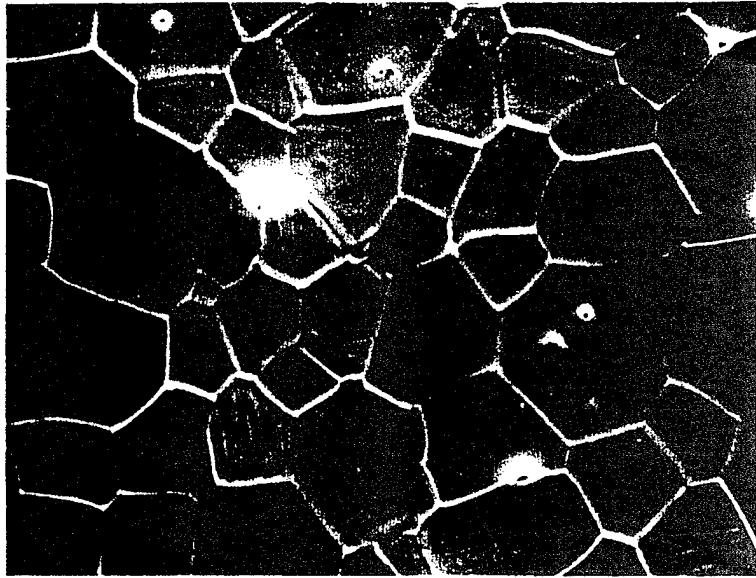
(a)
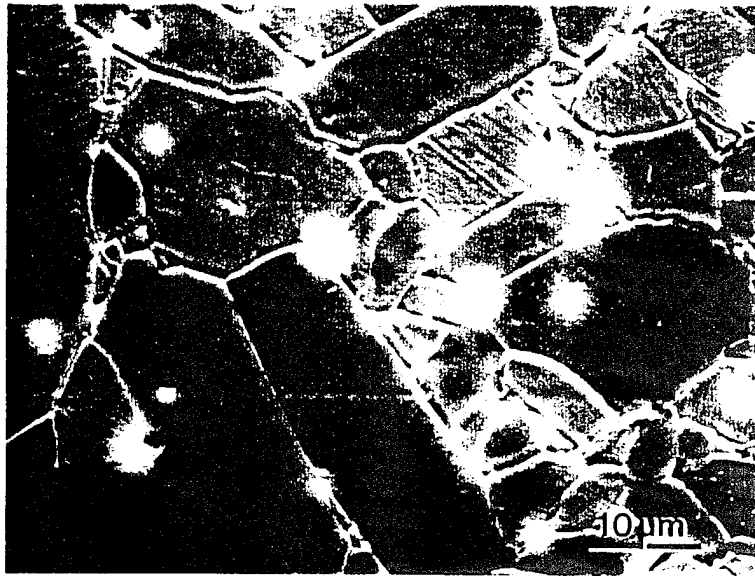
(b)

Figure 1. SEM micrographs showing the (a) high-purity alumina (b) commercial-purity aluminas sintered at 1600°C/5h.
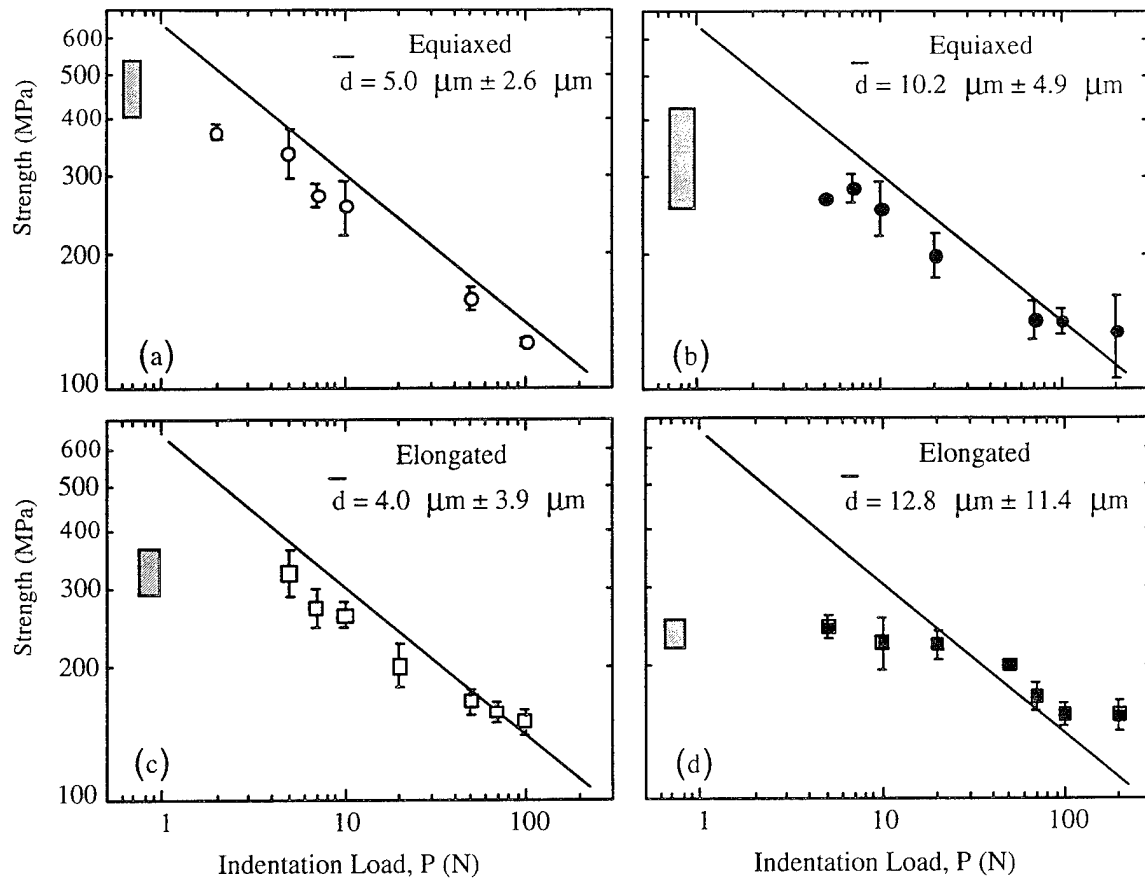
Figure 2. Strength as a function of indentation load (log-log scale) for the f-eq (a), c-eq (b), f-el (c), and c-el (d) alumina. See text for details.
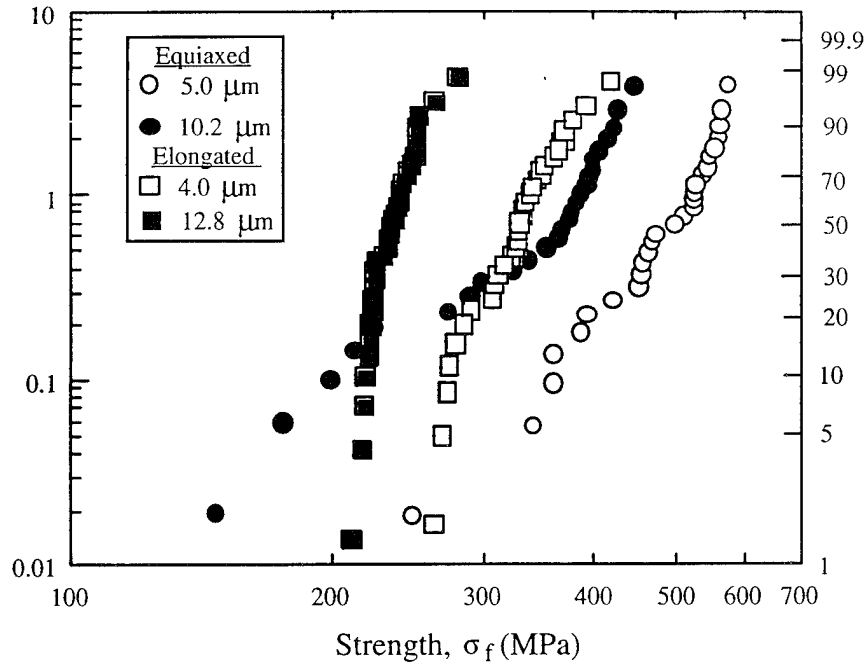
Figure 3. Weibull plot for polished specimens for the four aluminas. Although the high-purity, equiaxed aluminas have a higher average strength, the commercial-purity, elongated microstructure show the higher reliability.
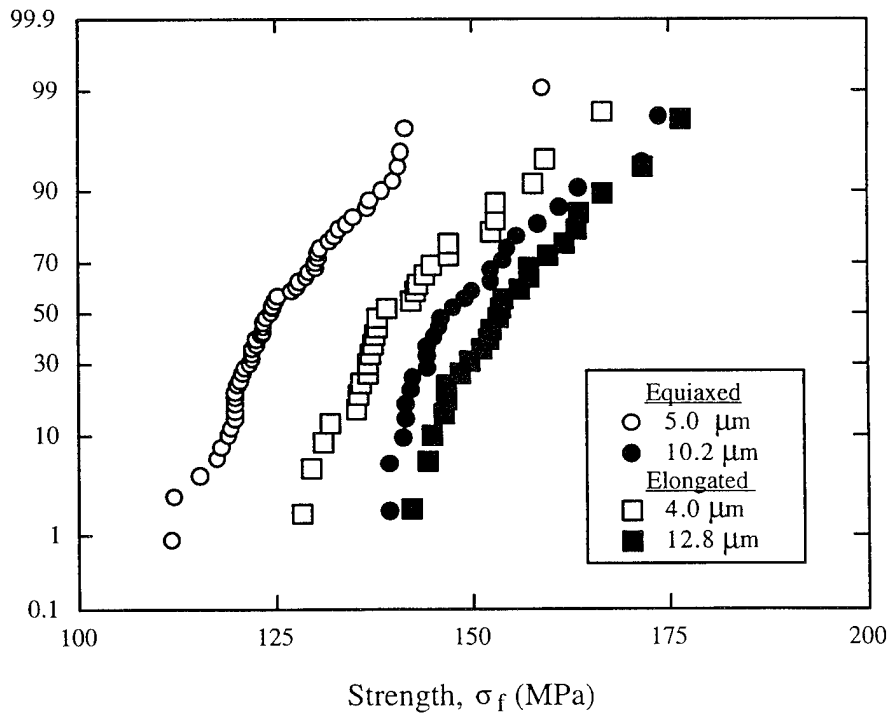

Figure 4. Strength variability for specimens that failed from 100 N Vickers indentations plotted using a probability scale. The fine-grain aluminas have a lower mean strength but the variability in strength is similar in all of the materials.
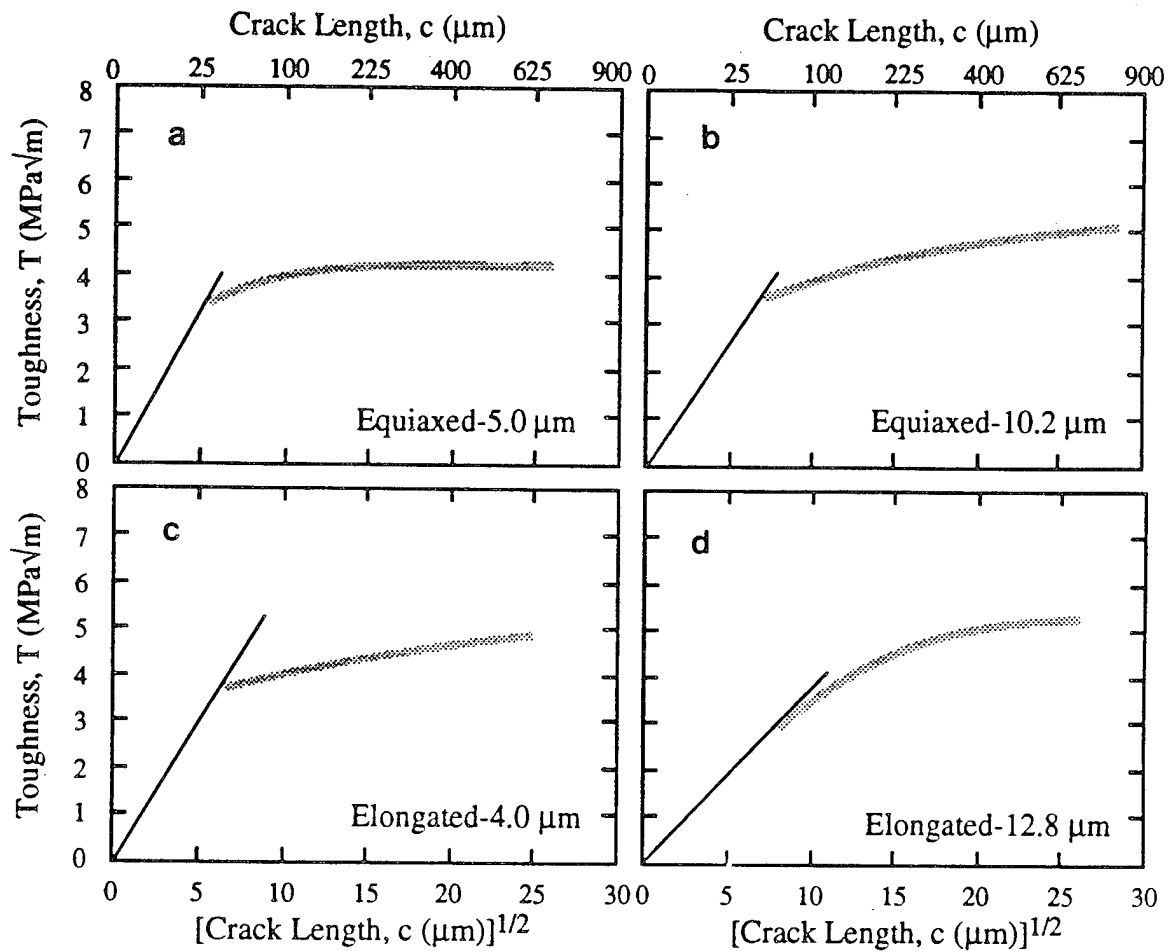
Figure 5. Toughness curves calculated from the indentation-strength data. Only the c-el alumina (d) exhibits pronounced T-curve behavior.
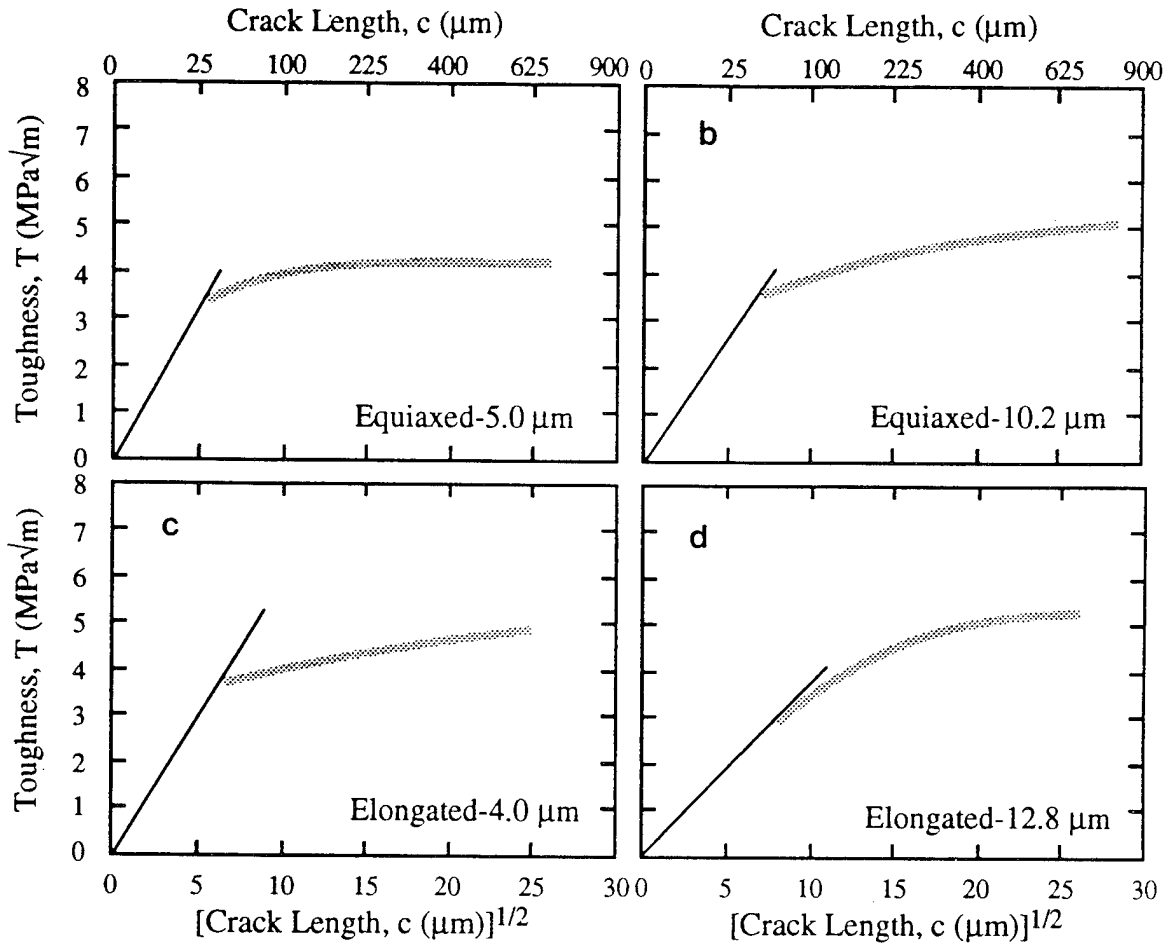
Figure 5. Toughness curves calculated from the indentation-strength data. Only the c-el alumina (d) exhibits pronounced T-curve behavior.

APPENDIX 8

EFFECT OF HEAT TREATMENT ON GRAIN SIZE, PHASE ASSEMBLAGE AND MECHANICAL PROPERTIES OF 3 mol% Y-TZP

by

Laurence Ruiz

Department of Materials Science and Engineering
Carnegie Mellon University
Pittsburgh, PA 15213

and

Michael J. Readey

Sandia National Laboratories
Glass and Electronic Ceramics
Department 1845, MS 0333
Albuquerque, NM 87185-0333

submitted to the:

Journal of the American Ceramic Society

Submitted August, 1994

Revised January, 1996

1

EFFECT OF HEAT TREATMENT ON GRAIN SIZE, PHASE ASSEMBLAGE AND MECHANICAL PROPERTIES OF 3 mol% Y-TZP

by

Laurence Ruiz*

Department of Materials Science and Engineering
Carnegie Mellon University
Pittsburgh, PA 15213

and

Michael J. Readey+**

Sandia National Laboratories
Glass and Electronic Ceramics
Department 1845, MS 0333
Albuquerque, NM 87185-0333

+ Member, American Ceramic Society

* Now at: Laboratoire de Metallurgie Chimique
Departement des Materiaux
Ecole Polytechnique Federale de Lausanne
MX-C Ecublens
CH-1015 Lausanne
Switzerland

** Correspondence should be sent to this author.

EFFECT OF HEAT TREATMENT ON GRAIN SIZE, PHASE ASSEMBLAGE AND MECHANICAL PROPERTIES OF 3 mol% Y-TZP

ABSTRACT

The effect of heat-treatment on the grain size, phase assemblage, and mechanical properties of a 3 mole percent Y-TZP ceramic was investigated. Specimens were initially sintered for two hours at 1450°C to near theoretical density; some specimens were then heat treated at 1550°C, 1650°C, 1750°C or 1850°C to coarsen the microstructure. The average grain size increased with heat treatment from < 0.5 μm to ~ 10 μm. Phase analyses revealed predominantly tetragonal and cubic phases below 1750°C, with a significant decrease in tetragonal content and increase in monoclinic content for temperatures > 1750°C. The maximum fraction of tetragonal phase that transformed during fracture corresponded with the largest tetragonal grain size of ~ 5-6 μm. Strength was on the order of 1 GPa, and was surprisingly insensitive to heat-treatment temperature and grain size, contrary to previous studies. The fracture toughness increased from 4 $MPa.m^{1/2}$ to 10 $MPa.m^{1/2}$ with increasing grain size, owing to an increasing transformation zone size. Grain sizes larger than 5-6 μm spontaneously transformed to monoclinic phase during cooling. Such critical grain sizes are much larger than found in past investigations, and may be due to the greater fraction of cubic phase present which decreases the strain energy arising from crystallographic thermal expansion anisotropy of the tetragonal phase.

EFFECT OF HEAT TREATMENT ON GRAIN SIZE, PHASE ASSEMBLAGE AND MECHANICAL PROPERTIES OF 3 mol% Y-TZP

I. Introduction

The relationships between microstructure and mechanical properties in Y-TZP ceramics have been studied extensively over the past decade.[1-4] Generally, it has been found that Y-TZP ceramics have high strength (~ 1 GPa) and fracture toughness (~ 4-5 $MPa.m^{1/2}$), making them attractive candidates for a number of demanding structural applications. It is also well established that these desirable mechanical properties are strongly influenced by grain size. For example, maximum strength is usually achieved with a small grain size (< 1 μm), whereas maximum toughness occurs at larger grain sizes (~ 2 μm). Swain and Becher have examined this grain size effect and have shown that larger tetragonal zirconia grains in TZP ceramics have a greater propensity to undergo the stress-induced phase transformation to the equilibrium monoclinic structure, resulting in an enhanced toughness.[5,6] At the same time, the strength decreases due to an increasing flaw size and more pronounced R-curve effect.[7-9]

Based on these results, several investigators have advocated coarsening Y-TZP microstructures by long, isothermal heat treatments at lower temperatures (*i.e.*, 1400-1500°C). The motivation for such long heat treatments at lower temperatures lies with the phase equilibria: lower temperatures maximize the fraction of tetragonal phase, resulting in a greater volume fraction of material available for transformation, and a potentially higher fracture toughness. For example, Swain obtained a fracture toughness of ~ 12 $MPa.m^{1/2}$ in a 2 mol % Y-TZP by coarsening the microstructure at 1500°C for approximately one hundred hours.[5] While this is approach is desirable from a technical perspective, coarsening for shorter periods of time by simply increasing the heat-treatment temperature is preferable in industrial environments for economic reasons. However, such coarsening treatments *may* influence the phase assemblage,

4

thus deleteriously affecting the mechanical properties. For instance, in 2 mol % Y-TZP, increasing the heat-treatment temperature has little influence on phase assemblage; equilibrium phase diagrams indicate > 90% tetragonal phase up to ~ 1700°C.[10] But in the 3 mole % Y-TZP ("3Y-TZP") system, which is more important commercially due to its greater ease of processing, the phase diagram (Figure 1) indicates that typical sintering temperatures (~ 1400-1600°C) lie within the tetragonal and cubic phase fields, and that increasing the heat-treatment temperature increases the fraction of cubic phase, with an attendant decrease in the tetragonal phase content.[10] Thus, while it is often more practical to coarsen the microstructure by increasing the heat-treatment temperature, one may also adversely affect the mechanical properties by decreasing the amount of tetragonal phase available for transformation.

On the other hand, it has also been shown by several investigators that the largest tetragonal grain size in Y-TZP that can be metastably retained to room temperature is of the order 1 μm,[11] depending on composition. In addition to composition, the critical grain size is influenced by the internal residual stresses owing to thermal contraction mismatch between neighboring tetragonal grains.[12,13] In c-ZrO_2, thermal expansion is isotropic, with an expansion coefficient that is roughly intermediate to the coefficient in the a- and c-directions in t-ZrO_2.[14,15] Hence the increased cubic fraction resulting from higher heat treatment temperatures should decrease the strain energy associated with thermal expansion anisotropy in t-ZrO_2 and thus may increase the critical tetragonal grain size, allowing for greater flexibility in processing.

In this study, we systematically investigated the effect of isochronal heat treatments at elevated temperatures on grain size, phase assemblage and mechanical properties of a 3Y-TZP. In particular, our study examined the extent of improvement or degradation of mechanical properties with increasing grain size but decreasing volume fraction of the transformable t-ZrO_2 phase. We then correlated these changes to the transformability of the tetragonal phase. Our

5

results suggest that the heat-treatment scheme used in this study results in much different properties than obtained by simply sintering at elevated temperatures, as was often done in past studies.

II Experimental Procedure

(1) *Material Processing*

A 3 mole % Y-TZP powder (HSY-3, Zirconia Sales of America, Atlanta, GA) having a nominal particle size of 0.15 µm and a purity greater than 99.9%* was uniaxially pressed (as-received) into disks at 80 MPa in a hardened steel die using a 1% stearic acid-propanol solution as a die lubricant. The disks were then cold-isostatically pressed at 210 MPa to increase the green density and minimize density gradients. The dimensions of the green disks measured approximately 27 mm in diameter and 4 mm in thickness. All specimens were then covered with powder of the same composition and fired in air to 1450°C for 2 h in a $MoSi_2$ resistance furnace. Some specimens were given an additional heat treatment by heating from the 1450°C sintering temperature to 1550, 1650, 1750, or 1850°C and holding for a period of 2 h. Heating rates were 5°C/min and cooling rates were 10°C/min from the maximum temperature to ~ 1000°C, whereby specimens were furnace cooled. Sintered densities were determined from Archimedes' method using distilled water as the immersion medium.

(2) *Microstructure Analysis*

All specimens were initially ground to an approximate thickness of 2 mm using a 40 µm diamond wheel and then polished on one side to a 1 µm diamond finish using standard

---

* manufacturer's claimed purity

7ceramographic techniques. Some specimens were thermally etched at 1400°C for 30 minutes to reveal the microstructure. Grain size data were obtained from representative scanning electron micrographs (SEM) of polished and etched surfaces using a semi-automatic image analysis system (Image 1.45, National Institute of Health, Bethesda, MD). The average grain size and grain size distributions were determined by measuring the area of at least 125 grains for each heat-treatment; grain areas were measured digitally and then converted to diameters assuming the grains were spheres. No further corrections were made to account for stereological effects from 2D images.

(3) Phase Analysis

X-ray diffraction was used to determine the phase content of the heat-treated Y-TZP ceramics (Cu Kα radiation, λ=0.15418 nm). X-ray spectra of ground, polished, and fracture surfaces were obtained from the same specimen by x-raying the ground (40 μm) and polished (1 μm) surfaces before strength testing, and the fractured surface after testing. Phase analyses were performed by first fitting the $(111)_{t+c}$ and $(11\text{-}1)_m$ peaks using a non-linear Lorentzian function (Peakfit 3.0, Jandel Scientific, Corte Madera, CA). The fraction of m-ZrO_2 was then calculated from integrated intensities using the method of Porter and Heuer.[16] The fraction of c-ZrO_2 was assumed to be the equilibrium volume fraction at the heat-treatment temperature, and was estimated using the lever rule and the phase diagram by Scott (Figure 1).[10] The fraction of t-ZrO_2 phase was then determined from:

$$f_t = 1 - f_c - f_m \qquad [1]$$

where f represents the volume fraction of each phase. This method slightly underestimates f_t, as undoubtedly some intragranular precipitation of the tetragonal phase will occur during cooling

from the sintering temperature. We also attempted to determine the fraction of c-ZrO_2 directly from the ratio polymorph method by determining the integrated intensities of the $(400)_c$, $(004)_t$, and $(220)_t$ peaks using the same non-linear Lorentzian peak-fitting routine as before. Values of the cubic phase fraction tended to vary approximately $\pm$ 3-4 percent about the equilibrium value determined from the phase diagram. Such variability was attributed to the low intensity and the significant overlap of the $(400)_c$ and $(220)_t$ peaks, making it difficult to deconvolute and measure the integrated intensities without undue error. The equilibrium values were therefore used for simplicity. Moreover, recent evidence by Sanchez-Bajo *et al.* suggest that thermodynamic equilibrium is achieved in relatively short periods of time at temperatures similar to those used in this study.[17]

Of particular interest is the fraction of available t-ZrO_2 that undergoes a stress-induced martensitic phase transformation during fracture or grinding. This was determined from:

$$f_{t \rightarrow m} = \frac{f_t(\text{polished}) - f_t(\text{fractured or ground})}{f_t(\text{polished})} \qquad [2]$$

The transformation zone depth was also calculated to correlate to the fracture toughness. Zone depths were calculated from XRD data using the method of Mori *et al.*[18]

(4) Mechanical Properties

The strengths of at least five heat-treated specimens were obtained by loading the disks in biaxial flexure (flat on 3-ball) using the polished side as the tensile surface. Specimens were quickly loaded to failure using a screw-driven universal testing machine (Instron Model 1122, Canton, MA) using a cross-head speed of 500 mm.min^{-1}. Strength was calculated from the maximum load, specimen and fixture dimensions using equations for thin plates.[19]

Previous investigators have shown that the fracture toughness in Y-TZP ceramics is

nearly characterized by a single-value, K_{IC}; there is little R-curve behavior in Y-TZP.[20-22] This

provides for the use of straightforward, conventional methods to determine the fracture

toughness as a function of heat-treatment. In this study, fracture toughness was determined from

a variety of indentation tests. In one series of tests, a 300 N Vickers diamond indent was placed

in the center of the polished specimen (the prospective tensile surface). The radial crack

dimensions were measured optically. A drop of silicon oil was placed on the indent to minimize

environmentally assisted subcritical crack growth. Specimens were then loaded to failure as

before. The fracture toughness was estimated from the strength and indent load using the method

of Chantikul *et al.*, namely[23]

$$K_{IC} = \eta(E/H)^{1/8}(\sigma P^{1/3})^{3/4} \qquad [3]$$

where $\eta = 0.59$ (a constant), E the elastic modulus, H the hardness, σ the strength, and P the

indentation load (300 N). The elastic modulus was measured acoustically using the pulsed-echo

overlap method.[24] The hardness was estimated from measurements of the indentation

impression using

$$H = P/2a^2 \qquad [4]$$

where a is the impression half diagonal.[25] Toughness was also calculated directly from the

crack lengths using the method of Anstis *et al.*[26], recently modified by Kaliszewski and

co-workers[27] to account for the effect of the compressive stresses due to the surrounding

transformation zone:

$$K_{IC} = 0.019(E/H)^{1/2}P/c^{3/2} \qquad [5]$$

where c is the radial crack dimension (measured from the center of the indent impression).

We appreciate that indentation-based calculations of toughness are suspect owing to the effect of the transformation zone, a point also recognized by Kaliszewski *et al.*, even after they accounted for the influence of transformation-induced compressive stresses on the indentation stress field. To overcome this weakness, we also calculated the toughness from indented specimens that were subsequently annealed to remove both the indentation-induced residual tensile stresses and the transformation-induced compressive stresses. In this test, a 200 N Vickers indentation was placed in the center of the polished surface as before, and the specimen subsequently annealed in air at 1000°C for 1 hour. Crack lengths were measured before and after annealing, and the strength determined as usual. The fracture toughness was then calculated from:

$$K_{IC} = \psi \sigma c^{1/2} \qquad [6]$$

where Ψ is the crack geometry factor. Fractographic analyses of the fine-grain Y-TZP ceramics revealed that crack profiles were semi-elliptical in shape, and identical to those observed by Dransmann *et al.*[28] Therefore we used their shape factor correction of 1.025 for a semi-elliptical crack. (Identifying the crack profile in the coarse-grained Y-TZP ceramics was more difficult, hence we assumed that the profiles remained constant and independent of heat treatment. Crack lengths were thus measured directly from the surface trace of radial cracks.)

For comparison with transformation-toughening models, we also determined the fracture toughness using the calculated transformation zone depths and the equation from McMeeking and Evans, where:[29]

$$K_{IC} = K_{matrix} + \Delta K \qquad [7]$$

where K_{matrix} is the baseline toughness of the matrix, assumed to be 2 MPa.m$^{1/2}$,[9] and ΔK is the

increase due to transformation toughening:

$$\Delta K = \frac{\zeta V_f e^t E \sqrt{h}}{1-\upsilon} \qquad [8]$$

where ζ is a constant dependent upon the mechanism of the *t-m* transformation (~ 0.22),[30] V_f is

the volume fraction of *t*-ZrO_2 that transforms near the crack tip, e^t is the unconstrained

transformation strain (~ 0.05), h is the transformation zone width, and υ is Poisson's ratio (0.31).

III. Results

(1) Microstructure

The densities of all specimens exceeded 98% of theoretical, and approached 99.5% of

theoretical density for specimens sintered at 1450°C (physical properties are summarized in

Table I). The density decreases slightly with increasing heat-treatment temperature due to the

presence of a few residual pores, indicated by an increase in the fraction of open (apparent)

porosity. However, the decrease in density is also attributed to the increasing fraction of cubic

phase, which has a lower density than tetragonal ZrO_2.[31] The increasing porosity and cubic phase

explain the trends in hardness and elastic modulus, which also decrease slightly with increasing

heat-treatment temperature.

Figure 2 (a-e) shows representative SEM micrographs of polished and thermally etched

Y-TZP specimens heat treated at 1450-1850°C. The grain size is small (~ 0.3 μm) for the

1450°C specimen (Figure 2a), with a few coarser grains (1 μm) evident. Transmission electron

microscopy (TEM) by Rühle *et al.*[32] has shown that the fine grains are typically *t*-ZrO_2 and the

larger grains *c*-ZrO_2. At 1550°C, the microstructure becomes coarser, but more bimodal (Figure

2b-note the change in magnification): the smaller matrix grains increase in size to approximately

1 μm while the larger c-ZrO_2 grains increase to ~ 3 μm. At 1650°C, the microstructure becomes coarser still (Figure 2c), with the finer matrix grains growing to about 2-3 μm, and the larger grains attaining diameters of ~ 6-8 μm. The microstructure for specimens heat treated at 1750°C (Figure 2d) appears less bimodal; the distinction between the finer matrix grains and the coarser grains becomes less evident as all grains are approximately 6-8 μm in size. There is also some evidence of a substructure in some of the grains, possibly due to the presence of some intragranular precipitation, although this was not confirmed in this study. Y-TZPs heat treated at 1850°C showed a grain size approaching 10 μm (Figure 2e). More importantly, many grains have transformed from t to m symmetry, evidenced by characteristic twinning features (indicated by the arrows in the figure). This indicates that these grains have exceeded a critical grain size and transformed during cooling from the thermal-etch treatment. Intergranular microcracks are occasionally visible, extending across several grains.

Figure 3 plots the average grain size as a function of heat-treatment temperature; the error bars represent ± one standard deviation. The average grain size for the 1450°C heat treatment is ~ 0.3 μm, and increases rapidly with increasing temperatures to a maximum value of approximately 10 μm for the 1850°C heat-treatment. Recall that several grains in the 1850°C specimen appeared to have transformed spontaneously, whereas no evidence of transformation was visible on the 1750°C Y-TZPs. This suggests a critical grain size >5 μm, much larger than the 1 μm determined in prior studies.

(2) Phase Analysis

Figure 4 shows typical x-ray diffraction patterns for (a) polished, (b) fractured, and (c) ground surfaces of heat-treated Y-TZP. In this case, the heat-treatment temperature was 1650°C, although the patterns are typical for all temperatures (with the exception of the 1850°C

specimen). For example, on polished surfaces, generally only the $(111)_{t+c}$ peak was observed; the 1850°C heat treatment showed considerably more monoclinic phase present. The monoclinic content increased dramatically on fracture surfaces, as indicated by the increase in $\{111\}_m$ intensities; the increase was less dramatic on ground surfaces. A clear shoulder exists on the $(111)_{t+c}$ peak of ground surfaces, which did not correspond to t, m, or c-ZrO_2, but was present on all ground XRD patterns. Kitano *et al.*[33] also observed this shoulder in XRD patterns of ground surfaces of Y-TZP ceramics, and attributed it to a metastable rhombohedral phase that results from a stress-induced transformation of the tetragonal phase during grinding.

The various phase fractions obtained from the integrated intensities of deconvoluted XRD patterns for (a) polished, (b) fractured, and (c) ground surfaces are shown in Figure 5, and summarized in Table II. For the polished surfaces (Figure 5a), only the tetragonal and cubic phases are present up to 1850°C, where the tetragonal content quickly decreases to zero. (The cubic phase content is estimated from the phase diagram in Figure 1, and therefore increases continuously with increasing heat-treatment temperature.) Correspondingly, no monoclinic phase was observed below 1850°C, but then increased dramatically at 1850°C.

Phase content on fracture surfaces is shown in Figure 5b (the data for the cubic phase fraction have been omitted for clarity). The tetragonal phase fraction for 1450°C heat treatments is lower than observed on polished surfaces, indicating the occurrence of t-m transformation, and is consistent with the observed increase in monoclinic content. The fraction of tetragonal phase decreases significantly at 1550°C, with a corresponding increase in the fraction of monoclinic phase, indicating that more of the available tetragonal phase is undergoing the stress-induced t-m transformation during strength testing. The fractions of tetragonal and monoclinic phases then remain nearly constant until 1850°C, where the t-phase decreases to zero, and the m-phase attains its maximum value.

The changes in *t*-phase and *m*-phase contents are similar on ground surfaces, but more gradual. In fact, *t*-ZrO$_2$ does not change appreciably until the 1650°C heat treatment (Figure 5c). Surprisingly, some *t*-phase exists after grinding specimens heat treated at 1850°C, suggesting that localized heating during the grinding process retransforms some monoclinic grains back to tetragonal symmetry, an observation also made by Green *et al.* in Ce-TZP ceramics.[34]

The fraction of *t*-phase that transformed to monoclinic during fracture or grinding (determined from equation [2]) is shown in Figure 6 (normalized to the fraction of available *t*-ZrO$_2$). Clearly, a greater fraction of *t*-ZrO$_2$ transformed on fracture surfaces than on ground surfaces, suggesting that the use of ground surfaces may not be suitable to assess the transformability of the tetragonal phase, although the trends are similar. Nonetheless, the fraction of *t*-phase that transforms increases with increasing heat-treatment temperature to a maximum between 1650 and 1750°C. (All of the available *t*-phase in the 1850°C specimen spontaneously transforms during cooling, so there is no *t-m* transformation during fracture or grinding.) It is also worth noting that 70% of the available *t*-phase transforms martensitically during fracture. This is much greater than reported by other investigators, who argued that the variability in solute concentration from grain to grain inhibits a significant fraction of grains from undergoing a stress-induced transformation.[32,35]

The significant fraction of zirconia that has undergone the stress-induced transformation during fracture is reflected in the transformation zone depth, shown in Figure 7 as a function of heat-treatment temperature. The zone is initially small, of the order of 1 μm, consistent with previous studies, but increases markedly with increasing heat-treatment temperature to a maximum near 5 μm. However, caution should be exercised when interpreting these XRD results. For example, a simple calculation of the penetration depth of Cu Kα radiation at 2θ=28° gives a depth of about 5.6 μm,[36] identical to the maximum value measured here. Thus it is likely

that the actual transformation zone widths exceed the sensitivity of the technique.

(3) Mechanical Properties

Strength as a function of heat-treatment temperature is shown in Figure 8. Note that for all heat treatments, the average strength was near or exceeded 1 GPa.[*] The strength was also surprisingly independent of heat treatment, at least within experimental scatter (standard deviation was approximately 20%). This result was unexpected, primarily because of the general belief that coarsening the grain size in TZP ceramics results in a decrease in strength.

The fracture toughness values determined for the heat-treated Y-TZPs were based on indentation tests, therefore it is worthwhile observing the general radial crack patterns in the indented specimens. Typical indentation patterns generated from a 300 N Vickers indentation are shown in the optical micrographs in Figure 9. At 1450°C (Figure 9a), the radial cracks are all well developed, and extend approximately 300 μm from the corners of the indentation impression. At 1550 and 1650°C, the cracks are shorter, with at least one crack much shorter than the others (Figure 9b and c, respectively). This is a commonly observed phenomenon in zirconia ceramics. Braun and Cook have shown that such cracks are "trapped" by the compressive stresses due to the surrounding transformation zone.[37] Also notable is some surface roughness near the indentation impression (recall these are bright field images), related to surface uplift due to the transformation. The roughness becomes more pronounced in the 1750°C specimen, as does the propensity for crack trapping; no cracks escape out of the rough region surrounding the indentation impression (Figure 9d). The surface uplift is better illustrated using Nomarski interference contrast, shown for the 1750°C specimen in Figure 10. Note that the

---

[*] Strength and toughness were not measured on the 1850°C specimens because they were severely microcracked.

uplift extends approximately half of the impression diagonal, and that all of the radial cracks lie within the uplifted region. Close observation of the uplifted region also shows individual grains approximately 5 μm in diameter. In addition, several grains in the uplifted region appear to be twinned.

The fracture toughness values calculated from equations [3], [5] and [6] (using measured values of elastic modulus, hardness, and Poisson's ratio from Table I) are shown in Figure 11, and summarized in Table III. Fracture toughnesses determined from transformation zone widths (equations [7-8]) are also summarized in Table III for comparison. As can be seen in Figure 11, there is considerable scatter among the various calculations, whereas the scatter within any particular method is relatively small (on the order of 5%). Only at the higher fracture toughnesses do the different methods converge. The equation proposed by Chantikul *et al.* tends to result in values higher than average, whereas the Kaliszewski modification to the Anstis equation gives the most conservative result. The calculation based on the Griffith equation and annealed, elliptical indentation cracks gives intermediate, and most likely the best estimate of the fracture toughness. Nonetheless, in all cases the fracture toughness increases with heat-treatment temperature, achieving a maximum of ~ 10 MPa.m$^{1/2}$ for the 1750°C heat treatment.

IV. Discussion

The primary motivation for this study was to determine whether the mechanical properties of a 3 mole % Y-TZP ceramic are compromised by coarsening the microstructure at elevated temperatures as opposed to prolonged periods at lower temperatures. For example, coarsening at elevated temperatures for short periods of time, while perhaps more economical, increases the cubic phase fraction, and thus decreases the fraction of transformable tetragonal

phase. Our results clearly demonstrate that the mechanical properties are not adversely affected by such heat treatments, but in fact are optimized at elevated temperatures. Specifically, sintering to near full density at 1450°C followed by heat treatment at 1750°C produced ceramics with strengths in excess of 1 GPa and fracture toughnesses of approximately 10 MPa.m$^{1/2}$. It is noteworthy that such high heat-treatment temperatures are rarely used in the processing of Y-TZP ceramics, mainly because full density can be achieved at much lower sintering temperatures, but also because of the prevailing philosophy that the mechanical properties will be severely degraded either by a decrease in the fraction of transformable tetragonal phase, or by the grain size exceeding the critical grain size, leading to spontaneous transformation during cooling. Our results show that with the heat treatments conducted in this study, critical grain sizes of approximately 5 μm are possible, much larger than observed in previous investigations, suggesting that the critical grain size is also a function of heat treatment, or more likely, a some combination of the phases present and the internal residual stresses derived from thermal expansion anisotropy.

One of the most surprising results of this study is the high strength *and* the high fracture toughness achieved for the 1750°C heat treatment; strengths of 1000 MPa and fracture toughnesses of 10 MPa.m$^{1/2}$ are rarely achieved in the same Y-TZP.* Furthermore, the presence of the tetragonal phase at room temperature with grain sizes of the order of 5-6 μm has not been reported; other studies have suggested a critical grain size of 1-2 μm for a 3 mole percent Y-TZP.[11] Considering the body of literature that suggests that strength decreases with

---

* Some studies have reported fracture toughnesses in excess of 10 MPa.m$^{1/2}$. However, the methods used to determine these values are suspect; Y-TZP is extremely notch sensitive, making measurements from conventional single-edge notched beam (SENB) tests dubious at best. Moreover, fracture toughness values based solely on indentation crack sizes overestimate the fracture toughness unless the effect of the transformation stress field and crack shapes are taken into account, as in this study.

increasing grain size, we have since reproduced the experiments outlined in this study with similar results.** At present it is not clear why our results differ from those in the literature. Evidently, first sintering at 1450°C and then heat treating at elevated temperatures is fundamentally different than merely sintering at the same elevated temperature. We are currently attempting to characterize microstructural differences resulting from such heat treatments in greater detail, such as the presence of intragranular tetragonal phase.

Generally it has been observed that a lower volume fraction of transformable *t*-phase increases the critical grain size in Y-TZP. In our study, the fraction of c-ZrO_2, which is increased by heat treating at elevated temperatures, results in a larger critical tetragonal grain size. One possibility for the larger critical grain size may be the lower strain energy due to thermal expansion anisotropy. For example, the (isotropic) thermal expansion coefficient for the cubic phase falls between the thermal expansion coefficients for the *a*- and *c*-directions of the tetragonal phase. Thus, while the *magnitude* of the internal residual stresses is the same (determined by thermal expansion mismatch), the total strain energy is related to how these stresses are distributed throughout the volume of material. Hence, the lower volume fraction of tetragonal phase implies a lower overall strain energy. The effect of this lower strain energy may be to increase the barrier to nucleation, thus preventing *spontaneous* transformation, allowing a greater fraction of tetragonal grains to undergo a *stress-induced* transformation, thereby increasing the fracture toughness by expanding the transformation zone size.

** Actually, we have reproduced the results in two separate laboratories. Originally these tests were conducted at Carnegie Mellon University. We have since processed a second batch of material at Sandia National Laboratories, with similar microstructures and mechanical properties. In reproducing the results we have learned that heat treating materials at temperatures just slightly above 1750"C, with grain sizes somewhat greater than the 5 microns measured here, results in virtually no tetragonal phase retained to room temperature.

The apparent constant strength with increasing grain size is also contrary to other investigations in Y-TZP, showing strength inversely proportional to grain size. Swain and Rose have argued that in Y-TZP, with little transformation plasticity, strength is governed largely by the critical flaw size, typical of other brittle ceramics that obey the Griffith strength relation. The observed strength decrease is believed to arise because the critical flaw size scales with the grain size.[30] To explain our contrary results, we surmise that the increasing fracture toughness compensates for the increasing flaw size, resulting in a nearly constant strength. In fact, a simple analysis using equation [6] shows that if the flaw size increases in proportion to the grain size, the constant strength can be explained almost entirely by the offsetting increase in fracture toughness. Alternatively, one could invoke arguments of enhanced R-curve behavior to explain the near constant strength, although *pronounced* R-curve behavior has not been observed in most Y-TZP ceramics. The presence of R-curve behavior was not determined in this study, and is currently part of on-going research.

The increase in fracture toughness is undoubtedly due to an increasing transformation zone size in specimens heat treated at elevated temperatures: the *t*-phase, while present in lower volume fractions, is much more transformable than for the finer grains attained at lower temperatures. This allows the stress-induced phase transformation to be nucleated at lower stresses, thus extending the zone width farther from the crack tip. Such transformability is readily apparent in Figure 11, which shows the uplift, twinned grains, and trapped radial cracks surrounding the indentation impression. The extent of such uplift is rarely observed in Y-TZP, and is more typical of indentation patterns in tough Mg-PSZ or Ce-TZP.

While the extensive surface uplift and large amount of stress-induced *t-m* phase transformation observed in these Y-TZP's suggests that most of the toughening arises due to transformation toughening, we do not rule out the possibility of a contribution from ferroelastic

domain switching. For example, Virkar and Matsumoto noted in x-ray diffraction experiments of Y-TZP extensive reorientation of the tetragonal phase under a grinding stress. They concluded that such a reorientation absorbs energy due to the grinding stresses, and thus acts as an additional toughening mechanism.[38] Ferroelastic domain switching in Y-TZP was further substantiated in tests by Srinivasan *et al.*, Chan and coworkers.[39,40] Additionally, Baker, Faber and Readey showed that the fracture toughness in bismuth vanadate (a known ferroelastic material) increased by over 50% when grain reorientation is operative.[41] Hence, while most of the toughening can be explained by transformation toughening, ferroelastic domain switching may also contribute to the high toughness observed in these Y-TZP ceramics.

Another point worth noting concerns the methods employed to determine the fracture toughness in these Y-TZP ceramics. As is often observed with toughness measurements in zirconia, there is considerable discrepancy among the several measuring techniques. We believe that the most accurate method for determining the fracture toughness in this study utilizes the strength obtained from specimens containing annealed indentation flaws (equation [6]), where the annealing process removes the indentation-induced and transformation-induced residual stresses. The parameters used to calculate the toughness in this case, namely the strength, flaw size, and flaw shape, are readily determined, providing a less ambiguous estimate of the fracture toughness. In our tests, the indentation cracks sizes and shapes were determined directly from fracture surfaces, and were found to correspond almost exactly to the crack morphologies observed by Dransmann *et al.*,[28] who also observed semi-elliptical cracks. We point out that the shape factor for semi-elliptical cracks results in a more conservative estimate of the fracture toughness (by nearly 20%) compared to estimates incorporating shape factors using the more familiar semi-circular, half-penny cracks.

Finally, this study cautions against using transformation zone depths calculated from

x-ray diffraction of fracture surfaces to assess the transformability of the *t*-phase. For example, the data suggest that the zone depth reaches a maximum, then remains relatively unchanged for heat treatments at 1650 and 1750°C, suggesting a maximum in transformability. However, it is easy to show that the penetration depth of the x-ray radiation corresponds almost exactly to this plateau value.[36] Hence transformation zone measurements can grossly underestimate the actual depth, and as a consequence underestimate the toughness determined from such measurements. Moreover, we have shown that using ground surfaces to asses the transformability of tetragonal zirconia can also be misleading. Ground surfaces always contained less monoclinic phase than fracture surfaces. This was also observed by Green *et al.*[34] for Ce-TZP ceramics. They postulated that the low thermal conductivity of zirconia, and the heat generated during the grinding process (in spite of using a coolant) produced localized elevated temperatures at the ground surface, thus decreasing the driving force for the transformation. Another explanation is that the grinding stresses are not as high as stresses that cause fracture, and therefore are not sufficient to cause widespread transformation.

V. Conclusions

In spite of decreasing the fraction of transformable tetragonal phase, coarsening Y-TZP microstructures at elevated temperatures for relatively short periods of time does not degrade the mechanical properties of the ceramic. In fact, the fracture toughness and strength are greatly enhanced at the higher temperatures, primarily due to enhanced transformability of the *t*-phase. Moreover, we have obtained tetragonal grain sizes that are much coarser than obtained in previous studies. These grains transform at lower stresses, thus allowing for a much larger transformation zone and hence higher fracture toughnesses. These properties were obtained by

first sintering at 1450°C, followed by heat treating at 1750°C. Evidently this processing scheme results in microstructures that behave differently than if sintered directly at the higher heat-treatment temperature. The reasons for this difference are unclear, but the result is a ceramic that has both high strength *and* high toughness, a combination of properties that is rarely achieved in 3Y-TZP.

Acknowledgments

References ·

1. K. Tsukuma, Y. Kubota, and T.Tsukidate. "Thermal and Mechanical Properties of Y_2O_3-Stabilized Tetragonal Zirconia Polycrystals"; pp. 382-90 in Advances in Ceramics, Vol. 12, *Science and Technology of Zirconia II.* Edited by N. Claussen, M. Rühle, and A.H. Heuer. The American Ceramic Society, OH, 1984.

2. V. Gross, and M.V. Swain, "Mechanical Properties and Microstructure of Sintered and Hot Isostatically Pressed Yttria-Partially Stabilized Zirconia (Y-PSZ)," *J. Aust. Ceram. Soc.*, 22 [1] 1-12 (1986).

3. M. Shimbo, M. Itoh, M Ueki, Y. Miyano, S. Ishihara, and T. Fujita, "Stress-Induced Transformation and Toughening of Yttria-Stabilized Zirconia"; pp. 415-22 in Advances in Ceramics, Volume 24A, *Science and Technology of Zirconia III.* Edited by S. Somiya, N. Yamamoto, and H. Hanagida. American Ceramic Society, OH, 1988.

4. Tsukuma and T. Takahata, "Mechanical Property and Microstructure of TZP and TZP/Al_2O_3 Composites"; pp. 123-36 in Advanced Structural Ceramics, Volume 78. Edited by P.F. Becher, M.V. Swain, and S. Somiya. Materials Research Society, Pittsburgh, 1987.

5. M.V. Swain, "Grain Size Dependence of Toughness and Transformability of 2 mol % Y-TZP Ceramics," *J. Mat. Sci. Lett.*, 5 1159-1162 (1986).

6. P.F. Becher and M.V. Swain, "Grain-Size Dependent Transformation Behavior in Polycrystalline Tetragonal Zirconia," *J. Am. Ceram. Soc.*, 75 [3] 493-502 (1992).

15. D.J. Green, R.H.J. Hannink and M.V. Swain, p. 222 in Transformation Toughened Ceramics. CRC Press, FL, 1989.

16. D.L. Porter and A.H. Heuer, "Microstructure Development in Mg-PSZ," *J. Am. Ceram. Soc.*, 62 [5-6] 298-305 (1979).

17. F. Sanchez-Bajo, F.L. Cumbrera, F. Guiberteau, and A. Dominguez-Rodriquez, "Microstructural Characterization of Y-PSZ (4 mol%) Polycrystals by means of X-Ray Diffraction Experiments", Materials Letters 15 39-44 (1992).

18. Y. Mori, Y. Kitano, A. Ishitani and T. Masaki, "X-Ray Determination of Transformation Zone Size in Toughened Zirconia Ceramics," *J. Am. Ceram. Soc.*, 71 [7] C322-C324 (1988).

19. ASTM, F-394-78, "Standard Test Method for Biaxial Flexure Strength (Modulus of Rupture) of Ceramic Substrates" pp. 422-426 in ASTM Annual Book of Standards. Volume 15.02, Section 15. American Society of Testing and Materials, Philadelphia, PA, (1994).

20. R.W. Steinbrech, unpublished work.

21. M.J. Readey, C.L. McCallen, P.D. McNamara, and B.R. Lawn, "Correlations between Flaw Tolerance and Reliability in Zirconia," *J. Mat. Sci.*, 28 6748-52 (1993).

22. M.J. Readey and C.L. McCallen, "Microstructure, Flaw Tolerance, and Reliability of Ce-TZP and Y-ZP Ceramics," *J. Am. Ceram. Soc.*, 78 [10] 2769-76 (1995).

23. P. Chantikul, G.R. Anstis. B.R. Lawn, and D.B. Marshall, "A Critical Evaluation of Indentation Techniques for Measuring Fracture Toughness: II, Strength Method." *J. Am. Ceram. Soc.*, **64** [9] 539-543 (1981).

24. E.P. Papadakis, "New, Compact Instrument for Pulse-Echo Overlap Measurements of Ultrasonic Wave Transmit Time," *Rev. Sci. Instrum.*, **47** [7] 806-13 (1976).

25. B.R. Lawn, p. 259 in Fracture of Brittle Solids, 2nd Edition. Cambridge University Press, Cambridge, 1993.

26. G.R. Anstis, P. Chantikul, B.R. Lawn, and D.B. Marshall, "A Critical Evaluation of Indentation Techniques for Measuring Fracture Toughness: I, Direct Crack Measurements." *J. Am. Ceram. Soc.*, 64 [9] 533-538 (1981).

27. M.S. Kaliszewski, G. Behrens, A.H. Heuer, M.C. Shaw, D.B. Marshall, G.W. Dransmann, R.W. Steinbrech, A. Pajares, F. Guiberteau, F.L. Cumbrera, and A. Domingues-Rodriguez, "Indentation Studies on Y_2O_3-Stabilized ZrO_2: I, Development of Indentation-Induced Cracks." *J. Am. Ceram. Soc.*, **77** [5] 1185-93 (1994).

28. G.W. Dransmann, R.W. Steinbrech, A. Pajares, F. Guiberteau, A. Domingues-Rodriguez and A.H. Heuer, "Indentation Studies on Y_2O_3-Stabilized ZrO_2: II, Toughness Determination from Stable Growth of Indentation-Induced Cracks," *J. Am. Ceram. Soc.*, **77** [5] 1194-201 (1994).

29. R.M. McMeeking and A.G. Evans, "Mechanics of Transformation-Toughening in Brittle Materials," *J. Am. Ceram. Soc.*, **65** [5] 242-246 (1982).

30. M.V. Swain and L.R.F. Rose, "Strength Limitations of Transformation-Toughened Zirconia Alloys," *J. Am. Ceram. Soc.*, **69** [7] 511-518 (1986).

31. D.J. Green, R.H.J. Hannink and M.V. Swain, p. 220-221 in <u>Transformation Toughened Ceramics.</u> CRC Press, FL, 1989.

32. M. Rühle, N. Claussen, and A.H. Heuer, "Microstructural Studies of Y_2O_3-Containing Tetragonal ZrO_2 Polycrystals (Y-TZP)," pp. 352-370 in Advances in Ceramics, Vol. 12, *Science and Technology of Zirconia II*. Edited by N. Claussen, M. Rühle, and A.H. Heuer. The American Ceramic Society, OH, 1984.

33. Y. Kitano, Y. Mori, A. Ishitani, and T. Masaki, "A Study of Rhombohedral Phase in Y_2O_3-Partially Stabilized Zirconia," pp. 17-24 in Advanced Structural Ceramics, Materials Research Society Symposium Proceedings, Volume 78. Edited by P.F. Becher, M.V. Swain, and S. Somiya. Materials Research Society, Pittsburgh, PA, 1987.

34. D.J. Green, R.H.J. Hannink and M.V. Swain, p. 149 in <u>Transformation Toughened Ceramics.</u> CRC Press, FL, 1989.

35. D.B. Marshall, personal communication.

36. B.D. Cullity, pp. 292-295 in <u>Elements of X-Ray Diffraction</u>, 2nd edition. Addison-Wesley Publishing, Reading, 1978.

37. R.F. Cook and L.M. Braun, "Trapped Cracks at Indentations; II, Fracture Mechanics Model," *J. Mat. Sci.*, **29**, 2192-2204 (1994).

38. A.V. Virkar and R.L.K. Matsumoto, "Toughening Mechanism in Tetragonal Zirconia Polycrystalline (TZP) Ceramics," pp. 653-662 in Advances in Ceramics, Vol. 24: Science and Technology of Zirconia, III. Edited by S. Somiya, N. Yamamoto, and H. Hanagida. American Ceramic Society Press, OH, 1988.

39. G.V. Srinivasan, J.F. Jue, S.Y.Kuo, and A.V. Virkar, "Ferroelastic Domain Switching in Polydomain Tetragonal Zirconia Single Crystals," *J. Am. Ceram. Soc.*, **72** [11] 2098-103 (1989).

40. C.J. Chan, F.F. Lange, M.F. Rühle, J.F. Jue and A.V. Virkar, "Ferroelastic Domain Switching in Tetragonal Zirconia Single Crystals-Microstructural Aspects," *J. Am. Ceram. Soc.*, **74** [4] 807-13 (1991).

41. T.L. Baker, K.T. Faber, and D.W. Readey, "Ferroelastic Toughening in Bismuth Vanadate," *J. Am. Ceram. Soc.*, 74 [7] 1619-23 (1991).

List of Figures

Figure 1. Phase diagram showing the ZrO_2-rich side of the ZrO_2-Y_2O_3 equilibrium phase diagram (after Scott[10]). The dashed lines correspond to the temperature region of interest in this study. As the heat-treatment temperature is increased, there is a reduction in the fraction of transformable tetragonal phase.

Figure 2. Scanning electron micrographs of polished and thermally etched surfaces of 3 mole % Y-TZP ceramics sintered at 1450°C for two h (a), and subsequently heat treated for two h at (b) 1550°C, (c) 1650°C, (d) 1750°C, and (e) 1850°C. At 1450°C, the grain size is small and uniform. The microstructure coarsens at the higher heat-treatment temperatures, and shows a more bimodal size distribution containing larger, c-ZrO_2 grains surrounded by a finer, t-ZrO_2 matrix. At the higher temperatures, the microstructure becomes more uniform again. Eventually, the microstructure exceeds some critical grain size and the t-phase spontaneously transforms to monoclinic symmetry, evidenced by the twinned (arrowed) features in (e).

Figure 3. The average grain diameter as a function of heat-treatment temperature. The grain size is initially sub-micron, but coarsens at an increasing rate to approximately 10 μm at the highest heat-treatment temperature. Error bars represent ± one standard deviation about the mean.

Figure 4. Representative x-ray diffraction patterns for (a) polished, (b) fracture, and (c) ground surfaces. These patterns in particular are for the Y-TZP heat-treated at 1650°C. On the polished surface, only c- and t-ZrO_2 are observed. Fracture surfaces show a significant fraction of m-ZrO_2. Ground surfaces also show the existence of m-ZrO_2, but less than on fracture surfaces. A distinct shoulder exists on the $(111)_{t+c}$ peak at ~ 30° 2θ. This was commonly observed on all ground surfaces, and is possibly a metastable rhombohedral phase that occurs only on abraded surfaces.

Figure 5. Fraction of c-, t-, and m-ZrO$_2$ as a function of heat-treatment temperature for (a) polished surfaces, (b) fracture surfaces. (c) ground surfaces. In (a), the cubic content increases owing to equilibrium volume fraction determined from the lever rule and the phase diagram. Correspondingly, the tetragonal content decreases. The fraction of monoclinic phase is zero up to the highest temperature tested, where it abruptly increases, indicating spontaneous transformation from the cooling temperature. For fracture surfaces, the monoclinic phase generally increases with temperature, with an associated decrease in t-phase, owing to stress-induced transformation. Ground surfaces show a similar trend, but the fraction m-ZrO$_2$ does not increase as quickly.

Figure 6. The fraction of transformed t-phase as a function of heat-treatment temperature for fractured and ground surfaces. For fracture surfaces, the fraction of t-ZrO$_2$ initially increases dramatically with increasing temperature, then appears to reach a plateau, followed by a precipitous decrease at 1850°C. This decrease is undoubtedly due to spontaneous transformation of all the t-ZrO$_2$ from the heat-treatment temperature, leaving none available for the stress-induced transformation. Ground surfaces show a similar trend. but with less t-phase transforming.

Figure 7. Transformation zone depth as a function of heat-treatment temperature for t-phase that has undergone a stress-induced transformation (only the fracture surface data are shown). Consistent with the data in figure 7, the zone depth increases quickly to a maximum of ~ 5 μm, followed by a rapid decrease. Note however, that the plateau is more likely due to a limitation in x-ray penetration (also about 5 μm) rather than a maximum in transformation zone depth.

Figure 8. Strength as a function of heat-treatment temperature. Strength is of the order 1000

MPa and relatively constant over the entire heat-treatment range, contrary to previous

investigations. Error bars correspond to ± one standard deviation about the mean.

Figure 9. Bright-field optical micrographs showing 300 N indentation patterns for Y-TZP

ceramics sintered at 1450°C for two h (a), and subsequently heat treated for two h at (b) 1550°C,

(c) 1650°C, and (d) 1750°C. In (a) the radial cracks are well developed, and extend several

hundred microns from the indentation impression. In (b) and (c), some surface texture becomes

evident near the impression; radial crack lengths are decreasing, and one or more cracks is

trapped. In (d), significant surface texture is evident, and all cracks are trapped within the

transformation zone.

Figure 10. Bright-field optical micrograph using Nomarski interference contrast of the specimen

heat treated at 1750°C showing the indentation pattern of a 300 N indent. Considerable surface

rumpling is observed, extending approximately 100 μm from the edges of the indent impression.

Evidence of twinning is present in some of the grains. Such crack patterns and surface rumpling

are common in high toughness zirconia ceramics such as Mg-PSZ and Ce-TZP.

Figure 11. Fracture toughness as a function of heat-treatment temperature. Fracture toughness is

calculated from: Chantikul *et al.*, eqn. [3], (◆), Kaliszewski *et al.*, eqn. [5] (■), and Griffith's

eqn. [6] (●). The toughness increases with heat-treatment temperature to a maximum of ~ 10

MPa.m$^{1/2}$. Chantikul's expression overestimates the toughness through most of the testing range,

whereas Kaliszewski's underestimates the toughness. Griffith's expression, based on the

measured strength, crack size and shape, yields the most accurate estimate of the toughness.

Table I. Physical Properties of Heat Treated 3 mol% Y-TZP Ceramics

Heat-Treatment Temperature (°C)[+]	Sintered Density (g/cm^3)	Apparent Porosity (%)	Grain Size (μm)	Hardness (GPa)	Elastic Modulus (GPa)	Poisson's Ratio
1450	6.05 ± 0.04	0.13	0.3 ± 0.1	12.7	218	0.31
1550	6.00 ± 0.02	0.17	0.6± 0.2	12.2	212	0.31
1650	6.00 ± 0.01	0.33	1.8 ± 0.7	11.6	211	0.31
1750	5.96 ± 0.02	0.24	5.1 ± 2.5	11.3	206	0.32
1850	*	*	10.1 ± 3.4	*	*	*

[+] Specimens were intially sintered at 1450oC for 2 hours; subsequent heat-treatments were for two hours at 1550, 1650, 1750, and 1850°C.

* Not measured due to severe microcracking.

Table II. Experimental Phase Content of Heat Treated Y-TZP Ceramics

Heat-Treatment Temperature (°C)	Surface State	Cubic Phase (%)	Tetragonal Phase* (%)	Monoclinic Phase* (%)
1450	Polished	25	75	0
	Fractured	25	51	24
	Ground	25	59	16
1550	Polished	28	72	0
	Fractured	28	24	48
	Ground	28	52	20
1650	Polished	32	68	0
	Fractured	32	20	48
	Ground	32	53	15
1750	Polished	38	62	0
	Fractured	38	18	44
	Ground	38	30	32
1850	Polished	46	0	54
	Fractured	46	0	54
	Ground	46	13	41

* Precision is approximately ± 5% of the calculated value.

Table III. Mechanical Properties of Heat Treated Y-TZP Ceramics

Heat-Treatment Temperature ($^{\circ}$C)	σ (MPa)	K_{IC} - I (MPa.m$^{1/2}$)	K_{IC} - II (MPa.m$^{1/2}$)	K_{IC} - III (MPa.m$^{1/2}$)	K_{IC} - IV (MPa.m$^{1/2}$)
1450	1079 ± 162	5.8 ± 0.2	4.3 ± 0.1	5.0 ± 0.6	3.6
1550	1039 ± 187	8.3 ± 0.5	5.0 ± 0.3	6.8 ± 0.3	8.4
1650	968 ± 200	8.6 ± 0.5	6.9 ± 0.4	8.1 ± 0.5	9.2
1750	1089 ± 81	9.4 ± 0.2	10.6 ± 0.7	9.7 ± 0.4	7.7

I: determined from equation [3]

II: determined from equation [5]

III: determined from equation [6]

IV: determined from equations [7-8]

Figure 1 (Ruiz/Readey)

Figure 2 (Ruiz/Readey)   135

(a)

(b)

Figure 2 (Ruiz/Readey)

(c)

(d)

Figure 2 (Ruiz/Readey) 137
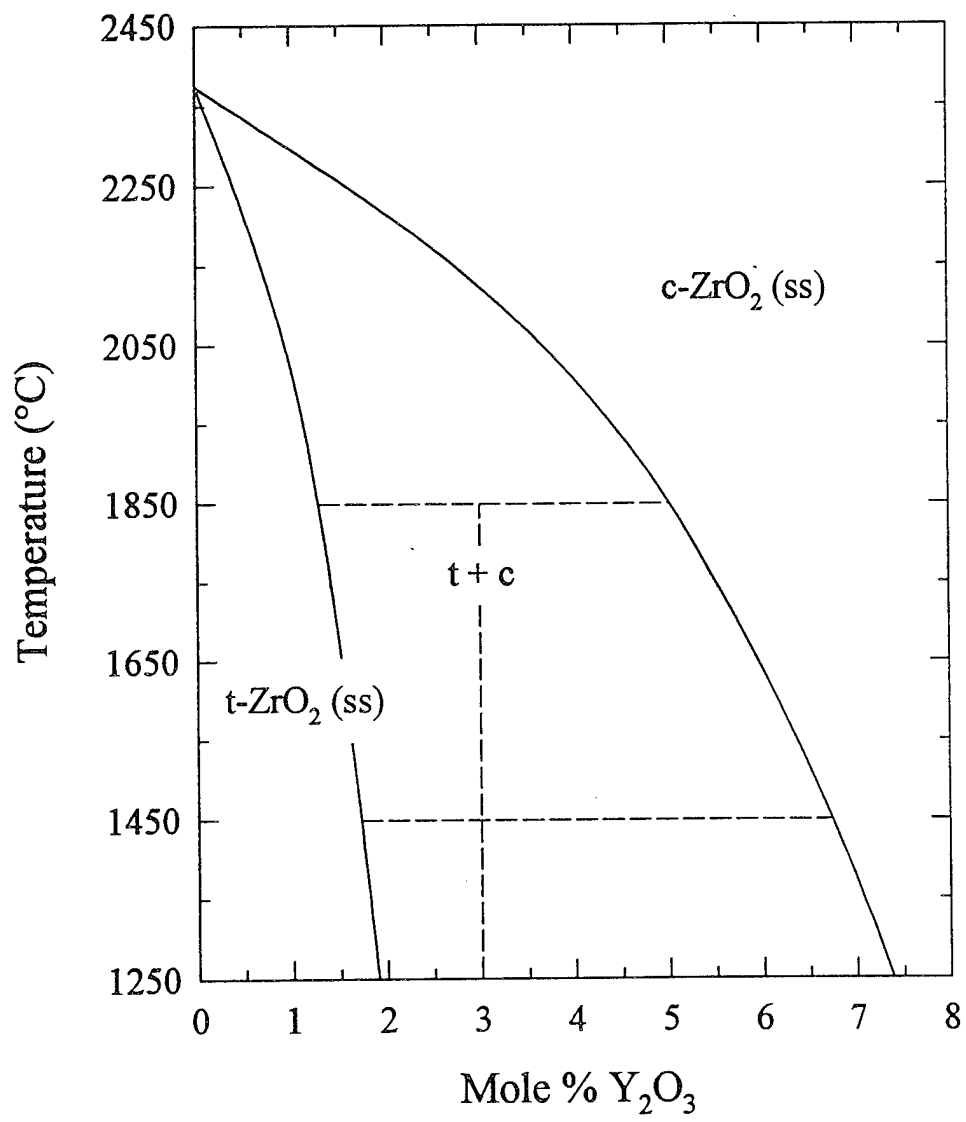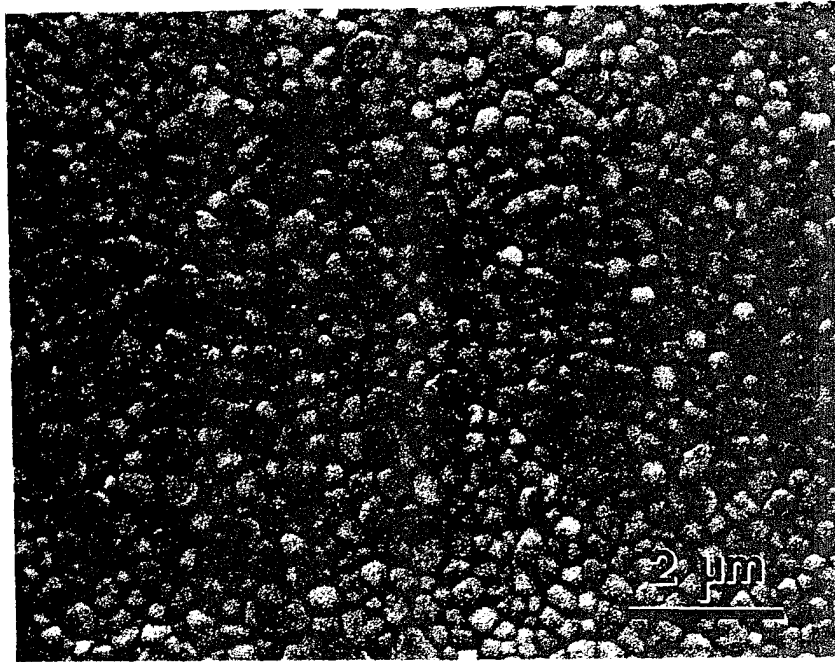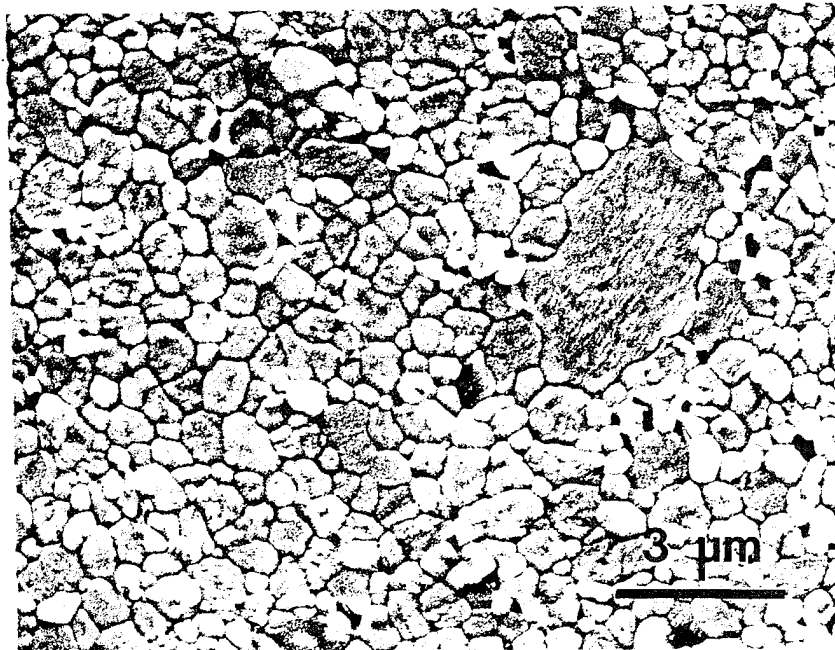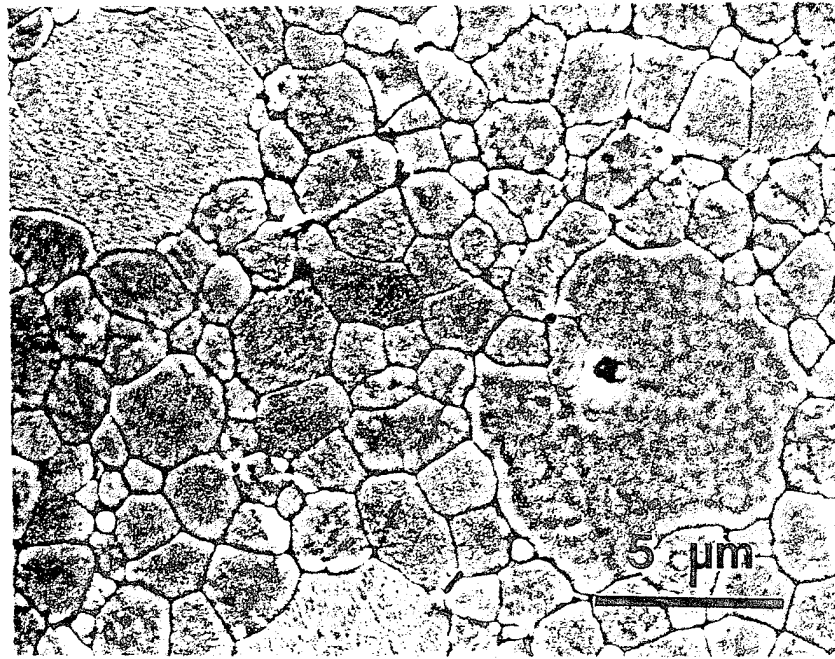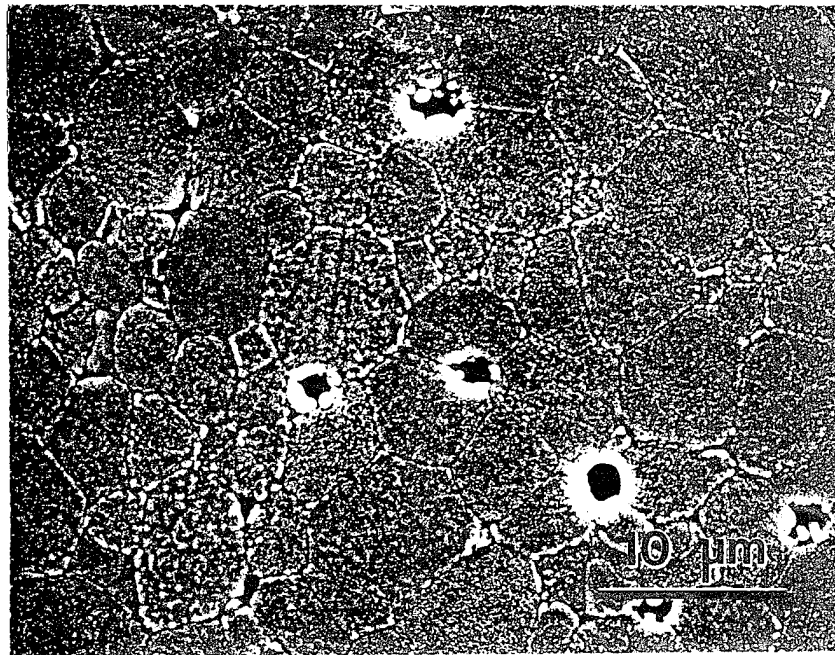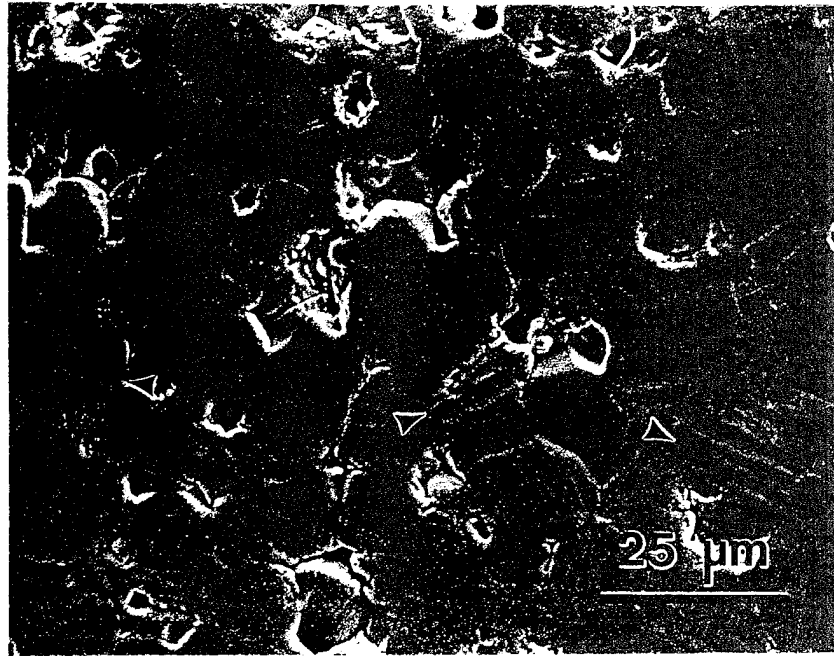
(e)

Figure 3 (Ruiz/Readey)
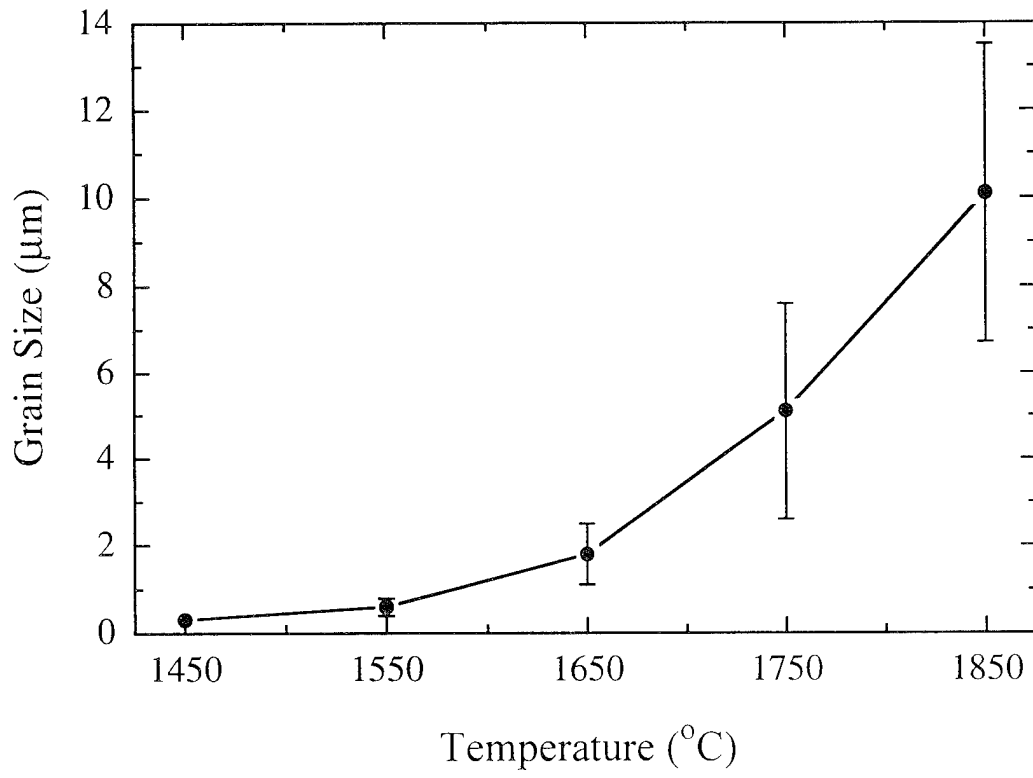
Figure 4 (Ruiz/Readey)
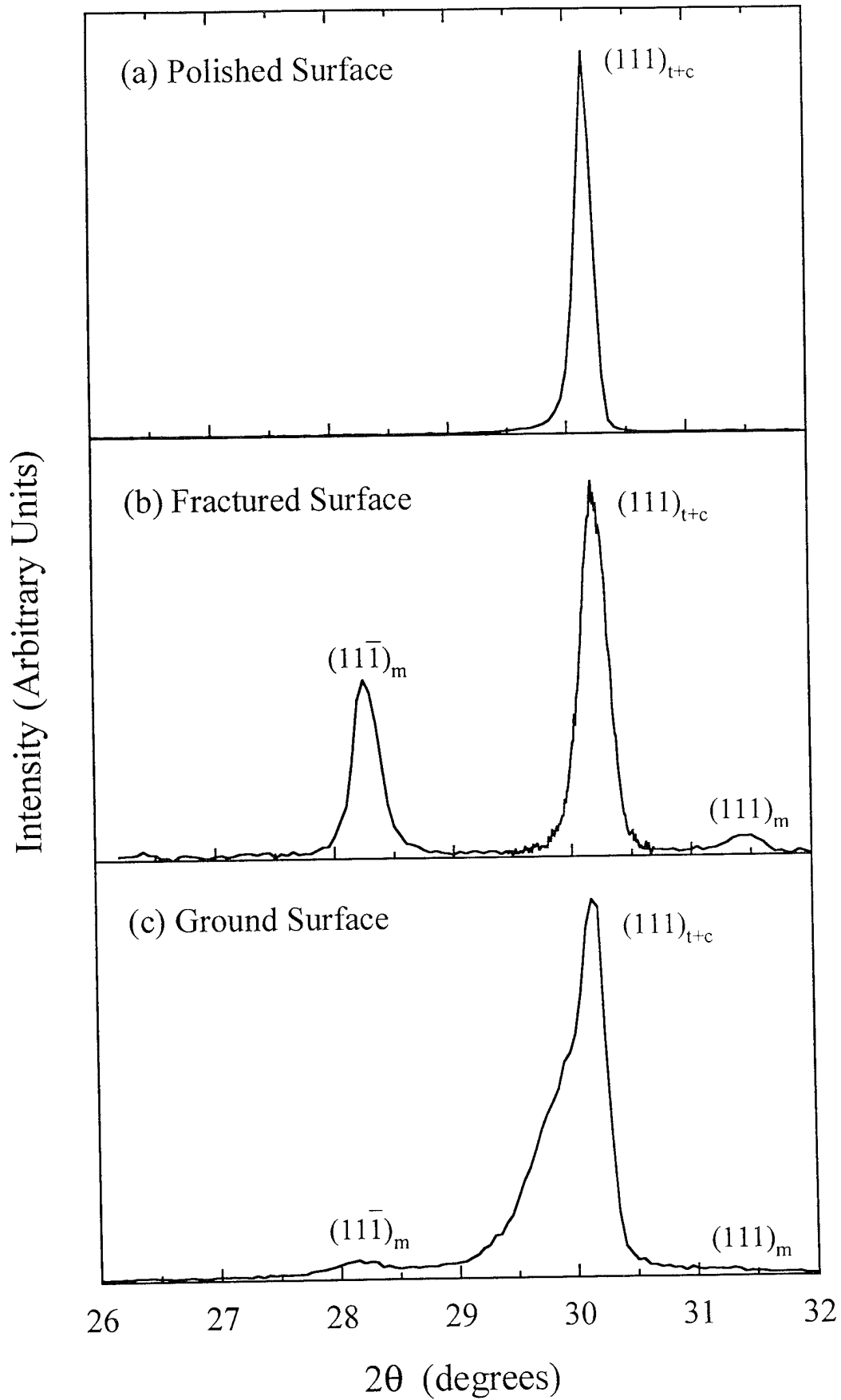
Figure 5 (Ruiz/Readey)
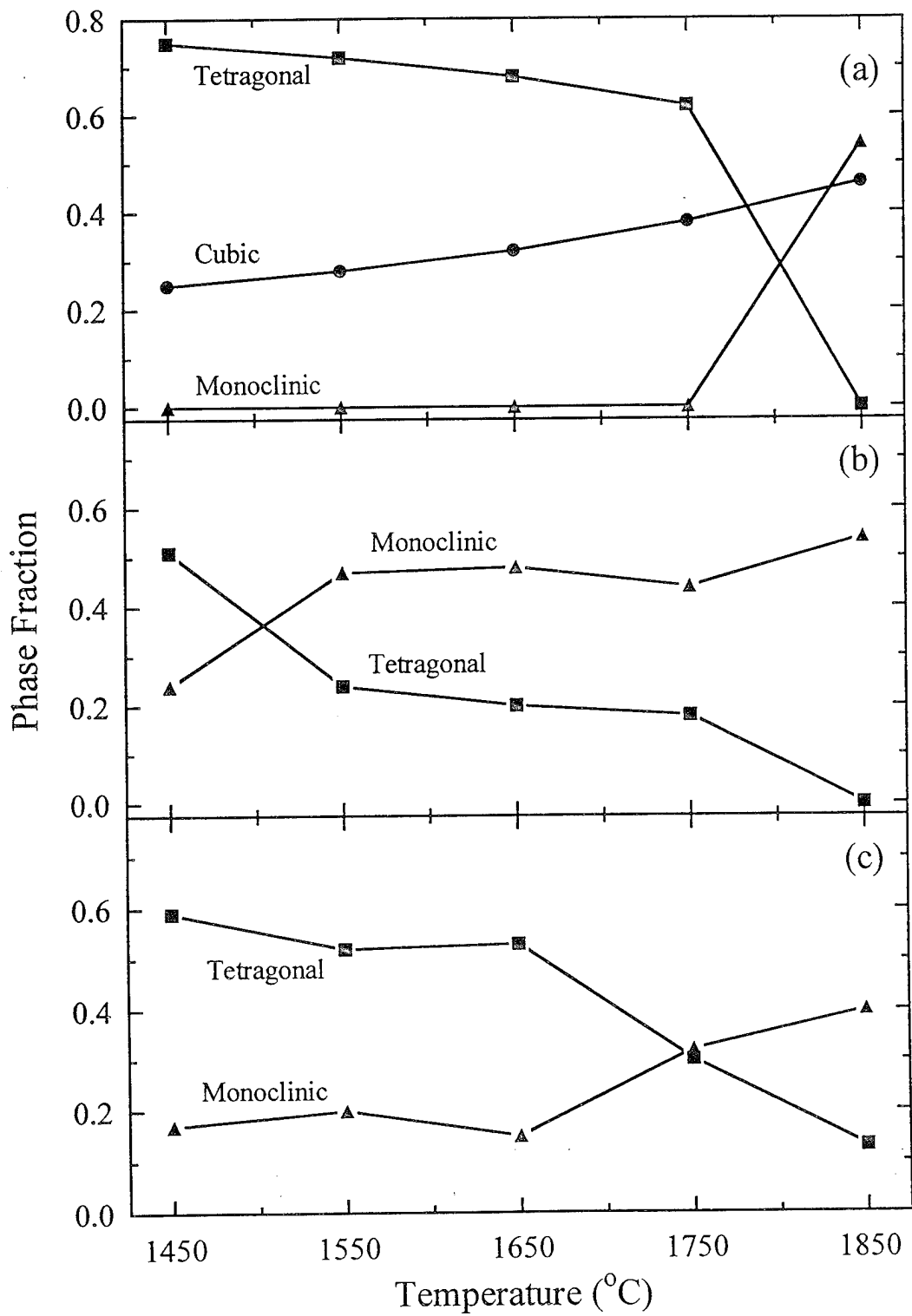
Figure 6 (Ruiz/Readey)
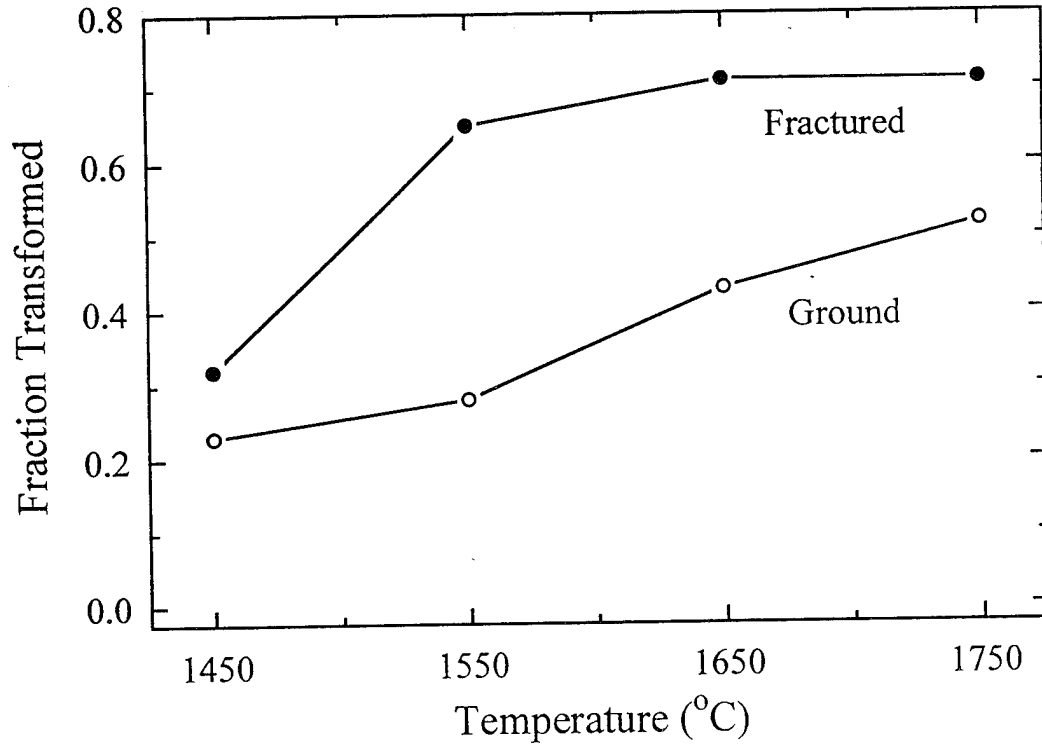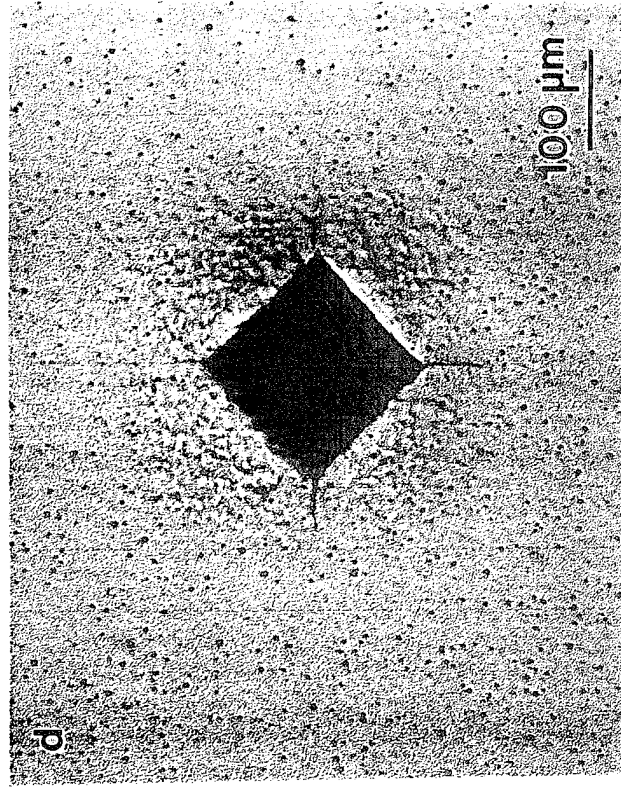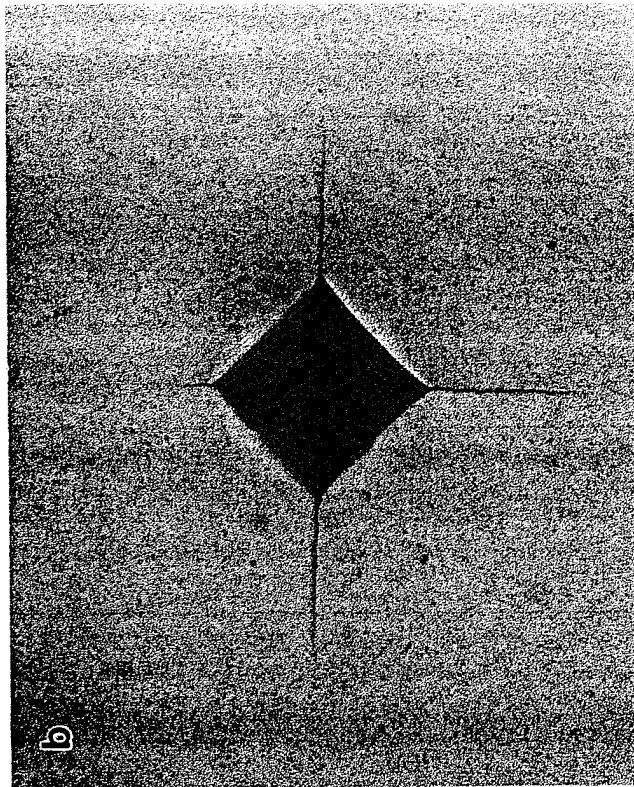
Figure 7 (Ruiz/Readey)
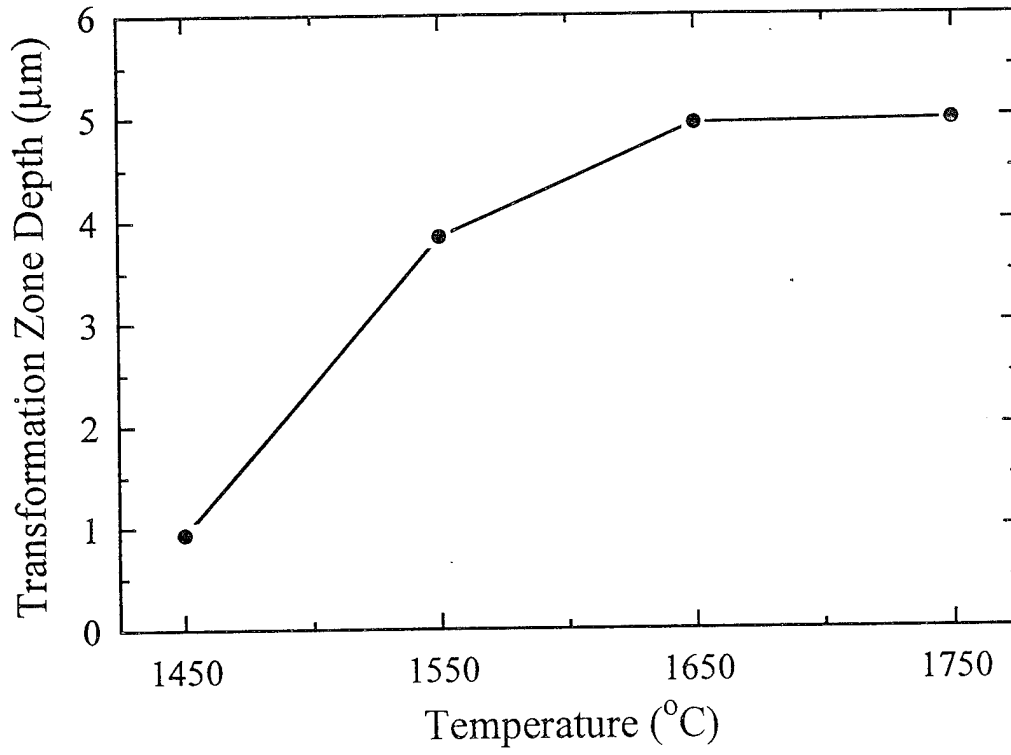
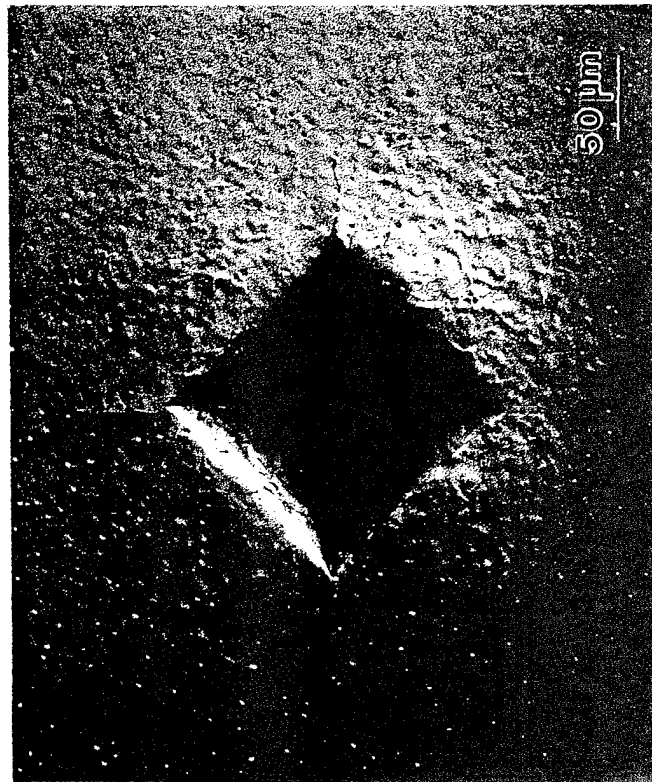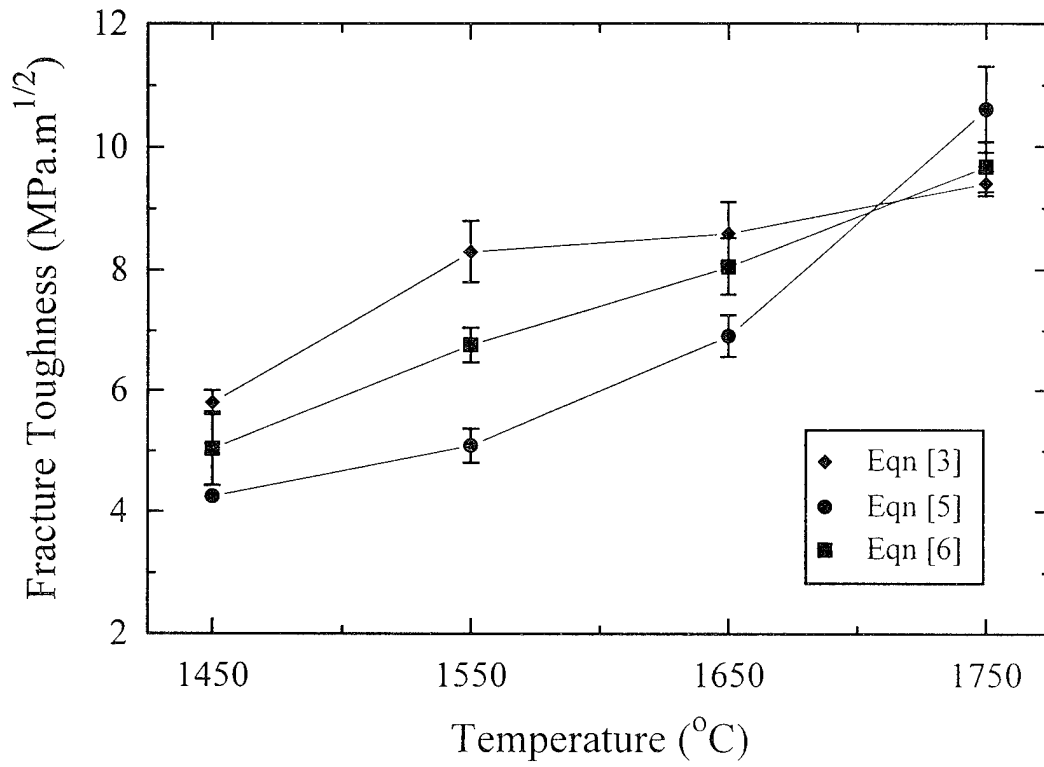Figure 8 (Ruiz/Readey)

Figure 9

Figure 10 145
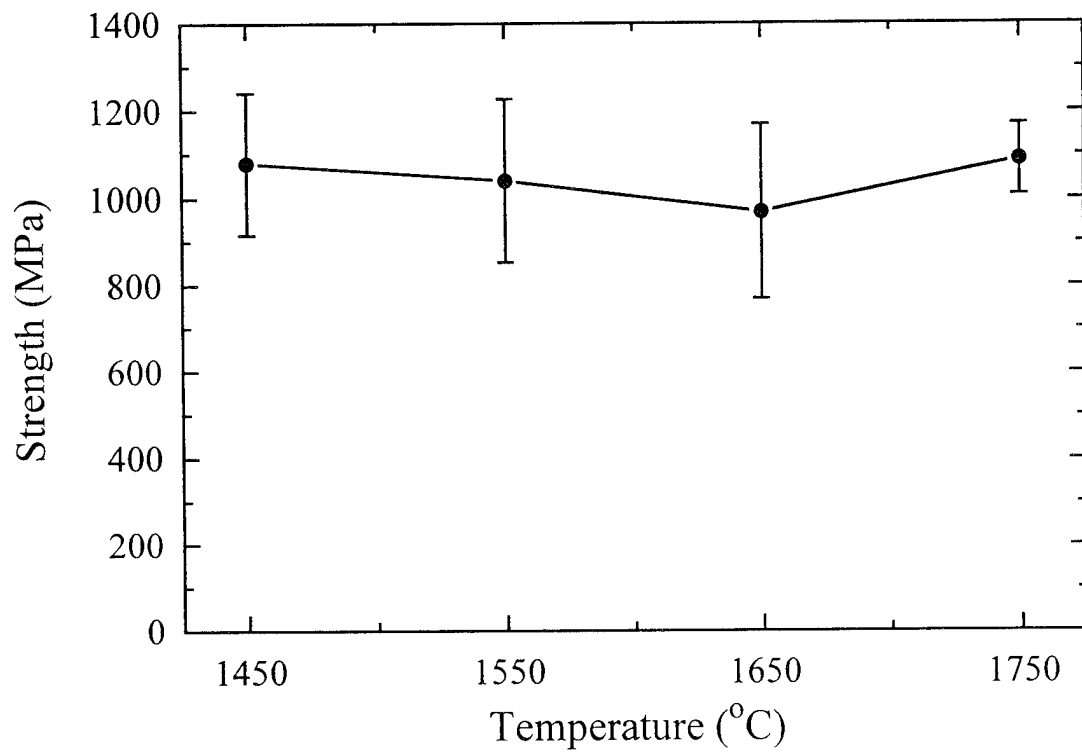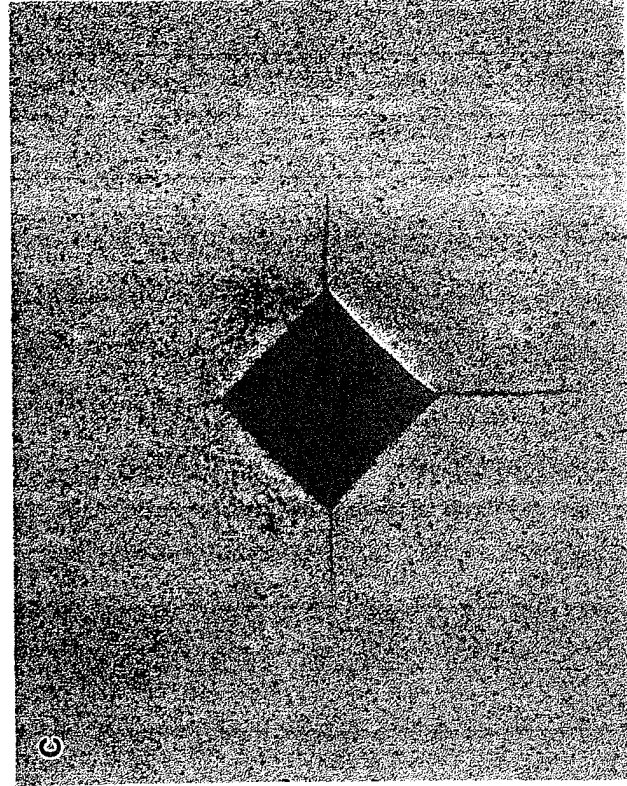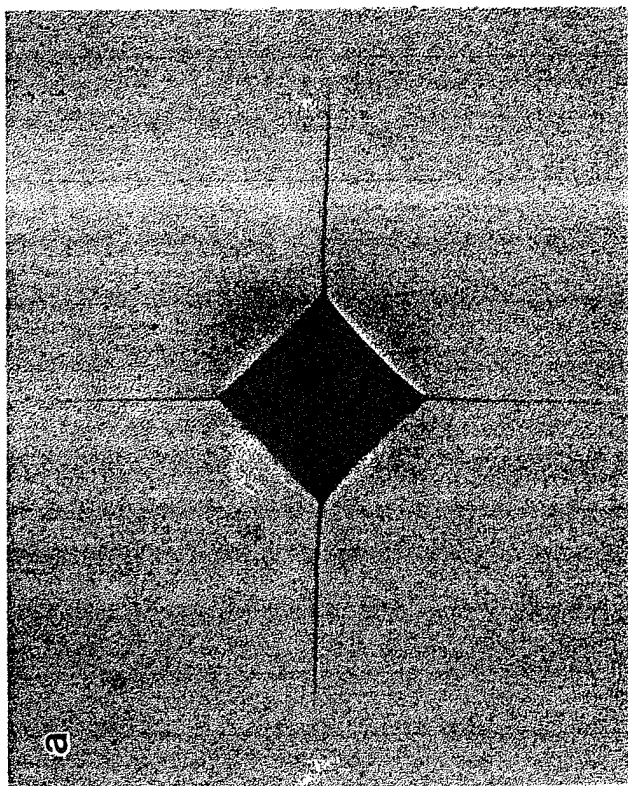
Figure 11 (Ruiz/Readey)

APPENDIX 9

CRACK STABILITY AND STRENGTH VARIABILITY IN ALUMINA CERAMICS WITH T-CURVE BEHAVIOR

ABSTRACT

Four batches of alumina ceramics were manufactured, characterized, and tested to determine the influence of microstructure on strength variability. Two batches of materials were produced from a high-purity starting powder and had an equiaxed grain morphology, one with a mean grain size of 5 μm and the other with a mean grain size of approximately 10 μm. Two batches of material with similar mean grain sizes were also manufactured from a lower purity starting powder which resulted in materials with an elongated grain shape and a broad grain size distribution. Mechanical tests indicated that only the coarse-grained, lower purity alumina exhibited strong flaw tolerance and T-curve behavior. *In-situ* crack studies confirmed that this was the only material for which significant stable crack extension occurred from flaws free of contact-induced residual stress. Strength tests on polished specimens indicated that the highest mean strength was achieved in fine-grained materials with little or no flaw tolerance. However, the lowest strength variability was measured in the coarse grained, lower purity alumina which exhibited strong T-curve behavior. The improved mechanical reliability that was observed in this material are rationalized in terms of T-curve behavior and its resultant influence on crack stability.

KEY WORDS

Alumina, T-curve, crack stability, strength variability, flaw tolerance, Weibull modulus, indentation

CRACK STABILITY AND STRENGTH VARIABILITY IN ALUMINA CERAMICS WITH T-CURVE BEHAVIOR

Desiderio Kovar[*][†]

Department of Materials Science and Engineering

Carnegie Mellon University

Pittsburgh, PA 15213-3890

Stephen J. Bennison[†]

E.I. du Pont de Nemours and Co., Inc.

Central Research and Development

Experimental Station, Bldg. E356/311

Wilmington, DE 19880-0356

Michael J. Readey[†]

Sandia National Laboratories

Glass and Electronic Ceramics

MS 0333, Organization 1845

Albuquerque, NM 87185-0333

[*] Now at University of Michigan, Materials Science and Engineering Department, Ann Arbor, MI 48109-2136
[†] Member of the American Ceramic Society

Four batches of materials were manufactured from two different commercially available alumina powders; a 99.7% alumina (A-16 SG, ALCOA Industrial Chemicals) and an 99.99% alumina (AKP-50, Sumitomo Chemical America Inc.). Specimens were prepared using conventional powder processing by first uniaxially pressing the as-received powders in a high-purity graphite die at 21 MPa into disk-shaped compacts. The compacts were then individually cold isostatically pressed at 276 MPa to eliminate gradients in the green density present after uniaxial pressing.

Specimens were packed in loose powder of identical composition to the compacts, placed into an alumina crucible, and fired in air. Fine-grained specimens were fired at 1600°C for 5 hours while coarse-grained specimens were fired at 1700°C for 25 hours. A heating rate of 5°C/min. and a cooling rate of 10°C/min. were used for all four batches of materials.

After firing, selected specimens were ground and polished to facilitate examination of the microstructure. The mean grain size, grain size distribution, and grain shape distribution for each material were determined using a computer-assisted image analysis system; details of this procedure are given elsewhere.[7] The densities of the materials were measured using Archemedes' method to an accuracy of ±0.001 g/cm^3 using water as an immersion medium.[8]

B. Mechanical Properties

1. Indentation-Strength Tests

Biaxial flexure specimens were used to measure the strength of each material. They were prepared by grinding and polishing one side of the disk-shaped specimens using successively finer metal-bonded diamond grinding pads and diamond paste until the specimens had a mirror-like finish. Indentations were placed in the center of the polished

CRACK STABILITY AND STRENGTH VARIABILITY IN ALUMINA CERAMICS WITH T-CURVE BEHAVIOR

I. Introduction

It has been suggested that mechanical reliability of ceramics can be improved by altering their microstructure. In particular, in materials that have a crack length-dependent toughness or T-curve, stable crack extension often precedes catastrophic failure. In such instances, it has been shown that strength becomes insensitive to the initial flaw size.[1] Because strength variability in many brittle materials is dependent on the flaw size distribution, it has been suggested that decreased strength variability should result.[2-4] However, the occurrence and amount of crack stability depends on the initial flaw size as well as the nature of the flaw.[5] For example, tensile residual stresses that arise due to sharp-particle contact cause stable crack extension in materials which exhibit little or no T-curve behavior.[6] Similarly, residual stresses due to thermal expansion anisotropy may also influence crack growth behavior from natural flaws such as pores or microcracks.

In this study, alumina with different microstructural features such as grain size and grain shape were systematically manufactured, characterized, and tested. Crack stability and T-curve behavior were measured using indentation flaws to initiate failure. In addition, the influence flaw history on mechanical reliability was investigated by measuring strength variability from both natural and indentation flaws in materials that exhibit varying degrees of T-curve behavior.

II. Experimental Procedure

A. Materials

employed to facilitate the location of the crack tips. The individual crack lengths were measured to a resolution of between 0.5-10 μm, depending on the magnification. The tests were performed by increasing the load in increments of 10-100 N until crack extension in one or more of the surface traces of the indentation cracks was apparent. When crack growth was detected, each of the traces were measured before again increasing the load. This was continued repeatedly until the specimen failed. Usually, four radial cracks emanated from the indentation corners immediately following indentation. However, at lower indentation loads or when the grain size in the material was large, it was common for more than four cracks to be present. Independent of the morphology of the cracks, after an initial period in which all of the cracks would grow, two cracks on opposite sides of the indentation impression would inevitably become dominant as the load was increased and, at this point, the other cracks would stop growing. Thus, the surface trace, c, was taken as average length of the two dominant radial cracks.

3. T-Curve Behavior

Short-crack T-curve behavior was determined using the method developed by Braun et al.[1] This technique requires that the indentation parameters χ and ψ be calibrated for a material that exhibits no T-curve behavior. It is assumed that these coefficients do not vary as a function of grain size or with small changes in the composition of the material. Thus, once these parameters are determined for a control material, the T-curves for similar materials may be deconvoluted from their indentation-strength response.

4. Strength Variability from Polished Specimens

The natural strength of each material was measured using unindented, polished biaxial flexure specimens identical to those used to measure indentation strength. Tests

disks using a Vickers diamond indentor with a dwell time of 10 seconds at loads ranging between 5-200 N. The indentation cracks were immediately covered with silicone oil (Dow Corning Diffusion Pump Oil, Midland MI) after indentation to minimize the introduction of moisture into the indentation cracks. Specimens were then rapidly loaded at a constant cross-head displacement rate (7.6 mm/min.) in biaxial tension using a servo-hydraulic testing machine (MTS 810, MTS, Minneapolis, MN) according to ASTM F394.[9] The strength was calculated using thin-plate theory from the peak load and the specimen dimensions. All specimens were examined after testing to ensure that fracture originated from the indentation cracks. Only data from specimens that failed from indentations were included in the results.

2. Crack Stability

Crack-growth studies were performed using larger biaxial flexure disks with a nominal diameter of 52 mm and a thickness of 4 mm. These specimens were prepared in an identical manner to the smaller disks used to measure the indentation-strength response described in Section II-B-1. Because moisture has been shown to have a profound influence on both the equilibrium crack size and crack configuration,[10] specimens were dried and indented in a dry-box (moisture content <0.20 ppm). Some specimens were immediately placed into a specially designed testing apparatus that is described in detail elsewhere.[1] Other specimens were removed from the dry-box after indentation and annealed in air for 4 hours at 1100°C to remove the indentation residual stress. Following the annealing treatment, the specimens were dried before being placed into the testing apparatus.

The testing apparatus consisted of a sealed chamber, a load cell, and a piezoelectric driver that allowed the load to be applied to the system while monitoring the surface traces of the indentation cracks *in situ* using an optical microscope. Lens magnifications were varied from 50-1000x and brightfield, darkfield, and Nomarski contrast modes were

indentation crack sizes tended to be normally distributed, the strengths were assumed to follow a normal distribution. In addition, all of the strength data fit a Gaussian distribution well whereas a poor fit was obtained using a Weibull distribution. The coefficient of variation, C_V, for each batch of material was calculated by taking the ratio of the standard deviation to the mean. To facilitate comparisons between the strength variability of the materials, the data was plotted on a *probability scale* where the slope of a line is equal to the inverse of the standard deviation. Thus, the slope of a line on a Weibull plot is a measure of the relative strength variability, while the slope of a line on a probability plot is a measure of the absolute strength variability. However, C_V, like the Weibull modulus, is a measure of the relative strength variability.

III. Results

A. Material Characterization

SEM micrographs of representative polished and thermally-etched specimens are shown in Figure 1a-d. The densities of the materials appear very high and measurements confirmed that they exceed 98.5% in all of the materials. The lower purity aluminas exhibit a relatively broad grain size distribution and many of the grains are tabular or elongated. In contrast, the higher purity aluminas have a narrow grain size distribution and an equiaxed grain morphology. The mean grain sizes for the fine and coarse-grained, lower purity aluminas are 4.0 and 12.7 μm, respectively while the mean grain sizes for the higher purity aluminas are 5.0 and 10.2 μm. Grain size distributions are shown for the four materials in Figure 2a-d. The distributions reveal that normal grain growth occurs in both material systems as the distributions are self similar for a given powder purity. They also confirm that the higher purity aluminas have a narrower grain size distribution compared to the lower purity aluminas.

were performed as described in Section II-B-1. A minimum of 24 specimens were tested

for each batch of material. The strength of each specimen within a batch was ranked from

lowest to highest and the probability of failure, P_f, for the ith specimen was assigned using

the following estimator:

$$P_f = \frac{i - 0.5}{n} \qquad (1)$$

where n is the number of specimens tested in each batch. The strength distributions were

assumed to follow a two-parameter Weibull distribution. The maximum likelihood method

was used the Weibull parameters and a boot-strap technique was used to estimate the

confidence limits on the Weibull modulus.[11] To facilitate qualitative comparisons between

the strength variability of the materials, the data was plotted on a traditional Weibull scale

(ln ln [1/[1-P_f)]) versus ln [strength]).

5. Strength Variability from Indented Specimens

Because it is likely that flaw populations change when the microstructure of a

material is altered, it is difficult to directly determine the influence of microstructure on the

strength distributions. For example, changes is strength variability may be due to

differences in flaw populations or may result from T-curve behavior. To isolate these

effects, a batch of specimens were fractured using controlled indentation flaws to initiate

failure. All of the specimens were indented at a load of 100 N and fractured using the

procedure described in Section II-B-3. This load was sufficiently large to ensure that the

indentation was the critical flaw in all of the specimens.

The Weibull distribution was not used to characterize the strength distribution for

indented specimens because weak link statistics, and therefore the Weibull distribution, are

no longer appropriate when a single dominant flaw is introduced into specimens. Since the

of the indentation load. This compares to the theoretical prediction that the critical crack size should be 2.5 times greater than the initial indentation flaw size for a material with a constant fracture toughness.[12] The crack path in this material was a mixture of transgranular and intergranular. In some cases, small microcracks were observed to open at grain boundaries as the crack propagated in their vicinity. However, microcracking was not profuse and was isolated to only a few grain boundaries.

In Figure 6, crack length versus applied load is shown for the c-el alumina in the as-indented condition at two different indentation loads. As with the f-eq material, the crack moved irregularly, jumping at least a facet length or more as the crack propagated. However, compared to the f-eq alumina, the tendency towards intergranular cracking was much greater in this material. Also, because of the larger grain size and the elongated grain shape, the crack path was much more tortuous and instances of grain bridging more numerous. SEM micrographs of the fracture surfaces for the four materials are shown in Figure 7a-d at the same magnification. These images confirm that the tendency towards intergranular cracking is much greater in the lower purity alumina compared to the higher purity aluminas. In addition, the roughness of the fracture surfaces increase dramatically as the grain size is increased and the powder purity is decreased.

D. Crack Stability from Annealed Indentations

In Figure 8, crack length is plotted as a function of applied stress for specimens that were annealed following indentation. Compared to the as-indented (unannealed) specimens, all of the annealed specimens failed at higher loads, consistent with the notion that the residual stress field due to the indentation was removed during annealing. However, in contrast to the unannealed specimens where all of the materials exhibited substantial stable crack extension, virtually no stable crack growth was observed in any of

Grain shape distributions are shown in Figure 3a-d. The grain shape also remains self-similar as the mean grain size is increased for both the lower and higher purity aluminas. However, the grain shape is significantly more elongated for the lower purity aluminas with mean aspect ratios greater than 2.0 compared to approximately 1.5 in the higher purity aluminas.[*]

B. Indentation-Strength

The indentation strength responses for the four aluminas are shown in Figure 4a-d. The solid line in each plot is the theoretical behavior for a material with a constant toughness and has a slope of -1/3.[12] The hatched box on the left side of each plot represents the strength distributions for polished but <u>unindented</u> specimens.

The indentation-strength response for the f-eq material exhibits classically brittle behavior with a slope very similar to the theoretical behavior for materials with a constant toughness while the c-eq and the f-el materials exhibit a slight deviation from the theoretical line. In contrast, the c-el material exhibits the largest deviation from the theoretical line indicating that the strength of this material exhibits the greatest degree of flaw tolerance.

C. Crack Stability

Crack length as a function of applied stress (log-log) is shown for the fine-grained, homogeneous alumina in Figure 5 in the as-indented condition. As the applied load was increased, the indentation cracks grew in an irregular fashion jumping one or more facet lengths before arresting. This behavior was independent of the indentation load or the crack length. When the crack length reached a critical value, the crack began to accelerate and the specimen failed. In the fine-grained, homogenous alumina, this critical crack length, c_M, was about 2.8 times greater then the initial indentation crack size, independent

---

[*] The materials will be abbreviated "f" or "c" for fine or coarse-grained and "eq" or "el" for equiaxed or elongated (e.g. "f-eq" for fine-grained, equiaxed alumina).

secondary flaw population, only the c-el alumina, which exhibits strong T-curve behavior, shows a statistically higher Weibull modulus.

2. Indented Specimens

Strength distributions from indented specimens are plotted using a probability scale in Figure 11. As expected from the indentation strength test, the f-eq alumina exhibits the lowest mean strength at an indentation load of 100 N. The c-eq and the f-el aluminas have similar mean strengths which are slightly higher than the f-eq alumina and the c-el material exhibits the highest mean strength. The coefficients of variation in strength range from 5.7 to 6.7% and thus, statistically, there is no difference in strength variability between materials. These results would seem to imply that the microstructure does not influence the strength variability of alumina. However, despite the fact that controlled indentation flaws were used to initiate failure, the critical flaw size distributions are not equivalent in these material as illustrated in Figure 12. From these micrographs it is apparent that indentations in the f-eq material are well behaved and exhibit little variability in crack length. In contrast, variability in crack length and morphology increase dramatically in the more flaw tolerant materials.

Crack lengths were measured in an attempt to quantify the flaw size distribution and a summary of these results is shown in Table II. The quantitative measurements agree with the qualitative observations; the f-eq alumina exhibits the least variability in indentation crack size with a coefficient of variation in crack length of 5.0% while the coefficient of variation in the other aluminas varied from 8.3% to 11.7%. Thus, although the overall strength variability does not appear to be sensitive to the microstructure, the indentation crack sizes are. In fact, the relationship between variability in the initial indentation crack size and microstructure is similar to that between flaw tolerance and microstructure; variability in crack sizes increases with grain size and grain aspect ratio. Most significantly, although the <u>variability in the indentation flaw size increases dramatically with</u>

10

the materials except for the c-el alumina. Cracks in this material grew to roughly two times their initial size before catastrophic failure ensued.

E. T-curve Behavior

Using the indentation strength data, the parameters χ and ψ were determined to be 0.100 and 1.00, respectively. This compares to previous estimates for similar alumina ceramics of 0.071-0.082 for χ and 0.77-1.26 for ψ. T-curves deconvoluted from the indentation strength data using these estimates of the indentation parameters are shown in Figure 9 for each of the four aluminas. The T-curve for the f-eq alumina rises slowly and quickly reaches a plateau toughness of approximately 3.6 MPa√m within 250 μm. The T-curves for the c-eq and f-el aluminas also rise slowly but continues to increase to a toughness of approximately 5 MPa√m at a crack length of 1000 μm. The c-el alumina exhibits the most pronounced T-curve behavior, beginning at a lower toughness and rising much more quickly than the T-curves for the other materials.

F. Strength Variability

1. Polished Specimens

Weibull plots from polished specimens are shown for the four materials in Figure 10. The Weibull moduli and the 90% confidence limits on the Weibull moduli are shown in Table I. The Weibull moduli vary from 7.8 and 5.3 for the f-eq and c-eq aluminas to 9.2 and 14.8 for the f-el and c-el aluminas. From the confidence limits, a statistical difference exists between the Weibull modulus for the c-el alumina and all of the other aluminas and between the c-eq and f-el aluminas. The low Weibull modulus of the c-eq alumina has been attributed to a secondary population of abnormal grains which did not exist in the other three materials.[6] If the data is censored to eliminate specimens that failed from this

B. T-Curve Behavior

There are a number of important features that are apparent from the T-curves measured using the indentation strength method. First, T-curve behavior does not come without penalty. Consistent with previous observations in alumina and other grain bridging ceramics, the increase in toughness at longer crack lengths comes at the expense of the short-crack toughness.[17-19] For instance, although the fine-grained equiaxed material had the lowest long crack toughness, it had the highest short-crack toughness. Thus, the shape of the T-curve is tied to the microstructure by the grain size, grain shape, and the tendency for intergranular cracking. Materials that contain coarse, elongated grains and fracture intergranularly exhibited the steepest T-curves and the greatest increase in toughness.

C. Crack Stability

Stable crack extension depends on a number of factors including the initial flaw size, the shape and magnitude of the T-curve, as well as the nature of the critical flaw.[5] The criterion for fracture based on linear elastic fracture mechanics states that if the applied stress intensity, K_I, exceeds the toughness, T, then crack growth occurs. However, if the T-curve rises very quickly, stable crack extension may precede catastrophic failure. The amount of stable extension is governed by the derivative of the applied stress intensity , dK_I/dc and the derivative of the toughness, dT/dc. Stable crack extension occurs in materials with a rising toughness until:

$$\frac{dK_I}{dc} > \frac{dT}{dc} \qquad (2)$$

grain size and grain aspect ratio, the strength variability is not affected by changes in the indentation flaw size distribution .

IV. Discussion

A. Flaw Tolerance

The current results illustrate that the flaw tolerance behavior of alumina ceramics are not controlled merely by the mean grain size. For example, although the f-eq alumina and the f-el alumina had similar mean grain sizes, the flaw tolerance and T-curve behavior were much more pronounced in the f-el alumina. In addition, the f-eq alumina and the c-eq alumina exhibit similar behavior despite a factor of 2.5 difference in the mean grain size. Thus, microstructural characteristics other than grain size such as grain shape, grain size distribution, and grain boundary toughness can have a pronounced influence on the toughness characteristics in alumina ceramics. For example, previous work has shown that broadening the grain size distribution does not lead to more pronounced flaw tolerance in high-purity alumina ceramics because larger grains fracture transgranularly and therefore do not contribute to enhanced grain bridging.[6] Similarly, in our current study, only very modest flaw tolerance was observed in the high purity aluminas even as the grain size was coarsened by more than a factor of 2.

Previous studies on aluminas indicate that in all but the purest materials, a glassy phase is present at many of the grain boundaries following sintering.[13, 14] In addition to providing an easier path for crack propagation, this glassy phase results in a broader grain size distribution and elongated or tabular shaped grains.[15] Thus, larger, more effective grain bridges and hence improved flaw tolerance are observed in the lower purity aluminas compared to high-purity aluminas with similar mean grain sizes.[16, 17]

11

Although all of the aluminas exhibit some degree of T-curve behavior, the c-el alumina clearly exhibits the strongest T-curve behavior. In fact, based on the tangency construction, this is the only material that has a T-curve that is sufficiently steep to allow stable crack extension from flaws free of contact-induced residual stresses (e.g. natural flaws). Recall that when the indentations were annealed to remove the residual stress (See Figure 8.), we observed significant stable crack extension only in the c-el alumina.

These results show that the nature of the flaw plays an important role in determining whether the strength of a material is sensitive to the initial flaw size. For example, although materials that exhibit weak T-curve behavior exhibit stable crack extension from indentation flaws, the strength of the material shows a strong dependence on the indentation flaw size. When the same material fails from a natural flaw, no stable crack extension is observed and again the strength is again dependent on the initial flaw size. It is only for materials that exhibit very strong T-curve behavior where flaw tolerance is observed from both natural and contact-induced flaws.

D. Strength Variability from Polished Samples

The Weibull plot in Figure 10 shows that strength variability decreases with increasing flaw tolerance for the materials tested. Similar results were found by Ting *et al.* for a variety of alumina ceramics; the highest Weibull modulus was obtained in the alumina with broadest grain size distribution and an elongated grain shape while the lowest Weibull modulus was obtained for the material with an equiaxed grain morphology and a narrow grain size distribution.[20] Hirosaki *et al.* and Hoffman and Petzow both found similar results for another grain bridging ceramic, silicon nitride.[21, 22] Ting *et al.* and Hirosaki *et al.* argued that the decreased strength variability in materials with increased heterogeneity in the microstructure was due to a narrowing in the critical flaw size distribution. They suggested that in materials that have a narrow grain size distribution, there is a decreased

14

at which point the specimen fails catastrophically. For typical natural flaws, the applied stress intensity is given by:

$$K_I = \sigma \psi \sqrt{c} \qquad (3)$$

Thus, a simple graphical criterion for crack stability can be given by plotting the applied stress intensity versus the square root of the crack length and then superimposing the T-curve on this plot (the tangency construction). However, when contact-induced residual stresses are present (e.g. an indentation flaw), they provide an additional driving force for crack extension. It has been shown that for indentation cracks, this driving force can be accounted for by subtracting the stress intensity due to the indentation residual stress from the toughness.[12] Thus for contact-induced flaws, the toughness, T_R, is given by:

$$T_R = T - \frac{\chi P}{c^{3/2}} \qquad (4)$$

The advantage of subtracting the indentation residual stress intensity from the toughness rather than adding it to the applied stress intensity as is usually done is that the conventional graphical tangency construction can still be performed.

The T-curves determined from the indentation strength data along with the tangency constructions are shown for the four materials in Figure 13a-d for indentation flaws and for natural flaws. As expected, all of the materials are predicted to exhibit stable crack extension from indentation flaws based on the tangency construction. Indentation flaws in the f-eq alumina should grow to 2.6 times their initial size before the specimens catastrophically fail. In the f-el, c-eq, and c-el materials with stronger T-curve behavior additional stabilization is predicted up to approximately 4 times the initial flaw size. Comparing the observed crack stability from Figures 5 and 6 with the predicted amount of crack stability, good agreement is seen.

13

One method of introducing controlled critical flaws with stress intensities that can be accurately computed is through the use of indentation flaws.[24]

For example, the strength distribution shown in Figure 11 for specimens indented at a load of 100 N revealed that there was essentially no difference in the variability in strength in aluminas with vastly different microstructures. However, measurements of the indentation crack sizes revealed that the distribution in the crack sizes varied greatly depending on the material. Cracks in the c-el alumina had more than twice the variability compared to the f-eq alumina, yet no difference in strength variability was detected. This suggests that narrowing of the critical flaw size distribution by itself cannot account for the reduction in strength variability that was measured in the c-el material.

Further evidence that the critical flaw size distribution cannot be the only factor that controls strength in grain bridging materials was provided by the crack growth tests on indented and annealed specimens. These tests conclusively demonstrated that even when a flaw is not subject to the strong residual stress associated with indentations, stable crack extension is observed in materials with strong T-curve behavior whereas no significant crack stability was observed in aluminas with less pronounced T-curve behavior. While the influence of flaw size distribution cannot be discounted, this suggests that the stabilizing influence of T-curve behavior must also play an important role in reducing strength variability in materials that exhibit strong T-curve behavior.

V. Conclusions

Four batches of alumina ceramics with different microstructural features were manufactured from two commercially available alumina powders. The lower purity aluminas exhibited a broader grain size distribution and a more elongated shape compared to the higher purity aluminas with similar mean grain sizes and an examination of the fracture mode revealed that the lower purity aluminas had a greater propensity to crack

probability of encountering a large, strength controlling defect. Since large defects occur in only a limited number of specimens, there is greater variability in strength for such materials. In contrast, they argued, materials with heterogeneous microstructures contain a more uniform dispersion of large flaws, and therefore these materials exhibit less variability in strength.

Hoffman and Petzow argued that it is T-curve behavior rather than a narrowing in the flaw size distribution is responsible for the reduced strength variability that is observed in grain bridging ceramics; little experimental evidence was offered to support this supposition. One method of distinguishing whether T-curve behavior or changes in the critical flaw size distribution are responsible for the changes strength distributions involves quantifying the critical flaw population. However, as was stated earlier, it is often the case that the failure origin cannot be determined in some of the specimens; it is particularly difficult in coarse-grained ceramics.

Even when the failure origin can be unambiguously determined, it is usually not possible to accurately assess the influence of the critical flaw size population. Consider the simplest case of a Griffith-like flaw; despite the fact that the crack size can be specified precisely, one must also know the geometry of the flaw to calculate the toughness. For example, even if it is known that an annular flaw surrounding a pore was responsible for failure, the crack shape parameter, and therefore the applied stress intensity, can vary by more than a factor of 2 depending on the assumptions regarding the size of the annular crack in relation to the pore.[23] Additional complications arise if one considers more realistic crack geometries or the influence of residual stresses that act on the crack. Thus, it quickly becomes clear that flaw size is only one of many factors that influence the strength of a specimen.

E. Strength Variability from Indented Specimens

have high mean strength, they exhibit poor strength variability and their strength is particularly susceptible to contact-induced damage. Coarsening the microstructure of the high-purity alumina does not significantly increase the flaw tolerance because grain bridging is limited. As a result, this material exhibits poor strength variability and a moderate susceptibility to contact-induced flaws. Despite the presence of a broader grain size distribution, elongated grain shape, and decreased the strength of grain boundaries, the fine-grained lower purity alumina exhibits similar properties. It is only when these microstructural feature are combined with a larger grain size that significant grain bridging occurs. T-curve behavior in this material is sufficiently strong to stabilize both natural and contact-induced flaws. As a result, this material exhibits low strength variability from natural flaws and strong flaw tolerance to post-processing induced flaws.

Acknowledgments

intergranularly. A combination of large, elongated grains and intergranular fracture resulted in strong grain bridging in the coarse-grained lower purity alumina. As a result, this material exhibited greatly reduced flaw sensitivity to indentations and significant T-curve behavior. *In-situ* crack propagation tests confirmed that this was the only material that exhibited significant stable crack extension from flaws free of contact-induced residual stress.

Strength tests on polished specimens showed that the coarse-grained, lower purity alumina exhibited less strength variability compared to the other materials. Because of the difficulties in quantifying critical flaw populations, however, it could not be determined from this data alone if the differences in strength variability were due to changes in the critical flaw population as the microstructure was altered or if instead differences in strength variability were due to flaw tolerance associated with T-curve behavior. Strength tests on specimens indented at a load of 100 N were used as a means of introducing controlled flaws into the material and then measuring the response of the strength distributions. These tests, revealed that there was no statistical difference in strength variability between materials at a given indentation load. Examination of the indentation cracks showed that the variability in the crack sizes increased dramatically as the grains size or grain aspect ratio was increased. Despite this increase in variability in the critical crack size with increasing heterogeneity in the microstructure, no increase in variability in strength was detected. Based on crack stability measurements and strength variability measurements from indented specimens, the reduced strength variability that is observed on polished specimens for the alumina with the coarse-grained, elongated microstructure can not be accounted for simply by changes in the critical flaw population.

From a practical point of view, these results have many important implications with respect to materials selection when reliability of a component is crucial. To produce components that are reliable, the strength of a material must be insensitive to both natural and processing flaws. For example, while it is true that fine-grained, high-purity aluminas

Boiling Water"; pp. 5-7 in Vol. 15.01, Edited by P.C. Fazio, *et al.* ASTM, Philadelphia, PA, 1992.

[9]Anon, F 394-78 Standard Test Method for Biaxial Flexure Strength (Modulus of Rupture) of Ceramic Substrates"; Vol. 15.02, *Glass; Ceramics Whitewares.* Edited by P.C. Fazio, *et al.* American Society for Testing and Materials, Philadelphia, PA, 1978.

[10]R.F. Cook and G.M. Pharr, "Direct Observation and Analysis of Indentation Cracking in Glasses and Ceramics," *J. Am. Ceram. Soc.,* **74** [4] 787-817 (1990).

[11]C.A. Johnson and W.T. Tucker, "Advanced Statistical Concepts of Fracture in Brittle Materials"; pp. 709-715 in Engineered Materials Handbook, Vol. 4, *Ceramics and Glasses.* ASM International, Materials Park, OH, 1992.

[12]B.R. Lawn, *Fracture of Brittle Solids.*, 2nd ed. Cambridge University Press, Cambridge, UK, 1993.

[13]C.A. Bateman, S.J. Bennison, and M.P. Harmer, "Mechanisms for the Role of Magnesia in the Sintering of Alumina Containing Small Amounts of Liquid Phase," *J. Am. Ceram. Soc.,* **72** [7] 1241-1244 (1989).

[14]C.A. Handwerker, P.A. Morris, and R.L. Coble, "Effects of Chemical Inhomogeneities on Grain Growth and Microstructure in Al_2O_3," *J. Am. Ceram. Soc.,* **72** [1] 130-136 (1989).

[15]H. O'Donnel, M.J. Readey, and D. Kovar, "The Effect of Glass Additions on the Indentation Strength Behavior of Alumina," *J. Am. Ceram. Soc.,* **78** [4] 849-856 (1995).

References

[1]L.M. Braun, S.J. Bennison, and B.R. Lawn, "Objective Evaluation of Short Crack Toughness Curves Using Indentation Flaws: Case Study on Alumina-Based Ceramics," *J. Am. Ceram. Soc.*, **75** [11] 3049-3057 (1992).

[2]C.J. Fairbanks, B.R. Lawn, R.F. Cook, and Y.M. Mai, "Microstructure and the Strength of Ceramics"; Fracture Mechanics of Ceramics, Vol. 8, Edited by R.C. Bradt, D.P.H. Hasselman, and F.F. Lange. Plenum Publishing Corp., New York, NY, 1986.

[3]R.F. Cook and D.R. Clarke, "Fracture Stability, R-curves and Strength Variability," *Acta Metall.*, **36** [3] 555-562 (1988).

[4]M.J. Readey, P.D. McNamara, C.L. McCallen, and B.R. Lawn, "Correlations Between Flaw Tolerance and Reliability in Zirconia Ceramics," *J. Mat. Sci.*, **28** 6748 (1993).

[5]S.J. Bennison and B.R. Lawn, "Flaw Tolerance in Ceramics with Rising Crack Resistance Characteristics," *J. Mat. Sci.*, **24** 3169-3175 (1989).

[6]D. Kovar and M.J. Readey, "Grain Size Distributions and the Mechanical Reliability of Alumina," *J. Am. Ceram. Soc.*, **In Press** (1995).

[7]D. Kovar and M.J. Readey, "Role of Grain Size in Strength Variability of Alumina," *J. Am. Ceram. Soc.*, **77** [7] 1928-1938 (1994).

[8]Anon, C 20-92 Standard Test Methods for Apparent Porosity, Water Absorption, Apparent Specific Gravity, and Bulk Density of Burned Refractory Brick and Shapes by

[23]G.C. Sih, *Handbook of Stress Intensity Factors.*, vol. 1. pp. 3.3.1-1 Lehigh University, Bethlehem, PA, 1973.

[24]B.R. Lawn, "The Indentation Crack as a Model Surface Flaw"; pp. 1-25 in Fracture Mechanics of Ceramics, Vol. 5, *Surface Flaws, Statistics, and Microcracking.* Edited by R.C. Bradt, A.G. Evans, D.P.H. Hasselman, and F.F. Lange. Plenum Press, New York, NY, 1983.

[16]R.F. Cook, S.W. Freiman, and T.L. Baker, "Effect of Microstructure on Reliability Predictions for Glass Ceramics," *Mat. Sci. Eng.*, **77** 199-212 (1986).

[17]P. Chantikul, S.J. Bennison, and B.R. Lawn, "Role of Grain Size in the Strength and R-Curve Properties of Alumina," *J. Am. Ceram. Soc.*, **73** [8] 2419-2427 (1990).

[18]N.P. Padture, J.L. Runyan, S.J. Bennison, L.M. Braun, and B.R. Lawn, "Model for Toughness Curves in Two-Phase Ceramics: II. Microstructural Variables," *J. Am. Ceram. Soc.*, **76** [9] (1993).

[19]N.P. Padture, S.J. Bennison, and H.M. Chan, "Flaw-Tolerance and Crack-Resistance Properties of Alumina–Aluminum Titanate Composites with Tailored Microstructures," *J. Am. Ceram. Soc.*, **76** [9] 2312-2320 (1993).

[20]J.-M. Ting, R.Y. Lin, and Y.-H. Ko, "Effect of Powder Characteristics on Microstructure and Strength of Sintered Alumina," *Am. Ceram. Soc. Bull.*, **70** [7] 1167-1172 (1991).

[21]N. Hirosaki, Y. Akimune, and M. Mitomo, "Effect of Grain Growth of β-Silicon Nitride on Strength, Weibull Modulus, and Fracture Toughness," *J. Am. Ceram. Soc.*, **76** [7] 1892-1894 (1993).

[22]M.J. Hoffman and G. Petzow, "Microstructural Design of Si_3N_4 Based Ceramics"; pp. 3-14, in Silicon Nitride Ceramics: Scientific and Technological Advances, Vol. 287, Materials Research Society Proceedings (Boston, MA, 1992). Edited by I.-W. Chen, *et al.* MRS, Pittsburgh, PA, 1989.

7.   SEM micrographs of the fracture surfaces of the a) f-eq b) c-eq, c) f-el, and d) c-el aluminas showing that the lower purity aluminas exhibit a larger fraction of intergranular cracking compared to the higher purity aluminas. Because of its tendency to fracture intergranularly and its large, elongated grain morphology, the c-el alumina exhibits the roughest fracture surface.

8.   Crack length versus applied stress for specimens indented at a load of 100 N and then annealed for a) f-eq b) c-eq, c) f-el, and d) c-el aluminas. Only the c-el alumina exhibits significant stable crack extension prior to catastrophic failure.

9.   T-curves deconvoluted from indention-strength data for the a) f-eq b) c-eq, c) f-el, and d) c-el aluminas. The thin, solid lines represent the applied stress intensity necessary to cause failure in indented specimens at indentation loads ranging from 2 N to 200 N. The broader lines are a fit to the common tangency of the applied stress intensity lines and represent the T-curves for each material.

10.   Weibull plot for polished specimens showing that , although the f-eq alumina exhibits highest mean strength, the c-el alumina exhibits the highest Weibull modulus.

11.   Strength distributions plotted on a probability scale for specimens containing 100 N indentations. There is no statistical difference in strength variability for indented materials in any of the materials.

12.   Optical micrographs of 100 N indentations in the a) f-eq b) c-eq, c) f-el, and d) c-el aluminas showing that variability in the indentation crack size increases with grain size and grain aspect ratio.

FIGURE CAPTIONS

1.   SEM micrographs of polished and thermally-etched a) f-eq, b) c-eq, c) f-el, and d) c-el alumina ceramics.

2.   Grain size distributions for the a) f-eq b) c-eq, c) f-el, and d) c-el aluminas. Grain size distributions remain self-similar with increasing grain size for a given powder purity. However, the lower purity aluminas exhibit broader grain size distributions.

3.   Grain aspect ratio distributions are shown for the a) f-eq b) c-eq, c) f-el, and d) c-el aluminas. The lower purity aluminas have a more elongated grain shape compared to the high purity aluminas.

4.   Indentation strength plots are shown for the a) f-eq b) c-eq, c) f-el, and d) c-el aluminas. The solid line represents the theoretical behavior for a material with a constant toughness and the hatched box indicates the natural strength for polished, unindented specimens. Only the c-el alumina exhibits strong flaw tolerance as evidenced by the deviation from the solid line.

5.   Crack lengths measured during slow fracture tests on indented specimens are shown as a function of the applied stress for the f-eq alumina for a variety of indentation loads. Arrows indicate the position where unstable crack growth begins. Stable crack extension is observed until the crack length reaches approximately 2.5 times the initial crack size, independent of the indentation load in this material.

6.   Crack length versus applied stress is shown for the c-el alumina at indentation loads of 50 and 100 N. In both cases stable crack extension occurs to a crack length greater than four times the initial indentation crack size before catastrophic failure ensues.

TABLE CAPTIONS

I.   Characteristic strengths, Weibull moduli, and 90% confidence intervals for the Weibull moduli (m_5 and m_{95}) for the four aluminas. The c-el alumina exhibits significantly less strength variability compared to the other aluminas.

II.   A comparison of the indentation crack lengths for the four aluminas used in this study at an indentation load of 100 N. Note that the variability in crack length increases with increasing grain size and aspect ratio.

13.   T-curves and tangency constructions are shown for the a) f-eq b) c-eq, c) f-el, and d) c-el aluminas. The solid lines are the T-curves for natural flaws while the shaded lines are the T-curves for indentation flaws (P = 100 N). The initial crack size is given by c_o and the dashed lines represent the tangency condition where catastrophic failure occurs at a crack length c_f. While all of the materials are predicted to exhibit stable crack extension from indentation flaws, only c-el alumina exhibits stable extension from natural flaws.

Material	Crack Length (μm)	C_v (%)
f-eq	221 ± 11	5.0
c-eq	182 ± 21	11.7
f-el	181 ± 15	8.3
c-el	192 ± 22	11.6

Table II

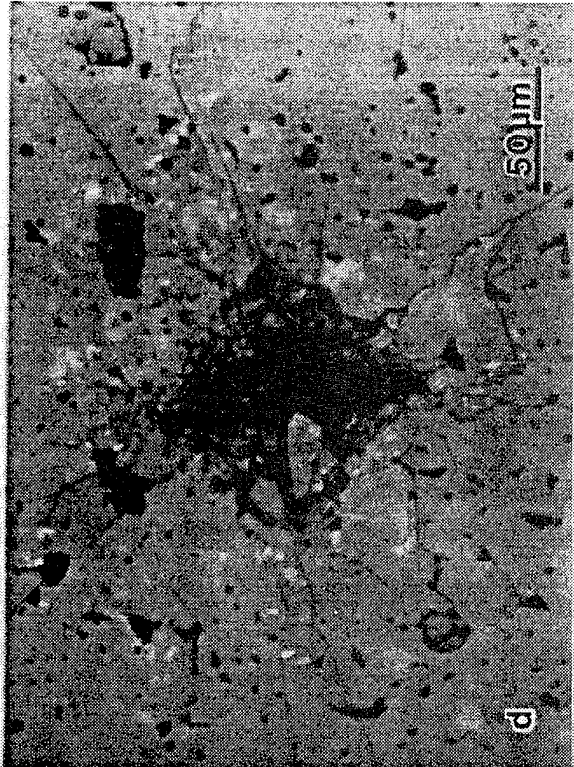| Material	σ_o	m	m_5	m_{95}
f-eq	507	7.8	6.1	10.5
c-eq	369	5.3	4.2	7.1
f-el	346	9.2	7.4	11.9
c-el	243	14.8	12.1	19.8

Table I
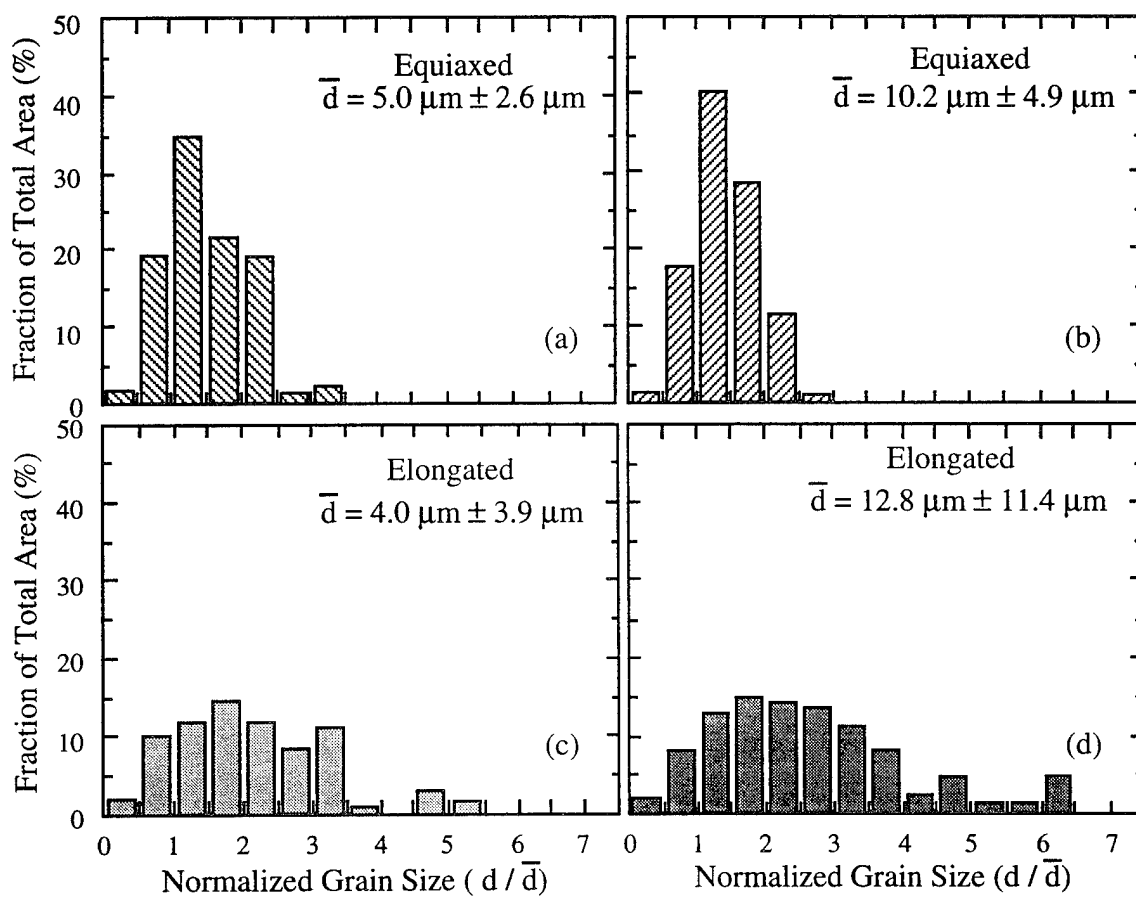
Figure 2
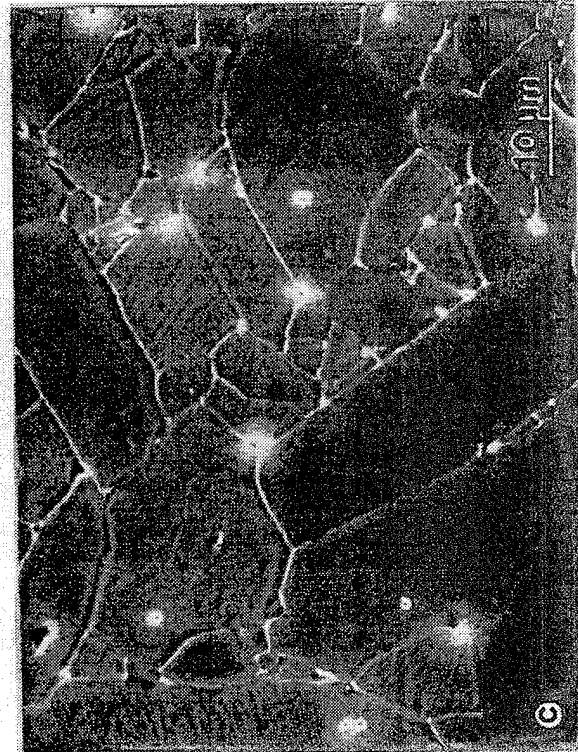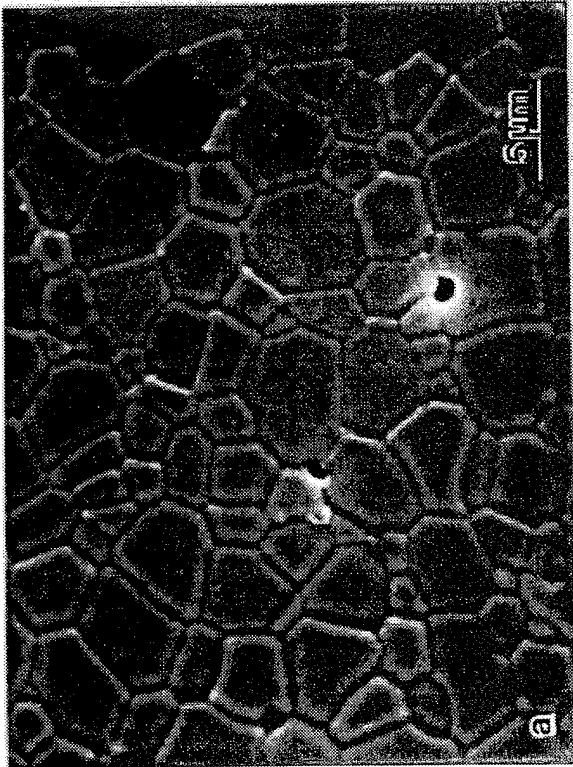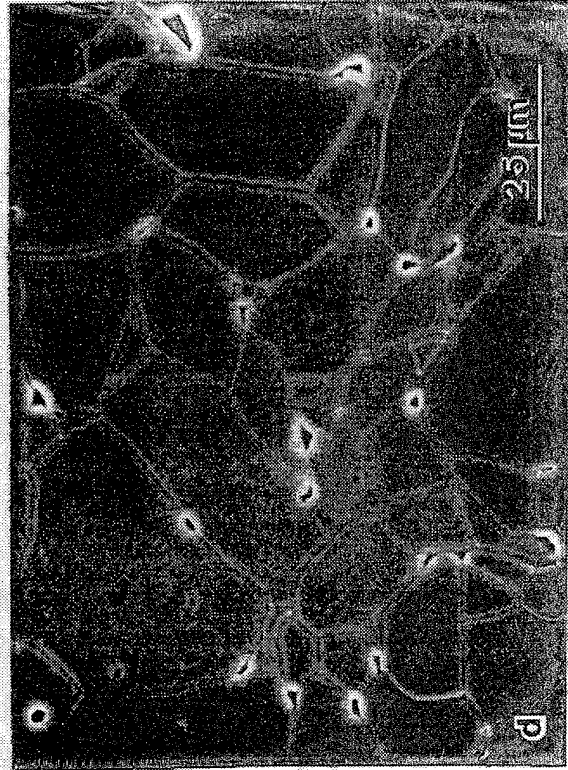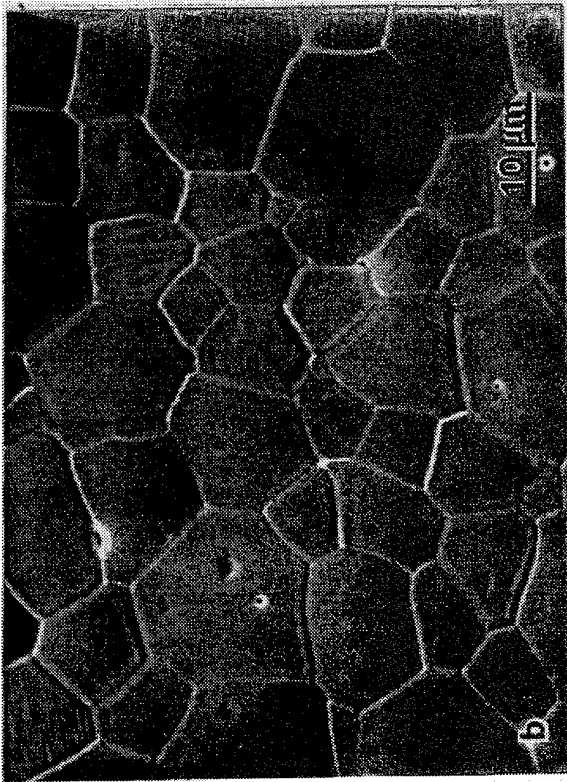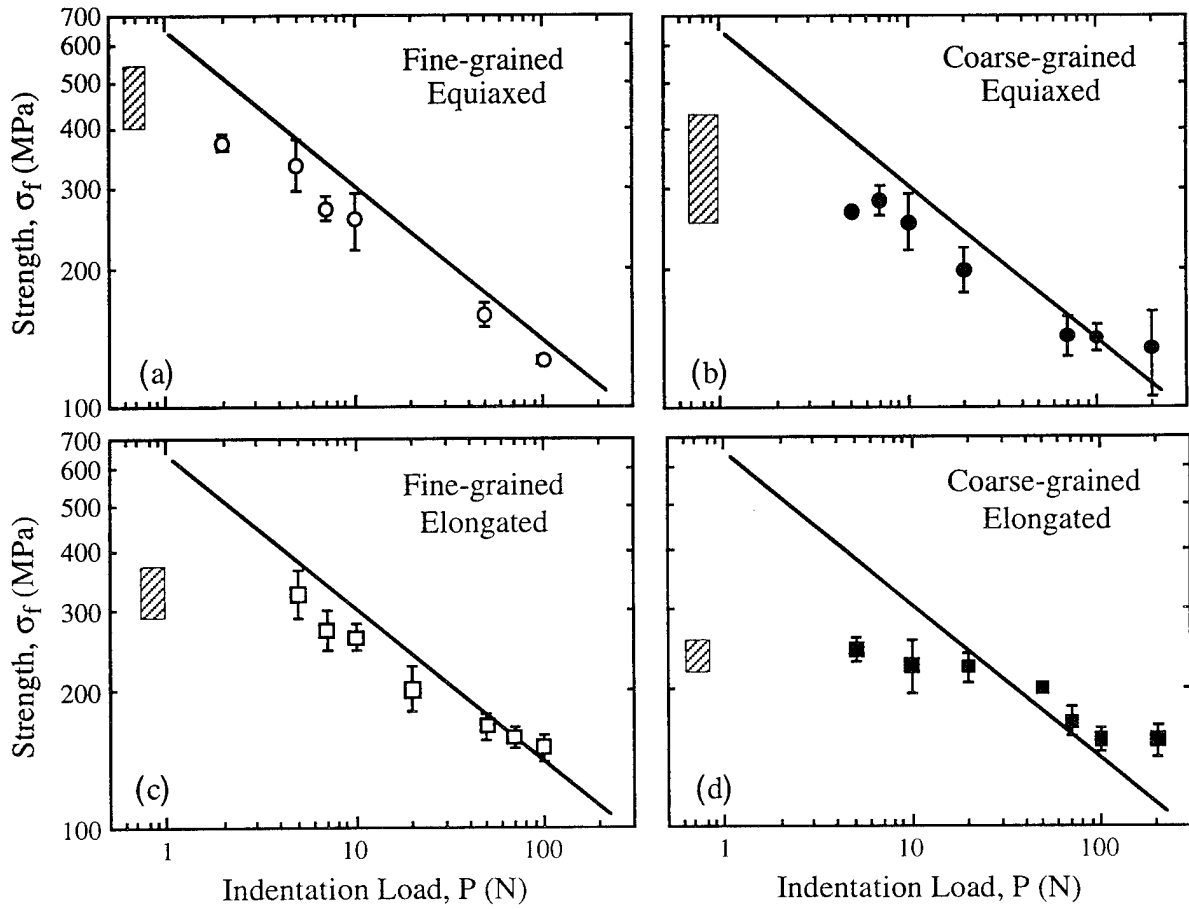
Figure 4
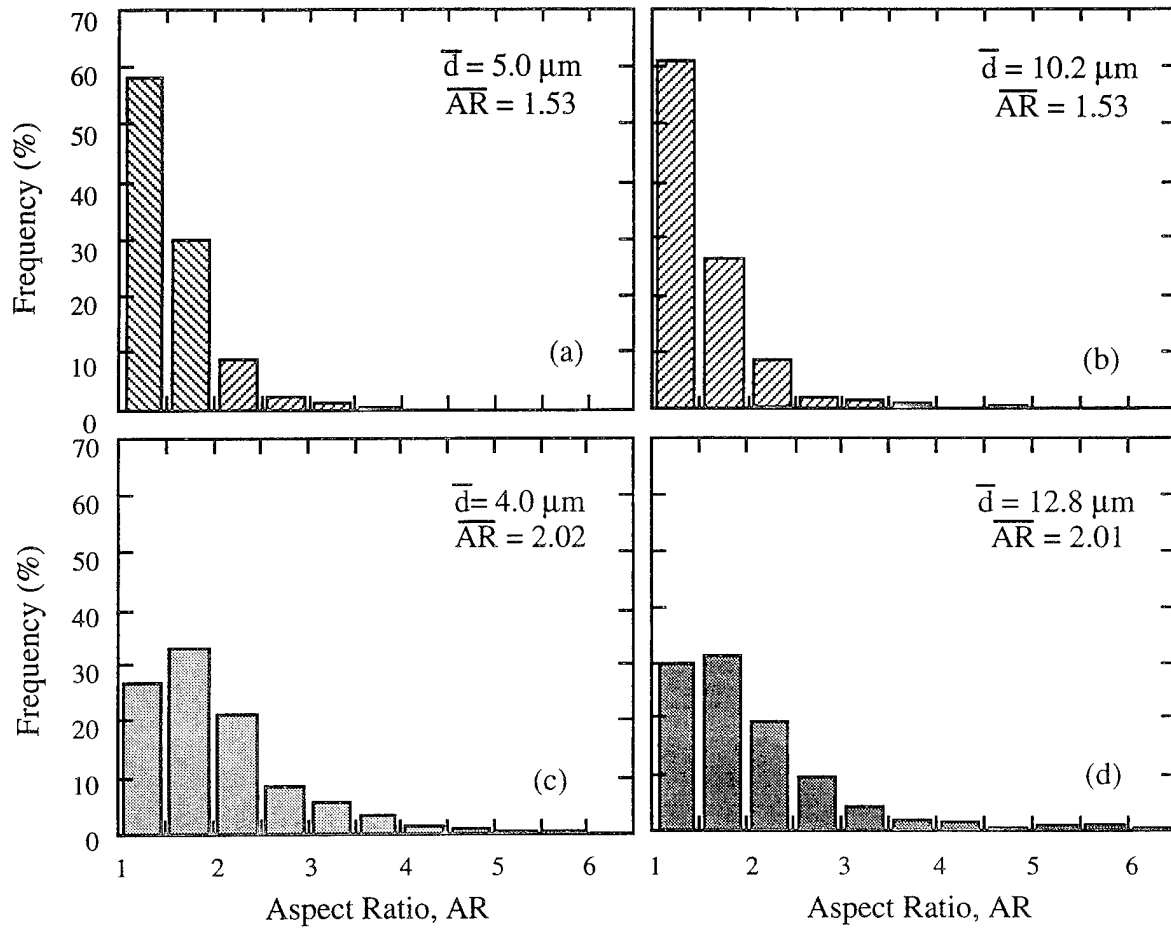
Figure 3
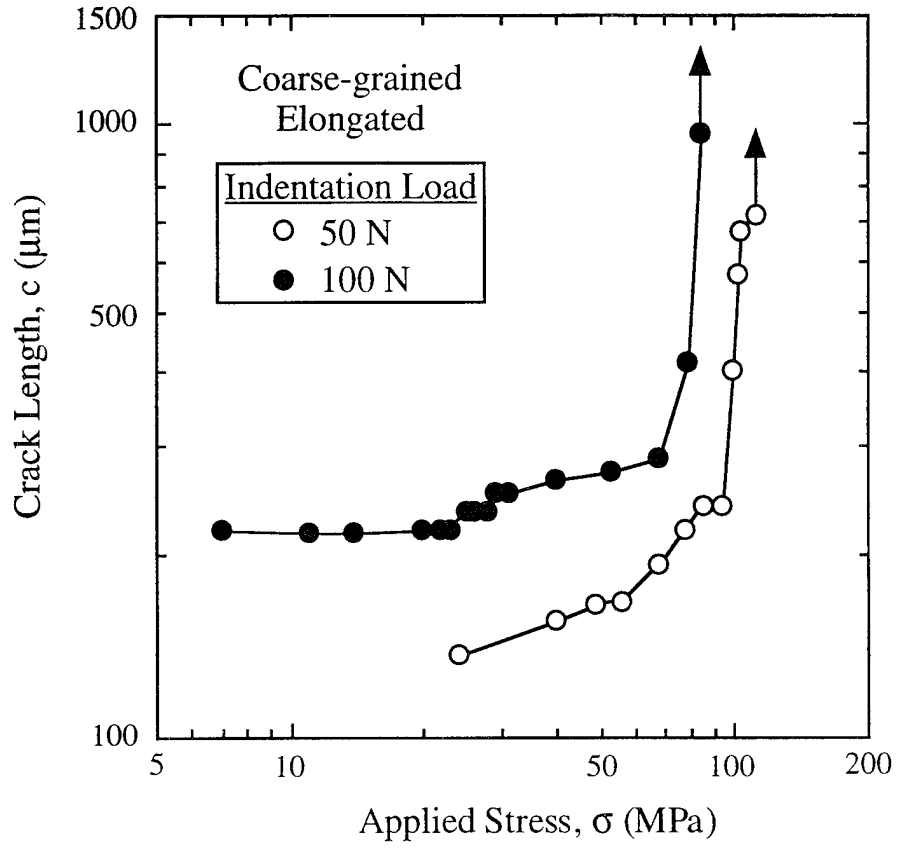
Figure 6
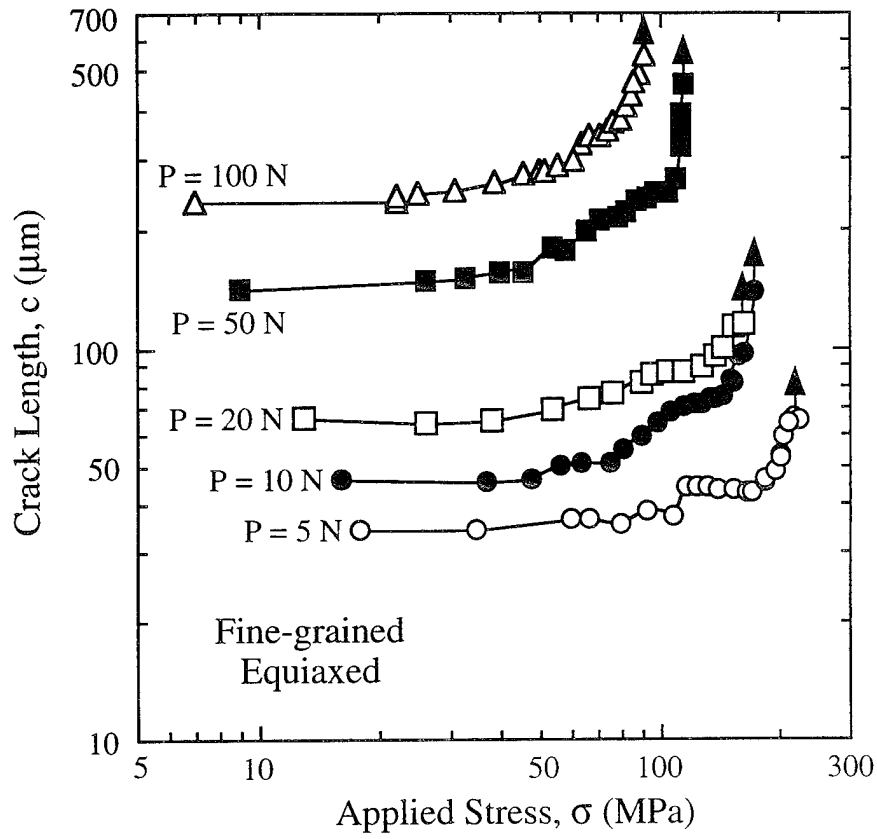
Figure 5
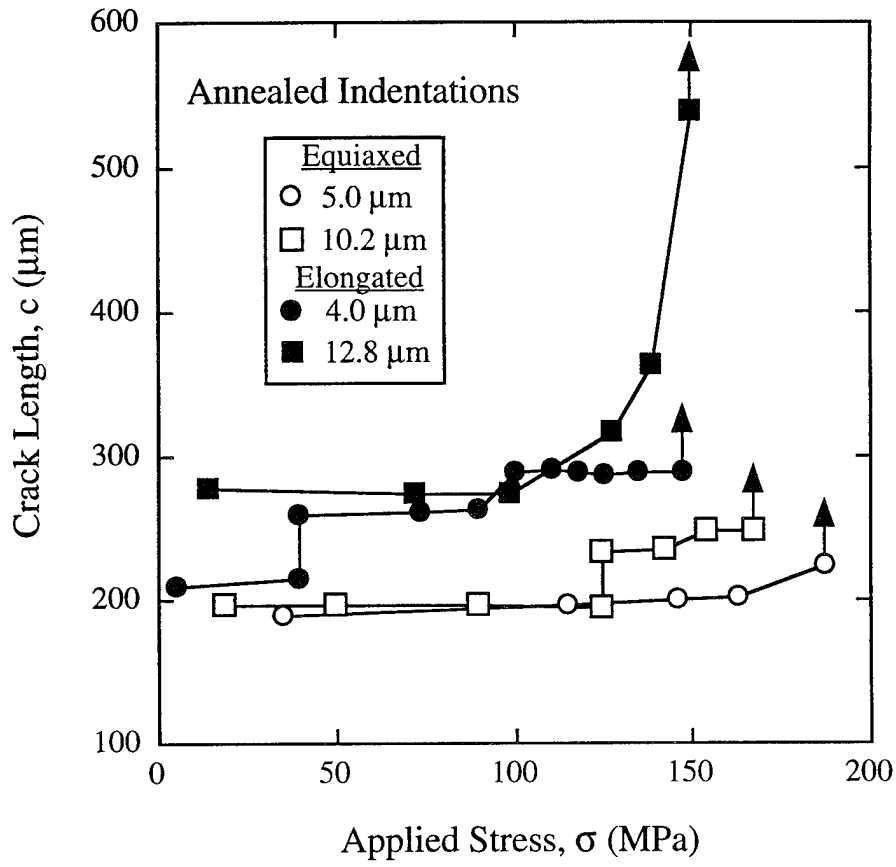
Figure 8

Figure 10

Figure 9

50μm

Figure 11

Figure 13